Topics in Organometallic Chemistry 56

Pierre H. Dixneuf
Henri Doucet *Editors*

C-H Bond Activation and Catalytic Functionalization II

Springer

56
Topics in Organometallic Chemistry

Aims and Scope

The series *Topics in Organometallic Chemistry* presents critical overviews of research results in organometallic chemistry. As our understanding of organometallic structure, properties and mechanisms increases, new ways are opened for the design of organometallic compounds and reactions tailored to the needs of such diverse areas as organic synthesis, medical research, biology and materials science. Thus the scope of coverage includes a broad range of topics of pure and applied organometallic chemistry, where new breakthroughs are being achieved that are of significance to a larger scientific audience.

The individual volumes of *Topics in Organometallic Chemistry* are thematic. Review articles are generally invited by the volume editors. All chapters from Topics in Organometallic Chemistry are published OnlineFirst with an individual DOI. In references, Topics in Organometallic Chemistry is abbreviated as Top Organomet Chem and cited as a journal.

More information about this series at http://www.springer.com/series/3418

Pierre H. Dixneuf • Henri Doucet
Editors

C-H Bond Activation and Catalytic Functionalization II

With contributions by

J.-M. Basset · O. Baudoin · D. Bézier · M. Brookhart · A.B. Charette · N. Chatani · D. Dailler · G. Danoun · R. Dey · K. Hirano · L. Ilies · W.D. Jones · S. Kavitake · M. Miura · E. Nakamura · M.K. Samantaray · Z.-J. Shi · D. Sustac Roman · T. Zhou

Springer

Editors
Pierre H. Dixneuf
Université de Rennes
Rennes
France

Henri Doucet
Université de Rennes
Rennes
France

ISSN 1436-6002 ISSN 1616-8534 (electronic)
Topics in Organometallic Chemistry
ISBN 978-3-319-24802-8 ISBN 978-3-319-29319-6 (eBook)
DOI 10.1007/978-3-319-29319-6

Library of Congress Control Number: 2015959030

Printed on acid-free paper

This Springer imprint is published by Springer Nature
The registered company is Springer International Publishing AG Switzerland

Preface

The metal-catalysed C–H bond dual activation and functionalisation have brought in the last two decades a revolution for the direct synthesis of complex molecules and molecular materials. Now the functionalisation of sp^2C–H bond for cross-coupled C–C or C-heteroatom bond formation presents advantages to replace, with better atom economy, the classical catalytic cross-coupling reactions involving a stoichiometric amount of an organometallic. In parallel the sp^3C–H bond activation, besides a faster access to natural products, is offering the possibility to functionalise alkanes in connection with renewable energy.

Whereas functional groups have shown efficiency to direct activation of neighbouring C–H bonds, as molecules containing multiple C–H bonds, the successive activations of several of these C–H bonds remain a challenge. Initially expensive metal catalysts have shown their efficiency to activate C–H bonds, but now many examples of cheap and environment-tolerant first-row metal catalysts are promoting useful activations. Examples of C–H bond functionalisation can now be performed in green solvents and even in water.

This volume gathers innovative contributions for a wide range of catalytic C–H bond functionalisations. They involve a variety of metal catalysts from Pd, Rh, Ir and Ru complexes to Fe, Ni, Cu and Ag derivatives, including surface organometallics, and they point out the importance of ancillary or transient ligands forcing the metal site to activate C–H bonds by several complementary processes. In addition this volume presents many new applications for cross C–C and C-heteroatom bond couplings and new synthetic methods, supported by mechanistic and computational studies, and examples of functionalisation of cyclopropanes or fullerenes and addresses problems of regioselectivity. The sp^3C–H bond activation reveals crucial aspects for the synthesis of natural products and for the dehydrogenation and functionalisation of alkanes.

The wide range of innovations presented here, on the concepts of C–H bond activations and their multiple profits, should be a source of inspiration for researchers and industry engineers to discover more efficient catalysts or to transfer the processes to industrial applications. They should attract teachers and students motivated by innovations, catalysis and sustainable development. They are

expected to initiate new ideas to discover new catalytic and cascade transformations.

We are grateful to all the chapter authors, experts in various complementary fields, who have contributed to create this multiple-facet volume.

We dedicate this volume to all chemists and students who are contributing, via C–H bond activation and functionalisation, to discover safe, catalytic transformations that will be profitable for our society.

Rennes, France

Pierre H. Dixneuf
Henri Doucet

Contents

Iron-Catalyzed C–H Bond Activation 1
Laurean Ilies and Eiichi Nakamura

Nickel-Catalyzed C–H Bond Functionalization Utilizing an *N*,*N*′-Bidentate Directing Group 19
Naoto Chatani

Copper-Mediated Intermolecular C–H/C–H and C–H/N–H Couplings via Aromatic C–H Cleavage 47
Koji Hirano and Masahiro Miura

The Effects of Ancillary Ligands on Metal–Carbon Bond Strengths as Determined by C–H Activation 67
William D. Jones

Catalytic C–H Bond Functionalization of Cyclopropane Derivatives . . . 91
Daniela Sustac Roman and André B. Charette

Silver-Mediated Direct sp^3 C–H Bond Functionalization 115
Taigang Zhou and Zhang-Jie Shi

Applications of Catalytic Organometallic C(sp^3)–H Bond Functionalization 133
David Dailler, Grégory Danoun, and Olivier Baudoin

New Concept of C–H and C–C Bond Activation via Surface Organometallic Chemistry 155
Manoja K. Samantaray, Raju Dey, Santosh Kavitake, and Jean-Marie Basset

Transfer Dehydrogenations of Alkanes and Related Reactions Using Iridium Pincer Complexes 189
David Bézier and Maurice Brookhart

Index 209

Top Organomet Chem (2016) 56: 1–18
DOI: 10.1007/3418_2015_129

Published online: 8 August 2015

Iron-Catalyzed C–H Bond Activation

Laurean Ilies and Eiichi Nakamura

Abstract Iron-catalyzed C–H bond activation followed by C–C bond formation has received much attention in recent years, motivated by the environmental and economical merits of iron, as well as the scientific challenge in controlling and understanding the reactivity of iron species. This review describes the utilization of iron as a catalyst for directed C–H bond activation, followed by C–C bond formation. Catalytic activation of $C(sp^2)$-H and $C(sp^3$-H) bonds, followed by oxidative reaction with nucleophiles, or reaction with electrophiles is described. Reactions of substrates possessing a directing group are mainly discussed, but other substrates are also presented. Carbon–heteroatom bond formation is also briefly discussed.

Keywords C–C bond formation · C–H bond activation · Iron

Contents

1 Introduction 2
2 Functionalization of $C(sp^2)$–H Bonds 2
2.1 Substrates Possessing a Directing Group 2
2.2 Other Substrates 11
3 Functionalization of $C(sp^3)$–H Bonds 14
3.1 Substrates Possessing a Directing Group 14
3.2 Other Substrates 14
4 Conclusion 16
References 16

L. Ilies (✉) and E. Nakamura (✉)
Department of Chemistry, The University of Tokyo, School of Science, Hongo, Bunkyo-ku, Tokyo 113-0033, Japan
e-mail: laur@chem.s.u-tokyo.ac.jp; nakamura@chem.s.u-tokyo.ac.jp

1 Introduction

Transition-metal-catalyzed carbon–hydrogen (C–H) activation followed by carbon–carbon (C–C) bond formation has become one of the most active research topics in recent synthetic chemistry, because it could enable the straightforward, step-efficient construction of the framework of target molecules [1–5]. However, there are serious challenges to overcome for the development of these reactions: the C–H bond is thermodynamically stable and difficult to cleave, especially in the presence of other functional groups, typically more labile; also, to differentiate between the many C–H bonds in an organic molecule is a formidable task. Utilization of a directing group, which coordinates the metal catalyst and cleaves the proximity C–H bond selectively in an intramolecular-like fashion, has been a popular strategy to overcome these problems. Late-transition metals such as Pd, Ru, Rh, Ir, etc. have been extensively investigated for this purpose, and versatile and efficient catalytic systems based on these metals have been achieved. However, economic and environmental incentives shifted the interest to first-row transition metals (base metals) for C–H bond activation [6]. Among these, iron is the most abundant transition metal, inexpensive, and nontoxic, and therefore, it has attracted special attention for catalysis [7, 8].

This review describes the utilization of iron as a catalyst for directed C–H bond activation, followed by C–C bond formation. Nondirected reactions, many of which proceed through radical pathways, are briefly discussed. Carbon–heteroatom bond formation is briefly discussed, and reactions where iron acts as a Lewis acid or simply as a radical initiator are outside the scope of this review. Several reviews or minireviews discussing iron-catalyzed C–H bond activation have been published recently [9–16].

2 Functionalization of C(sp^2)–H Bonds

2.1 Substrates Possessing a Directing Group

Cyclometalation reactions using iron complexes have been known for a long time [17–20]. Of special interest for the development of a catalytic reaction under mild conditions are the reports that iron(0) complexes can oxidatively add into the *ortho* C–H bond of an aromatic imine (Eq. 1), and alkyliron(II) complexes can cleave an *ortho* C–H bond with elimination of alkane (Eq. 2) [21, 22].

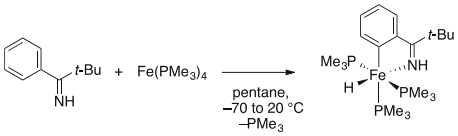

(1)

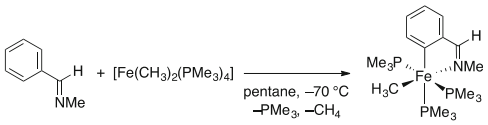

(2)

2.1.1 Catalytic Reactions with Nucleophilic Reagents

After the relatively numerous reports on cyclometalation reactions using iron complexes, the first example of a catalytic reaction was reported in 2008, when Nakamura and collaborators reported that arylpyridines and congeners can be arylated with diarylzinc generated in situ from a Grignard reagent and $ZnCl_2$·TMEDA in the presence of a catalytic amount of Fe(III) salt, a bipyridine-type ligand, and a dihaloalkane oxidant (Eq. 3) [23]. The reaction proceeded in high yield at 0°C, with selectivity for the monoarylated product.

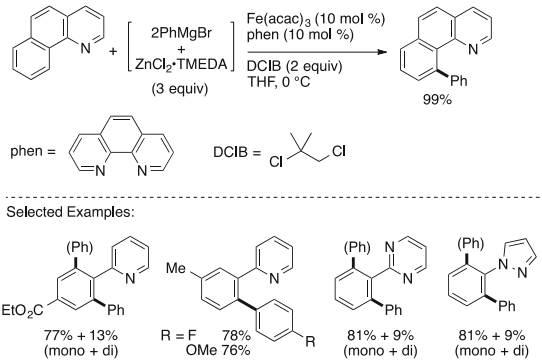

(3)

The same group reported 1 year later that aromatic imines can also be *ortho* arylated under similar conditions, and the resulting imine was hydrolyzed during acidic workup to the corresponding ketone (Eq. 4) [24]. The C–H bond was preferentially functionalized in the presence of a reactive bromide, triflate, or tosylate group, in contrast with palladium catalysis, where the halide reacts selectively (Eq. 5). Nakamura group also demonstrated that dioxygen can be used as an alternative oxidant, albeit the reaction efficiency decreased [25].

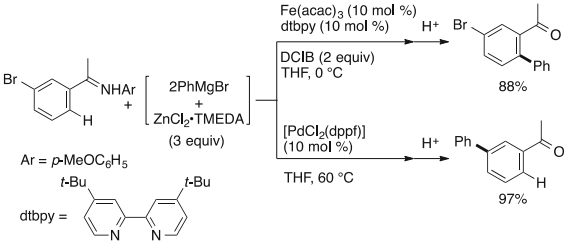

(4, 5)

Under similar reaction conditions, *N*-methylbenzamides were *ortho* arylated with diarylzinc (Eq. 6) [26]. The reaction proceeded selectively and only the

monoarylated product was obtained, presumably because of the steric bias induced by the *ortho* substituent, which disturbs the cyclometalation step.

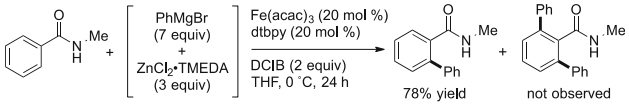

(6)

The oxidative reaction of amides with diarylzinc reagents was reported by Ackermann [27]. The use of a bidentate directing group containing a triazole moiety (TAM) was crucial for the efficiency of the reaction (Eq. 7).

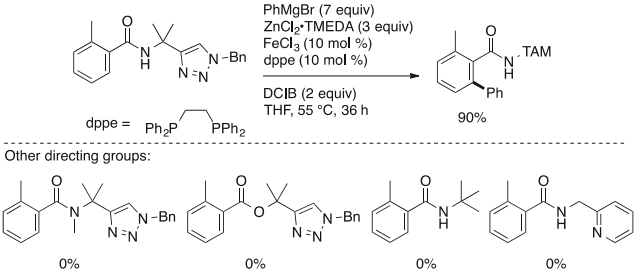

(7)

The arylation of arylpyridines (Eq. 8) and aromatic amines (Eq. 9) can also be achieved using Grignard reagents [28]. For these reactions, the slow addition of the Grignard reagent proved crucial in order to prevent excessive homocoupling of the organometallic reagent [29, 30], and under the slow addition condition, the *ortho*-arylated compounds were obtained in high yield. DuBois used similar reaction conditions to investigate the arylation of various heterocyclic substrates such as pyridines, thiophenes, and furans (Eq. 10) [31].

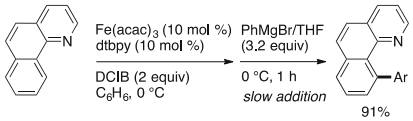

(8)

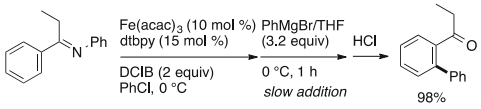

(9)

(10)

The mechanism of these reactions is largely unknown. Nakamura showed [28] that the reaction requires an oxidant for catalyst turnover and to accelerate reductive elimination, and the reaction with a stoichiometric amount of iron in the absence of an oxidant, followed by high deuterium incorporation upon quenching with

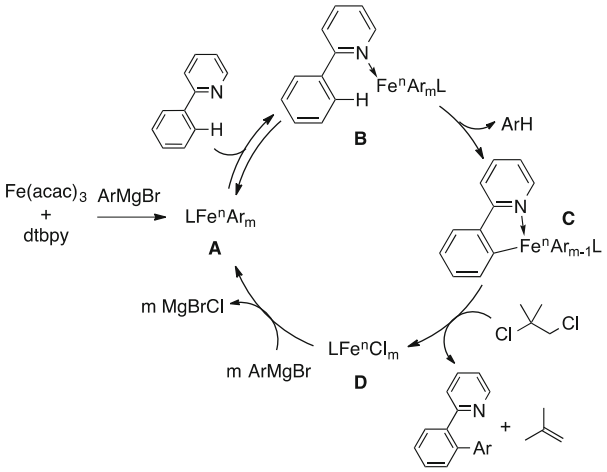

Fig. 1 A proposed catalytic cycle for the iron-catalyzed oxidative C–H functionalization with organometallic reagents

deuterium oxide (Eq. 11), suggested the intermediacy of a ferracycle. Kinetic isotope effect experiments showed a large value for the intermolecular (3.4) and intramolecular (3.1) competition, indicating that coordination of the pyridyl group to the iron catalyst takes place in a reversible manner and that the following C–H bond-cleavage step is the first irreversible step of the catalytic cycle [32]. Taking also into account the cyclometalation reaction with diorganoiron complexes depicted in Eq. 2, the authors proposed the catalytic cycle in Fig. 1. An organoiron species **A** generated from the iron(III) salt and the organometallic reagent [33] reversibly coordinates the substrate and then cleaves the *ortho* C–H bond to generate metallacycle **C**. This complex is stable in the absence of the oxidant as shown by the deuterium-labeling experiment but readily undergoes reductive elimination in the presence of a dichloroalkane oxidant to give the *ortho*-arylated product and regenerate the catalyst. The valence of iron during this catalytic cycle is unclear: formation of a homocoupling product (Ar–Ar) suggests that iron is reduced to a lower valence; however, subsequent work from Nakamura group (vide infra) showed that an iron(III) species is competent for C–H activation, and therefore, the reduction of iron may occur outside the catalytic cycle.

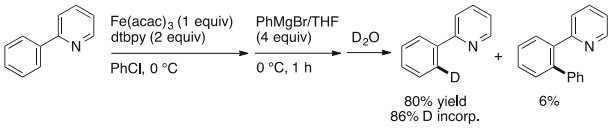

(11)

The group of Nakamura reported that an alkene possessing a pyridine or imine group can be arylated with Grignard reagents in a stereoselective fashion (Eq. 12) [34]. The reaction proceeded within 5 min at 0°C to give the *Z* product when chlorobenzene was used as a solvent or the *E* product when THF was used as a solvent. Control experiments showed that the *Z* product forms first and then isomerizes in the presence of THF.

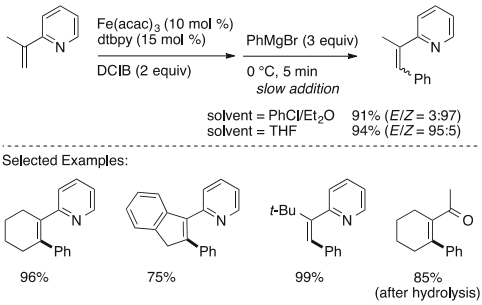

(12)

To circumvent the use of organometallic reagents, the group of Nakamura used aryl bromides in the presence of metallic magnesium for the *ortho* arylation of arylpyridines and aromatic imines (Eq. 13) [35]. It was assumed that a Grignard reagent is generated in situ, possibly facilitated by the iron catalyst [36–38]. Dioxane was used as a cosolvent in order to retard the generation rate of the Grignard reagent and its subsequent homocoupling, rather than to generate a diarylmagnesium reagent, which a control experiment showed to be low yielding.

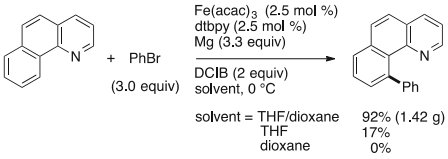

(13)

A common problem of these reactions was the rather restricted reaction scope and versatility. Because a significant amount of homocoupling of the organometallic reagent was observed and based on previous knowledge [33], it was assumed that iron was reduced to a lower-valent species (or a mixture of species) and combined with the use of a reactive organozinc or organomagnesium reagent, the reaction scope and functional group tolerance were poor. Ilies and Nakamura found a solution to this problem: if iron could be stabilized as an iron(III) species by the use of appropriate ligands and a milder organometallic reagent, a more versatile catalytic system was expected. And indeed, by using an organoborate as the organometallic reagent [39, 40] in the presence of an iron(III) salt, a diphosphine ligand, a zinc salt cocatalyst, and a dihalide oxidant, the coupling of a variety of aryl, heteroaryl, and alkenyl amides possessing a bidentate 8-quinolylamide group [41–43] with aryl and alkenyl boron reagents was achieved (Eq. 14) [44]. The stereospecific alkene–alkene coupling to produce (*Z*,*E*) or (*Z*,*Z*) dienes or trienes is especially noteworthy. The homocoupling of the organometallic reagent was observed in a trace amount for the catalytic reaction, and in small amount (13%) for the reaction using a stoichiometric amount of iron, demonstrating that the iron(III) species is not reduced by the organometallic reagent. Combined with the poor activity of an Fe(II) precursor, the authors concluded that an organoiron(III) species is responsible for cleaving the C–H bond. The zinc salt was considered to assist the transfer of the organic group from borate to iron [45, 46]. The authors also suggested the low-valent iron species that is generated after reductive elimination may be stabilized by spin delocalization over the diphosphine ligand and quinolylamine directing group [47].

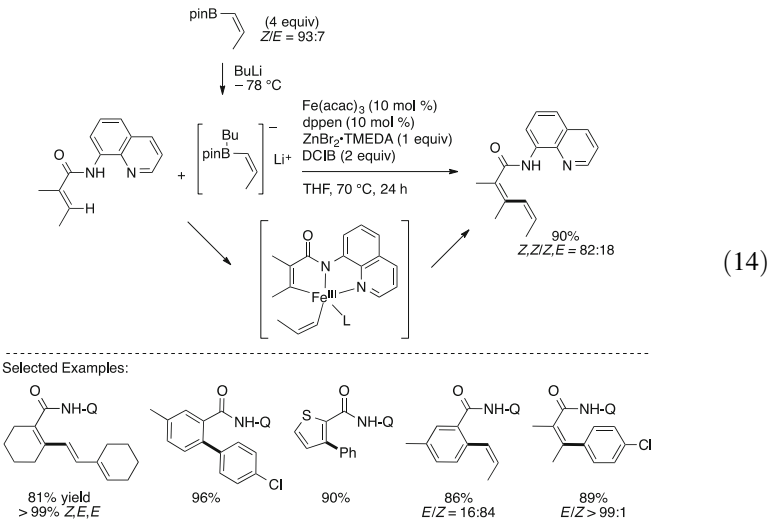

(14)

Ilies and Nakamura recently reported the alkylation of alkene-, arene-, and heteroareneamides possessing the 8-aminoquinolyl group with alkylzinc halides (Eq. 15) [48]. The use of a bidentate directing group was crucial in order to prevent the β-hydride elimination of the alky liron intermediate; the reaction of a substrate possessing a monodentate directing group such as pyridine with phenethylzinc halide resulted in the recovery of the starting material together with formation of styrene. Notably, the homocoupling of the organometallic reagent was also suppressed, suggesting that an organoiron(III) species is the active species. The stereospecific reaction of acrylamide is especially noteworthy, because the reaction of this substrate is typically sluggish under C–H bond activation conditions.

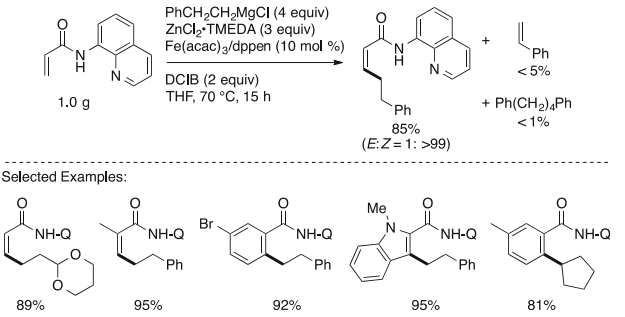

(15)

2.1.2 Catalytic Reactions with Electrophilic Reagents

The reactions described in the previous paragraph utilize an organometallic reagent as the reaction partner under oxidative conditions. From a practical point of view, the use of an electrophilic, neutral reagent as the reaction partner is more attractive. However, if an organometallic reagent is used as a base in the presence of an electrophile, the oxidative reaction between the C–H substrate and the

organometallic reagent and the reaction between the organometallic reagent and the electrophile compete with the desired reaction of the C–H substrate with the electrophile.

The first successful example of this type of reaction was reported by Ilies and Nakamura in 2013 (Eq. 16) [49]. They utilized a bidentate 8-quinolylamide directing group, a diphosphine ligand, and a bulky organozinc reagent as the base, to succeed in coupling an aromatic carboxamide with allyl phenyl ether in high yield, and with suppression of the oxidative reaction of the substrate with the organometallic reagent, or the cross-coupling between the allyl ether and the diorganozinc. Various aromatic carboxamides reacted well, but the scope of the allyl ether was limited. A deuterium-labeling experiment showed that the allylation reaction proceeds with γ-selectivity, and an intermolecular KIE experiment showed that the C–H bond activation step is not involved in the turnover-limiting step. The authors also showed that 1-arylpyrazoles and congeners can also be allylated with allyl phenyl ether using iron catalysis [50]. The authors also achieved an amination reaction under similar conditions, where an *N*-chloroamine was used as the electrophile (Eq. 17) [51].

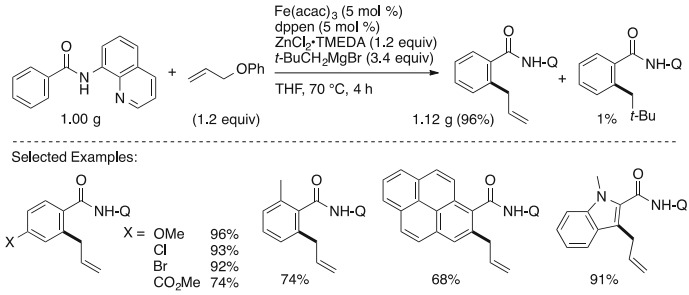

(16)

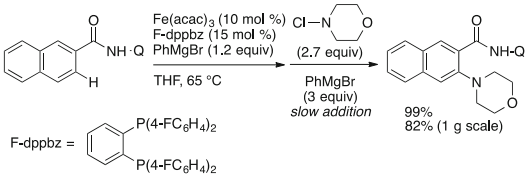

(17)

Iron-catalyzed alkylation of carboxamides possessing an 8-aminoquinolyl group with alkyl tosylates and halides was reported by Ilies and Nakamura [52], and at the same time the reaction of similar substrates with alkyl halides was reported by Cook [53, 54].

Ilies and Nakamura reported the iron/diphosphine-catalyzed reaction of arene-, heteroarene-, and alkeneamides with primary and secondary alkyl tosylates or halides (Eq. 18) [52]. The reaction of acyclic alkenes substrated proceeded stereoselectively, and acyclic secondary tosylates could be introduced without isomerization of the alkyl group to the linear one. A chiral alkyl center underwent isomerization, and a cyclopropylalkyl group reacted with the opening of the cyclopropyl ring, suggesting that the alkyl iron species has a radical character. Homocoupling of the organozinc halide that

was used as a base was not observed, suggesting that an organoiron(III) may be the active species. Control experiments showed that under the reaction conditions, alkyl tosylates and chlorides are converted into the corresponding bromides.

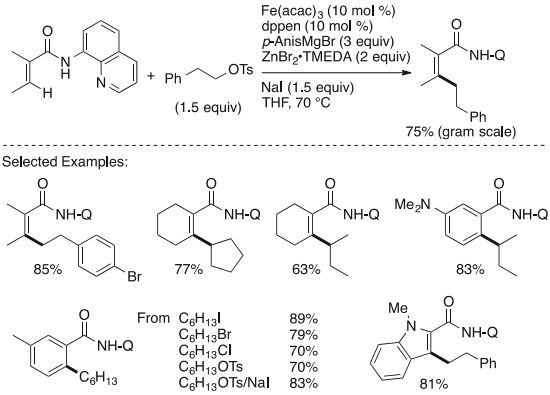

(18)

Cook reported the iron/diphosphine-catalyzed alkylation of arene-, heteroarene-, and alkeneamides with primary alkyl halides (Eq. 19) [53] and, shortly after, the alkylation of aromatic amides with benzyl chlorides and secondary alkyl bromides (Eq. 20) [54]. The reaction with primary alkyl bromides proceeded well for aromatic, heteroaromatic, and alkenyl amides; despite using phenylmagnesium bromide as a base, the reaction with benzyl chlorides proceeded well under air. As previously observed by Nakamura [28, 34], the slow addition of the Grignard reagent was crucial in order to achieve high yields, presumably because of the competing homocoupling [29]. Secondary alkyl bromides and iodides could be employed in the reaction with benzamides, but acyclic secondary alkyls underwent partial isomerization to the linear alkyl.

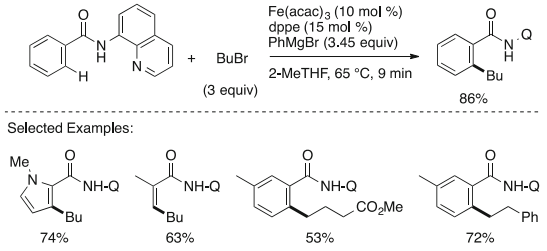

(19)

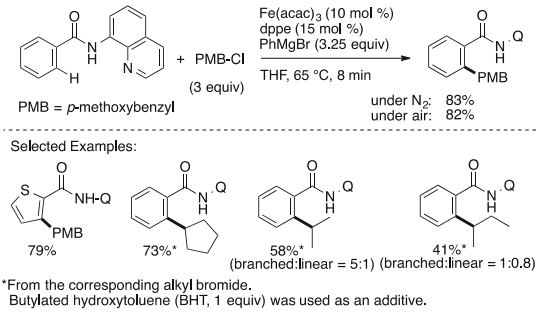

(20)

The iron-catalyzed directed C–H alkylation and alkenylation of indole derivatives possessing an imine group with alkenes and alkynes, respectively, was reported by Yoshikai (Eqs. 21 and 22) [55]. Inspired by an analogy with cobalt catalysis [56], they used an *N*-heterocyclic carbene as a ligand, cyclohexylmagnesium chloride as a base, and TMEDA as an essential additive for the reaction with alkenes, whereas phenylmagnesium bromide was the base of choice, and TMEDA was not necessary for the reaction with alkynes. The reaction with styrene derivatives proceeded regioselectively to give the branched product; however, other terminal alkenes such as 1-octene did not react. *β*-Substituted styrenes could also be employed in this reaction. Diaryl-, arylsilyl-, and alkylsilyl-substituted alkynes gave the (*E*)-alkenylated product, but in some cases isomerization was observed. A dialkylalkyne was much less reactive. Based on deuterium-labeling experiments, the authors proposed that the Grignard reagent reduces the iron precatalyst to a low-valent iron-NHC species, which after coordination to the imine directing group oxidatively adds the C–H bond. Next the alkene or alkyne undergoes migratory insertion into the iron hydride complex, followed by reductive elimination to give the product.

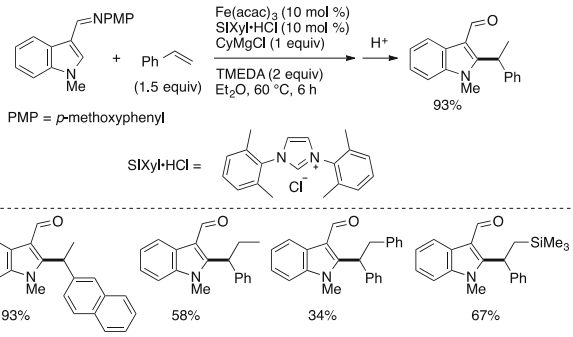

(21)

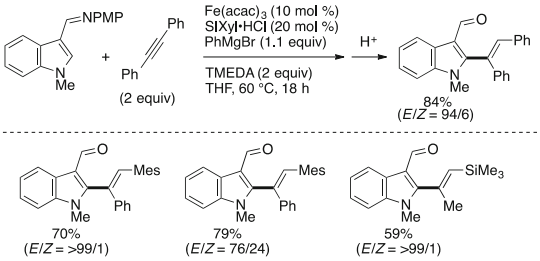

(22)

2.2 *Other Substrates*

It has been known from the 1970s that an iron complex can cleave the C–H bond of an arene [57, 58]. However, the exploitation of this reactivity for the development of a catalytic reaction has been largely neglected to date. An early attempt was described in 1987 [59], when Jones reported that an iron–isocyanide complex can insert the isocyanide group into the C–H bond of benzene upon irradiation with light, and in the presence of added isonitrile and high dilution, the reaction was catalytic in iron, albeit the turnover was low (Eq. 23).

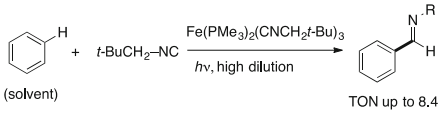

(23)

In 2010, the groups of Charette and Lei independently reported an iron/diamine-catalyzed reaction of aryl iodides or bromides with a solvent amount of arene at 80–90°C (Eqs. 24 and 25) [60, 61]. A mixture of *ortho*-, *meta*-, and *para*-isomers was obtained when substituted arenes were used as the substrate, the *ortho*-isomer being the major product. The Charette group reported a KIE value of 1.04, while Lei group measured a KIE of 1.7. Based also on reaction inhibition by a radical scavenger, Charette suggested that radical processes are involved. Recent studies have revealed that cross-coupling of an aryl halide with an arene can proceed in the absence of a transition metal catalyst ([62] and references therein).

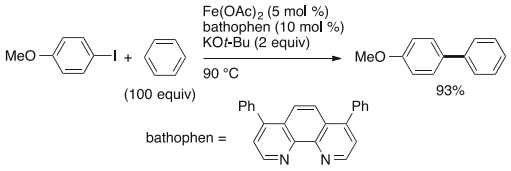

(24)

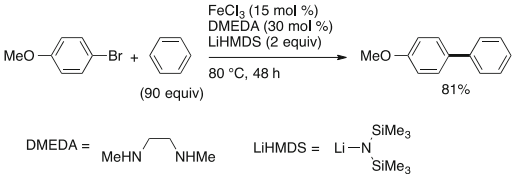

(25)

Hu and Yu reported an iron/macrocyclic polyamine-catalyzed reaction of arylboronic acids with a large excess of pyrrole or pyridine at 130°C under air (Eqs. 26 and 27) [63], based on their previous studies on iron-mediated reactions (initial report using a stoichiometric amount of iron: [64]). Pyrrole derivatives were arylated at 2-position in good yield (Eq. 26), but when pyridine was used as a substrate, the catalyst turnover was poor and 2-arylpyridine was obtained together with a small amount of 3-aryl- and 4-arylpyridine (Eq. 27). Because a catalytic amount of a radical scavenger did not inhibit the reaction, the authors proposed an oxoiron complex as the active species to activate the *ortho*-hydrogen of the heterocycle via σ-bond metathesis and also performed a DFT analysis of the mechanism. A related iron-catalyzed reaction of aryl boronic acids with heteroarenes was reported by Singh and Vishwakarma [65].

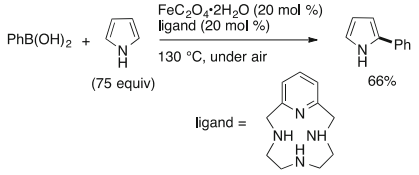

(26)

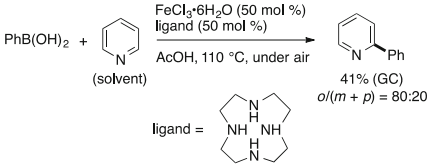

(27)

Shirakawa and Hayashi reported the iron-catalyzed oxidative coupling of arylboronic acids with arenes and heteroarenes (Eq. 28) [66]. They used iron(III) triflate, a bipyridine-type ligand, and a peroxide as an oxidant. For substituted arenes, a mixture of *ortho*-, *meta*-, and *para*-substituted compounds was obtained, with modest selectivity for the *ortho*-isomer. The authors propose that Fe(III) mediates generation of *t*-BuO radical from the peroxide, which oxidizes the arylboronic acid to generate an aryl radical that adds to the arene substrate.

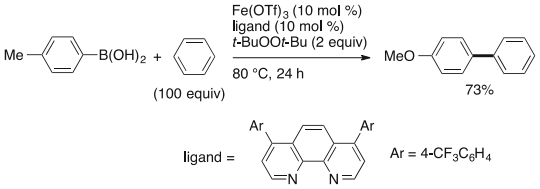

(28)

Nakamura reported that 2-biphenylmagnesium and congeners could be annulated with alkynes under mild reaction conditions in the presence of an iron catalyst and a dihalide oxidant to produce a variety of phenanthrene derivatives (Eq. 29) [67]. Based on deuterium-labeling experiments, the authors proposed the

intermediacy of a biphenyl metallacycle, formed through intramolecular activation of the *ortho*-hydrogen.

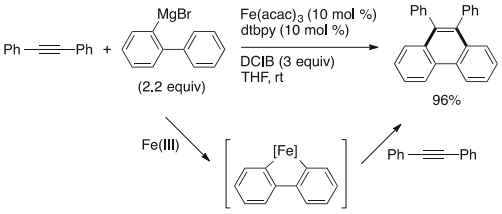

(29)

Nakamura group also reported the reaction of aryl Grignard reagents with two molecules of alkynes to produce polysubstituted naphthalenes (Eq. 30) [68]. Diarylalkynes reacted in good yield, but dialkylalkynes gave lower yield. A limitation of this reaction was the lack of regioselectivity when differently substituted substrates were used. The authors proposed that in situ-generated aryliron species carbometalate the alkyne [69–73], followed by C–H bond activation, insertion of a second molecule of alkyne, and finally reductive elimination to give the product.

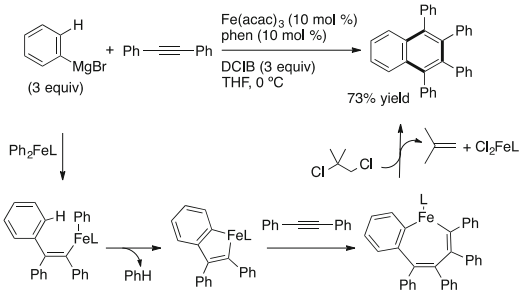

(30)

Iron-catalyzed silylation and borylation of a C–H bond has received much attention recently. Sunada and Nagashima reported that a disilaferracycle iron carbonyl complex can catalyze the C-3-selective silylation of indoles [74]. Ito and Nishiyama reported that a similar reaction can be catalyzed by a pincer iron complex containing a silyl ligand [75]. Ohki and Tatsumi reported that Cp*Fe complexes bearing imidazolium salts catalyze the borylation of furans and thiophenes [76]. The borylation of arenes catalyzed by nano-Fe2O3 was reported by Kuang and Wang [77]; a similar reaction was reported by Mankand, who used an iron–copper heterobimetallic complex under photochemical conditions [78], and by Bontemps, Sortais, Sabo-Etienne, and Darcel, who used a bis(diphosphine)iron complex under UV irradiation [79].

3 Functionalization of C(sp^3)–H Bonds

3.1 Substrates Possessing a Directing Group

Directed activation of a C(sp^3)–H bond by an iron complex was much less investigated than the reaction of C(sp^2)–H bonds. Li reported the phosphine-directed C (sp^3)–H to form an iron pincer complex (e.g., [80]). Ohki and Tatsumi reported that Cp*Fe complexes bearing imidazolium salts undergo cyclometalation through C–H activation or can cleave the C–H bond of a heteroarene [81].

Nakamura reported the first iron-catalyzed directed functionalization of C(sp^3)–H bonds in 2013 (Eq. 31) [82]. Propionamides bearing a bidentate directing group could be arylated with diarylzinc reagents in the presence of an iron/diphosphine catalyst and a dichloroalkane oxidant. The nature of the directing group and of the diphosphine ligand was crucial for the success of this reaction, presumably because of stabilization of the putative organoiron intermediate. The reaction proceeded exclusive at the methyl C–H in the presence of a benzyl C–H, suggesting the intermediacy of organometallic species rather than a radical mechanism. The distance between the C–H bond and the directing group proved also important, and elongation of this distance resulted in shutting off the reaction.

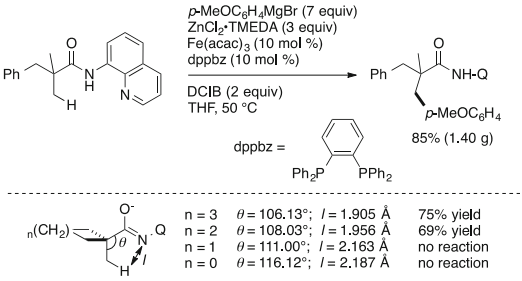

(31)

Ackermann showed that a bidentate directing group containing a triazole moiety can also be used for this reaction, under otherwise very similar conditions (Eq. 32) [27].

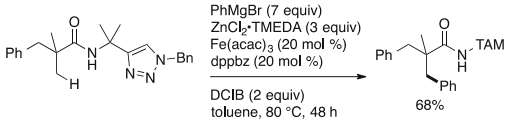

(32)

3.2 Other Substrates

Hartwig showed in 1997 that an iron boryl complex can cleave the C–H bond of a simple alkane under photochemical conditions [83, 84], but this reactivity was not exploited for C–C bond formation to date.

Nakamura observed the α-arylation of THF by an diorganozinc reagent in the presence of an iron/bipyridine-type ligand and 4-iodotoluene that presumably acted

as an oxidant (Eq. 33) [85]. Based on this initial lead, a reaction that combines radical and organometallic reactivity of iron to achieve α-functionalization of aliphatic amines through 1,5-hydrogen transfer was designed (Eq. 34).

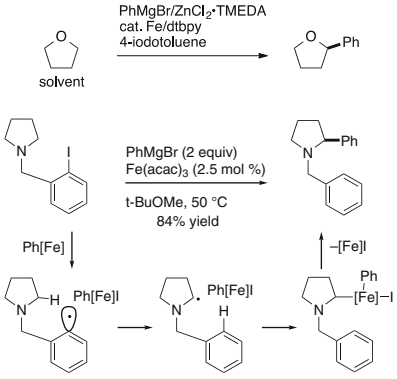

(33)

(34)

The α-arylation of ethers was further developed by Vishwakarma [86, 87], who reported that in situ-prepared Grignard reagents react with THF to give the corresponding 2-arylated compounds (Eq. 35). Despite its low solubility, iron oxide was the catalyst of choice, and high yields were reported.

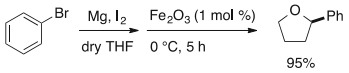

(35)

The arylation of cyclic and acyclic alkenes at the allylic position with Grignard reagents was accomplished by Nakamura by using an iron/xantphos catalyst and mesityl iodide as an oxidant (Eqs. 36 and 37) [88]. The alkene was used in large excess, and the TON of the reaction reached 240. Control experiments supported the intermediacy of a π-allyliron rather than a Heck-type mechanism.

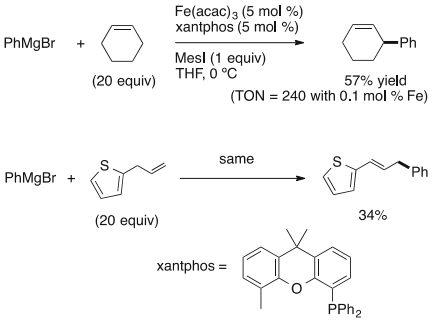

(36, 37)

A large number of cross-dehydrogenative couplings using iron catalysis under oxidative conditions have been reported [89, 90]. The coupling of sp^3–sp^3, sp^3–sp^2, and sp^3–sp bonds has been achieved. These reactions proceed through iron-mediated electron-transfer processes and are outside the scope of this review.

4 Conclusion

Iron-catalyzed C–H bond activation followed by C–C bond formation has received much attention in recent years, motivated by the environmental and economical merits of iron, as well as the scientific challenge in controlling and understanding the reactivity of iron species. Robust catalytic systems have been developed for directed C–H bond functionalization with organometallic reagents or with electrophiles, and in some cases versatility and efficiency rivaling precious metal catalysis have been achieved. Several examples of directed $C(sp^3)$–H activation have also been reported. Nondirected reactions have mostly relied on electron-transfer processes, especially the reactions of $C(sp^3)$–H bonds. While the pace of recent developments is impressive, it can be said that the potential of iron catalysis for C–H bond functionalization is far from being fulfilled. The repertoire of reactions is still limited, as is the variety of substrates available; many of these reactions use reactive organometallics as a base, and in many cases functional group tolerance or product selectivity is unsatisfactory. Two of the biggest obstacles in the development of these reactions are the lack of mechanistic understanding and implicitly the lack of guidelines for controlling the reactivity of iron species. It is the belief of the authors that in the near future these challenges will be successfully addressed, and efficient iron catalysts for versatile C–H bond functionalization will be achieved.

References

1. Dyker G (ed) (2005) Handbook of C–H transformations. Wiley-VCH, Weinheim
2. Godula K, Sames D (2006) Science 312:67
3. Gutekunst WR, Baran PS (2011) Chem Soc Rev 40:1976
4. Wencel-Delord J, Glorius F (2013) Nat Chem 5:369
5. Segawa Y, Maekawa T, Itami K (2015) Angew Chem Int Ed 54:66
6. Nakamura E, Sato K (2011) Nat Mater 10:158
7. Plietker B (ed) (2008) Iron catalysis in organic chemistry. Wiley-VCH, Weinheim
8. Bolm C (2009) Nat Chem 1:420
9. Kulkarni A, Daugulis O (2009) Synthesis 4087
10. Sun C-L, Li B-J, Shi Z-J (2011) Chem Rev 111:1293
11. Bauer I, Knölker H-J (2015) Chem Rev 115:3170
12. Yoshikai N (2014) Iron-catalyzed cross-coupling reactions. In: Marek I, Rappoport Z (eds) The chemistry of organoiron compounds. Wiley, Chichester
13. Ambhaikar NB (2015) Iron-catalyzed C–H activation. In: Li JJ (ed) C–H bond activation in organic synthesis. CRC, Boca Raton
14. Mihovilovic MD, Schnürch M (2014) ChemCatChem 6:2194
15. Su B, Cao Z-C, Shi Z-J (2015) Acc Chem Rev 48:886
16. Nakamura E, Yoshikai N (2010) J Org Chem 75:6061
17. Bagga MM, Pauson PL, Preston FJ, Reed RI (1965) Chem Commun 543
18. Baikie PE, Mills OS (1966) Chem Commun 707
19. Bagga MM, Flannigan WT, Knox GR, Pauson PL, Preston FJ, Reed RI (1968) J Chem Soc C 36
20. Alper H, Chan ASK (1971) Chem Commun 1203

21. Klein H-F, Camadanli S, Beck R, Leukel D, Flörke U (2005) Angew Chem Int Ed 44:975
22. Camadanli S, Beck R, Flörke U, Klein H-F (2009) Organometallics 28:2300
23. Norinder J, Matsumoto A, Yoshikai N, Nakamura E (2008) J Am Chem Soc 130:5858
24. Yoshikai N, Matsumoto A, Norinder J, Nakamura E (2009) Angew Chem Int Ed 48:2925
25. Yoshikai N, Matsumoto A, Norinder J, Nakamura E (2010) Synlett 313
26. Ilies L, Konno E, Chen Q, Nakamura E (2012) Asian J Org Chem 1:142
27. Gu Q, Al Mamari HH, Graczyk K, Diers E, Ackermann L (2014) Angew Chem Int Ed 53:3868
28. Yoshikai N, Asako S, Yamakawa T, Ilies L, Nakamura E (2011) Chem Asian J 6:3059
29. Cahiez G, Chaboche C, Mahuteau-Betzer F, Ahr M (2005) Org Lett 7:1943
30. Nagano T, Hayashi T (2005) Org Lett 7:491
31. Sirois JJ, Davis R, DeBoef B (2014) Org Lett 16:868
32. Simmons EM, Hartwig JF (2012) Angew Chem Int Ed 51:3066
33. Bedford RB (2015) Acc Chem Rev 48:1485
34. Ilies L, Asako S, Nakamura E (2011) J Am Chem Soc 133:7672
35. Ilies L, Kobayashi M, Matsumoto A, Yoshikai N, Nakamura E (2012) Adv Synth Catal 354:593
36. Bogdanovic B, Schwickardi M (2000) Angew Chem Int Ed 39:4610
37. Czaplik WM, Mayer M, Jacobi von Wangelin A (2009) Angew Chem Int Ed 48:607
38. Czaplik WM, Mayer M, Jacobi von Wangelin A (2011) ChemCatChem 3:135
39. Kobayashi Y, Mizojiri R (1996) Tetrahedron Lett 37:8531
40. Hatakeyama T, Hashimoto T, Kondo Y, Fujiwara Y, Seike H, Takaya H, Tamada Y, Ono T, Nakamura M (2010) J Am Chem Soc 132:10674
41. Zaitsev VG, Shabashov D, Daugulis O (2005) J Am Chem Soc 127:13154
42. Rouquet G, Chatani N (2013) Angew Chem Int Ed 52:11726
43. Daugulis O, Roane J, Tran LD (2015) Acc Chem Res 48:1053
44. Shang R, Ilies L, Asako S, Nakamura E (2014) J Am Chem Soc 136:14349
45. Bedford RB, Hall MA, Hodges GR, Huwe M, Wilkinson MC (2009) Chem Commun 6430
46. Bedford RB, Gower NJ, Haddow MF, Harvey JN, Nunn J, Okopie RA, Sankey F (2012) Angew Chem Int Ed 51:5435
47. Blanchard S, Derat E, Murr M, Fensterbank L, Malacria M, Mouries-Mansuy V (2012) Eur J Inorg Chem 376
48. Ilies L, Ichikawa S, Asako S, Matsubara T, Nakamura E (2015) Adv Synth Catal. doi:10.1002/adsc.201500276
49. Asako S, Ilies L, Nakamura E (2013) J Am Chem Soc 135:17755
50. Asako S, Norinder J, Ilies L, Yoshikai N, Nakamura E (2014) Adv Synth Catal 356:1481
51. Matsubara T, Asako S, Ilies L, Nakamura E (2014) J Am Chem Soc 136:646
52. Ilies L, Matsubara T, Ichikawa S, Asako S, Nakamura E (2014) J Am Chem Soc 136:13126
53. Monks BM, Fruchey ER, Cook SP (2014) Angew Chem Int Ed 53:11065
54. Fruchey ER, Monks BM, Cook SP (2014) J Am Chem Soc 136:13130
55. Wong MY, Yamakawa T, Yoshikai N (2015) Org Lett 17:442
56. Gao K, Yoshikai N (2014) Acc Chem Res 47:1208
57. Tolman CA, Ittel SD, English AD, Jesson JP (1978) J Am Chem Soc 100:4080
58. Baker MV, Field LD (1986) J Am Chem Soc 108:7433
59. Jones WD, Foster GP, Putinas JM (1987) J Am Chem Soc 109:5047
60. Vallée F, Mousseau JJ, Charette AB (2010) J Am Chem Soc 132:1514
61. Liu W, Cao H, Lei A (2010) Angew Chem Int Ed 49:2004
62. Yanagisawa S, Itami K (2011) ChemCatChem 3:827
63. Wen J, Qin S, Ma L-F, Dong L, Zhang J, Liu S-S, Duan Y-S, Chen S-Y, Hu C-W, Yu X-Q (2010) Org Lett 12:2694
64. Wen J, Zhang J, Chen S-Y, Li J, Yu X-Q (2008) Angew Chem Int Ed 47:8897
65. Singh PP, Aithagani SK, Yadav M, Singh VP, Vishwakarma RA (2013) J Org Chem 78:2639
66. Uchiyama N, Shirakawa E, Nishikawa R, Hayashi T (2011) Chem Commun 47:11671
67. Matsumoto A, Ilies L, Nakamura E (2011) J Am Chem Soc 133:6557

68. Ilies L, Matsumoto A, Kobayashi M, Yoshikai N, Nakamura E (2012) Synlett 23:2381
69. Hojo M, Murakami Y, Aihara H, Sakuragi R, Baba Y, Hosomi A (2001) Angew Chem Int Ed 40:621
70. Shirakawa E, Yamagami T, Kimura T, Yamaguchi S, Hayashi T (2005) J Am Chem Soc 127:17164
71. Zhang D, Ready JM (2006) J Am Chem Soc 128:15050
72. Yamagami T, Shintani R, Shirakawa E, Hayashi T (2007) Org Lett 9:1045
73. Shirakawa E, Ikeda D, Masui S, Yoshida M, Hayashi T (2012) J Am Chem Soc 134:272
74. Sunada Y, Soejima H, Nagashima H (2014) Organometallics 33:5936
75. Ito J, Hosokawa S, Khalid HB, Nishiyama H (2015) Organometallics 34:1377
76. Hatanaka T, Ohki Y, Tatsumi K (2010) Chem Asian J 5:1657
77. Yan G, Jiang Y, Kuang C, Wang S, Liu H, Zhang Y, Wang J (2010) Chem Commun 46:3170
78. Mazzacano TJ, Mankad NP (2013) J Am Chem Soc 135:17258
79. Dombray T, Werncke CG, Jiang S, Grellier M, Vendier L, Bontemps S, Sortais J-B, Sabo-Etienne S, Darcel C (2015) J Am Chem Soc 137:4062
80. Xu G, Sun H, Li X (2009) Organometallics 28:6090
81. Ohki Y, Hatanaka T, Tatsumi K (2008) J Am Chem Soc 130:17174
82. Shang R, Ilies L, Matsumoto A, Nakamura E (2013) J Am Chem Soc 135:6030
83. Waltz KM, Hartwig JF (1997) Science 277:211
84. Waltz KM, Hartwig JF (2000) J Am Chem Soc 122:11358
85. Yoshikai N, Mieczkowski A, Matsumoto A, Ilies L, Nakamura E (2010) J Am Chem Soc 132:5568
86. Singh PP, Gudup S, Ambala S, Singh U, Dadhwal S, Singh B, Sawant SD, Vishwakarma RA (2011) Chem Commun 47:5852
87. Singh PP, Gudup S, Aruri H, Singh U, Ambala S, Yadav M, Sawant SD, Vishwakarma RA (2012) Org Biomol Chem 10:1587
88. Sekine M, Ilies L, Nakamura E (2013) Org Lett 15:714
89. Li C-J (2009) Acc Chem Res 42:335
90. Li Z (2014) Org Chem Front 1:194

Top Organomet Chem (2016) 56: 19–46
DOI: 10.1007/3418_2015_117

Published online: 13 June 2015

Nickel-Catalyzed C–H Bond Functionalization Utilizing an *N*,*N*′-Bidentate Directing Group

Naoto Chatani

Abstract This review discusses the use of nickel catalysts and *N*,*N*′-bidentate directing groups, such as 2-pyridinylmethylamine, 8-aminoquinoline, and derivatives thereof, which constitute a powerful combination for the chelation-assisted functionalization of C–H bonds.

Keywords C–H activation · C–H functionalization · Chelation assistance · Nickel

Contents

1 Introduction 20
2 C(sp^2)-H Activation 21
2.1 Oxidative Cycloaddition of C(sp^2)–H Bonds with Alkynes 21
2.2 Alkylation of C(sp^2)–H Bonds 24
2.3 Arylation of C(sp^2)–H Bonds 27
2.4 Alkynylation of C(sp^2)–H Bonds 28
2.5 Cross-Dehydrogenative Coupling of C(sp^2)–H Bonds with Toluene C–H Bonds 30
2.6 Carbonylation of C(sp^2)–H Bonds 31
2.7 C–S Bond Formation 32
3 C(sp^3)–H Activation 34
3.1 Arylation of C(sp^3)–H Bonds 34
3.2 Alkylation of C(sp^3)–H Bonds 38
3.3 Carbonylation of C(sp^3)–H Bonds 39
3.4 C–S Bond Formation 39
3.5 C–N Bond Formation 41
4 Elaboration of Directing Groups 41
5 Conclusions 43
References 45

N. Chatani (✉)
Department of Applied Chemistry, Osaka University, Suita, Osaka 565-0871, Japan
e-mail: chatani@chem.eng.osaka-u.ac.jp

1 Introduction

A wide variety of transition metal complexes, such as Pd, Ru, Rh, and Ir, have been used as catalysts in a variety of catalytic functionalizations of C–H bonds, such as arylation, alkenylation, alkylation, carbonylation, dehydrogenation, amination, oxidation, silylation, and borylation [1–9]. Among the transition metal complexes used thus far in the functionalization of C–H bonds, the most powerful and extensively studied involve Pd complexes. Pd complexes are known to show a high catalytic activity in a wide variety of functionalization reactions of C–H bonds. Because of this, many groups are now using Pd catalysts in the development of such functionalization reactions. Mechanistic studies of the Pd-catalyzed functionalization of C–H bonds, including stoichiometric reactions, have also been conducted. However, the recent focus on developing synthetic methodology for various functionalization reactions using less costly and more abundant first row metals, such as Fe, Co, Ni, and Cu, is a challenging task. Ni catalysts are of particular interest in this area [10, 11].

In 1963, an early example of the stoichiometric cyclometalation of C–H bonds was reported by Kleiman and Dubeck (Scheme 1) [12]. Thus, the reaction of azobenzene with $NiCp_2$ resulted in the formation of a cyclometalated complex. Although the mechanism responsible was not discussed, the cleavage appeared to proceed through σ-bond metathesis. A chelation-assisted cylometalation using Pd complexes was also reported by Cope and coworkers in 1965 [13]. Since then, cyclopalladation has been extensively studied [14, 15], in which the cleavage of C–H bonds proceeds through an S_EAr-type or concerted metalation–deprotonation (CMD) mechanism. A wide variety of new reactions have arisen from the cyclopalladated intermediates. In contrast, examples of stoichiometric amounts of Ni complexes involving the activation of C–H bonds are still very rare. In 2014, Zargarian finally reported on a stoichiometric reaction of bis(phosphinite) derivatives with $NiBr_2$, in which the cleavage of C–H bonds was proposed to proceed through a S_EAr-type mechanism based on the observation that electron-donating substituents facilitate the reaction (Scheme 2) [16].

A pioneering example of the Ni-catalyzed functionalization of C–H bonds was reported by Cavell, who reported on the Ni(0)-catalyzed alkylation of C–H bonds in imidazolium salts with alkenes leading to the production of linear alkylation products [17]. The addition of 2 equiv. of PPh_3 is essential for the effective catalytic reaction. The oxidative addition of C–H bonds to $Ni(PPh_3)_n$, which is generated in situ, was proposed to initiate the catalytic cycle (Scheme 3).

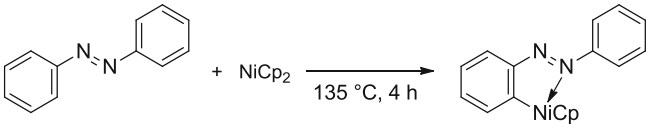

Scheme 1 Cyclometalation using $NiCp_2$ complex

Scheme 2 Cyclometalation using $NiBr_2$

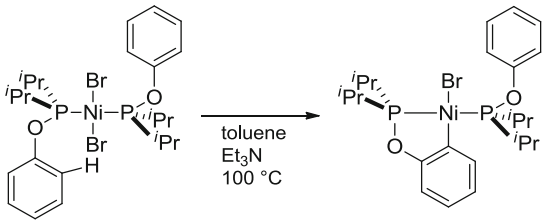

Scheme 3 Imidazolium C–H/alkene coupling reaction

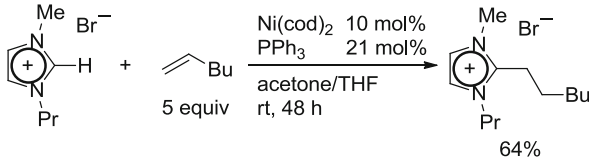

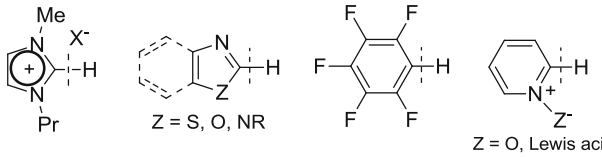

Fig. 1 Representative substrates applicable to the Ni-catalyzed functionalization of C–H bonds

Following this pioneering report, a number of the Ni-catalyzed functionalization of C–H bonds have been reported. However, the functionalization of C–H bonds catalyzed by Ni complexes is limited to C–H bonds in specific aromatic systems, such as pyridine or activated pyridine derivatives and highly perfluorinated benzene and azole derivatives, in which an acidic C–H bond is present (Fig. 1) [18]. On the other hand, examples of the nickel-catalyzed activation of non-acidic C–H bonds in benzene rings are rare. Recently, Chatani reported on the use of a powerful combination of a Ni catalyst and an *N*,*N*′-bidentate directing group in the chelation-assisted functionalization of C–H bonds, which is a promising chelation system for developing new types of Ni-catalyzed functionalization of C–H bonds. Since then, various transformations of C–H bonds catalyzed by Ni complexes have been reported [19, 20]. This review focuses on the Ni-catalyzed functionalization of C–H bonds by taking advantage of *N*,*N*′-bidentate directing groups. A pioneering example of an *N*,*N*′-bidentate directing group was reported by Daugulis [21].

2 C(sp^2)-H Activation

2.1 Oxidative Cycloaddition of C(sp^2)–H Bonds with Alkynes

In 2011, Chatani and coworkers reported on the Ni(0)-catalyzed oxidative cycloaddition of aromatic amides **1** to internal alkynes for the synthesis of isoquinolone derivatives **2** (Scheme 4) [22]. A similar transformation was previously reported

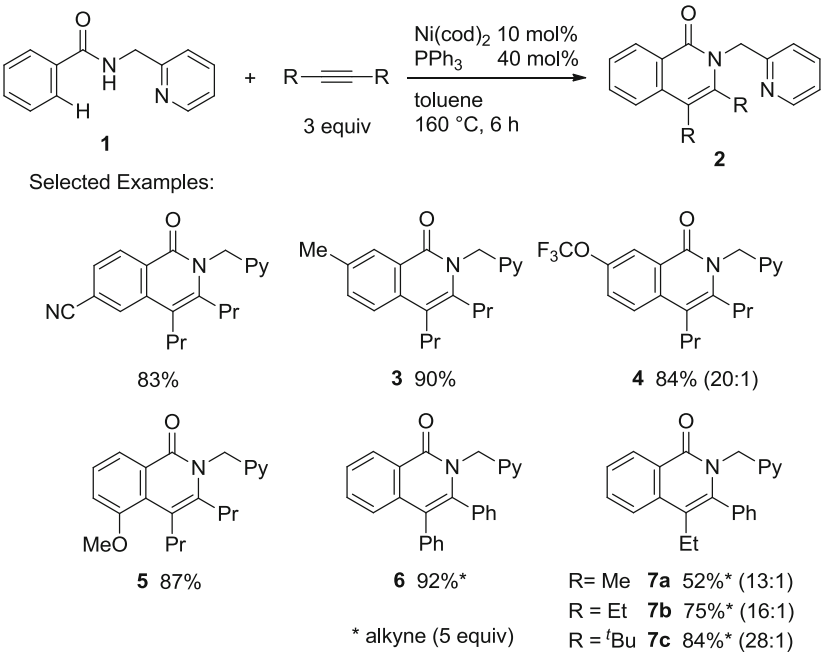

Scheme 4 Ni-catalyzed oxidative cycloaddition reaction with alkynes

using Rh(III) as the catalyst [23, 24]. However, the reaction does not require the addition of a metal oxidant or an intramolecular sacrificed oxidizing substituent in the substrate, in contrast to the Rh(III) system. Instead, an alkyne functioned as the hydrogen acceptor. Later, Pd(II) [25] and Ru(II) were also found to catalyze oxidative cycloaddition of aromatic amides to internal alkynes leading to isoquinolones [26] (for the Ru(II)-catalyzed isoquinolone synthesis utilizing an 8-aminoquinoline directing group, see [27]). However, the use of an inexpensive and abundant metal, such as Ni as the catalyst, is significant. A key to the success of this reaction was the utilization of a 2-pyridinylmethylamine moiety as the directing group. Among the directing groups examined, a 2-pyridinylmethylamine was found to be a superior directing group.

Various functional groups, such as methoxy, amino, trifluoromethoxy, acetyl, cyano, and acetal groups, are tolerated in the reaction. The reaction of a *meta*-methyl- and trifluoromethoxy-substituted aromatic amide gave **3** and **4**, respectively, in which the less-hindered C–H bond was selectively cleaved. In sharp contrast, in the case of a *meta*-methoxy-substituted substrate, the hindered C–H bonds were cleaved to afford **5**. The difference in regioselectivity between **4** and **5** is worthy of attention. These results suggest that steric effects are a major factor in this type of reaction, but the electronic nature of the substituents also can have a significant effect on the regioselectivity of the reaction if they contain a lone pair of electrons. Diphenylacetylene also participates in the oxidative cycloaddition, as in **6**. Unsymmetrical alkynes and phenyl alkyl alkynes regioselectively gave the

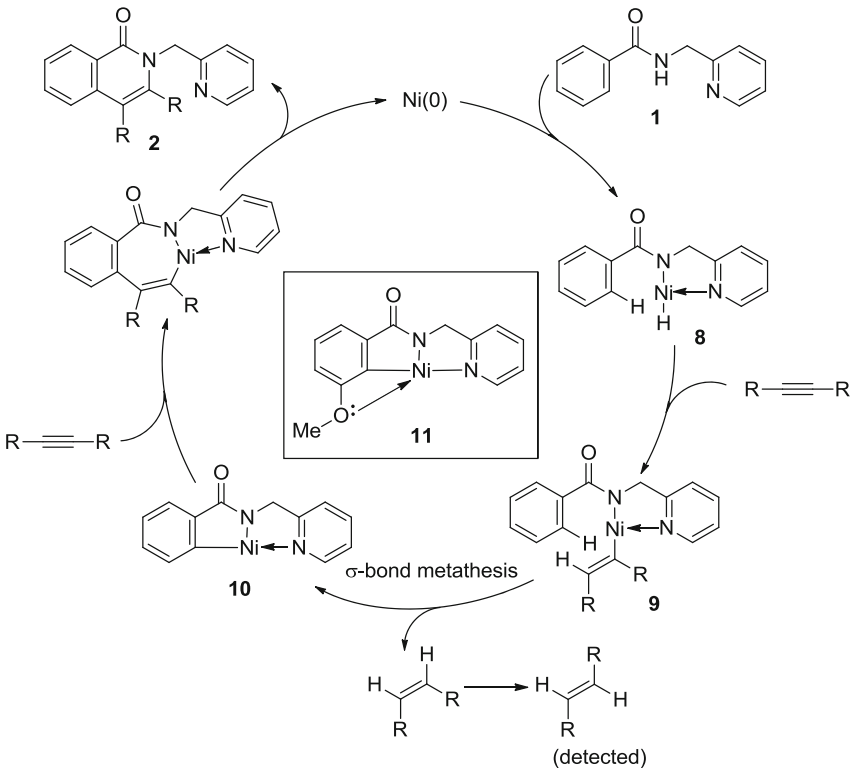

Scheme 5 A proposed reaction mechanism for the Ni-catalyzed oxidative cycloaddition with alkynes

corresponding isoquinolones **7**, in which the phenyl group is attached to the carbon adjacent to a nitrogen atom. The regioselectivity increased with increasing size of the alkyl group.

A proposed mechanism for the oxidative cycloaddition with alkynes is shown in Scheme 5. The reaction starts from the coordination of the pyridine nitrogen in the amide **1** to the nickel(0) center followed by the oxidative addition of a N–H bond to give the nickel hydride complex **8**. The insertion of the alkyne into the Ni–H bond of **8** affords the vinyl nickel complex **9**. Cleavage of the *ortho*-C–H bond with the concomitant formation of an alkene (experimentally detected) gives the *ortho*-metalated complex **10**. The cleavage of C–H bonds is proposed to proceed through σ-bond metathesis. Insertion of the alkyne into the C–Ni bond in complex **10**, followed by a reductive elimination, results in the formation of an isoquinolone **2**, with regeneration of the active nickel(0) species. The proposed intermediate, which switches the regioselectivity of *meta*-methoxy substrate, is depicted as the complex **11**. According to the proposed mechanism, in which the alkyne functions as a hydrogen acceptor, 2 equiv. of alkynes is required and 1 equiv. of alkenes would be formed. In fact, stilbene was formed in 81% yield, which is comparable to that for **6** (92%) in the reaction of **1** with diphenylacetylene.

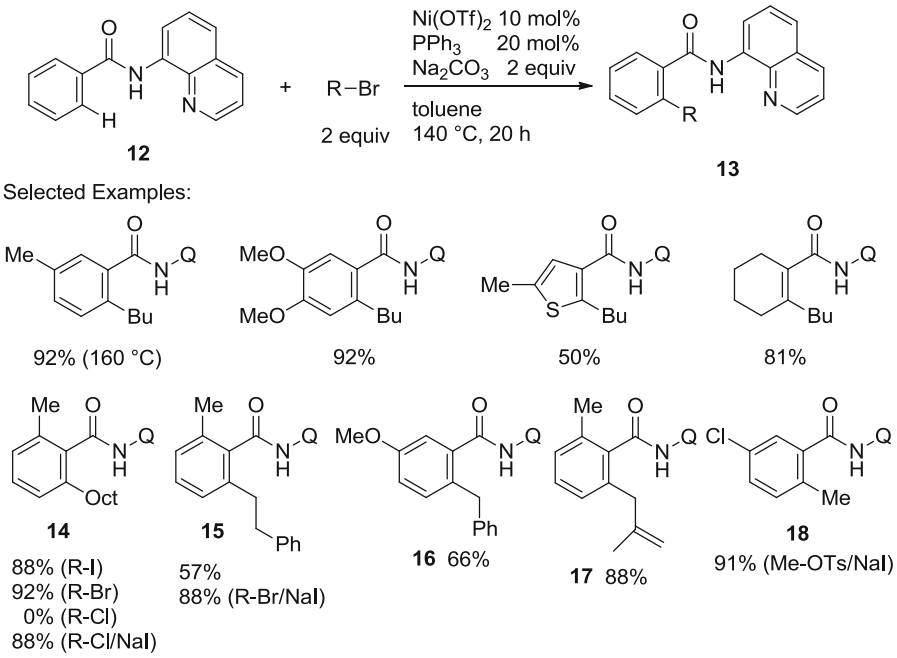

Scheme 6 Ni-catalyzed alkylation of C–H bonds with primary alkyl halides

2.2 *Alkylation of C(sp^2)–H Bonds*

The direct arylation of C–H bonds with aryl halides or pseudo halides has been extensively studied to construct biaryls as one of the alternative cross-coupling reactions because biaryls find widespread applications as building blocks for organic materials, fine chemicals, and pharmaceuticals. In sharp contrast, examples of the direct alkylation of C–H bonds with alkyl halides are limited because the oxidative addition of alkyl halides to transition metal complexes is an unfavorable process and the resulting alkylmetal complexes tend to undergo β-hydride elimination (for a review on C–H alkylation, see [28]). In 2013, Chatani reported on the Ni(II)-catalyzed alkylation of C–H bonds in aromatic amides **12** with alkyl halides (Scheme 6) [29, 30]. Among various directing groups tested, only an 8-aminoquinoline directing group gave the alkylation products **13**. The addition of PPh_3 was essential for the success of the reaction. In the absence of PPh_3, no product was formed. The addition of NaI was also found to promote the reaction. An alkyl chloride showed no reactivity, but the reaction with an alkyl chloride in the presence of 2 equiv. of NaI dramatically increased the product yield, as in **14**. The addition of NaI was also effective in the case of reactions with relatively less-reactive alkyl bromides, as in **15**. Not only alkyl halides but also benzyl bromide and allyl bromide were also applicable to the reaction, as in **16** and **17**. Because examples of the methylation of C(sp^2)–H bonds with methyl halides

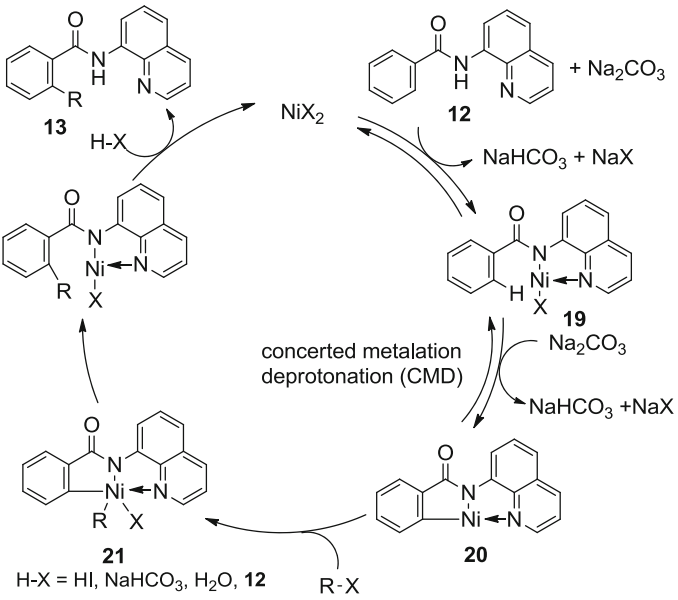

Scheme 7 A proposed reaction mechanism for the Ni-catalyzed alkylation of C–H bonds

(or pseudohalide) are very rare, the methylation of C–H bonds continues to be a significant challenge. The use of a combination of methyl tosylate/NaI afforded the methylation product **18** in 91% yield.

To gain insights into the reaction mechanism, various mechanistic experiments, including deuterium-labeling experiments, competition experiments, radical clock experiments, and radical trap experiments, have been carried out. These mechanistic studies indicated that (1) the cleavage of C–H bonds is reversible, (2) a free radical is not involved, and (3) Ni(II) is a key catalytic species. A proposed mechanism for the Ni-catalyzed alkylation of C–H bonds is shown in Scheme 7 [29, 30]. The coordination of amide **12** to the Ni(II) center gives the nickel complex **19** with the concomitant generation of HX. This step is accelerated by the base. The complex **19** undergoes cyclometalation to give the *ortho*-metalated complex **20**. The cleavage of C–H bonds appears to proceed via a CMD (concerted metalation deprotonation) mechanism [31]. This step is a reversible and rapid step and is not the rate-determining step. The oxidative addition of R–X gives the Ni(IV) species **21**, which undergoes reductive elimination followed by protonation to afford the alkylation product **13** with the regeneration of Ni(II) species.

The reaction with secondary halides under the reaction conditions suitable for the reaction with primary alkyl bromides gave no alkylation products (Scheme 6). However, Ackermann recently successfully found the optimal reaction conditions for the Ni(II)-catalyzed alkylation of C–H bonds with secondary alkyl halides using essentially the same chelation system (Scheme 8) [32]. The reaction gave the mono-alkylation products **22** with excellent selectivity. More significantly, less-reactive

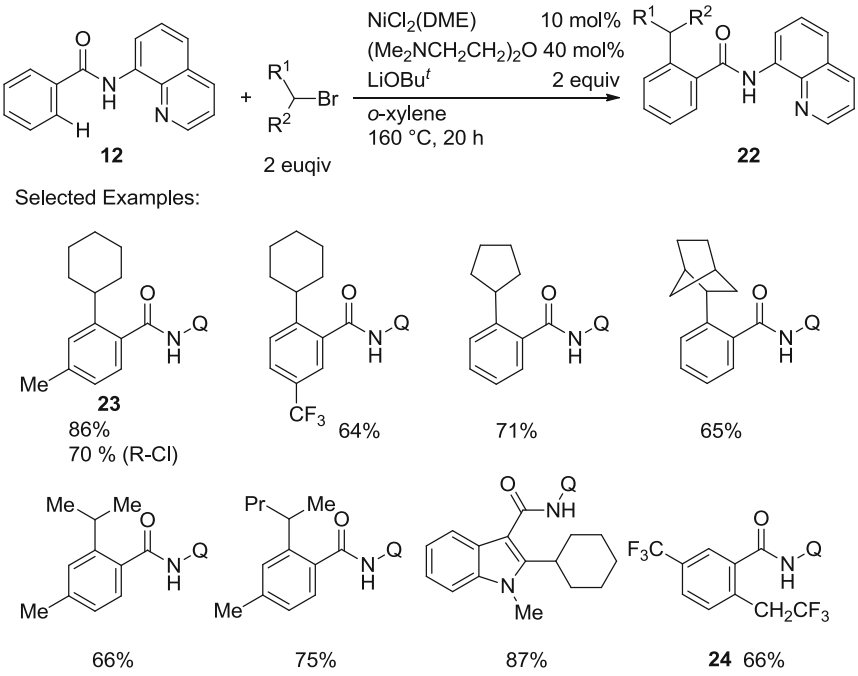

Scheme 8 Ni-catalyzed alkylation of C–H bonds with secondary alkyl halides and trifluoroethyl halide

secondary alkyl chlorides were also applicable to the reaction, as in **23**. Various secondary alkyl bromides including cyclic and acyclic halides participate in the reaction without any evidence of isomerization or rearrangement. Similar to the results reported by Chatani and coworkers [29, 30], H/D exchange took place only at the *ortho*-position, providing a strong support for the occurrence of a reversible C–H bond cleavage. In addition, competition experiments showed that electron-withdrawing groups on the aromatic ring facilitate the reaction. The trifluoroethylation of C–H bonds was also achieved, as in **24**.

It was found that a variety of groups, such as alkyl, benzyl, allyl, and methyl groups, can be installed at the *ortho*-position in the Ni-catalyzed reaction of C–H bonds with alkyl halides or pseudohalides (Schemes 6 and 8) [29, 30, 32]. Zeng recently reported on the Ni(0)-catalyzed *ortho*-allylation of C–H bonds in aromatic amides using an 8-aminoquinoline as the directing group with allyl phosphates (Scheme 9) [33]. In this reaction, Ni(II) complexes also showed catalytic activity, but $Ni(cod)_2/PCy_3$ was the most active catalyst. This C–H allylation proceeds with complete α- and *E*-selectivity. The addition of 2,4-di-*tert*-butyl-4-methylphenol (BHT), a radical scavenger, had no obvious effect on the conversion, suggesting that a free radical is not involved in the reaction pathway.

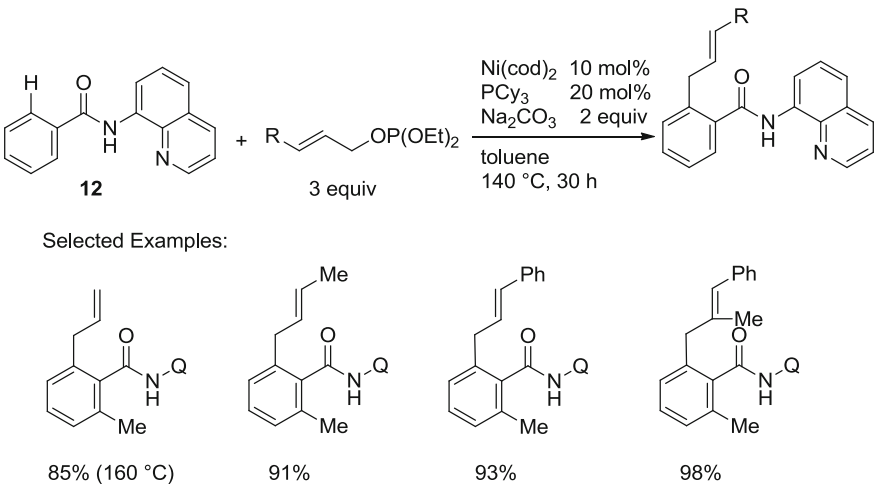

Scheme 9 Ni-catalyzed allylation of C–H bonds with ally phosphates

2.3 Arylation of C(sp^2)–H Bonds

Chatani recently developed the Ni(II)-catalyzed arylation of aromatic amides containing an 8-aminoquinoline as the directing group with aryl iodides as coupling partners (Scheme 10) [34]. In this system only the 8-aminoquinoline moiety gave the desired *ortho*-phenylation product. Unlike the alkylation of C–H bonds shown in Scheme 6 [29, 30], the addition of a phosphine ligand was not required for the reaction to proceed. The reaction showed a high efficiency with broad functional group tolerance. The scope of the reaction is broad with regard to both aromatic amide and coupling partner. The reaction with 1,4-diiodebenzene gave **26**, in which one of the iodides remained intact. Some heteroaromatic iodides, such as 7-iodo-1H-indole and 2-iodothiophene, also participate in the arylation of C–H bonds as coupling partners to give **27** and **28**, respectively.

To gain insights into the reaction mechanism, several mechanistic experiments, including deuterium-labeling experiments, competition experiments, radical trapping experiments, and Hammett studies, have been conducted. The results of deuterium-labeling experiments indicated that the cleavage of C–H bonds is reversible and it does not appear to be the rate-determining step. The competition experiments and Hammett studies indicated that the presence of an electron-withdrawing group in the aromatic amides and an electron-donating group in the aryl iodides accelerates the reaction, suggesting that the reductive elimination step appears to be the rate-determining step. The reaction was not completely inhibited in the presence of the radical scavenger, 2,2,6,6-tetramethylpiperidine 1-oxyl (TEMPO). A proposed mechanism, based on the above observations, for the Ni-catalyzed alkylation of C–H bonds is shown in Scheme 11. The mechanism is essentially the same as that proposed for the alkylation of C–H bonds shown in

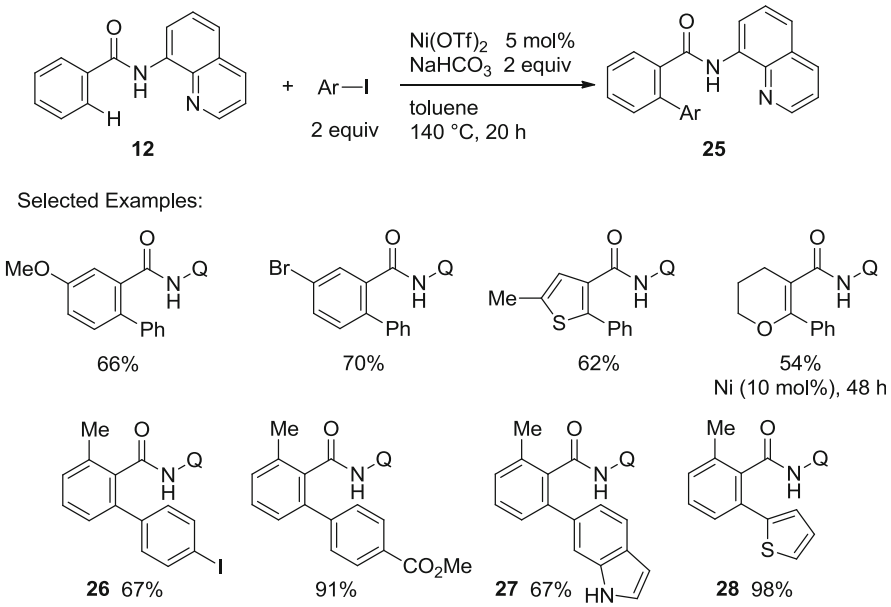

Scheme 10 Ni-catalyzed arylation of C–H bonds with aryl iodides

Scheme 7. The oxidative addition of Ar–I to the cyclometalated Ni(II) complex **20** leads to the formation of the Ni(IV) species **29**, which undergoes a reductive elimination followed by protonation to give the final arylation product **25** with the regeneration of the active Ni(II) species. Based on competition experiments and Hammett studies, the reductive elimination, which appears to be the rate-determining step, would proceed through the transition state **30** in which a developing negative charge is stabilized by electron-withdrawing groups **R** on the aromatic amides and a developing positive charge is stabilized by electron-donating groups **Z** on the aryl iodides.

2.4 Alkynylation of C(sp^2)–H Bonds

Shi recently reported on the Ni(II)-catalyzed alkynylation of aromatic amides containing a (pyridine-2-yl)isopropylamine (PIP) as the directing group with ethynyl bromides as coupling partners (Scheme 12) [35]. When *meta*-substituted aromatic amides were employed, the alkynylation occurred at the sterically more accessible position. A wide variety of functional group were tolerated. The scope of the reaction with respect to ethynyl bromides was wide. Not only a triisopropylsilyl (TIPS) group but also a trimethylsilyl (TMS), alkyl, and aryl-substituted alkynes were applicable to the reaction. The reaction proceeded with a high catalyst turnover number (TON) of up to 196.

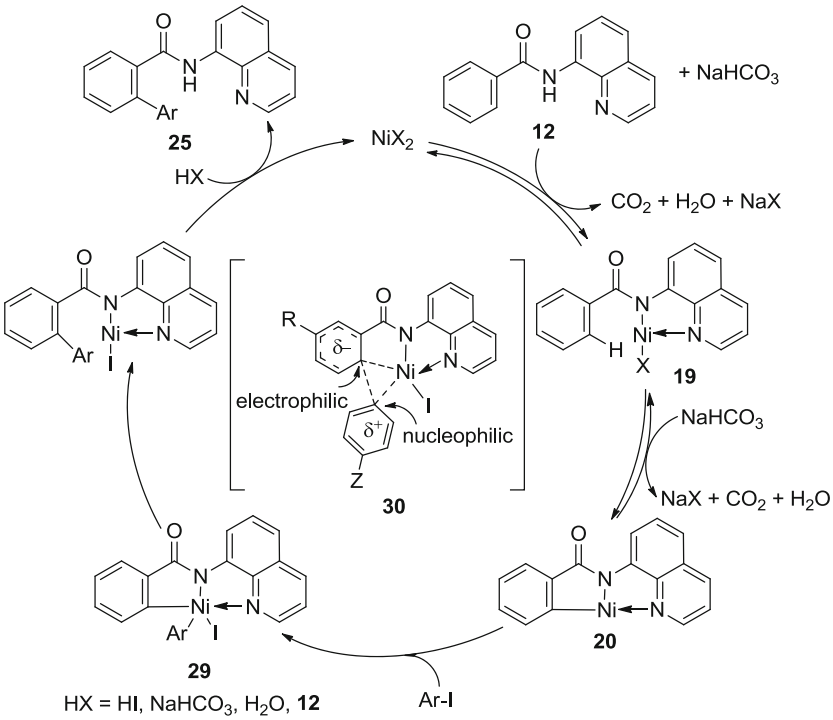

Scheme 11 A proposed reaction mechanism for the Ni-catalyzed arylation of C–H bonds

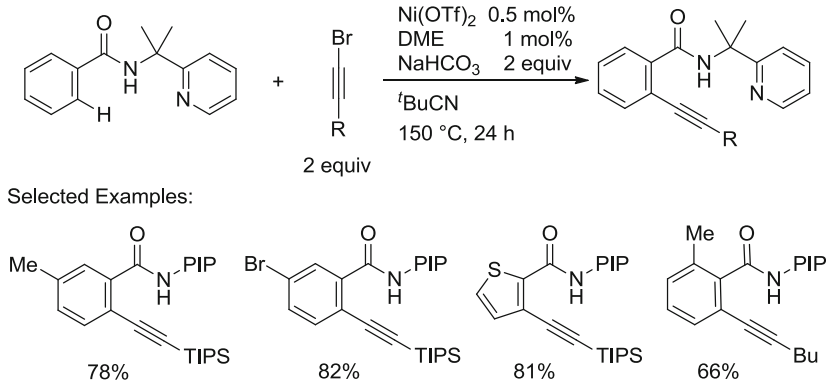

Scheme 12 Ni-catalyzed alkynylation of C–H bonds with ethynyl bromides

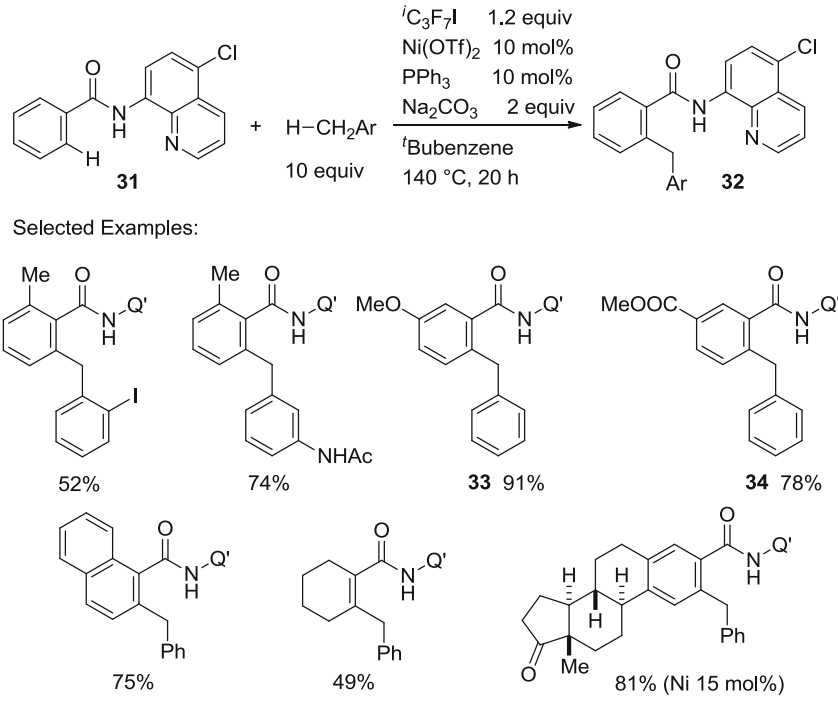

Scheme 13 Ni(II)-catalyzed benzylation of C–H bonds via cross-dehydrogenative coupling of C–H bonds

2.5 *Cross-Dehydrogenative Coupling of C(sp^2)–H Bonds with Toluene C–H Bonds*

Among catalytic functionalizations of C–H bonds developed so far, cross-dehydrogenative coupling of C–H bonds is one of the most ideal C–H functionalizations because the new C–C bond is formed by the direct connection of two different C–H bonds, thus avoiding the generation of stoichiometric amounts of halogenated or organometallic byproducts [36–38]. However, most of the examples reported so far involve the coupling of C(sp^2)–H/C(sp^2)–H bonds. Chatani reported on the Ni(II)-catalyzed benzylation of *ortho*-C–H bonds in aromatic amides with toluene derivatives using an 8-amino-5-choloroquinoline as the directing group (Scheme 13) [39]. The reaction is tolerant to a wide variety of functional groups. When *meta*-substituted aromatic amides were used, benzylation products were selectively obtained through the cleavage of the less-hindered C–H bonds, as in **33** and **34**.

A proposed mechanism is depicted in Scheme 14. The most important issue to be understood is the nature of the actual benzylation species and how it is generated. The generation of a benzyl radical species is proposed as the key species, which is generated by the SET (single-electron transfer) from the base, Na_2CO_3 to $^{i}C_3F_7I$ to

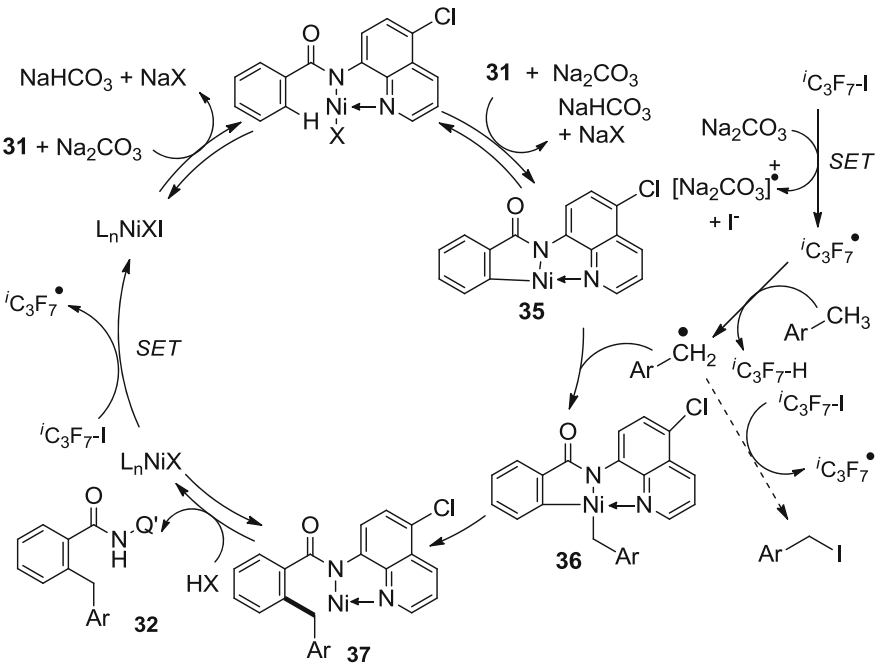

Scheme 14 A proposed reaction mechanism for the Ni-catalyzed cross-dehydrogenative coupling of C–H bonds with toluene C–H bonds

generate a $^{i}C_3F_7$ radical. The radical abstracts a hydrogen from toluene to give a benzyl radical, which reacts with the cyclometalated complex **35** to generate a Ni (III) complex **36**. Reductive elimination from **36** releases the benzylation product **32** and a Ni(I) complex. The Ni(I) complex abstracts an iodine atom from $^{i}C_3F_7I$ to generate Ni(II) complex and a $^{i}C_3F_7$ radical. In fact, the addition of TEMPO completely quenched the reaction, suggesting that a free radical species is involved in the reaction. The generation of benzyl iodide as the electrophilic counter partner also cannot be excluded.

2.6 Carbonylation of C(sp^2)–H Bonds

The use of *N*,*N*′-bidentate directing group in the carbonylation of C–H bonds has been achieved by the use of carbon monoxide (CO) as the carbonyl source in conjunction with $Ru_3(CO)_{12}$ [40] or $Co(acac)_2$ as the catalysts [41]. Ge recently reported on the Ni(II)/Cu(II)-catalyzed carbonylation of benzamides containing an 8-aminoquinoline as the directing group with DMF as the carbonyl source (Scheme 15) [42]. The presence of both a Ni and a Cu catalyst was required for the reaction to proceed. The product yield was improved by the addition of a

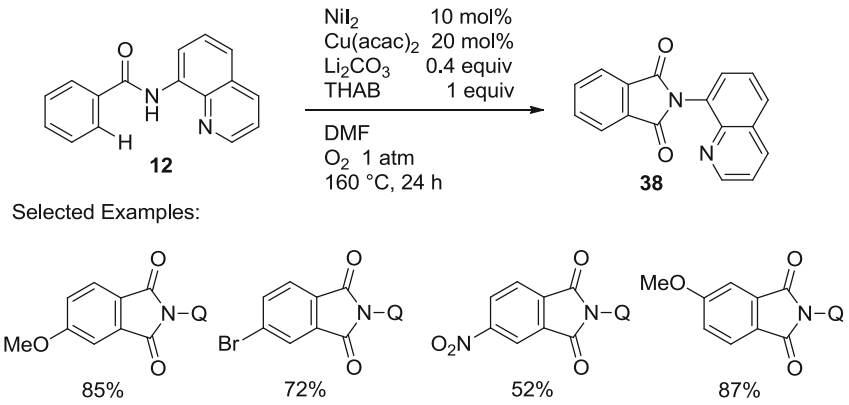

Scheme 15 Ni(II)-catalyzed carbonylation of C–H bonds

quaternary ammonium salt, tetraheptylammonium bromide (THAB). The reaction shows a high functional group compatibility. When ^{13}C-labeled DMF, the carbonyl group being labeled, was used as the solvent, only a trace amount of ^{13}C was incorporated into the product **38**, indicating that the carbonyl group in DMF is not the source of CO. The results from some control experiments with various nitrogen-containing solvents resulted in the suggestion that the source of the incorporated CO in **38** is mainly the methyl group in DMF.

A deuterium-labeling experiment was carried out to probe the reaction mechanism. The results indicated that the H/D exchange at the *ortho*-position is reversible. A proposed mechanism is shown in Scheme 16. An iminium species **39**, which is proposed as the CO source, is generated in situ from DMF via a multistep process under Cu(II) catalyst with O_2. The reaction of cyclometalated complex **20** with **39** resulted in the formation of **40**, which is oxidized by Cu(II) under O_2 to give **41**. An intramolecular nucleophilic addition gives the intermediate **42**, which is followed by oxidation and hydrolysis to afford the phthalimide **38**.

2.7 C–S Bond Formation

Around the same time, the Lu, Shi, and Zhang groups independently reported on the Ni(II)-catalyzed thiolation of C–H bonds with disulfides, in which two different *N*, *N*′-directing groups were used as the directing group (Scheme 17). Lu (Scheme 17a) [43] and Shi (Scheme 17b) [44] used a PIP directing group and Zhang used an 8-aminoquinoline as the directing group (Scheme 17c) [45]. In all cases, the reactions showed a high degree of functional group tolerance. The scope of the reaction regarding aromatic amides and diaryl disulfides was broad. Curiously, Lu found that the addition of TEMPO inhibited the reaction, but in Shi and Zhang's systems, the addition of TEMPO had no effect on the efficiency of the reaction.

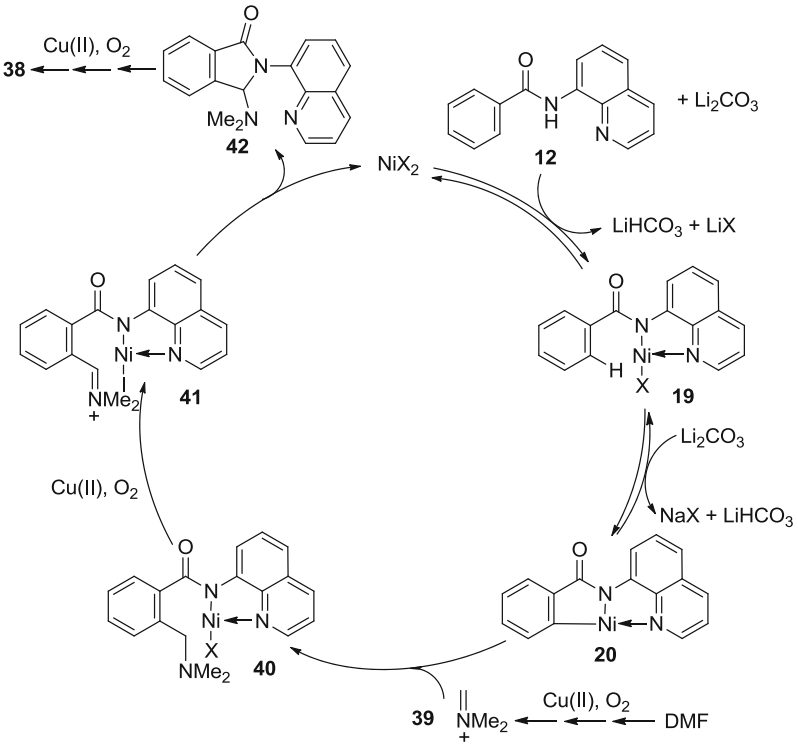

Scheme 16 A proposed reaction mechanism for the Ni-catalyzed carbonylation reaction

Based on their contradictory results, a different mechanism was proposed. Lu proposed a Ni(II)/Ni(III) catalytic cycle, in which the cyclometalated complex **20** reacts with a phenylsulfide radical to generate a Ni(III) intermediate, which is similar to the pathway from **35** to **37** in Scheme 14. However, Shi and Zhang proposed a Ni(II)/Ni(IV) cycle, in which diaryl disulfides undergo oxidative addition to the cyclometalated complex **20** to afford a Ni(IV) intermediate.

Chatani recently reported that the reaction of aromatic amides that contain a 5-chloro-8-aminoquinoine moiety as the directing group with arylsulfonyl chlorides in the presence of $Ni(OTf)_2$ as the catalyst results in sulfonylation at the *ortho*-position (Scheme 18) [46]. A blocking substituent, chloride, is required to avoid the sulfonylation at the quinoline ring at the 5-position. Various arylsulfonyl chlorides can be used as the coupling partner, as in **43**–**45**.

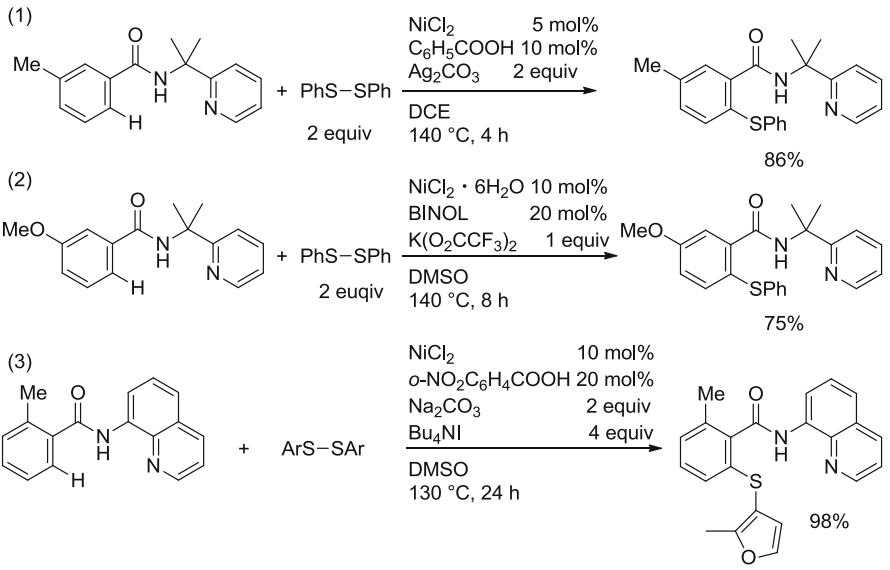

Scheme 17 Ni-catalyzed thiolation of C–H bonds with disulfides

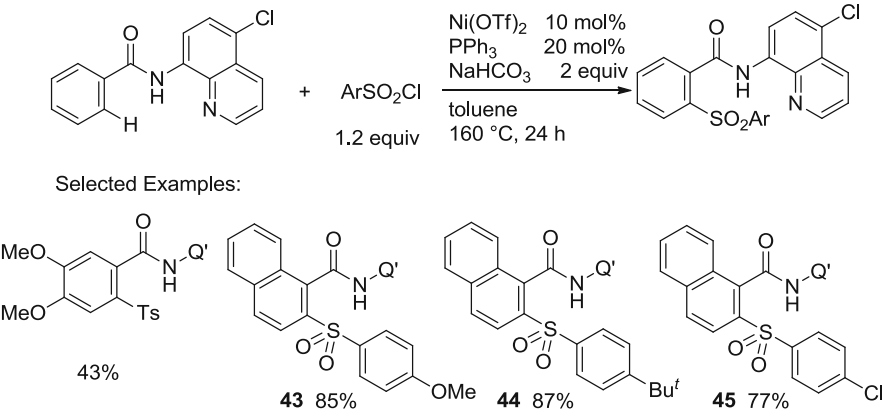

Scheme 18 Ni-catalyzed sulfonylation of C–H bonds

3 C(sp^3)–H Activation

3.1 Arylation of C(sp^3)–H Bonds

A wide variety of catalytic functionalizations of C(sp^2)–H have already been developed to date and have had a significant impact not only in the field of organic chemistry but also in related fields of chemistry. The methods have been applied to the synthesis of synthetically useful compounds, such as materials, fine chemicals,

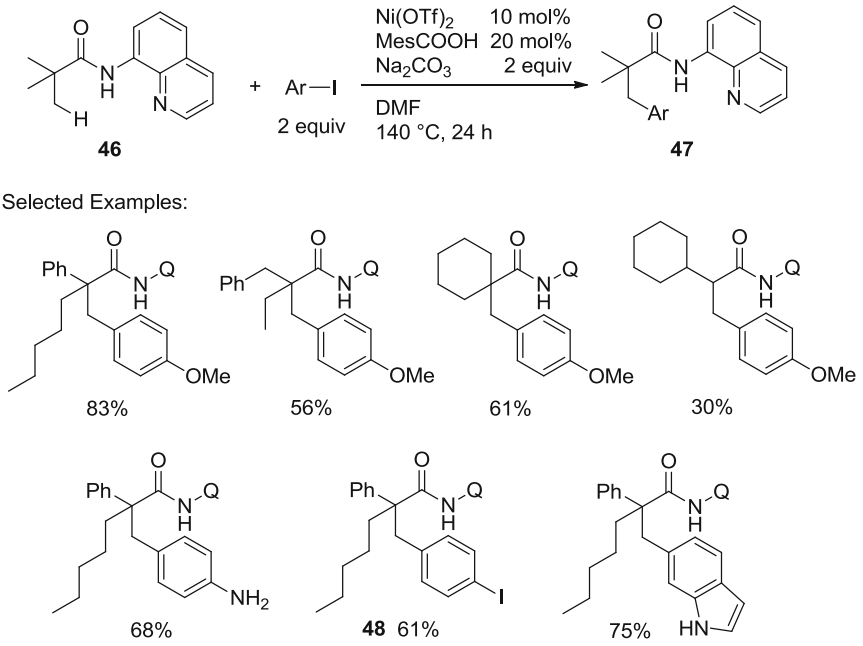

Scheme 19 Ni-catalyzed arylation of C–H bonds with aryl iodides

and pharmaceuticals. Much attention has been currently focused on the functionalization of C(sp^3)–H bonds, which continues to be a challenging issue. In 2014, Chatani reported the first example of the Ni(II)-catalyzed β-arylation of C(sp^3)–H bonds in aliphatic amides with aryl iodides (Scheme 19) [47]. Among the directing groups evaluated, only an 8-aminoquinoline was successful directing group. The addition of a sterically bulky carboxylic acid, such as 2,4,6-trimethylbenzoic acid (MesCOOH) as an additive, improved the efficiency of the reaction. The reaction was also significantly affected by the base used. Na_2CO_3 was found to be the best base for this reaction. Among the solvents examined, DMF was the solvent of choice. Curiously, not only Ni(II) complexes, such as $Ni(OTf)_2$, $NiCl_2$, and $Ni(OAc)_2$, but also a Ni(0) complex $Ni(cod)_2$ showed a high catalytic activity. The reaction took place only at the β-position. The reaction shows a high efficiency with a broad functional group tolerance. Even an iodide survived under the reaction conditions, as in **48**.

The reaction mechanism appears to be similar to those proposed for the alkylation and arylation of C(sp^2)–H bonds (Schemes 7 and 11). Mechanistic studies indicated that (1) the C–H bond cleavage is reversible and is not a difficult process, even in the case of strong C(sp^3)–H bonds; (2) the oxidation of a Ni(0) species to a Ni(II) species occurs, which is the actual catalytic species, by the Ar–I with the generation of the respective Ar–H; and (3) a single-electron transfer (SET) was not involved, based on radical trapping experiments with TEMPO. A proposed mechanism for the reaction is shown in Scheme 20. Coordination of the amide **46** to the

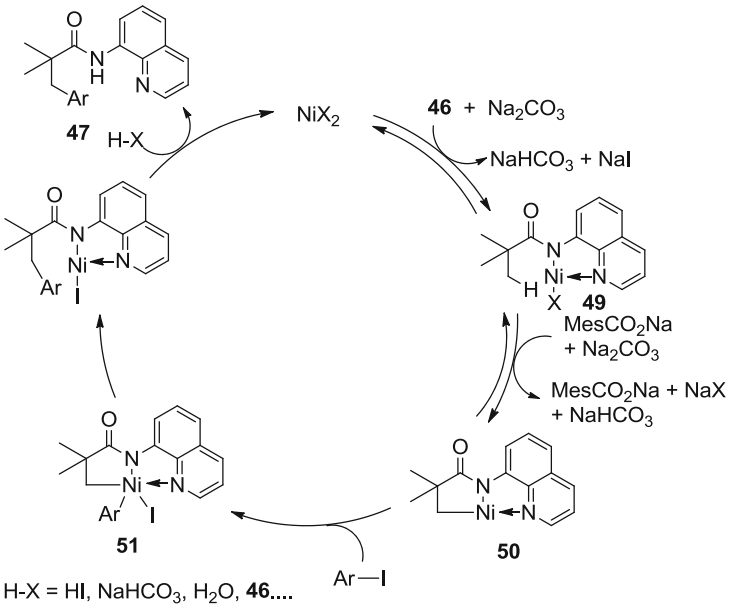

Scheme 20 A proposed reaction mechanism for the Ni-catalyzed arylation of C–H bonds

Ni(II) center followed by ligand exchange with the concomitant generation of HX gives the Ni complex **49**. The C–H bond in complex **49** undergoes cleavage at the β-position to give **50** via a CMD mechanism. The oxidative addition of an aryl iodide gives the high-valent Ni(IV) complex **51**, which undergoes reductive elimination followed by protonation to complete the catalytic cycle with the formation of the desired arylation product **47** with the regeneration of Ni(II). The cleavage of C–H bonds is reversible. The role of the carboxylic acid appears to be to accelerate the cleavage of C–H bonds and the reductive elimination step.

You also reported on the use of a similar system for the Ni(II)-catalyzed arylation of C(sp^3)–H bonds in aliphatic amides using an 8-aminoquinoline as a bidentate auxiliary directing group (Scheme 21) [48]. The addition of PPh_3 and DMSO improved the product yield. It is noteworthy that aryl bromides can be used as the coupling partner in this system, but the yield of the corresponding arylation products was slightly lower than those in the reaction with aryl iodides. The reaction was compatible with various functional groups, such as ketones, esters, amides, aldehydes, and cyano groups.

Since Sanford reported the first example of the Pd-catalyzed arylation of C–H bonds with diaryliodonium salts as coupling partners [49], the utilization of diaryliodonium salts in the functionalization of C–H bonds has been of great interest. However, all examples involved the use of Pd, Pt, and Cu as the catalyst. Chatani reported that diaryliodonium salts can also be used as coupling partners for the arylation of C(sp^3)–H bonds in place of aryl iodides using Ni(II) as the catalyst (Scheme 22) [50]. Arylated products were obtained in good yields even in the

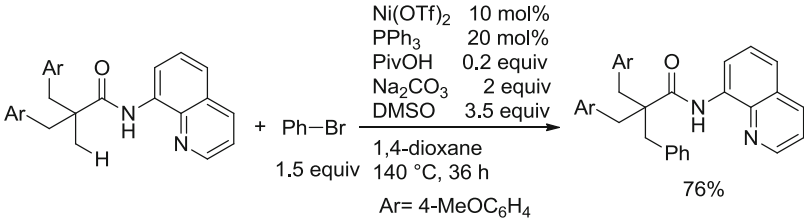

Scheme 21 Ni-catalyzed arylation of C–H bonds with aryl halides

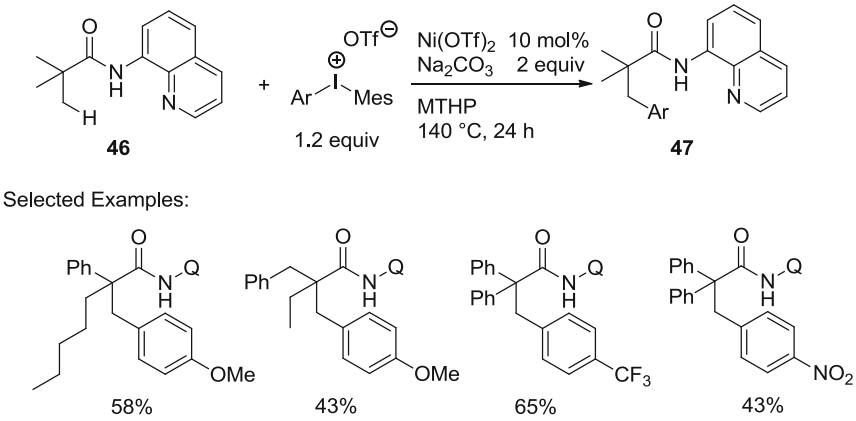

Scheme 22 Ni-catalyzed arylation of C–H bonds with diaryliodonium salts

absence of a carboxylic acid. The effect of the counter anion of the diaryliodonium salt was examined. Among the anions screened, a triflate was found to be a superior counterion. The use of tetrafluoroborates (BF_4^-) and hexafluorophosphates (PF_6^-) as counterions resulted in no reaction. Among the solvents examined, 4-methyltetrahydro-2H-pyrane (MTHP) was determined to be the solvent of choice. A competition experiment using electronically different diaryliodonium salts indicated that an electron-donating group facilitates the reaction, which is a similar tendency to that observed in the reaction with aryl iodides [47]. The addition of TEMPO had no effect on the reaction.

Alkenylation was also achieved using a Ni(II) catalyst and an 8-aminoquinoline directing group (Scheme 23) [51]. BINOL (1,1′-bi-2-naphthol) provided the best results among the various additives examined. The yield was improved when a combination of Li_2CO_3 and potassium trifluoroacetate (KTFA) along with BINOL was used. Various functional groups were tolerated under the reaction conditions. Even a bromo group remained intact, as in **52**. As a synthetic application of this alkenylation, a highly functionalized carboxamide **53** was prepared via a sequence involving a Ni(II)-catalyzed arylation step, Ni(II)-alkenylation, hydrogenation under Pd/C, and Ni(II)-catalyzed alkenylation.

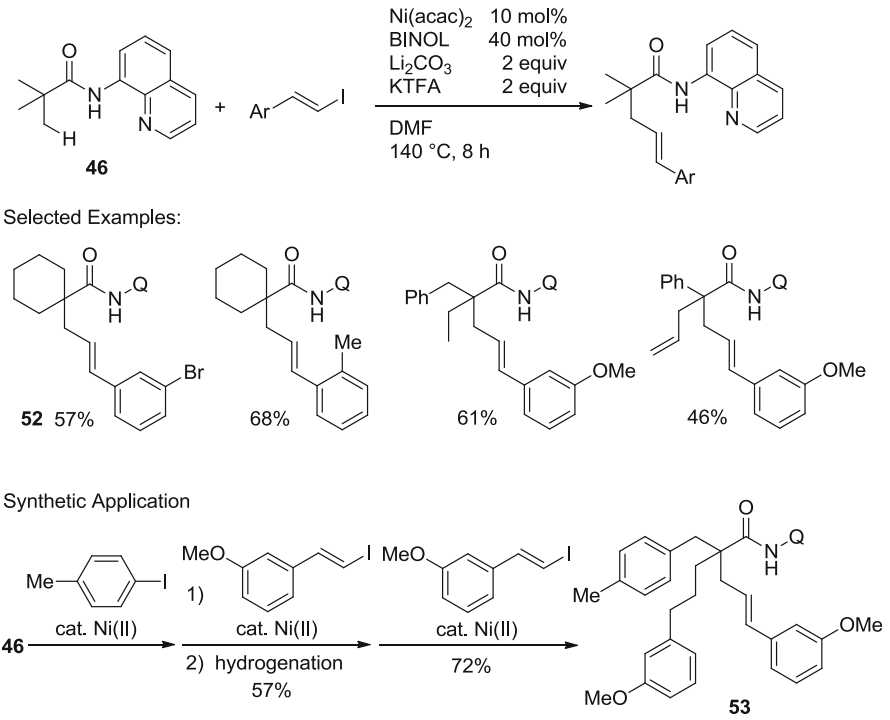

Scheme 23 Ni-catalyzed alkenylation of C–H bonds with aryl iodides

3.2 *Alkylation of C(sp^3)–H Bonds*

Ge reported on the Ni(II)-catalyzed alkylation of C(sp^3)–H bonds with alkyl halides by taking advantage of an 8-aminoquinoline directing group (Scheme 24) [52]. In sharp contrast to the arylation of C(sp^3)–H bonds [47], $Ni(cod)_2$ was not active as a catalyst. It was found that various phosphine ligands improved the product yield. Among the phosphine ligands screened, 1,2-bis(diphenylphosphino)benzene (dppbz) gave the best result. The reaction tolerated various functional groups, such as terminal alkenes (**55**), esters (**56**), cyano groups (**57**), and trifluoromethyl groups (**58**). It was found that alkyl iodides could be replaced with alkyl bromides with the addition of CsI, as in **55**–**57**.

In contrast to the mechanism proposed by Chatani (Schemes 7, 11, and 20), which involves a Ni(II)/Ni(IV) catalytic cycle, a Ni(II)/Ni(III) cycle was proposed. When TEMPO was added, the yield of the product **54** was decreased: 0 equiv. 86%, 3 equiv. 46%, and 8 equiv. trace. In addition, the corresponding pentyl TEMP ether was isolated. On the basis of these observations, a Ni(II)/Ni(III) catalytic cycle was proposed. The cyclometalated complex **50** reacts with an alkyl radical, which is generated through SET from a Ni(I) species to an alkyl halide with the concomitant generation of a Ni(II) species. In this catalytic system, H/D exchange did not take

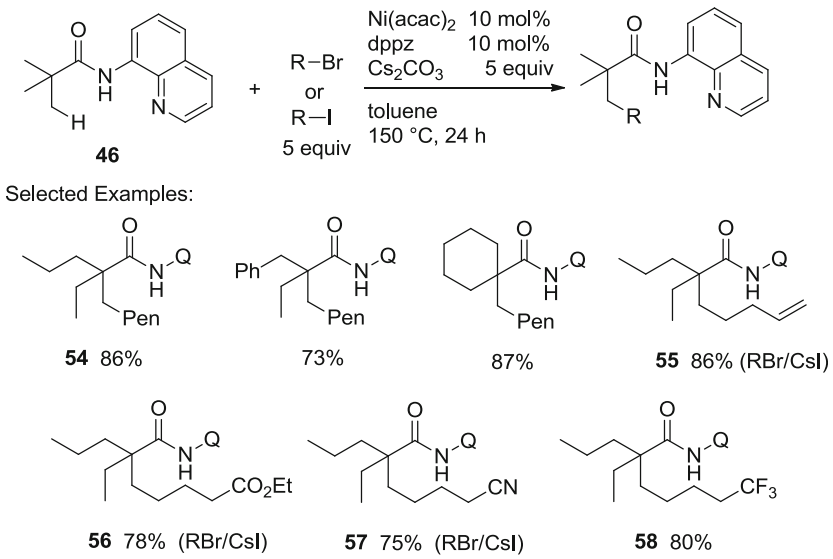

Scheme 24 Ni-catalyzed alkylation of C–H bonds with primary alkyl halides

place, suggesting that the cleavage of C–H bonds is irreversible, which is contrary to finding reported by Chatani [47].

3.3 Carbonylation of C(sp^3)–H Bonds

Ge reported on the Ni(II)/Cu(II)-catalyzed carbonylation of C(sp^2)–H bonds in aromatic amides containing an 8-aminoquinoline as the directing group with DMF as the carbonyl source (Scheme 15) [42]. This catalytic system was applicable to the carbonylation of C(sp^3)–H bonds (Scheme 25) [42]. A quaternary α-carbon to the carbonyl group in the substrates is required for the carbonylation to proceed. Contrary to the carbonylation of C(sp^2)–H bonds, in which the cleavage of C–H bonds is reversible, the cleavage of C–H bonds was irreversible in the carbonylation of C(sp^3)–H bonds, suggesting that the rate-determining step is the cyclometalation.

3.4 C–S Bond Formation

Zhang reported on the Ni(II)-catalyzed thiolation of C(sp^3)–H bonds in aliphatic amides containing an 8-aminoquinoline directing group with diaryl disulfides (Scheme 26) [53]. All examples involved the use of aliphatic amides having no hydrogen at the α-position. Diphenyl diselenide was also applicable to the reaction,

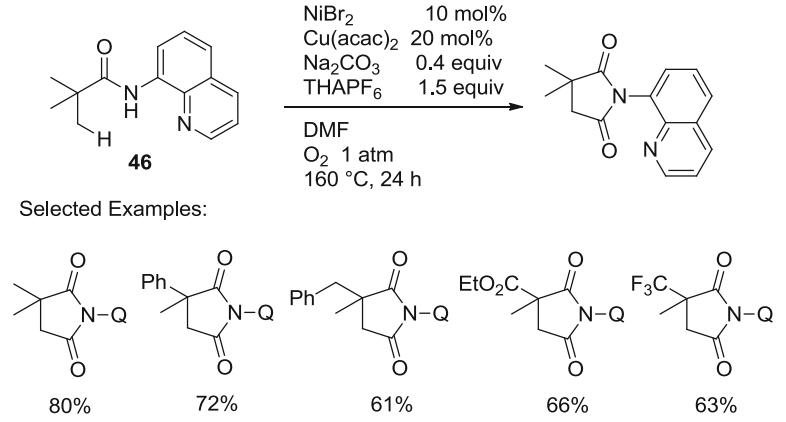

Scheme 25 Ni(II)-catalyzed carbonylation of C(sp^3)–H bonds

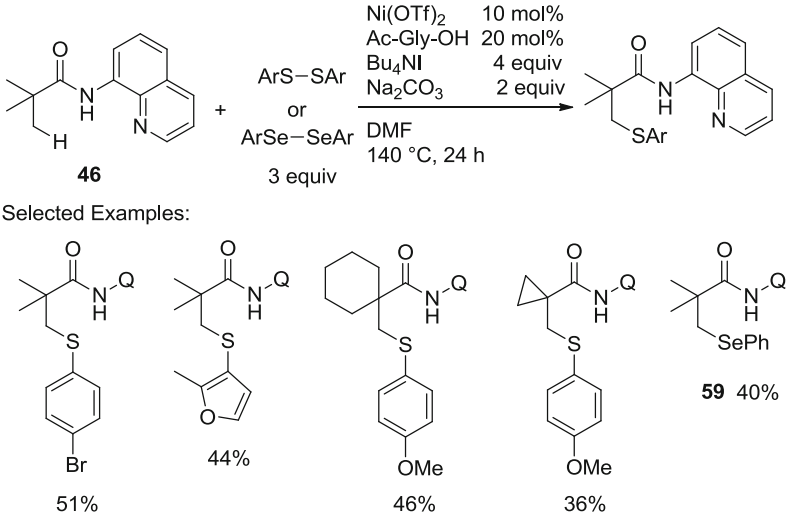

Scheme 26 Ni-catalyzed thiolation of C–H bonds with diaryl sulfides

as in **59**. The addition of TEMPO or BHF had a negligible effect on the reaction, suggesting that the reaction does not proceed through a free radical mechanism. The results of deuterium-labeling experiments indicated that H/D exchange took place only at the β-position indicating that the cleavage of C–H bonds is reversible.

Around the same time, Shi also developed the Ni(II)-catalyzed thiolation of C (sp^3)–H bonds in aliphatic amides with diaryl disulfides (Scheme 27) [54]. Mechanistic experiments using 1,4-dinitrobenzene, TEMPO, and 1,4-diphenylethylene indicated that a thioaryl radical is not involved in the reaction. Zhang and Shi proposed a Ni(II)/Ni(IV) catalytic cycle for the Ni(II)-catalyzed thiolation.

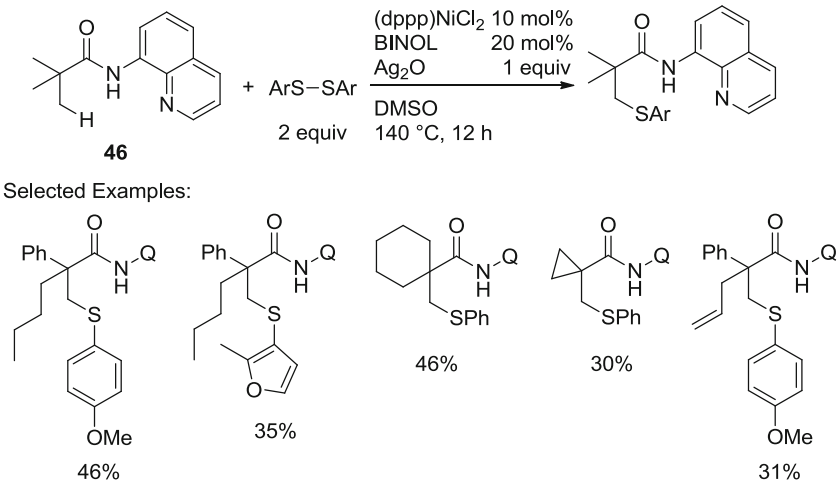

Scheme 27 Ni-catalyzed thiolation of C–H bonds with diaryl sulfides

3.5 C–N Bond Formation

Ge reported on the TEMPO-assisted Ni(II)-catalyzed intramolecular cyclization of C–H bonds in aliphatic amides leading to the formation of β-lactam derivatives with the assistance of an 8-aminoquinoline directing group (Scheme 28) [55]. Amidation took place at the methyl C–H bond preferentially over phenyl C–H bonds, as in **61**. If the substrate did not contain a methyl group at the β-position, the reaction took place at the benzylic C–H bonds, as in **62** and **63**. A 5-methoxy-8-aminoquinoline can be used as the directing group, as in **64**, and the directing group can be easily removed under oxidation conditions using cerium (IV) ammonium nitrate (CAN).

A Ni(II)/Ni(III) catalytic cycle is proposed (Scheme 29). Catalysis is initiated by the coordination of **46** to Ni(II) followed by a ligand exchange and the cleavage of C–H bonds gives the cyclometalated Ni(II) complex **50**, which is oxidized to the Ni (III) species **65** by TEMPO. Reductive elimination gives the desired product **60** with the generation of a Ni(I) species that is oxidized to Ni(II) species by TEMPO.

4 Elaboration of Directing Groups

Three different directing groups, such as 2-pyridinylmethylamine, 8-aminoquinoline or derivatives thereof, and (pyridine-2-yl)isopropylamine moieties, have been used as the directing group in Ni-catalyzed chelation-assisted C–H functionalization reactions. These directing groups are easily converted to other synthetically useful functional groups. Deprotection of an 8-aminoquinline moiety to carboxylic acids was easily achieved by hydrolysis under acidic conditions

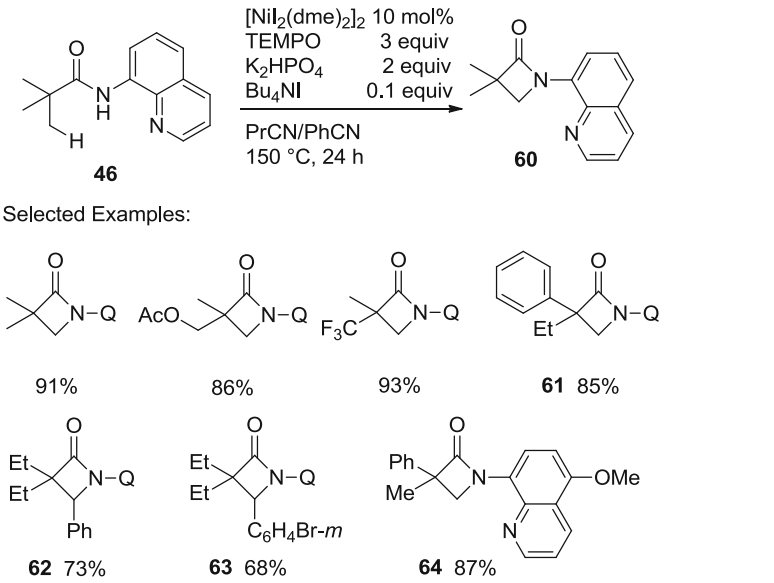

Scheme 28 Ni-catalyzed intramolecular amidation of C–H bonds

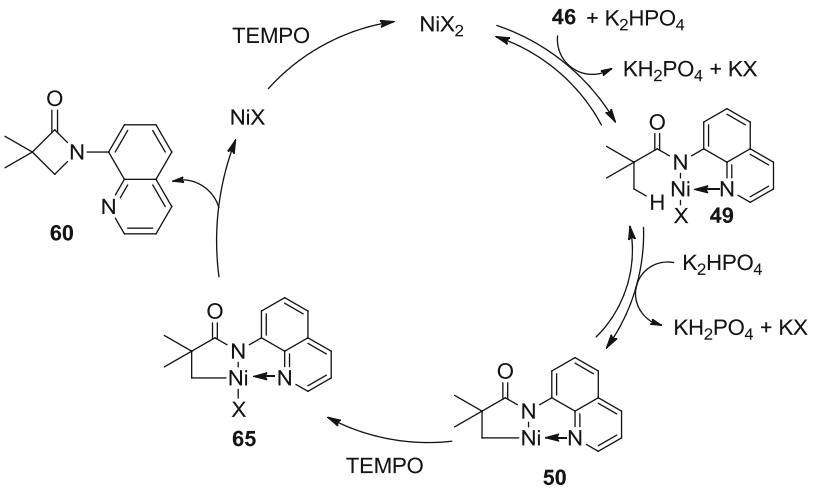

Scheme 29 A proposed reaction mechanism for the Ni-catalyzed amidation of C–H bonds

(Scheme 30a) [56] or basic conditions [57] (Scheme 30b). The 8-aminoquinoline moiety was removed by treatment with HCl in refluxing methanol [58] or BF_3•Et_2O in methanol at 100°C to give the corresponding ester [59]. The 8-aminoquinoline moiety was converted into the corresponding aldehydes via a reaction with Schwartz's reagent ($ZrHClCp_2$) [60] (Scheme 30c). The 2-pyridinyl-isopropylamine moiety can also be easily removed by a mild sequence consisting

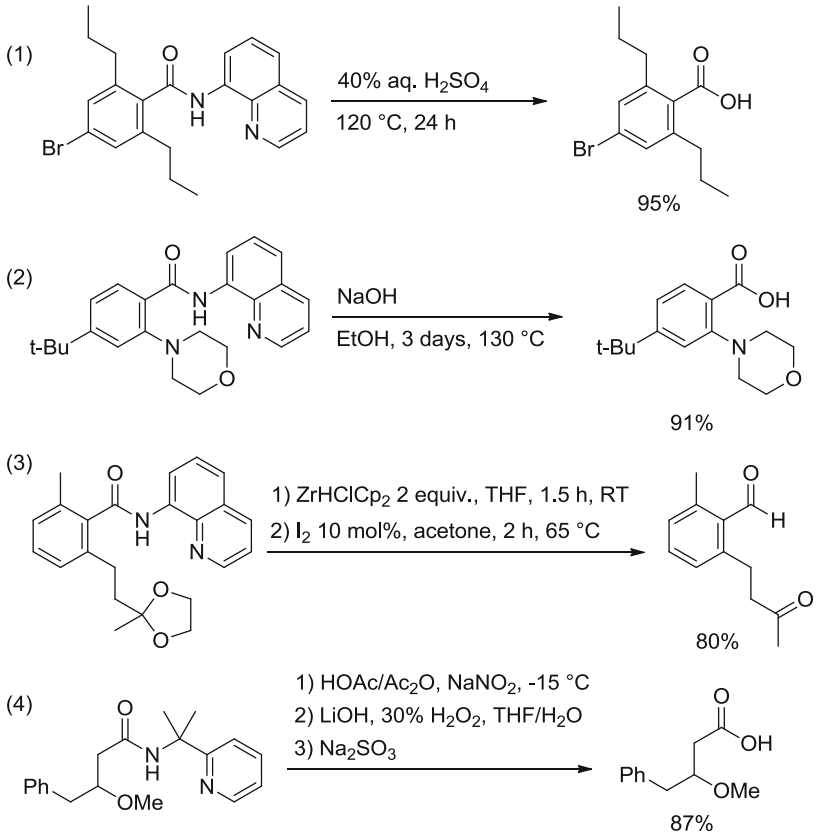

Scheme 30 Elaboration of directing groups

of *N*-nitrosylation, treatment with LiOOH, and reduction with Na_2SO_3 [61] (Scheme 30d).

5 Conclusions

A new chelation system using an *N*,*N*′-bidentate directing group has enabled the development of various types of Ni-catalyzed functionalizations of C–H bonds. In the case of previously reported systems, substrates that were applicable to the Ni-catalyzed functionalization of C–H bonds were limited to specific structures, such as pyridine or activated pyridine derivatives and highly perfluorinated benzene and azole derivatives, all of which contain an acidic C–H bond (Fig. 1) [17]. However, the combination of a Ni catalyst and an *N*,*N*′-bidentate directing group was found to be an excellent combination for the development of various Ni-catalyzed chelation-assisted functionalizations of C–H bonds, since the report by Chatani and

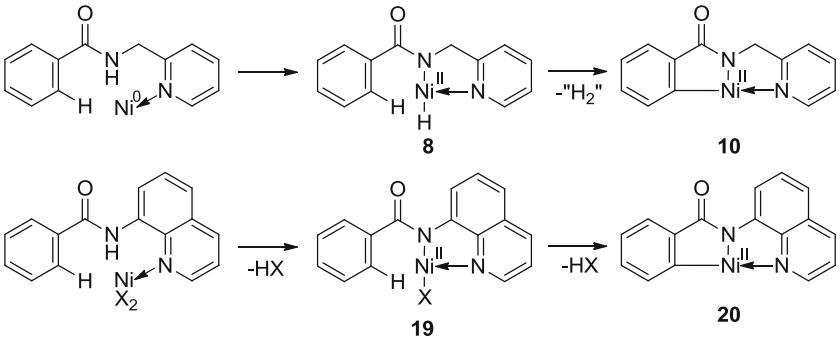

Scheme 31 Difference between Ni(0)/2-pyridineylmethylamine and Ni(II)/8-aminoquinoline systems

coworkers in 2011, on the use of an *N*,*N*′-bidentate directing group in the first example of the Ni-catalyzed chelation-assisted functionalization of C–H bonds [20].

The cleavage of C–H bonds in these Ni-catalyzed chelation systems appears to involve two different mechanisms depending on the system in use (Scheme 31). Substrates applicable to the *N*,*N*′-bidentate chelation system involve amides, which contain both an sp^2 nitrogen and the NH bonds. In both cases, the coordination of the sp^2 nitrogen to the Ni center initiates the catalysis. In the case of the Ni(0)/2-pyridineylmethylamine system, the cleavage of C–H bonds proceeds via σ-bond metathesis. In contrast, a CMD mechanism is operative in the case of Ni(II)/8-aminoquinoline. In any case, the catalytic Ni species forms a chemical bond to an sp^3 nitrogen by the coordination of sp^2 nitrogen followed by the reaction with a NH bond, as in **8** and **19**. This N–Ni bond formation is a key for the activation of *ortho*-C–H bonds.

One of the most important issues to be addressed in this area involves the mechanism responsible for the reaction. In sharp contrast to the Pd-catalyzed functionalization of C–H bonds, mechanistic studies dealing with the Ni-catalyzed functionalization of C–H bonds are limited. The oxidation state of the Ni intermediates is unclear. Catalytic Ni(II)/Ni(IV) or Ni(II)/Ni(III) cycles have been proposed, although no direct experimental evidences exist [62, 63]. The role of the guinoline ring is also unclear. In addition to serving as a directing group [64], it is likely that it plays other roles in the overall reaction. One possibility is that the 8-aminoquinoline moiety functions as an electron reservoir to stabilize the high-valent and unstable Ni(III) or Ni(IV) complex (for a review on redox non-innocent ligands, see [65]).

Reactions using a Ni catalyst and an *N*,*N*′-bidentate directing group have started to appear in the literature only in the last few years. As more mechanistic information emerges, new and more exciting advances can be anticipated.

References

1. Kakiuchi F, Chatani N (2003) Adv Synth Catal 345:1077–1101
2. Colby DA, Bergman RG, Ellman JA (2010) Chem Rev 110:624–655
3. Xu L-M, Li B-J, Yang Z, Shi Z-J (2010) Chem Soc Rev 39:712–733
4. Yamaguchi J, Yamaguchi AD, Itami K (2012) Angew Chem Int Ed 51:8960–9009
5. Li B, Dixneuf PH (2013) Chem Soc Rev 42:5744–5767
6. Wencel-Delord J, Glorius F (2013) Nat Chem 5:369–375
7. Gao K, Yoshikai N (2014) Acc Chem Res 47:1208–1219
8. Sarkar SD, Liu W, Kozhushkov SI, Ackermann L (2014) Adv Synth Catal 356:1461–1479
9. Miura M, Satoh T, Hirano K (2014) Bull Chem Soc Jpn 87:751–764
10. Tasker SZ, Standley EA, Jamison TF (2014) Nature 509:299–309
11. Ananikov VP (2015) ACS Catal 5:1964–1971
12. Kleiman JP, Dubeck M (1963) J Am Chem Soc 85:1544–1545
13. Cope AC, Siekman RW (1965) J Am Chem Soc 87:3272–3273
14. Dupont J, Consorti CC, Spencer J (2005) Chem Rev 105:2527–2572
15. Lyons TW, Sanford MS (2010) Chem Rev 110:1147–1169
16. Vabre B, Deschamps F, Zargarian D (2014) Organometallics 33:6623–6632
17. Clement ND, Cavell KJ (2004) Angew Chem Int Ed 43:3845–3847
18. Yamaguchi J, Moto J, Itami K (2013) Eur J Org Chem 19–30
19. Rouquet R, Chatani N (2013) Angew Chem Int Ed 52:11726–11743
20. Misal Castro LC, Chatani N (2015) Chem Lett 44:410–421
21. Roane J, Tran LD, Daugulis O (2015) Acc Chem Res 48:1053–1064
22. Shiota H, Ano Y, Aihara Y, Fukumoto Y, Chatani N (2011) J Am Chem Soc 133:14952–14955
23. Guimond N, Gouliaras C, Fagnou K (2010) J Am Chem Soc 132:6908–6909
24. Hyster TK, Rovis T (2010) J Am Chem Soc 132:10565–10569
25. Zhong H, Yang D, Wang S, Huang J (2012) Chem Commun 48:3236–3238
26. Ackermann L, Lygin AV, Hofmann N (2011) Angew Chem Int Ed 50:6379–6382
27. Allu S, Swamy KCK (2014) J Org Chem 79:3963–3972
28. Ackermann L (2010) Chem Commun 46:4866–4877
29. Aihara Y, Chatani N (2013) J Am Chem Soc 135:5308–5311
30. Aihara Y, Wülbern J, Chatani N (2015) Bull Chem Soc Jpn 88:438–446
31. Fagnou K (2010) Top Curr Chem 292:35–56
32. Song W, Lackner L, Ackermann L (2014) Angew Chem Int Ed 53:2477–2480
33. Cong X, Li Y, Wei Y, Zeng Z (2014) Org Lett 16:3926–3929
34. Yokota A, Aihara Y, Chatani N (2014) J Org Chem 79:11922–11932
35. Liu Y-J, Liu Y-H, Yan S-Y, Shi B-F (2015) Chem Commun 51:6388–6391
36. Li B-J, Shi Z-J (2012) Chem Soc Rev 41:5588–5598
37. Kuhl N, Hopkinson MN, Wencel-Delord J, Glorius F (2012) Angew Chem Int Ed 51:10236–10254
38. Girard SA, Knauber T, Li C-J (2014) Angew Chem Int Ed 53:74–100
39. Aihara Y, Tobisu M, Fukumoto Y, Chatani N (2014) J Am Chem Soc 136:15509–15512
40. Inoue S, Shiota H, Fukumoto Y, Chatani N (2009) J Am Chem Soc 131:6898–6899
41. Grigorjeva L, Daugulis O (2014) Org Lett 16:4688–4690
42. Wu X, Zhao Y, Ge H (2015) J Am Chem Soc 137:4924–4927
43. Yang K, Wang Y, Chen X, Kadi AK, Fun H-K, Sun H, Zhang Y, Lu H (2015) Chem Commun 51:3582–3585
44. Yan S-Y, Liu Y-J, Liu B, Liu Y-H, Shi B-F (2015) Chem Commun 51:4069–4072
45. Li C, Li D, Wang B, Yao J, Zhang Y (2015) Org Lett 17:1328–1331
46. Yokota A, Chatani N (2015) Chem Lett 44. doi:10.1246/cl.150239
47. Aihara Y, Chatani N (2014) J Am Chem Soc 136:898–901
48. Li M, Dong J, Huang X, Li K, Wu Q, Song F, You J (2014) Chem Commun 50:3944–3946
49. Kalyani D, Deprez NR, Desai L, Sanford MS (2005) J Am Chem Soc 127:7330–7331

50. Iyanaga M, Aihara Y, Chatani N (2014) J Org Chem 79:11933–11939
51. Liu Y-J, Zhang Z-Z, Yan S-Y, Liu Y-H, Shi B-F (2015) Chem Commun 51. doi:10.1039/c5cc02254a
52. Wu X, Zhao Y, Ge H (2014) J Am Chem Soc 136:1789–1792
53. Lin C, Yu W, Yao J, Wang B, Liu Z, Zhang Y (2015) Org Lett 17:1340–1343
54. Yan S-Y, Liu Y-J, Liu B, Liu Y-H, Zhang Z-Z, Shi B-F (2015) Chem Commun 51:7341–7344
55. Wu X, Zhao Y, Ge H (2014) Chem Eur J 20:9530–9533
56. Shabashov D, Daugulis O (2010) J Am Chem Soc 132:3965–3972
57. Tran LD, Roane J, Daugulis O (2013) Angew Chem Int Ed 52:6043–6046
58. Ano Y, Tobisu M, Chatani N (2011) J Am Chem Soc 133:12984–12986
59. Zhang SY, Li Q, He G, Nack WA, Chen G (2015) J Am Chem Soc 137:531–539
60. Rouquet G, Chatani N (2013) Chem Sci 4:2201–2208
61. Chen FJ, Zhao S, Hu F, Chen K, Zhang Q, Zhang SQ, Shi BF (2013) Chem Sci 4:4187–4192
62. Camasso NM, Sanford MS (2015) Science 347:1218–1220
63. Zheng B, Tang F, Luo J, Schultz JW, Rath NP, Mirica LM (2014) J Am Chem Soc 136:6499–6504
64. Tang H, Huang X-R, Yao J, Chen H (2015) J Org Chem 80. doi:10.1021/acs.joc.5b00580
65. Lyaskovskyy V, de Bruin B (2011) ACS Catal 2:270–279

Top Organomet Chem (2016) 56: 47–66
DOI: 10.1007/3418_2015_116

Published online: 10 June 2015

Copper-Mediated Intermolecular C–H/C–H and C–H/N–H Couplings via Aromatic C–H Cleavage

Koji Hirano and Masahiro Miura

Abstract Copper salts and complexes have recently received significant attention as less expensive and abundant alternatives to some noble transition metal catalysts such as palladium, rhodium, and ruthenium, in the research field of C–H activation. They not only replace the above precious metal catalysts in the known C–H transformations but also mediate unique, otherwise challenging, cross-coupling reactions involving C–H bond cleavage. This chapter mainly focuses on recent advances in the copper-mediated or copper-catalyzed intermolecular C–H/C–H and C–H/N–H aromatic couplings. Seminal mechanistic studies on the copper-mediated C–H functionalization are also discussed.

Keywords Aromatic compounds · C–C formation · C–N formation · Copper · Dehydrogenative coupling

Contents

1 Introduction 48
2 C–H/C–H Coupling 48
2.1 Alkynylation 49
2.2 Arylation 51
2.3 Alkylation 53
3 C–H/N–H Coupling 54
4 C–H/X–H Coupling with Other Heteroatom Nucleophiles 57
4.1 S-Nucleophiles 58
4.2 O-Nucleophiles 58
4.3 Miscellaneous Nucleophiles 59
5 Mechanistic Studies 60
6 Conclusion 62
References 63

K. Hirano (✉) and M. Miura (✉)
Department of Applied Chemistry, Faculty of Engineering, Osaka University, Suita, Osaka 565-0871, Japan
e-mail: k_hirano@chem.eng.osaka-u.ac.jp; miura@chem.eng.osaka-u.ac.jp

1 Introduction

Since the pioneering work on the ruthenium-catalyzed directed C–H alkylation by Murai and coworkers [1], the transition metal-mediated C–H functionalization has grown rapidly because of its possibility for transformation of ubiquitous C–H bonds to versatile functional groups in atom- and step-economical manners. While the second- and third-row transition metal catalysts such as palladium, rhodium, and ruthenium have initially been developed, for the realistic catalyst loading, many researchers then turned attention into less expensive and easy-to-handle first-row transition metals. Particularly, less toxic and abundant copper salts are attractive alternatives for the above noble metal catalysts and have great potential for ideal but greatly challenging intermolecular C–H/C–H and C–H/N–H couplings [2–6]. In 2006, two seminal examples for the C–H/N–H coupling were reported concurrently by Yu [7] and Chatani [8]. While not catalytic in copper, 2-phenylpyridine was found to undergo dehydrogenative amination with tosylamide or aniline without employing any precious metal catalysts (Eqs. 1 and 2). Since then, this research field has greatly progressed and is now one of the hottest areas in C–H functionalization. In this chapter, recent advances in the copper-mediated intermolecular dehydrogenative C–C and C–N aromatic couplings are summarized; the intramolecular version is not covered because the excellent review is now available [9]. Additionally, some related couplings with miscellaneous heteroatom nucleophiles and seminal mechanistic studies on the Cu-promoted C–H functionalization are also referred.

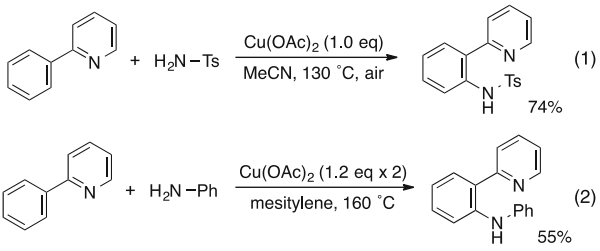

2 C–H/C–H Coupling

The transition metal-promoted C–C cross-coupling reaction ranks as the most important bond-forming strategy in modern organic synthesis. Traditionally, organic halides and organometallic reagents are employed as prefunctionalized starting materials [10–12]. On the other hand, the metal-mediated C–H activation can skip prefunctionalization steps such as halogenation and stoichiometric metalation. In particular, the dehydrogenative C–H/C–H coupling can be an ultimate C–C formation because no preactivation of both starting materials are needed. In this section, copper-mediated C–H/C–H aromatic couplings are divided into

three types of alkynylation, arylation, and alkylation, and their scope and limitations are described.

2.1 Alkynylation

Arylacetylenes are among the most fundamental and important π-conjugated systems in various areas of organic chemistry. A powerful and reliable approach to these molecules is the palladium/copper-catalyzed cross-coupling of aryl halides with terminal alkynes, also known as the Sonogashira coupling [13–16]. However, the stoichiometric halogenation of arenes is inevitable for the preparation of the starting halogenated arenes. Ultimately, the direct coupling between arenes and terminal alkynes via twofold C–H bond cleavage of both substrates is an ideal goal since no preactivation step is required. The first copper-mediated dehydrogenative alkynylation of aromatic compounds was reported by Miura and coworkers in 2010 (Eq. 3) [17]. The aromatic substrate is limited to some acidic 1,3-azoles, but preliminary attempts to apply catalytic conditions are also successful by using molecular oxygen as a terminal oxidant. Subsequently, the same group [18] and Su [19], independently, succeeded in the related direct alkynylation of polyfluoroarenes (Eqs. 4 and 5). A relatively strong base, LiO*t*Bu, is necessary, but the reaction proceeds well under mild conditions without special slow addition techniques.

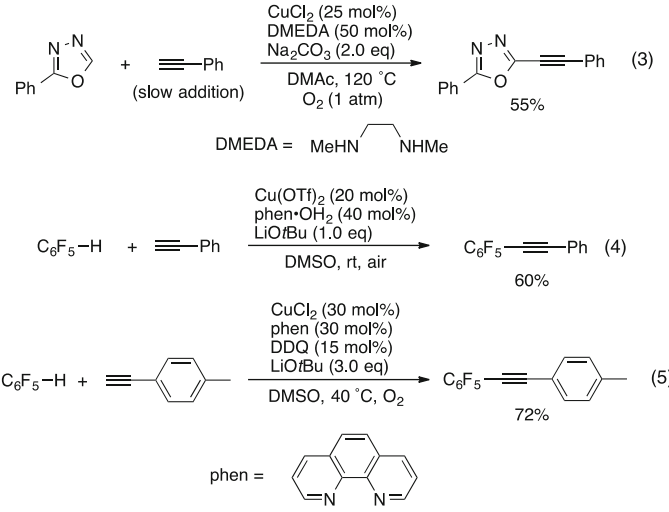

In the above leading work, the aromatic C–H cleavage step is apparently dependent on the acidity of aromatic C–H. The theoretical pK_a values of representative (hetero)aromatic compounds are shown in Table 1 [20].

Table 1 Theoretical pK_a values of some representative (hetero)aromatic compounds in DMSO

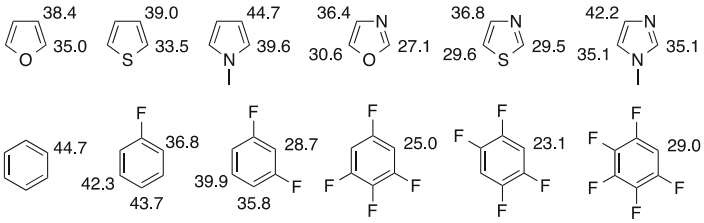

On the other hand, recent development of the bidentate coordination strategy [21, 22] successfully expands the substrate scope into the more general benzene derivatives. The first applicable directing group is the aminoquinoline-based *N*,*N*-bidentate amide, which was originally developed by Daugulis [23]. Although the dehydrogenative alkynylation occurs smoothly, probably because of the relatively high acidic nature of the aminoquinoline NH, the in situ generated alkynylated product spontaneously undergoes the subsequent annulation to provide the methylene isoindolinone skeleton (Eqs. 6 and 7) [24, 25]. More recently, Dai and Yu [26] and Shi [27] successfully suppress the undesired annulation by the oxazolinylaniline- and pyridinylpropylamine-modified coordinating moieties, respectively, and the desired alkynylated products were obtained in good yields (Eqs. 8 and 9). The latter two directing groups are easily removed under base-promoted hydrolysis conditions after the coupling reaction.

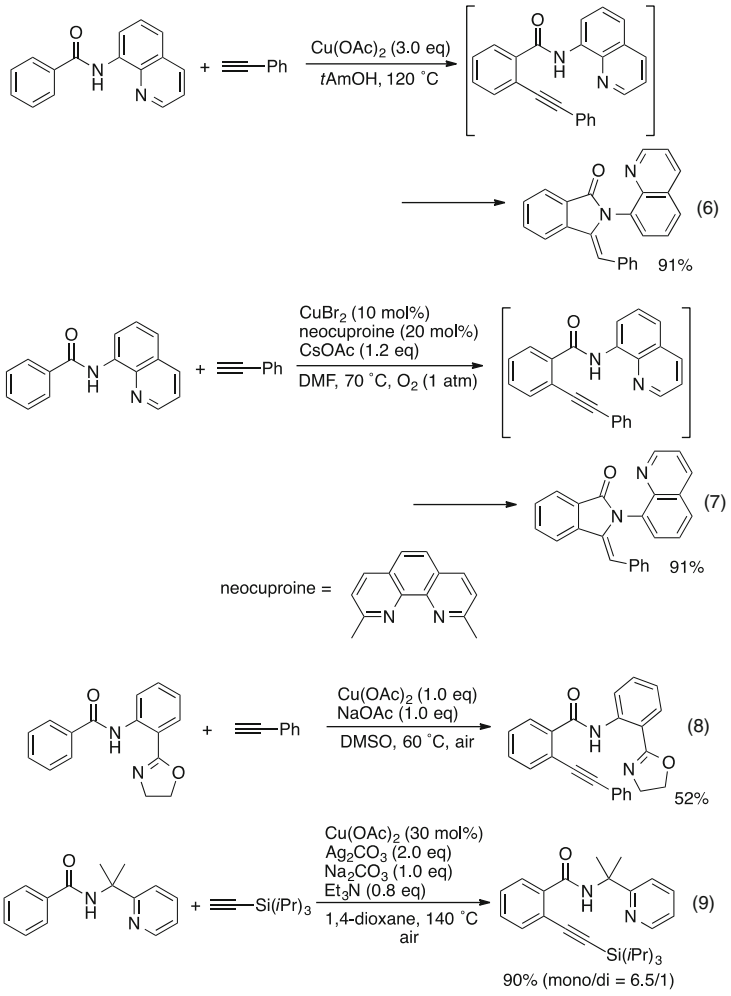

2.2 *Arylation*

Since the biaryl structures are prevalent cores in pharmaceutical targets and functional materials [28, 29], the dehydrogenative biaryl coupling of nonfunctionalized simple arenes has been extensively studied in recent years. Early successful examples with copper salts alone involve the cross-coupling reaction of relatively acidic 1,3-azoles and polyfluoroarenes (Eqs. 10–13) [30–33].

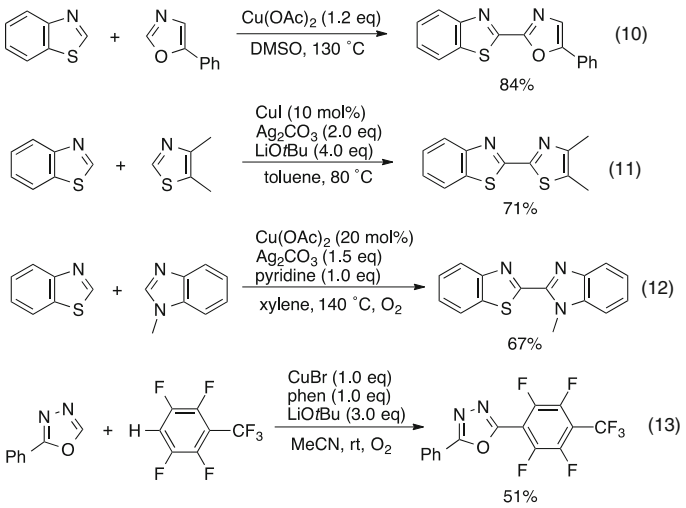

The application to less acidic, general arenes was first reported by the group of Hirano and Miura in 2011. Under $Cu(OAc)_2$/PivOH-promoted conditions, 2-phenylpyridine directly cross-couples with some 1,3-azoles (Eq. 14) [34]. The related dehydrogenative biaryl couplings of indoles, benzamides, and naphthylamines also proceed in the presence of $Cu(OAc)_2$, with the assistance of appropriate directing groups, to make the corresponding bi(hetero)aryl linkages efficiently (Eqs. 15–17) [35–37]. The directors except for the 2-phenylpyridine are readily attachable and detachable: 2-pyrimidyl (Eq. 16) and 8-aminoquinolinyl (Eq. 17) groups were removed smoothly by sodium alkoxide-mediated alcoholysis. Additionally, in some cases, the molecular oxygen renders the reaction catalytic in copper. The copper-based C–H/C–H coupling strategy can also be applicable to the regioselective direct heteroarylation of 2-pyridones at the C6 position (Eq. 18) [38].

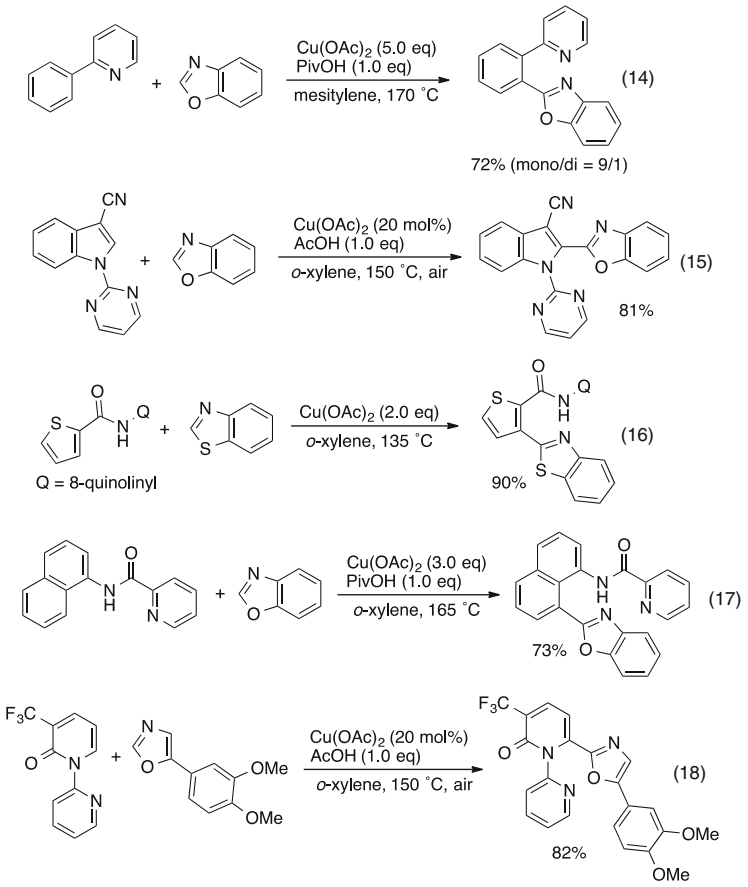

The same research group also developed the formal dehydrogenative construction of benzofuran- and indole–azole conjugations via an annulative metalation of ortho-alkynylphenols and ortho-anilines (Scheme 1) [39, 40]. In the case of the aniline, the substituent on the nitrogen is spontaneously removed after the C–C formation to form the free NH indole exclusively. This protocol requires the alkyne and heteroatom functions in one coupling partner but can provide a unique approach to the biologically important bi(heteroaryl)s from nonhalogenated and nonmetalated starting materials.

2.3 *Alkylation*

The copper-mediated dehydrogenative alkylation of aromatic compounds is less investigated, compared to the alkynylation and arylation in Sects. 2.1 and 2.2. The limited successful example includes the quinoline-containing benzamide and

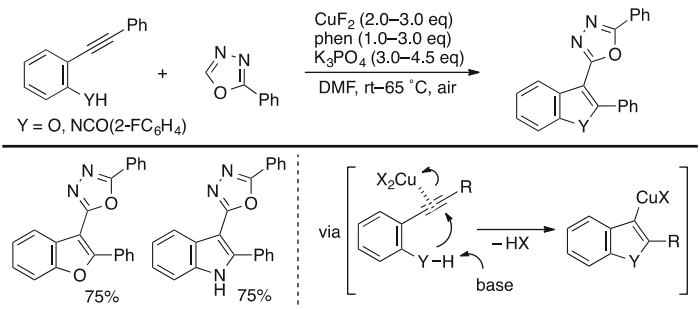

Scheme 1 Formal dehydrogenative construction of bi(heteroaryl)s via annulative metalation

relatively acidic active methylene compound, namely, ethyl cyanoacetate (Eq. 19) [41]. An initially formed alkylated product undergoes the intramolecular nucleophilic addition/tautomerization sequence to furnish the formally annulated product, isoquinolinone, in a good yield. Very recently, Dai and Yu succeeded in the annulation reaction of benzamide with malonates by the action of the oxazolinylaniline auxiliary (Eq. 20) [42]. While not dehydrogenative, the oxidative C–H trifluoromethylation with TMS-CF_3 also appears (Eq. 21) [43].

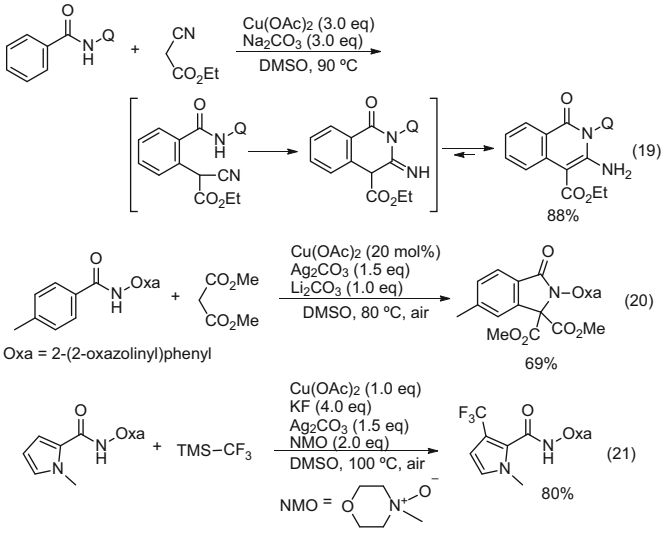

3 C–H/N–H Coupling

Due to the ubiquity of (hetero)arylamines in biologically active compounds, natural products, and organic functional materials, the aromatic C–N formation has been widely explored over the last two decades [44, 45]. Among them, the

dehydrogenative coupling with readily available (hetero)arenes and amines is ideal but difficult, particularly in an intermolecular manner, even with the noble transition metals such as palladium. The challenging aromatic C–H/N–H coupling has been recently achieved in copper-based systems.

The first copper-*catalyzed* intermolecular C–H/N–H coupling was reported by Mori and Schreiber, independently, in 2009 (Eqs. 22 and 23) [46, 47]. Although the scope of the aromatic compound is limited to the acidic 1,3-azoles, the catalytic turnover of copper is realized by an ideal oxidant, molecular oxygen. Subsequently, similar aminations of polyfluoroarenes (Eq. 24) and pyridine *N*-oxides (Eq. 25) were developed by Su [48] and the groups of Li [49], Wu, and Cui [50], respectively. When the biologically important sulfoximine is employed as a nitrogen source, the reaction proceeds smoothly even under ambient conditions, and the enantiopure substrate is converted into the product without affecting the enantiomeric excess (Eq. 26) [51].

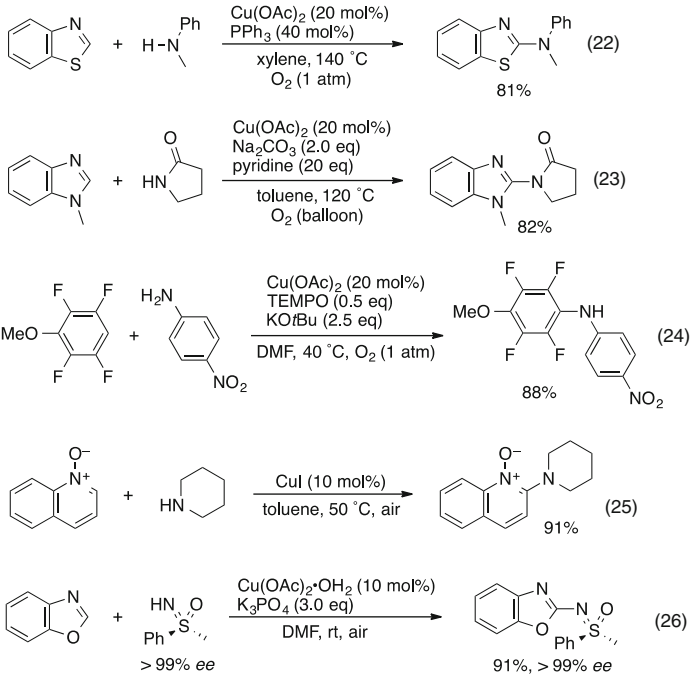

Meanwhile, Nicholas succeeded in the development of catalytic variants of work by Yu and Chatani in Eqs. (1) and (2). The key to the success is a careful choice of the solvent: an anisole/DMSO cosolvent system is essential for the good conversion (Eq. 27) [52]. Li and coworkers also reported the catalytic system with *tert*-butyl peroxide (TBP) as an oxidant (Eq. 28) [53]. In the latter case, an aminyl radical species might be involved in the C–N forming step [54], although the details are not clear. Additionally, the sulfoximine is also a promising coupling partner for 2-phenylpyridine, albeit with a stoichiometric amount of $Cu(OAc)_2$ (Eq. 29) [55].

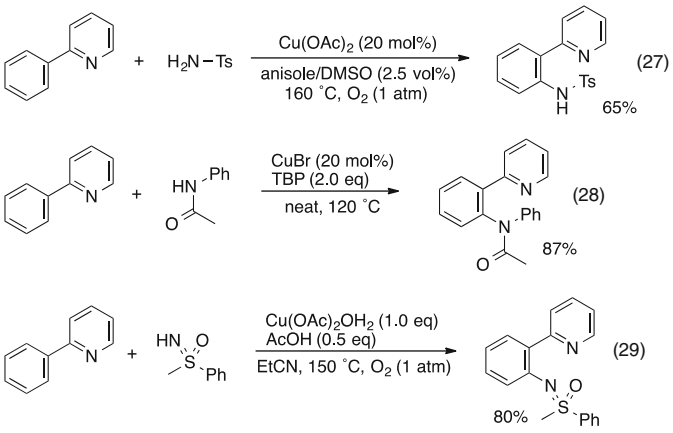

More general arenes and heteroarenes can be employed by the introduction of appropriate directing groups. Shen and coworkers reported the CuOAc/O_2-catalyzed C2-selective amination of *N*-(2-pyrimidyl)indoles with phthalimide (Eq. 30) [56].

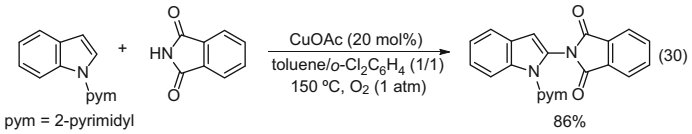

Similar to the C–H/C–H coupling mentioned in Section 2, some *N*,*N*-bidentate coordinating groups also work well in the C–H/N–H coupling. Benzamides bearing the quinoline moiety are directly aminated under the copper/silver bimetallic catalyst system, although the exact role of the silver salt is not clear (Eq. 31) [57]. The oxazoline-based double coordination strategy allows the otherwise difficult dehydrogenative C–N coupling of various heteroarenes and heteroarylamines to afford heteroatom-rich diarylamines of pharmaceutical importance (Eq. 32) [58]. Intriguingly, the scope of amines is complementary: in the former case, strongly basic alkylamines are applicable whereas the latter conditions accommodate less basic arylamines and amides.

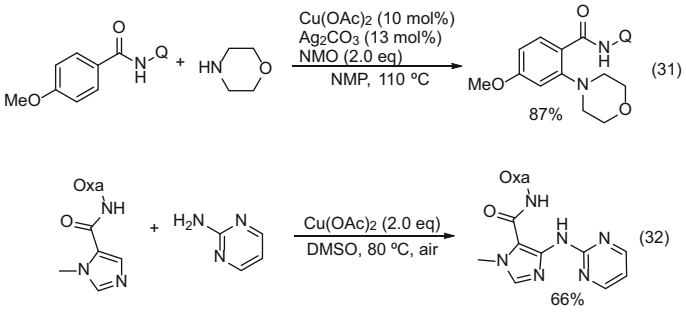

By using a picoline-type director, anilides can also couple with alkylamines in a dehydrogenative manner to form the corresponding 1,2-diaminobenzene derivatives (Eqs. 33 and 34) [59, 60]. The hypervalent I(III) reagent, $PhI(OAc)_2$ is a critical oxidant, and the reaction occurs under relatively mild conditions (rt–80 °C). The unique *ortho*-regioselectivity observed in the reaction of 1-naphthylamine and preliminary deuterium-labeling experiments suggests a single electron transfer (SET) mechanism, although the detailed pathway still remains obscure.

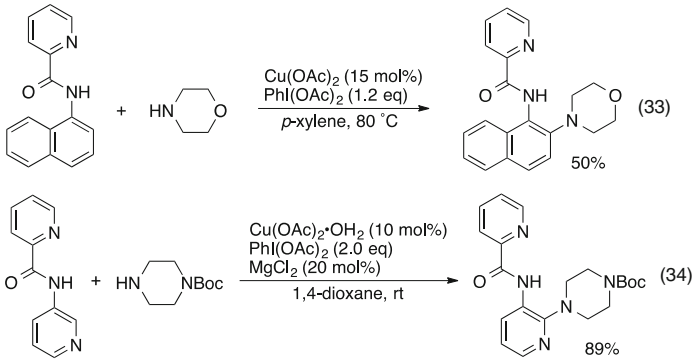

4 C–H/X–H Coupling with Other Heteroatom Nucleophiles

Some heteroatom nucleophiles other than amines also couples with aromatic C–H bonds under appropriate copper-based conditions to make the corresponding C–X bonds efficiently.

4.1 S-Nucleophiles

Several copper salts have been found to promote the dehydrogenative thiolation of 1,3-azoles with both aromatic and aliphatic thiols [61–66]. Especially, *N*-heterocyclic carbenes (NHCs)-ligated copper complexes show the high catalytic activity (Eq. 35) [66]. The thiolation of less acidic aromatic substrates is possible with the aid of Daugulis's quinoline-type bidentate coordinating group (Eq. 36) [67]. In this case, the corresponding disulfides, for example, $F_3CS–SCF_3$, are also effective thiolation reagents (Eq. 37) [68].

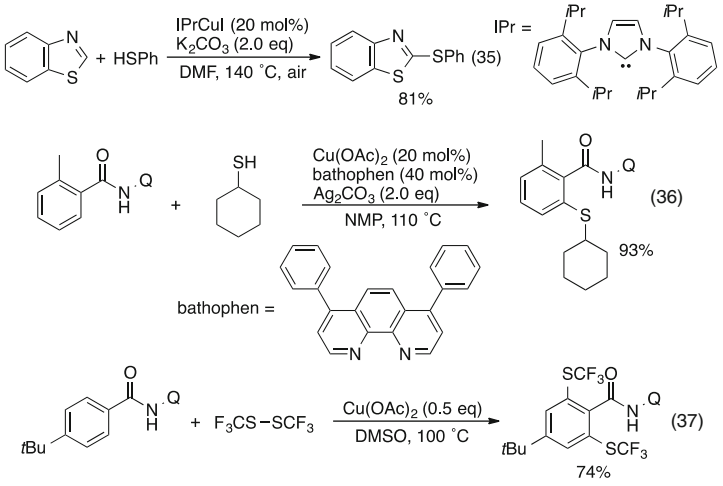

4.2 O-Nucleophiles

The C–H/O–H coupling of 2-phenylpyridine with primary and secondary aliphatic alcohols occurs in the presence of a $Cu(OAc)_2$ catalyst and $AgOTf/O_2$ dual oxidants (Eq. 38) [69]. Unfortunately, phenols in place of the alcohols result in no formation of the C–O coupling products, due to the dominant self-coupling under oxidative conditions. The use of the quinoline auxiliary overcomes this limitation, and phenol derivatives as well as easily-oxidizable allylic and benzylic alcohols can be employed (Eq. 39) [70]. Interestingly, with 3-aminophenol, the selective C–O formation over C–N formation is observed. Very recently, the group of Niu and Song introduced the unique *N,O*-bidentate directing group based on 2-aminopyridine *N*-oxide and succeeded in the copper-mediated dehydrogenative C–O coupling of aromatic compounds with both aromatic and aliphatic alcohols (Eqs. 40 and 41) [71, 72]. Unusual compatibility with aryl iodide as well as hexafluoro-2-propanol (HFIP) is observed.

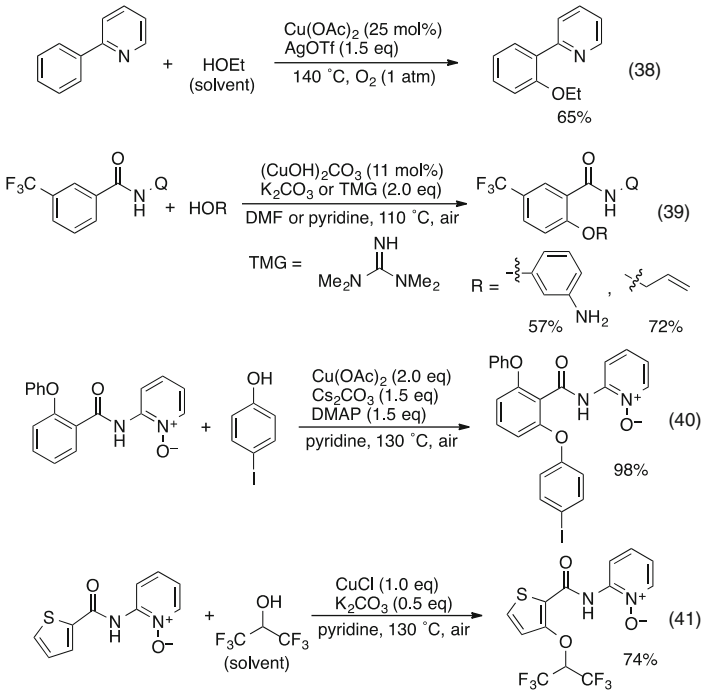

4.3 *Miscellaneous Nucleophiles*

The potential of P-based nucleophiles in the copper-promoted dehydrogenative aromatic coupling was reported by the research group of Chen and Yu (Eq. 42) [73]. With the assistance of the *N*,*N*-bidentate coordination of the aminoquinoline, the copper-catalyzed C–P formation of aromatics with dialkylphosphonates proceeds to produce the corresponding aryl phosphonates in good yields.

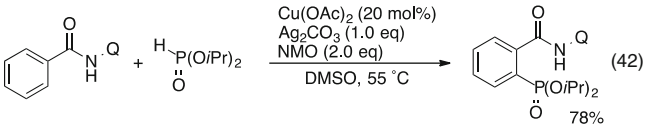

Some halogen sources, such as LiCl, NCS, and NIS, also couple with aromatic C–H bonds to form the corresponding C–halogen bonds under appropriate copper catalysis [7, 74–78]. Some representative examples are illustrated in Eqs. (43) to (45).

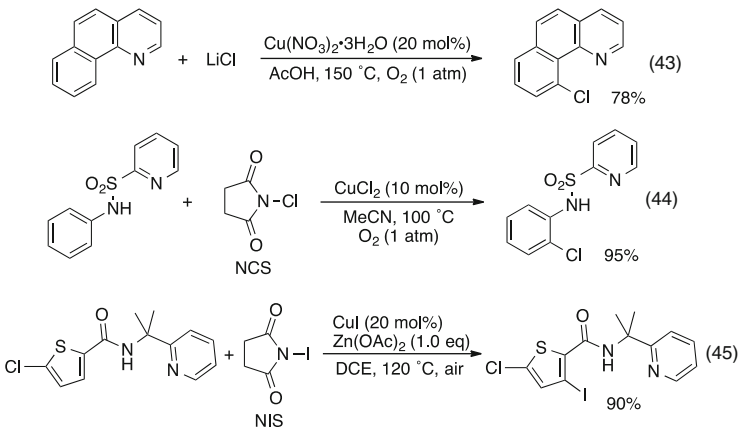

5 Mechanistic Studies

The detailed mechanism of copper-mediated dehydrogenative couplings mentioned above remains largely elusive because under oxidative conditions, copper complexes can have several oxidation states including Cu(0), Cu(I), Cu(II), and Cu(III). Despite such complications, seminal studies recently appear. In an early work by Yu in 2006 (Eq. 1) [7], a SET mechanism is proposed on the basis of deuterium-labeling experiments: no kinetic isotope effect (KIE) is observed in the intramolecular competition (Scheme 2). As exemplified by the chlorination, the pyridine directing group can coordinate to the Cu center to form ate-type complexes and induce the one-electron oxidation followed by ligand transfer regioselectively at the *ortho*-position. The second SET process by an additional Cu(II) species provides the observed C–H functionalized product.

On the other hand, a very unique redox system involving Cu(I)/Cu(II)/Cu(III) oxidation states was reported by Ribas, Stahl, and coworkers [79–81]. They extensively studied the reactivity of the triazamacrocyclic ligand with Cu(II) and successfully characterized C–H activated Ar–Cu(III) and Cu(I) complexes. The careful investigation of the reaction stoichiometry revealed that 0.5 eq of Ar–Cu(III) and 0.5 eq of Ar–Cu(I) are formed from 1.0 eq of Cu(II), thus suggesting an disproportionation of Cu(II) into Cu(III) and Cu(I) during the C–H activation event (Eq. 46). Upon treatment of the isolated Ar–Cu(III) complex with MeOH as an oxygen nucleophile, the C–H alkoxylated product and Cu(I) salt are obtained quantitatively (Eq. 47). A similar C–N bond formation occurs when NH pyridone is used as a nitrogen nucleophile.

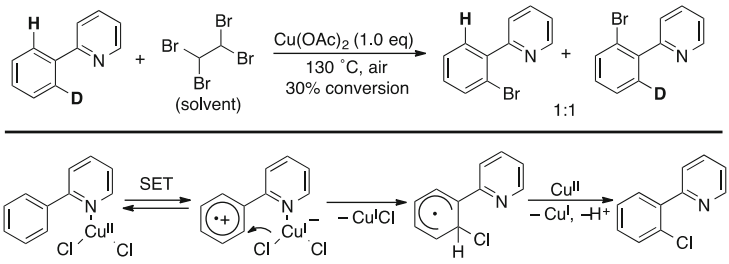

Scheme 2 A SET mechanism of Cu(II)-mediated C–H functionalization proposed by Yu

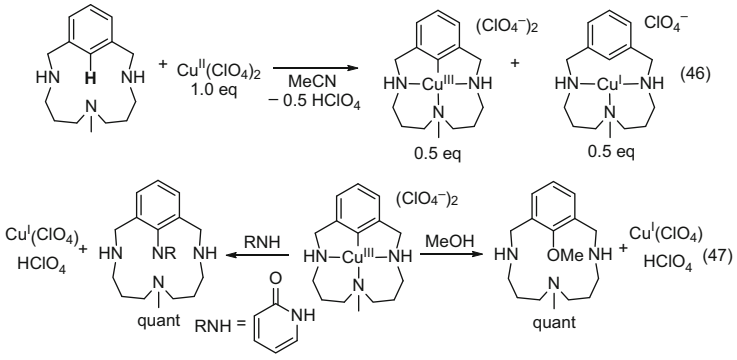

Based on the above outcomes, the mechanism of the Cu(II)/O_2-catalyzed C–H/O–H coupling of the macrocyclic arene with MeOH is proposed as shown in Scheme 3. An initial complexation of the arene with Cu(II) (**A**) is followed by C–H cupration with concomitant disproportionation by additional Cu(II) to form Ar–Cu(III) intermediate (**B**). Subsequent reaction with MeOH probably through reductive elimination furnish the C–O coupling product-ligated Cu(I) complex (**C**). The formed Cu(I) species is reoxidized by O_2 (**D**), and final ligand exchange with the starting arene liberates the product and regenerates the starting Cu(II) complex (**A**) to complete the catalytic cycle.

Additionally, the research group of Ertem and Stahl recently reported a condition-dependent, divergent mechanism in the Cu(II)-mediated C–H functionalization of the benzamide with Daugulis's auxiliary (Scheme 4) [82]. Under acidic chlorination conditions with a CuCl catalyst and LiCl in AcOH, the SET mechanism is operative, and the C–H chlorination occurs selectively at C5 position of the quinoline ring. A KIE value of 1.0 also supports the electron transfer system. In sharp contrast, under relatively basic conditions, the Cu$(OAc)_2$-mediated C–H/O–H coupling with MeOH proceeds exclusively at the *ortho*-position of the benzamide ring. A large KIE value of 5.7 as well as the observed site selectivity apparently indicates a different C–H activation mechanism. In the latter case, the reaction involves a Cu(I)/Cu(II)/Cu(III) organometallic pathway similar to that in Scheme 3. Particularly notable is the C–H activation at the Cu(II) center prior to the oxidation

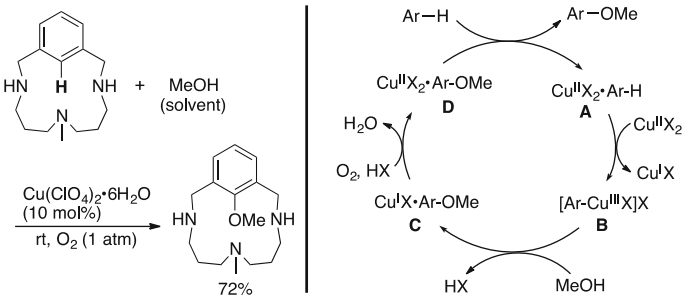

Scheme 3 A unique one-electron redox mechanism in Cu(II)-mediated C–H/O–H coupling

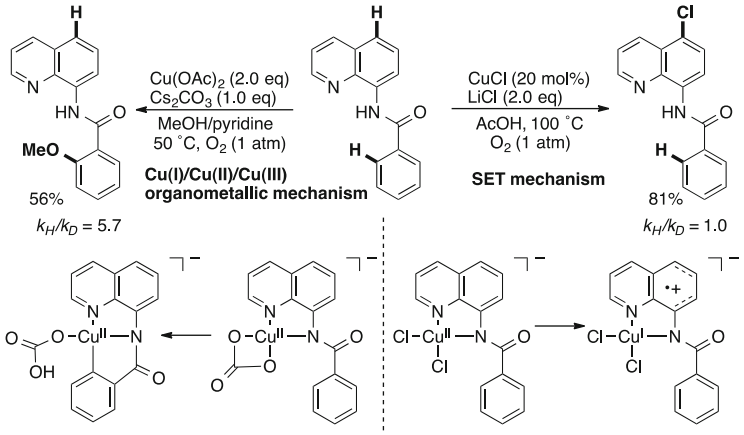

Scheme 4 A condition-dependent, divergent mechanism in Cu(II)-mediated C–H activation: SET vs organometallic pathway

(disproportionation) into the Cu(III), which is supported by DFT calculations (Scheme 5).

6 Conclusion

Over the last decade, the copper-mediated or copper-catalyzed C–H functionalization has been developed rapidly and greatly by significant efforts of many researchers, and cheap and abundant copper salts now can replace, to some extent, precedented noble transition metal catalysts such as Pd, Rh, and Ru. Moreover, some unique features of copper salts and complexes are observed. The intermolecular dehydrogenative cross-couplings mentioned in this chapter are such good examples, and they are otherwise challenging even under known noble transition metal catalysis. However, there is still a large room for further

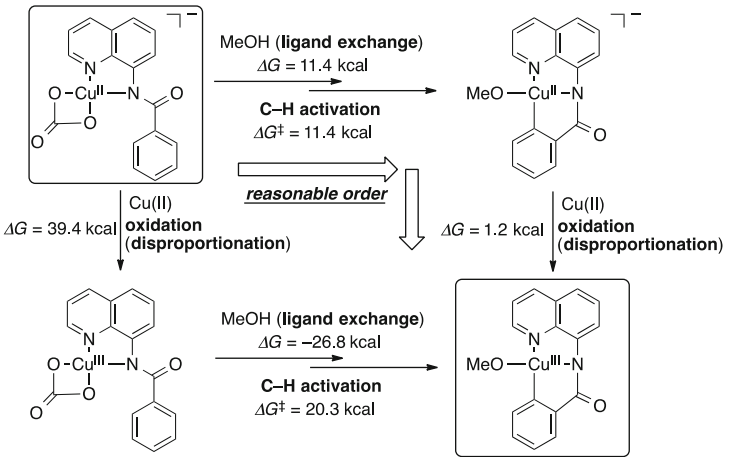

Scheme 5 DFT calculations for C–H activation: Cu(II) vs Cu(III)

development: improvement of turnover number (or frequency), use of atmospheric oxygen as an ideal terminal oxidant, activation of even more challenging sp^3 C–H bonds [83–85], and application to asymmetric catalysis. The clarification of detailed mechanisms and design of new Cu-based catalysis can address these problems and open a door to truly useful and practical synthetic transformation based on C–H activation chemistry.

References

1. Murai S, Kakiuchi F, Sekine S, Tanaka Y, Kamatani A, Sonoda A, Chatani N (1993) Nature 366:529
2. Daugulis O, Do H-Q, Shabashov D (2009) Acc Chem Res 42:1074
3. Kulkarni AA, Daugulis O (2009) Synthesis 24:4087
4. Wendlandt AE, Suess AM, Stahl SS (2011) Angew Chem Int Ed 50:11062
5. Hirano K, Miura M (2012) Chem Commun 48:10704
6. Hirano K, Miura M (2014) Top Catal 57:878
7. Chen X, Hao X-S, Goodhue CE, Yu J-Q (2006) J Am Chem Soc 128:6790
8. Uemura T, Imoto S, Chatani N (2006) Chem Lett 35:842
9. Guo X-X, Gu D-W, Wu Z, Zhang W (2015) Chem Rev 115:1622
10. de Meijere A, Diederich F (2004) Metal-catalyzed cross-coupling reactions, 2nd edn. Wiley-VCH, Weinheim
11. Tsuji J (2004) Palladium reagents and catalysts, 2nd edn. Wiley, Chichester
12. Miyaura N (2002) Top Curr Chem 2002:219
13. Chinchilla R, Nájera C (2007) Chem Rev 107:874
14. Doucet H, Hierso J-C (2007) Angew Chem Int Ed 46:834
15. Chinchilla R, Najera C (2011) Chem Soc Rev 40:5084
16. Thomas AM, Sujatha A, Anilkumar G (2014) RSC Adv 4:21688
17. Kitahara M, Hirano K, Tsurugi H, Satoh T, Miura M (2010) Chem Eur J 16:1722
18. Matsuyama N, Kitahara M, Hirano K, Satoh T, Miura M (2010) Org Lett 12:2358

19. Wei Y, Zhao H, Kan J, Su W, Hong M (2010) J Am Chem Soc 132:2522
20. Shen K, Fu Y, Li J-N, Liu L, Guo Q-X (2007) Tetrahedron 63:1568
21. Corbet M, Campo FD (2013) Angew Chem Int Ed 52:9896
22. Rouquet G, Chatani N (2013) Angew Chem Int Ed 52:11726
23. Zaitsev VG, Shabashov D, Daugulis O (2005) J Am Chem Soc 127:13154
24. Dong J, Wang F, You J (2014) Org Lett 16:2884
25. Zhang Y, Wang Q, Yu H, Huang Y (2014) Org Biomol Chem 12:8844
26. Shang M, Wang H-L, Sun S-Z, Dai H-X, Yu J-Q (2014) J Am Chem Soc 136:11590
27. Liu Y-J, Liu Y-H, Yin X-S, Gu W-J, Shi B-F (2015) Chem Eur J 21:205
28. Hassan J, Sévignon M, Gozzi C, Schulz E, Lemaire M (2002) Chem Rev 102:1359
29. Baumann M, Baxendale IR (2013) Beilstein J Org Chem 9:2265
30. Mao Z, Wang Z, Xu Z, Huang F, Yu Z, Wang R (2012) Org Lett 14:3854
31. Fan S, Chen Z, Zhang X (2012) Org Lett 14:4950
32. Qin X, Feng B, Dong J, Li X, Xue Y, Lan J, You J (2012) J Org Chem 77:7677
33. Zou L-H, Mottweiler J, Priebbenow DL, Wang J, Stubenrauch JA, Bolm C (2013) Chem Eur J 19:3302
34. Kitahara M, Umeda N, Hirano K, Satoh T, Miura M (2011) J Am Chem Soc 133:2160
35. Nishino M, Hirano K, Satoh T, Miura M (2012) Angew Chem Int Ed 51:6993
36. Nishino M, Hirano K, Satoh T, Miura M (2013) Angew Chem Int Ed 52:4457
37. Odani R, Hirano K, Satoh T, Miura M (2013) J Org Chem 78:11045
38. Odani R, Hirano K, Satoh T, Miura M (2014) Angew Chem Int Ed 53:10784
39. Hachiya H, Hirano K, Satoh T, Miura M (2011) Org Lett 13:3076
40. Oda Y, Matsuyama N, Hirano K, Satoh T, Miura M (2012) Synthesis 2012:1515
41. Zhu W, Zhang D, Yang N, Liu H (2014) Chem Commun 50:10634
42. Wang H-L, Shang M, Sun S-Z, Zhou Z-L, Laforteza BN, Dai H-X, Yu J-Q (2015) Org Lett 17:1228
43. Shang M, Sun S-Z, Wang H-L, Laforteza BN, Dai H-X, Yu J-Q (2014) Angew Chem Int Ed 53:10439
44. Surry DS, Buchwald SL (2011) Chem Sci 2:27
45. Monnier F, Taillefer M (2009) Angew Chem Int Ed 48:6954
46. Monguchi D, Fujiwara T, Furukawa H, Mori A (2009) Org Lett 11:1607
47. Wang Q, Schreiber SL (2009) Org Lett 11:5178
48. Zhao H, Wang M, Su W, Hong M (2010) Adv Synth Catal 352:1301
49. Li G, Jia C, Sun K (2013) Org Lett 15:5198
50. Zhu C, Yi M, Wei D, Chen X, Wu Y (2014) Cui X 16:1840
51. Miyasaka M, Hirano K, Satoh T, Kowalczyk R, Bolm C, Miura M (2011) Org Lett 13:359
52. John A, Nicholas KM (2011) J Org Chem 76:4158
53. Shuai Q, Deng G, Chua Z, Bohle DS, Li C-J (2010) Adv Synth Catal 352:632
54. Santoro S, Liao R-Z, Himo F (2011) J Org Chem 76:9246
55. Wang L, Priebbenow DL, Dong W, Bolm C (2014) Org Lett 16:2661
56. Xu H, Qiao X, Yang S, Shen Z (2014) J Org Chem 79:4414
57. Tran LD, Roane J, Daugulis O (2013) Angew Chem Int Ed 52:6043
58. Shang M, Sun S-Z, Dai H-X, Yu J-Q (2014) J Am Chem Soc 136:3354
59. Martínez ÁM, Rodríguez N, Arrayás RG, Carretero JC (2014) Chem Commun 50:2801
60. Li Q, Zhang S-Y, He G, Ai Z, Nack WA, Chen G (2014) Org Lett 16:1764
61. Fukuzawa S-I, Shimizu E, Atsuumi Y, Haga M, Ogata K (2009) Tetrahedron Lett 50:2374
62. Zhang S, Qian P, Zhang M, Hu M, Cheng J (2010) J Org Chem 75:6732
63. Zhou A-X, Liu X-Y, Yang K, Zhao S-C, Liang Y-M (2011) Org Biomol Chem 9:5456
64. Ranjit S, Lee R, Heryadi D, Shen C, Wu J, Zhang P, Huang K-W, Liu X (2011) J Org Chem 76:8999
65. Dai C, Xu Z, Huang F, Yu Z, Gao Y-F (2012) J Org Chem 77:4414
66. Inomata H, Toh A, Mitsui T, Fukuzawa S-I (2013) Tetrahedron Lett 54:4729
67. Yan X-B, Gao P, Yang H-B, Li Y-X, Liu X-Y, Liang Y-M (2014) Tetrahedron 70:8730

68. Tran LD, Popov I, Daugulis O (2012) J Am Chem Soc 134:18237
69. Bhadra S, Matheis C, Katayev D, Goosen LJ (2013) Angew Chem Int Ed 52:9279
70. Roane J, Daugulis O (2013) Org Lett 15:5842
71. Hao X-Q, Chen L-J, Ren B, Li L-Y, Yang X-Y, Gong J-F, Niu J-L, Song M-P (2014) Org Lett 16:1104
72. Zhang L-B, Hao X-Q, Zhang S-K, Liu K, Ren B, Gong J-F, Niu J-L, Song M-P (2014) J Org Chem 79:10399
73. Wang S, Guo R, Wang G, Chen S-Y, Yu X-Q (2014) Chem Commun 50:12718
74. Wang WH, Pan CD, Chen F, Cheng J (2009) Chem Commun 2009:6460
75. Mo S, Zhu YM, Shen ZM (2013) Org Biomol Chem 11:2576
76. Urones B, Martinez AM, Rodriguez N, Arrayas RG, Carretero JC (2013) Chem Commun 49:11044
77. Du Z-J, Gao L-X, Lin Y-J, Han F-S (2014) ChemCatChem 6:123
78. Li B, Liu B, Shi B-F (2015) Chem Commun 51:5093
79. Ribas X, Jackson DA, Donnadieu B, Mahía J, Parella T, Xifra R, Hedman B, Hodgson KO, Llobet A, Stack TDP (2002) Angew Chem Int Ed 41:2991
80. Huffman LM, Stahl SS (2008) J Am Chem Soc 130:9196
81. King AE, Huffman LM, Casitas A, Costas M, Ribas X, Stahl SS (2010) J Am Chem Soc 132:12068
82. Suess AM, Ertem MZ, Cramer CJ, Stahl SS (2013) J Am Chem Soc 135:9797
83. Wang Z, Ni J, Kuninobu Y, Kanai M (2014) Angew Chem Int Ed 53:3496
84. Wu X, Zhao Y, Zhang G, Ge H (2014) Angew Chem Int Ed 53:3706
85. Wang Z, Kuninobu Y, Kanai M (2014) Org Lett 16:4790

Top Organomet Chem (2016) 56: 67–90
DOI: 10.1007/3418_2015_138

Published online: 26 July 2015

The Effects of Ancillary Ligands on Metal–Carbon Bond Strengths as Determined by C–H Activation

William D. Jones

Abstract The activation of C–H bonds by oxidative addition in about 30 different substrates has been examined with three closely related metal species, [Tp′RhL], where L = CNneopentyl, PMe_3, and $P(OMe)_3$. Kinetic studies of the reductive elimination of R–H provided data to ascertain the relative metal–carbon bond strengths for a wide range of compounds. Trends in these bond strengths reveal that there are two classes of C–H substrates: parent hydrocarbons and substituted methanes. DFT calculations are used to support the observed trends, and some generalizations are made by comparison to other metal systems.

Keywords Bond strengths · Kinetics · Oxidative addition · Reductive elimination · Rhodium · Thermodynamics

Contents

1 Introduction 68
2 Hydrocarbon Activation by [Tp′Rh(CNR)] 68
3 Thermodynamic Determination of Rhodium–Carbon Bond Strengths in Tp′Rh(CNR)(R)H 72
4 Hydrocarbon Activation by [Tp′Rh(PMe_3)] 77
5 Thermodynamic Determination of Rhodium–Carbon Bond Strengths in Tp′Rh(PMe_3)(R)H 80
6 Hydrocarbon Activation by [Tp′Rh($P(OMe)_3$)] 82
7 Thermodynamic Determination of Rhodium–Carbon Bond Strengths in Tp′Rh[$P(OMe)_3$](R)H 84
8 Conclusions 88
References 88

W.D. Jones (✉)
Department of Chemistry, University of Rochester, Rochester, NY 14627, USA
e-mail: jones@chem.rochester.edu

1 Introduction

Carbon–hydrogen bond activation by transition metals has found its way to becoming an important aspect of organic synthesis. Metals have been found to break C–H bonds and then participate in follow-up reactions, oftentimes insertions of olefins or alkynes, that permit functionalization of a substrate or the formation of fused-ring systems. As this chemistry is developed, it is clear that selectivity in C–H bond activation is a critical issue that must be controlled to make a given functionalization reaction valuable.

In this chapter, we will present a summary of results that have been reported over the last 25 years with a transition metal complex that activates a wide variety of C–H bonds. As this chemistry developed, additional insight has been obtained that permitted further extensions of the work that have led to a deeper understanding of the factors that influence metal–carbon bond strengths. These bond strengths play an important role in determining the selectivity in reactions such as regioselective olefin insertions, so it is important to be able to predict how the formation of one bond vs. another will affect the thermodynamics. The importance of these factors will be revealed, and the effects of ancillary or "spectator" ligands on metal–carbon bond strengths will also be quantitatively analyzed and interpreted. This is all possible because the unsaturated metal fragment [Tp′RhL] where L = CNR, PMe_3, or $P(OMe)_3$ has proven to be very reactive toward a wide variety of C–H bonds, allowing the necessary comparisons to be made.

2 Hydrocarbon Activation by [Tp′Rh(CNR)]

We first reported that the 16-electron rhodium fragment [Tp′Rh(CNR)] where CNR = neopentyl isocyanide could activate hydrocarbon C–H bonds by irradiation of the carbodiimide precursor in benzene [1]. 366 nm irradiation of the yellow complex **1** led to the colorless phenyl hydride product in good yield. The quantum yield was determined to be 1.0 ± 0.3, which is higher than for many other organometallic photoprecursors [2–6]. Compound **1** is readily prepared by the reaction of phenyl azide with the $Tp'Rh(CNR)_2$.

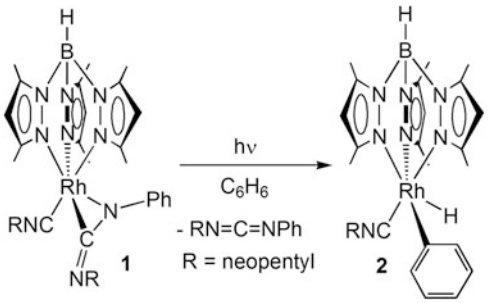

(1)

Benzene loss from **2** occurs upon warming to 80°C, with $\Delta G^{\ddagger} = 29.8$ kcal/mol in C_6D_6. The 16-electron fragment that apparently forms is rapidly trapped by the solvent to give **2**-d_6. The true mechanism, however, is one in which the benzene is displaced. If neopentyl isocyanide is added to **2**, a bimolecular reaction occurs to generate Tp′Rh(CNR)$_2$. The rate is first order in [CNR] at low isocyanide concentrations but zero order in [CNR] at high isocyanide concentrations, which is consistent with a pre-equilibrium between **2** and the η^2 complex (κ^2-Tp′)Rh(η^2-C_6H_6)(CNR) followed by associative substitution of the benzene at a square planar coordinatively unsaturated intermediate (Eq. 2). Further evidence for reversible formation of an η^2-benzene intermediate came from the observation of scrambling in the complex Tp′Rh(CNR)(C_6D_5)H. The hydride appears in all five locations on the phenyl group at the same rate, implying that the η^2-C_6D_5H complex is fluxional. Rh-phenyl rotation is hindered at room temperature, and at low T, five distinct phenyl resonances can be observed in the ^{1}H NMR spectrum [7].

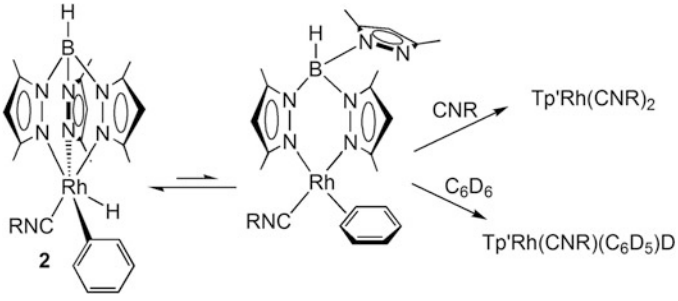

(2)

Complex **1** was found to activate a wide variety of hydrocarbons, including propane, pentane, cyclohexane, cyclopentane, methane, mesitylene, isobutene, and *t*-butylethylene [8, 9]. For linear hydrocarbons, a kinetic preference was observed for the exclusive activation of the C–H bonds of the terminal methyl groups. The activation of secondary C–H bonds was only observed when no other primary C–H bonds were available (e.g., cyclohexane, cyclopentane, cyclopropane [10]). With mesitylene, both aromatic and benzylic C–H bonds were cleaved. These observations were interpreted in terms of initial coordination of the hydrocarbon C–H bond to the 16-electron rhodium fragment, followed by rapid migration along the chain to

the end methyl group, where oxidative cleavage was rapid. This hypothesis was supported by experiments using deuterium-labeled alkyl deuterides. By monitoring the rates at which the deuterium appeared in the α and distal positions of the alkyl group vs. dissociation, the relative rates could be established as $k_{\text{C–H cleavage}} > k_{\text{migration}} > k_{\text{dissociation}}$ (Eq. 3) [11].

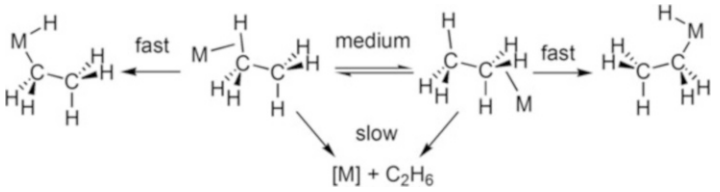

(3)

Further evidence for the intermediacy of alkane complexes came from studies of the reductive elimination of methane from Tp′Rh(CNR)(Me)H, **3**. Here, the rate of reaction with C_6D_6 to produce **2**-d_6 was found to be dependent on the concentration of C_6D_6 in inert C_6F_6 solvent. As with the reaction with isocyanide in Eq. 2, the rate was first order in $[C_6D_6]$ at low concentrations but less than first order at higher $[C_6D_6]$. These observations were treated in terms of a reversible equilibrium between **3** and an η^2-methane complex that then underwent bimolecular displacement by benzene. The reaction also shows a "solvent kinetic isotope effect," with the rate being faster in C_6H_6 than in C_6D_6 ($k_{C_6H_6}/k_{C_6D_6} = 1.08$). Since the rate-determining step involves bimolecular reaction with benzene, the rate is slightly different with C_6D_6 vs. C_6H_6 [12].

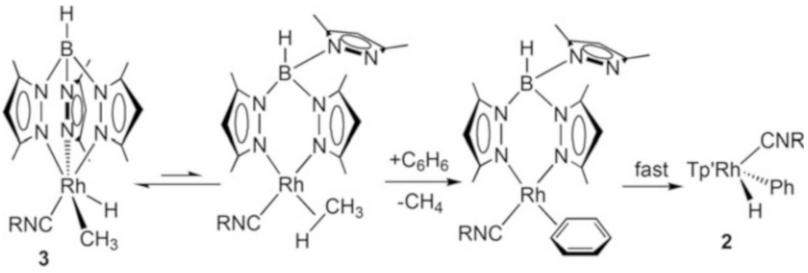

(4)

Terminal alkynes also add to [Tp′Rh(CNR)]. Irradiation of the carbodiimide complex **1** in neat 1-alkyne leads to the activation of the sp C–H bond. In cases where other "activatable" C–H bonds were presented, competitive C–H activation at these positions was observed. For example, *t*-butylacetylene and trifluoromethyl acetylene give exclusively alkynyl hydride products, whereas 1-octyne and trimethylsilylacetylene also give products resulting from methyl group activation. In both of the latter cases, the sp^3 C–H activation products are unstable and convert to the terminal alkynyl products at room temperature after a few days (Scheme 1). Similarly, the activation of arylalkynes leads to mixtures of sp and sp^2 C–H activation products. The unsaturated fragment [Tp′Rh(CNR)] was prepared either

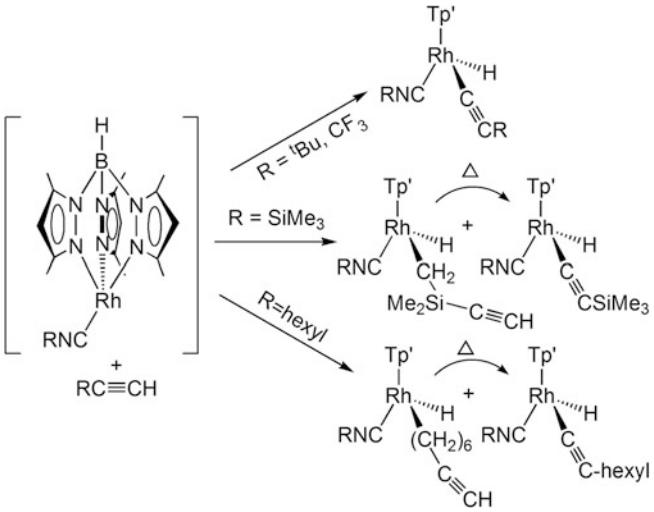

Scheme 1 Reactions of [Tp′Rh(CNR)] with terminal alkynes

by irradiation of **1** or by reductive elimination of methane from **3** in the presence of the alkyne [13].

The fragment [Tp′Rh(CNR)], prepared from irradiation of **1** or reductive elimination of methane from **3**, was found to react with a wide variety of substituted methanes. In each case, exclusive activation of the methyl C–H bond was observed, giving products of the type Tp′Rh(CNR)(CH_2X)H (X = *m*-xylyl, 2-propenyl, OMe, O^{t}Bu, CN, Cl, F, CF_3, C≡CMe, or C(=O)Me, Eq. 5) [14]. Difluoromethane also underwent clean oxidative addition of the C–H bond, but trifluoromethane proved unreactive, perhaps due to steric hindrance from the fluorines.

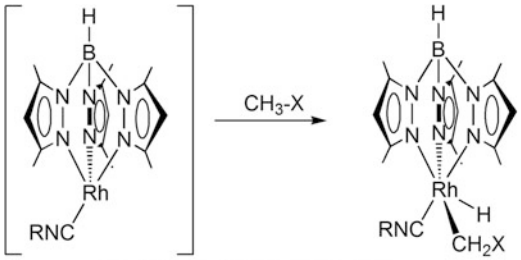

(5)

Irradiation of **1** in a series of linear nitriles was also examined and found to give terminal methyl activation products as the dominant species in all cases. Traces (~5%) of α-cyano C–H activation could be seen with propionitrile and butyronitrile (Eq. 6).

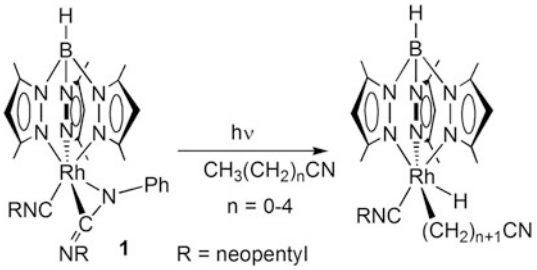

(6)

3 Thermodynamic Determination of Rhodium–Carbon Bond Strengths in Tp′Rh(CNR)(R)H

Through our studies of the above C–H activation reactions, we have found that we could do additional kinetic experiments to provide thermodynamic information on the stability of the various derivatives. These complexes all vary only in the hydrocarbyl group attached to rhodium – the spectator ligands are kept constant – so that relative bond strengths can be extracted from these studies.

The method employed uses three kinetic measurements to obtain the basic data needed to establish relative thermodynamic stabilities. The first two measurements needed to compare two complexes is the rate at which they reductively eliminate hydrocarbon. This is obtained by dissolving the pure compound in benzene-d_6 and then measuring the rate of the first-order reductive elimination. This rate constant can then be converted to a barrier height using the Eyring equation. The third kinetic measurement needed is to perform a competition between the two substrate hydrocarbons when they react with the [Tp′Rh(CNR)] fragment. This is accomplished by irradiation a solution of **1** in a 1:1 molar ratio of the two substrates. The ratio of the products gives the difference in the two barrier heights for C–H activation. The experiments are summarized in Scheme 2 for benzene vs. *t*-butylethylene, and the thermodynamic analysis is shown in Fig. 1.

From the two barrier heights for reductive elimination, combined with the kinetic selectivity, one can obtain the driving force ΔG^0 for the exchange of benzene for *t*-butylethylene in Tp′Rh(CNR)(R)H as shown in Fig. 1. This driving force has both enthalpic and entropic contributions. The enthalpic contributions depend on the relative Rh–C bond strengths (D_{rel}(Rh–C)) and the relative C–H bond strengths ($D_{R2–H} - D_{R1–H}$) in the bonds that are being broken and formed. The entropic contributions largely cancel out, since most of the molecule is the same on both sides of the reaction. There is one important entropic contribution that should be considered, however, and that is to account for the number of hydrogens that are available for activation.

In the present example, benzene has six hydrogens that can react, whereas *t*-butylethylene has only one hydrogen that can react (only the *trans* isomer is formed). Therefore, benzene is six times more likely to react compared to

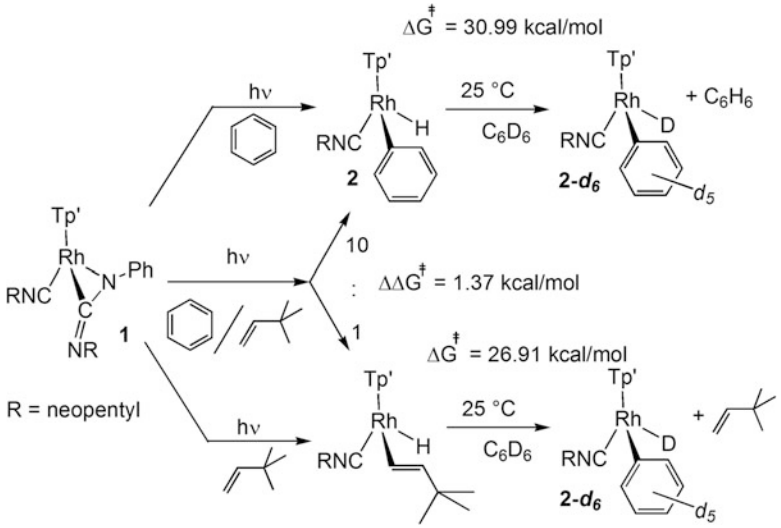

Scheme 2 Three kinetics experiments that allow determination of the driving force

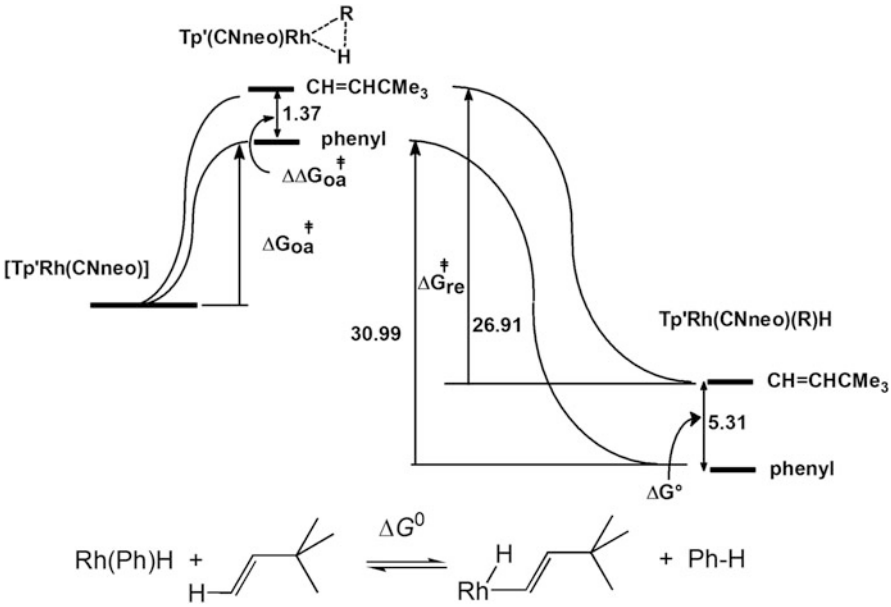

Fig. 1 Thermodynamic analysis of R–H activation equilibrium from the results of three kinetic experiments. Energies are in kcal mol^{-1}

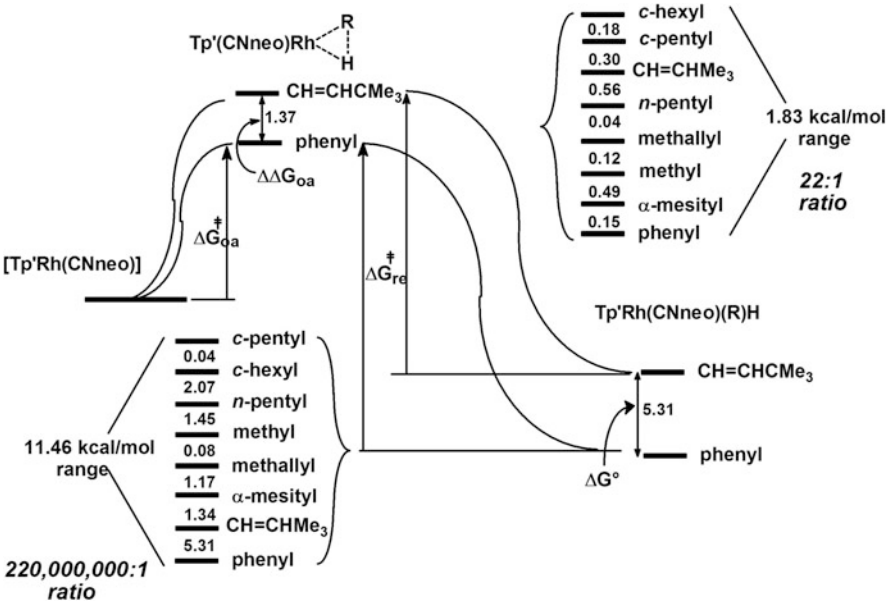

Fig. 2 Thermodynamic analysis of R–H activation equilibrium for several hydrocarbons. Reproduced with permission of the ACS from Jones and Wick [9]

t-butylethylene, and this statistical difference amounts to an entropic contribution to ΔG^0. Equation 7 summarizes how these terms combine for any two hydrocarbons to give the relative metal–carbon bond strength, D_{rel}(Rh–C), from the free energy of reaction:

$$D_{\text{rel}}(\text{Rh}-\text{C}) = \Delta G^0 - [D_{\text{R2}-\text{H}} - D_{\text{R1}-\text{H}}] - RT\ln(\#\text{H}_2/\#\text{H}_1) \qquad (7)$$

This analysis can be applied to all of the hydrocarbon activations discussed thus far, some of which are summarized in Fig. 2. The only requirement is that the C–H activation must give a single product and that the reductive elimination must cleanly give **2**-d_6. If the reductive elimination leads to a rearranged product, then Eq. 7 cannot be used. For example, the activation of cyclopropane leads to the C–H oxidative addition product. However, reductive elimination in C_6D_6 does not give **2**-d_6 but rather produces the metallocyclobutane. Therefore, cyclopropane does not appear in this scheme.

At this point, it is worth commenting on these hydrocarbon activations. First, from the competition experiments, all of the hydrocarbons are activated with similar barriers – that is, the $\Delta\Delta G^{\ddagger}$ only spans 1.8 kcal/mol, which corresponds to a 22:1 ratio at 25°C. This is because in the rate-determining step, the substrate is coordinating to the [Tp′Rh(CNR)] fragment via its C–H bond, and all of the hydrocarbons have similar binding affinities. For aromatic substrates, the arene can bind through its π-system, and this is why benzene and mesitylene are the

fastest substrates to be activated. After this, the kinetic selectivity largely follows steric accessibility to the C–H bond. The range for thermodynamic preference spans a much larger range, 220 million:1 or 11.5 kcal/mol. It is also noteworthy that the most preferred product is the one in which the strongest C–H bond has been broken, the phenyl hydride. This thermodynamic preference for breaking the strongest C–H bond can only be accounted for by the formation of an even more favorable rhodium–phenyl bond. It is the strength of the metal–carbon bond that is formed that drives these equilibria, not the strength of the C–H bond that must be broken. These are product driven equilibria, so the focus on the C–H bond strength to predict favorability is not warranted.

While all of the substrates discussed above are not shown in Fig. 2, the same analysis can be performed with all of them (alkynes, substituted methanes). One caveat that we encountered was that many of these substituted derivatives proved to be very stable. Loss of alkane from the *n*-pentyl hydride complex has a half-life of about an hour at 25°C. Methane loss from **3** has a half-life of about 5 h. Loss of benzene from **2**, however, is extremely slow (months), and therefore, the rate of benzene reductive elimination at 25°C was determined by extrapolation from the rate at higher temperatures. The Eyring plot of ln(*k*/T) vs. 1/T gave activation parameters for reductive elimination of benzene $\Delta H^{\ddagger} = 37.8$ (1.1) kcal/mol and $\Delta S^{\ddagger} = 23$ (3) e.u., which can be used to calculate the rate at other temperatures. As mentioned above, the substituted derivatives are much more stable. Reductive elimination of the alkynyl hydrides was examined at 100°C, as was the elimination of many of the substituted methyl derivatives. In these cases, the rate of benzene elimination was calculated from the Eyring parameters at the same temperature as that where the rate of reductive elimination was measured, so that the barriers could be directly compared as in Fig. 2. The determination of ΔG^0 for all substrates allows Eq. 7 to be used to determine relative metal–carbon bond strengths for these compounds. Table 1 summarizes these data, giving $\Delta\Delta G^{\ddagger}$, ΔG^0, and D_{rel}(Rh–C) for all substrates.

With D_{rel}(Rh–C) now available for all substrates, the data can be compared visually by plotting D_{rel}(Rh–C) vs. the C–H bond strength of the substrate. Figure 3 shows the resulting plot. The data fall into two classes of substrates. The parent hydrocarbon data are shown in blue, with the M–C_{sp} bonds being strongest and then the M–C_{sp2}, followed by the M–C_{sp3}. The line has a slope of 1.4, indicating that the range of metal–carbon bond strengths is about 40% greater than the range of carbon–hydrogen bond strengths. The data for the substituted methanes is shown in red. It is parallel with a slope of 1.4 also but is offset vertically by about 7 kcal/mol. This offset reflects the fact that the metal–carbon bonds are about 7 kcal/mol stronger than what you would expect based upon the strength of the C–H bond that is being broken. Also, while chloro and fluoro substituents are seen to strengthen the metal–methyl bond, all of the other substituents actually *weaken* the metal–methyl bond. This is actually to be expected, as bond strengths are based on homolysis, and these radicals are all stabilized by resonance. The unexpected 7 kcal/mol "increase" in bond strength is believed to be attributable to a greater ionic contribution to the metal–carbon bond with these substituents on the α-carbon.

Table 1 Kinetic and thermodynamic data for Tp′Rh(CNneopentyl)(R)H complexes

R	D(C–H)[a]	$\Delta\Delta G_{oa}^{\ddagger}$ vs. PhH	$\Delta G_{re}^{\ddagger}$	T_{re}(R–H)	ΔG^0 vs. PhH	#H	D_{rel}(M–C)
Ph-	112.9	0	30.95	296	0	6	0.0
t-Butylvinyl-	111.1	1.36	26.91	295	5.47	1	−6.2
Methyl-	105.0	0.70	23.52	296	8.17	4	−15.8
n-Pentyl-	100.2	0.79	22.43	296	9.35	6	−22.1
c-Pentyl-	95.6	1.78	21.18	296	11.59	10	−29.2
c-Hexyl-	99.5	1.80	21.40	296	11.39	12	−25.2
$CF_3C{\equiv}C$-	*135.4*[a]	0.75	30.10	373	−0.13	1	23.7
n-HexylC≡C-	*131.0*[a]	1.19	30.39	373	0.02	1	19.1
$Me_3SiC{\equiv}C$-	*131.6*[a]	0.62	32.50	373	−2.66	1	22.4
$Me_3CC{\equiv}C$-	*131.4*[a]	0.96	30.83	373	−0.65	1	20.2
PhC≡C-	*133.2*[a]	0.50	31.53	373	−1.81	1	23.2
p-$CF_3C_6H_4C{\equiv}C$-	*127.8*[a]	−0.09	31.83	373	−2.70	1	18.7
p-$MeOC_6H_4C{\equiv}C$-	*122.7*[a]	0.29	30.78	373	−1.27	1	12.1
-C_2H_4CN	*103.0*[a]	1.26	25.47	299	6.71	3	−16.2
-C_3H_6CN	*101.3*[a]	1.17	23.64	299	8.45	3	−19.6
-C_4H_8CN	*101.2*[a]	1.04	22.88	299	9.09	3	−20.4
-$C_5H_{10}CN$	*101.2*[a]	1.04	22.38	299	9.58	3	−20.9
-CH_2CN	94.8	1.48	31.36	373	−0.66	3	−17.0
-$CH_2C(Me){=}CH_2$	89.1	0.74	23.92	296	7.81	6	−31.6
α-Mesityl-	89.4	0.13	24.49	296	6.63	9	−30.4
-$CH_2C{\equiv}CCH_3$	90.7	0.44	26.98	340	3.44	6	−25.6
-$CH_2C(O)CH_3$	96.0	0.73	27.71	340	3.00	6	−19.9
-CH_2O^tBu	93.0	0.84	25.43	340	5.39	3	−24.9
-CH_2OCH_3	96.1	0.48	26.24	340	4.22	6	−21.0
-CH_2F	101.3	0.81	28.48	340	2.31	3	−13.5
-CHF_2	103.2	2.33	30.36	373	1.19	2	−10.2
-CH_2Cl	100.1	0.14	27.90	353	1.92	3	−14.3
-C_6F_5[b]	116.5	1.92	36.81	412	−6.57	1	11.2
-CH_2CF_3	106.7	1.63	27.90	340	3.71	3	−9.5

Terminal C–H bond strengths *in italics* for alkynes and nitriles were calculated using DFT; B3LYP/6-31G**

[a]Energies are in kcal mol^{-1}

[b]From Evans et al. [15]

For comparison with the experimental values, we have also calculated these same bond strength data using DFT with Tp′Rh(CNMe)(R)H as a model, with methylisocyanide replacing neopentylisocyanide. A plot of calculated relative Rh–C bond strengths vs. C–H bond strengths with these substrates also shows two distinct linear correlations with slopes of 1.59 and 1.46 for the two analogous sets of compounds (Fig. 4). While there is generally good agreement with the observed experimental trends in Rh–C bond strengths, DFT overestimates the range of Rh–C bond strengths by 10–15%.

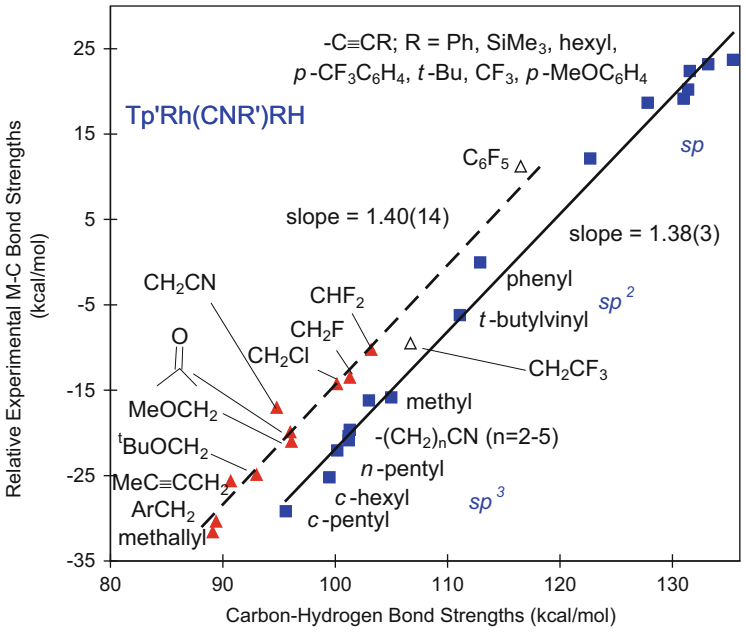

Fig. 3 Plot of relative experimental M–C bond strengths vs. C–H bond strengths. The *solid line* is fit to the hydrocarbons and aliphatic nitriles $-(CH_2)_n-CN$ ($n = 2–5$) (*blue filled box*, $y = 1.376x - 159.5$), and the *dashed line* is fit to the $-CH_2X$ substrates and $-CHF_2$ (*red filled triangle*, $y = 1.4024x - 154.6$). Also shown are $-C_6F_5$ and $-CH_2CF_3$ (Δ), which are not included in either fit. Experimental C–H bond strengths were used for all substrates except the alkynes and nitriles other than acetonitrile. Alkyne and nitrile C–H bond strengths were calculated (B3LYP) since experimental values are unavailable or have large errors [13]. The vertical separation of the lines at $D_{C-H} = 100$ kcal mol^{-1} is 7.5 kcal mol^{-1}. Reproduced with permission of the ACS from Jiao et al. [14]

4 Hydrocarbon Activation by [Tp′Rh(PMe$_3$)]

In order to investigate the effect of the ancillary ligands on the metal–carbon bond strengths, we also examined the reactivity of the fragment [Tp′Rh(PMe$_3$)] with hydrocarbons and substituted methyl derivatives. Here, the strongly electron-donating PMe$_3$ ligand replaces the electron-withdrawing neopentyl isocyanide ligand in the above studies and was anticipated to have a significant effect on the bond strengths.

To generate the 16-electron fragment, Tp′Rh(PMe$_3$)H$_2$ (**4**) was used as a photochemical precursor of the reactive intermediate [16, 17]. Irradiation of **4** in a variety of hydrocarbons led to the formation of oxidative addition products of the type Tp′Rh(PMe$_3$)(R)H (R = α-mesityl, *tert*-butylvinyl, CH_2O^tBu, $CH_2C{\equiv}CMe$, $CH_2C(=O)CH_3$, pentyl, cyclopentyl) along with a small amount of by-products Tp′Rh(PMe$_3$)$_2$ and Tp′Rh(PMe$_3$)R$_2$. The latter are formed as a result of photolysis of the product(s). As an alternative, Tp′Rh(PMe$_3$)MeH (**5**) was prepared by the

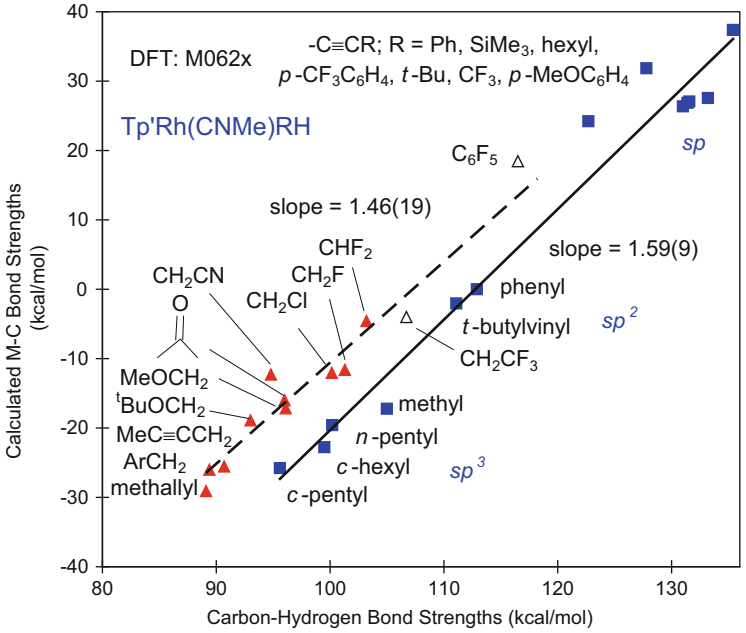

Fig. 4 DFT-calculated plot of relative M–C bond strengths vs. C–H bond strengths for Tp′Rh(CNMe)(R)H. The *lower line* is fit to the hydrocarbons (*blue filled box*, $y = 1.593x - 179.6$), and the *upper line* is fit to the $-CH_2X$ and CHF_2 substrates (*red filled triangle*, $y = 1.457x - 156.2$). Data for C_6F_5H and CH_3CF_3 activation is also shown (Δ), but not included in the fits. M062X method and basis set 6–31g** for first row atoms and pseudopotentials, additional functions optimized by Stuttgart group for atoms beyond the second row (see [13] for details on the choice of method). Experimental C–H bond strengths were used for all substrates except the alkynes. Alkyne C–H bond strengths were calculated (B3LYP) since experimental values are unavailable or have large errors [13]. The vertical separation of the lines at $D_{C-H} = 100$ kcal mol^{-1} is 9.7 kcal mol^{-1}. Reproduced with permission of the ACS from Jiao et al. [14]

reaction of Tp′Rh(PMe_3)MeCl with Cp_2ZrH_2. Loss of methane occurs rapidly at 30°C ($\tau_{1/2} = 35$ min), giving rise to an alternate thermal source of [Tp′Rh(PMe_3)]. During the isolation of **5**, some methane loss and activation of the THF solvent used in the synthesis produced variable quantities of Tp′Rh(PMe_3)(tetrahydrofuranyl)H, which is also a labile source of [Tp′Rh(PMe_3)]. Using **5**, many hydrocarbon and substituted methyl products could be prepared (Scheme 3) [18].

Reaction of mesitylene with **5** gave only the product of benzylic C–H activation, unlike the reaction with **1** which gave a 3:1 mixture of benzylic/aromatic C–H activation. The isonitrile ligand appears to induce less crowding at the metal center. As with **1**, CF_3H proved unreactive. Once again, steric inaccessibility of the C–H bond is believed to be responsible.

Irradiation of dihydride **4** in neat terminal alkyne led to C–H activation products, but the lengthy photolysis times led to decomposition products with many of the acetylenes. Methyl hydride **5** proved to be a good precursor for the activation of

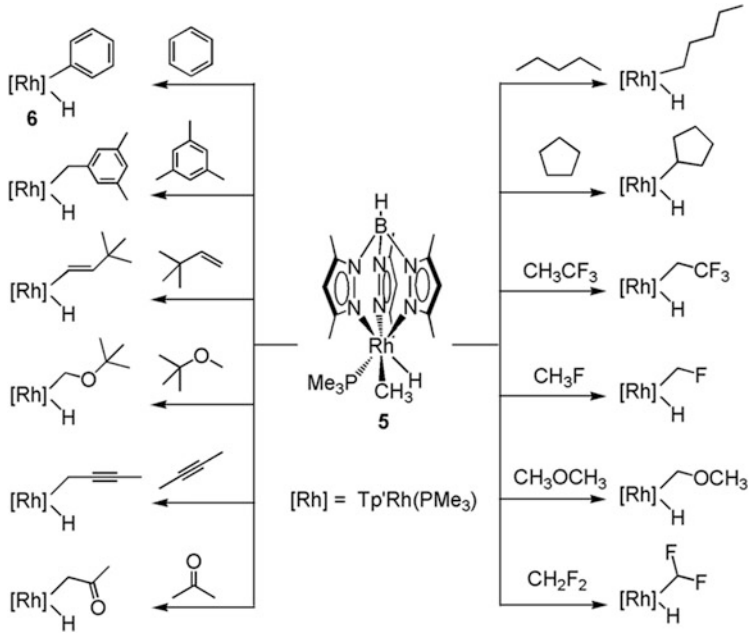

Scheme 3 Reactions of $Tp'Rh(PMe_3)$ with hydrocarbon substrates

terminal alkynes to give products of the type $Tp'Rh(PMe_3)(C{\equiv}CR)H$ ($R = {}^tBu$, $SiMe_3$. *n*-hexyl, *p*-$MeOC_6H_4$, CF_3, Ph, *p*-$CF_3C_6H_4$). In the latter three cases, competitive formation of the π-bound acetylene complex was also observed. Heating these samples to 140°C for several hours resulted in their complete conversion to the alkynyl hydride products (Eq. 8). These alkynyl hydride products proved to be very stable, as they could be chromatographed in air on the benchtop and the X-ray crystal structures of many of them could be obtained without derivatization [18].

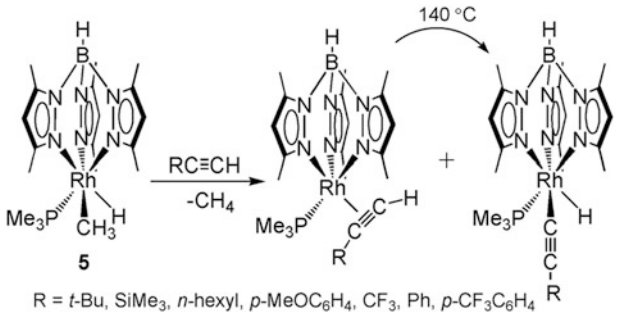

(8)

5 Thermodynamic Determination of Rhodium–Carbon Bond Strengths in Tp′Rh(PMe$_3$)(R)H

As was done previously, the kinetics of reductive elimination, combined with kinetic competition data, were used to obtain rhodium–carbon bond strengths with [Tp′Rh(PMe$_3$)] as the metal fragment. Thermolysis of each compound in C_6D_6 at 30°C was found to follow first-order reductive elimination kinetics, giving Tp′Rh(PMe$_3$)(C_6D_5)D (**6-*d*$_2$**). The only exception was the 2-butynyl hydride Tp′Rh(PMe$_3$)($CH_2C{\equiv}CCH_3$)H, which gave the η^2-butyne complex as confirmed by X-ray crystallography. This complex could therefore not be employed in the thermodynamic analysis. In comparison with the earlier case with Tp′Rh (neopentyl)($CH_2C{\equiv}CCH_3$)H, the elimination of 2-butyne cleanly led to the formation of **2-*d*$_6$**. Apparently the stronger donor PMe$_3$ allows for significant stabilization of the π-bound alkyne complexes.

Some of the compounds underwent reductive elimination far too slowly at 30°C for convenient measurement (e.g., alkynes), and therefore, they were conducted at elevated temperatures (140°C). In addition, since **6-d$_2$** is unstable at this temperature, C_6F_5H was added to trap the metal fragment following reductive elimination. To compare these barriers to those of the reductive elimination of **6**, the temperature dependence of the rate of elimination for **6** in C_6D_6 was measured, giving activation parameters $\Delta H^{\ddagger} = 32.6 \pm 3.3$ kcal mol^{-1} and $\Delta S^{\ddagger} = 10.9 \pm 0.2$ kcal mol^{-1} K^{-1}. Using these data, the barrier heights could be compared at the same temperature.

Kinetic competitions between a substrate and C_6H_6 were accomplished by irradiation of a solution of **4** in a mixture of the two substrates. The samples were irradiated for only a short time to avoid problems arising from secondary photolysis of the products. The ratio of the two products could be easily determined by ^{1}H NMR spectroscopy, giving the value for $\Delta\Delta G^{\ddagger}$. Competition data for methane was measured vs. pentane and then referred to benzene using the competition between pentane and benzene: $k_{\mathrm{PhH}}/k_{\mathrm{CH_4}} = \left(k_{\mathrm{PhH}}/k_{\mathrm{pentane}}\right)\left(k_{\mathrm{pentane}}/k_{\mathrm{CH_4}}\right)$.

As described above for [Tp′Rh(CNneopentyl)], the analysis of the data in Table 2 as in Fig. 1 and using Eq. 7 allows the determination of D_{rel}(Rh–C) for a large number of substrates. These Rh–C bond strengths can be plotted vs. the corresponding C–H bond strengths to give the overall trend as shown in Fig. 5. As before two trends clearly emerge. The first trend is seen joining the unsubstituted hydrocarbons with a slope of 1.54(4). This compares to the value seen with CNneopentyl as the ancillary ligand of 1.38(3). The effect of replacing the strong isocyanide π-acceptor with the strong PMe$_3$ σ-donor is to increase the slope of the line. This corresponds to a "stretching out" of the range of Rh–C bond strengths with the better σ-donor ligand; i.e., the PMe$_3$ derivative shows a wider range of selectivity. The second trend seen is in the methyl-substituted derivatives Rh–CH_2X. Again, a parallel line is observed with a slope of 1.71(8), which compares to the slope seen with L = CNneopentyl of 1.40(14). The line is offset vertically by about 8 kcal/mol, very similar to the values seen with L = CNneopentyl. The range

Table 2 Kinetic and thermodynamic data for Tp′Rh(PMe_3)(R)H complexes

R	D(C–H)[a]	$\Delta\Delta G_{oa}^{\ddagger}$ vs. PhH	$\Delta G_{re}^{\ddagger}$	T_{re}(R–H)	ΔG^0 vs. PhH	#H	D_{rel}(M–C)
Ph-	112.9	0	29.34	303	0.00	6	0.0
t-Butylvinyl-	111.1	0.83	27.99	303	2.18	1	−2.9
Methyl-	105.0	0.49	22.58	303	7.25	4	−14.9
n-Pentyl-	100.2	0.47	21.00	282	9.04	6	−21.7
c-Pentyl-	95.6	1.45	20.34	271	10.80	10	−28.4
$CF_3C{\equiv}C$-	*135.4*[a]	−0.77[a]	36.56	413	−9.19	1	32.7
n-HexylC≡C-	*131.0*[a]	0.36	34.31	413	−5.81	1	25.0
$Me_3SiC{\equiv}C$-	*131.6*[a]	0.27	37.50	413	−9.09	1	28.8
$Me_3CC{\equiv}C$-	*131.4*[a]	0.31	34.94	413	−6.49	1	26.1
PhC≡C-	*133.2*[a]	0.43	34.85	413	−6.28	1	27.6
p-CF_3phenylC≡C-	*127.8*[a]	−0.05	36.01	413	−7.91	1	23.9
p-MeOphenylC≡C-	*122.7*[a]	0.28	35.83	413	−7.41	1	18.3
Mesityl-	89.4	0.16	22.19	303	7.31	9	−31.1
-$CH_2C(O)CH_3$	96.0	0.97	26.67	303	3.64	6	−20.5
-CH_2O^tBu	93.0	0.66	25.70	303	4.30	3	−23.8
-CH_2OCH_3	96.1	0.34	26.31	303	3.37	6	−20.2
-CH_2F	101.3	0.03	28.75	340	0.22	3	−11.4
-CHF_2	103.2	−0.26	30.95	373	−2.63	2	−6.4
-CH_2CF_3	106.7	0.91	25.95	303	4.30	3	−10.1

Terminal C–H bond strengths *in italics* for alkynes were calculated using DFT; B3LYP/6-31g**
[a]Energies are in kcal mol^{-1}

of strengths for the substituted methyl derivatives is also "stretched out" for L = PMe_3 vs. L = CNneopentyl.

These trends can also be calculated using DFT and the full [Tp′Rh(PMe_3)] fragment as the model. The results are shown in Fig. 6. Two nearly parallel lines are seen, with the substituted methyl derivatives lying about 12 kcal/mol higher than the hydrocarbons. As before, the slopes by DFT show about 12–13% variance with experiment. The calculated slope for the hydrocarbons is too large, whereas the calculated slope for the substituted methyl derivatives is too small.

The larger slopes for L = PMe_3 vs. L = CNneopentyl indicate that the range of Rh–C bond strengths for the σ-donor complex is larger than for the π-acceptor complex. This has the experimental ramification that the weakest complexes with L = PMe_3 appear less stable than with L = CNneopentyl and that the strongest complexes with L = PMe_3 appear much more stable than with L = neopentyl. For example, Tp′Rh(CNneopentyl)(*n*-pentyl)H loses pentane with a half-life of about 1 h at 30°C, whereas Tp′Rh(PMe_3)(*n*-pentyl)H loses pentane with a half-life of about 30 min at only 9°C. Likewise, loss of phenylacetylene from Tp′Rh (CNneopentyl)(C≡CPh)H occurs with a half-life of about 74 h at 100°C, compared with 60 h at 140°C for Tp′Rh(PMe_3)(C≡CPh)H, a much more difficult elimination.

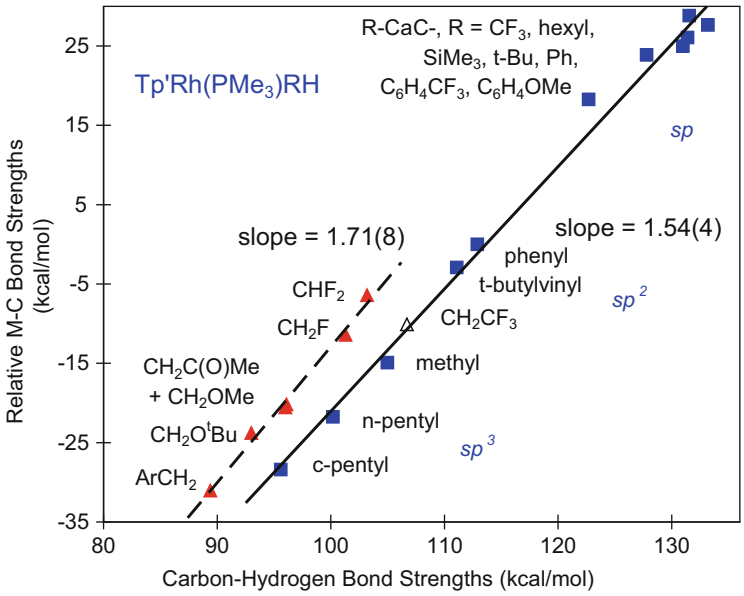

Fig. 5 Plot of relative experimental M–C bond strengths vs. C–H bond strengths for Tp′Rh(PMe_3)(R)H. The *solid line* is fit to the α-unsubstituted hydrocarbons (*blue filled box*, $y = 1.543x - 175.3$), and the *dashed line* is fit to the $–CH_2X$ substrates and $–CHF_2$ (*red filled triangle*, $y = 1.712x - 184.1$). $–CH_2CF_3$ is also shown but not included in either fit. Experimental C–H bond strengths were used for all substrates except the alkynes. Alkyne C–H bond strengths were calculated (B3LYP) since experimental values are unavailable [13]. The vertical separation of the lines at $D_{C–H} = 100$ kcal mol^{-1} is 8.1 kcal mol^{-1}. Reproduced with permission of the ACS from Jiao et al. [18]

6 Hydrocarbon Activation by [Tp′Rh(P(OMe)$_3$)]

As a third test of the effect of the ancillary or "spectator" ligand on the strength of the metal–carbon bond, we set out to use trimethylphosphite as the ligand. Trimethylphosphite is in between trimethylphosphine and neopentylisocyanide in donor/acceptor strength [19], and therefore, we predicted that the slope for the corresponding range of bond strengths should lie in between those found above. As with the PMe_3 series of compounds, two approaches were examined for the formation of the {Tp′Rh[P(OMe)$_3$]} fragment.

One approach uses Tp′Rh[P(OMe)$_3$]H_2 (**7**) as a photochemical precursor of the fragment, and the second uses Tp′Rh[P(OMe)$_3$]MeH (**8**) as the precursor [20]. As in the case with L = PMe_3, irradiation of **7** in hydrocarbon solvents gave the desired products but also showed evidence of several side products. The use of the thermal precursor showed improved product selectivity, and therefore, this was chosen as the route for preparing hydrocarbon activation products. As in the case of PMe_3, the activation of THF solvent during the preparation of **8** led to the formation of some Tp′Rh[P(OMe)$_3$](tetrahydrofuranyl)H in the solution containing **8**, but both served

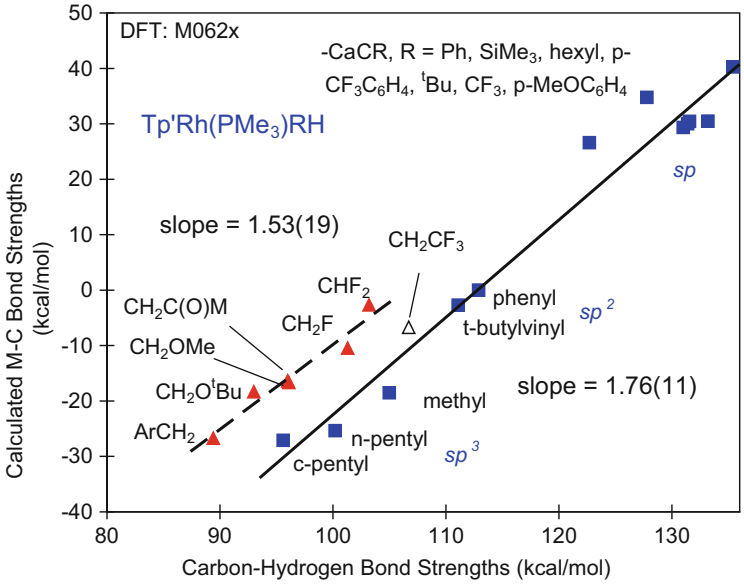

Fig. 6 DFT-calculated plot of relative M–C bond strengths vs. C–H bond strengths for Tp′Rh(PMe_3)(R)H. The *lower line* is fit to the hydrocarbons (*blue filled box*, $y = 1.531x - 162.9$), and the *upper line* is fit to the $-CH_2X$ and CHF_2 substrates (*red filled triangle*, $y = 1.756x - 198.0$). Data for CH_3CF_3 activation is also shown, but not included in the fits. M062X method and basis set 6–31g** for first row atoms and pseudopotentials, additional functions optimized by Stuttgart group for atoms beyond the second row. Experimental C–H bond strengths were used for all substrates except the alkynes. Alkyne C–H bond strengths were calculated (B3LYP) since experimental values are unavailable [13]. The vertical separation of the lines at $D_{C-H} = 100$ kcal mol^{-1} is 12.6 kcal mol^{-1}. Reproduced with permission of the ACS from Jiao et al. [18]

as efficient thermal precursors for {Tp′Rh[$P(OMe)_3$]}. Several hydrocarbon activation products were observed by exchange for methane in **8** (Scheme 4). In the alkyne activations, no evidence was seen for the formation of alkyne π-complexes, again pointing to the need for a strong σ-donor to be present to stabilize the η^2-ligation. In addition, the activation of pentane using **8** was unsuccessful, giving only decomposition after several hours. Instead, Tp′Rh[$P(OMe)_3$](*n*-pentyl)H was prepared by irradiation of **7** in pentane at 10°C. Also, attempted activation of cyclopentane, CH_3CF_3, and CH_2F_2 was unsuccessful, giving only small quantities of the desired products (not enough for use in kinetic studies).

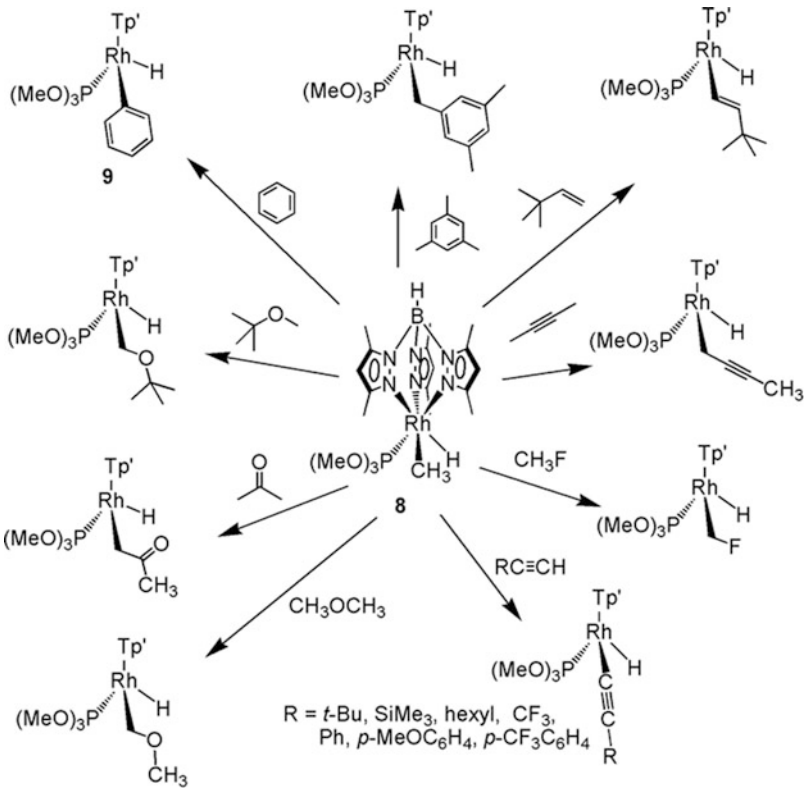

Scheme 4 Reactions of Tp′Rh[P(OMe)$_3$] with hydrocarbon substrates

7 Thermodynamic Determination of Rhodium–Carbon Bond Strengths in Tp′Rh[P(OMe)$_3$](R)H

As with the other ligands, reductive elimination studies were carried out in C_6D_6 solvent to generate hydrocarbon and Tp′Rh[P(OMe)$_3$](C_6D_5)D (**9-*d*$_6$**). The eliminations were carried out at temperatures between 20 and 140°C. To compare these elimination barriers with those of benzene, reductive elimination of C_6H_6 from **9** was carried out at 70–100°C and activation parameters measured for the reductive elimination. An Eyring plot gave $\Delta H^{\ddagger} = 30.7(6)$ kcal/mol and $\Delta S^{\ddagger} = 10.3(3)$ e.u. and permitted comparison of barriers in Fig. 1 at the same temperature. Table 3 summarizes the barrier heights measured and the temperature at which they were measured.

Competition experiments between benzene and the hydrocarbon substrates were examined by photolysis of **7** in a mixture of the two substrates as solvent. Examination of the NMR spectra after a short irradiation time provided the competition data, typically by examination of the area of the hydride resonances of the products.

Table 3 Kinetic and Thermodynamic data for Tp′Rh[P(OMe)$_3$](R)H complexes

R	D(C–H)[a]	$\Delta\Delta G_{oa}^{\ddagger}$ vs. PhH	$\Delta G_{re}^{\ddagger}$	T_{re}(R–H)	ΔG^0 vs. PhH	#H	D_{rel}(M–C)
Ph-	112.9	0	27.61	303	0.01	6	0.0
t-Butylvinyl-	111.1	1.10	27.20	303	1.51	1	−2.3
Methyl-	105.0	0.22	22.64	303	5.20	4	−12.9
n-Pentyl-	100.2	0.67	21.24	298	7.10	6	−19.8
$CF_3C{\equiv}C$-	*135.4*[a]	−0.81	35.01	413	−9.33	1	32.9
n-HexylC≡C-	*131.0*[a]	0.80	35.86	413	−8.57	1	27.7
$Me_3SiC{\equiv}C$-	*131.6*[a]	0.68	36.74	413	−9.58	1	29.3
t-ButylC≡C-	*131.4*[a]	0.89	36.85	413	−9.47	1	29.0
PhC≡C-	*133.2*[a]	0.19	36.63	413	−9.95	1	31.3
p-CF_3phenylC≡C-	*127.8*[a]	0.10	36.25	413	−9.67	1	25.6
p-MeOphenylC≡C-	*122.7*[a]	0.56	35.40	413	−8.35	1	19.2
α-Mesityl-	89.4	0.32	21.86	293	6.18	9	−29.9
-$CH_2C(O)CH_3$	96.0	0.54	25.39	303	2.77	6	−19.7
-$CH_2C{\equiv}CCH_3$	90.7	0.13	25.98	303	1.77	6	−24.0
-CH_2O^tBu	93.0	0.50	25.53	303	2.59	3	−22.1
-CH_2OCH_3	96.1	−0.25	25.24	303	2.13	6	−18.9
-CH_2F	101.3	−0.16	27.92	340	−0.84	3	−10.4

Terminal C–H bond strengths *in italics* for alkynes were calculated using DFT; B3LYP/6-31g**
[a]Energies are in kcal mol^{-1}

The combination of these competition barriers with the reductive elimination barriers gives relative metal–carbon bond strengths with trimethylphosphite as the ancillary ligand, as summarized in Table 3. A plot of D_{rel}(M–C) vs. D_{C-H} is shown in Fig. 7. Here once again, two parallel trends are seen, one for the parent hydrocarbons and one for the substituted methyl derivatives. The slope for the hydrocarbons is 1.55(4), which is similar to that seen with L = PMe_3 (1.54(4)) but smaller than that seen with L = CNneopentyl (1.38(3)). The slope for the substituted methyl derivatives is in between that seen with L = PMe_3 (1.71(8)) and L = CNneopentyl (1.46(19)). Therefore, the effect of the ancillary ligand on rhodium–carbon bond strengths parallels directly the donor ability of the ligand. The better the donor, the wider is the range of metal–carbon bond strengths.

Figure 8 shows the DFT-calculated version of bond strength trends for Tp′Rh[P(OMe)$_3$](R)H complexes. As with the previous two cases, the slopes of the lines are overestimated by about 10%. Does this mean that DFT calculations may be expected to also overestimate the slope in other metal systems? Eisenstein and Perutz made a series of such calculations for both Ti(R)(silox)$_2$(NHSi*t*-Bu$_3$) (silox = OSi*t*-Bu$_3$) and the simplified TpRh(CNMe)(R)H systems [21]. For both systems, about a dozen substrates were considered, and lines were produced with slopes of 1.08 and 1.22, respectively. However, both of these correlations included data for α-mesityl and allyl, and these data can be seen to lie above the correlation for the parent hydrocarbons. From the current studies, we now know why these data

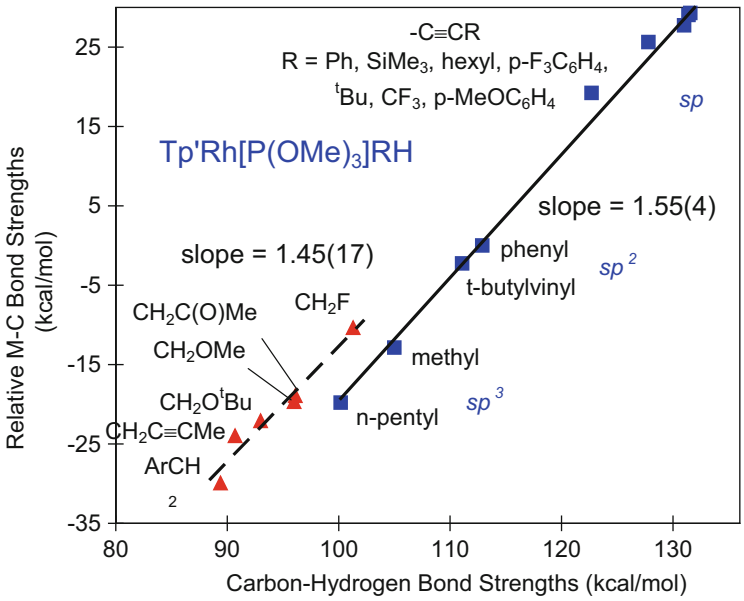

Fig. 7 Plot of relative Rh–R bond strength in Tp′Rh[P(OMe)$_3$](R)H vs. C–H bond strength of hydrocarbon substrates. Experimentally determined D(Rh–C) vs. D(C–H). The *solid line* is fit to the hydrocarbons (*blue filled box*, $y = 1.5501x - 174.59$), and the *dashed line* is fit to the –CH_2X substrates (*red filled triangle*, $y = 1.4535x - 158.06$). Experimental C–H bond strengths were used for all substrates except the alkynes. Alkyne C–H bond strengths were calculated (B3LYP) since experimental values are unavailable [13]. The vertical separation of the lines at $D_{C-H} = 100$ kcal/mol is 6.9 kcal/mol. Reproduced with permission of the RSC from Jiao et al. [20]

lie where they do. Recalculation of the Eisenstein and Perutz data without these points gives revised slopes of 1.33 and 1.71, respectively. The latter is about 24% higher than seen in Fig. 3 (slope = 1.39) and even higher by 7% than the DFT-calculated data seen in Fig. 4 (1.59). This difference between calculated slopes obtained by Eisenstein could be due to either use of a different functional (B3PW91 vs. MO62X) or use of a simplified model or both. The data for the titanium plot also included data for benzyl and methallyl. Removal of these data points gives a slope of 1.33 for the DFT-calculated bond strengths (B3PW91) vs. a slope of 1.35 for experiment, indicating very good agreement. Therefore, DFT can serve as a useful predictor of M–C bond trends, within the above limits.

Furthermore, the observation for all three ligands (PMe_3, $P(OMe)_3$, and CNneopentyl) of a vertical offset for substituted methyl derivatives of about 7 kcal/mol suggests this "additional" bond strength for these ligands might apply generally to other metal complexes. As seen with the data mentioned above by Wolczanski, the substituted methyl data points do indeed lie above the line joining hydrocarbons [22]. Data by Marks for Cp*$_2$Th(R)Cl also show α-benzyl to be an outlier from the trend of six other hydrocarbons [23]. Holland calculated a series of Fe–C bond strengths in (diimine)FeR complexes and found a good linear trend for

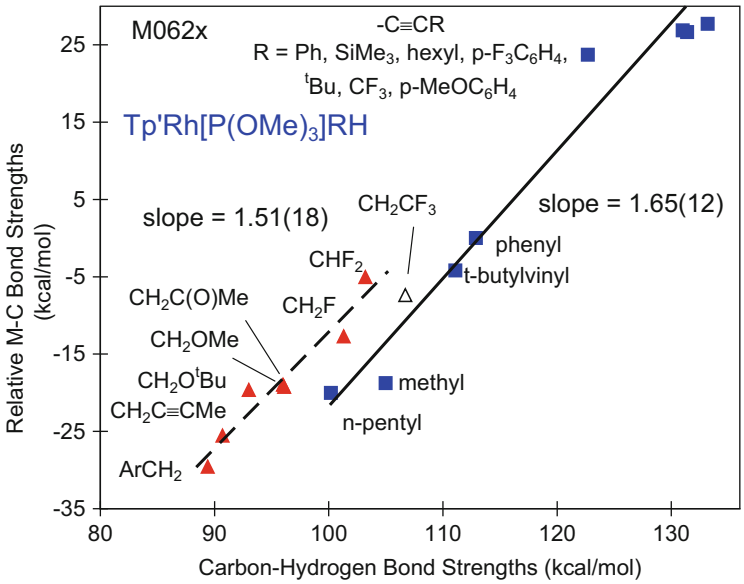

Fig. 8 DFT-calculated D(Rh–C) vs. D(C–H). The *solid line* is fit to the hydrocarbons (*blue filled box*, $y = 1.6527x - 187.02$), and the *dashed line* is fit to the $–CH_2X$ substrates and $–CHF_2$ (*red filled triangle*, $y = 1.508x - 162.94$). Also shown is $–CH_2CF_3$ (*open triangle*) which is not included in either fit. M062X method and basis set 6–31g** for first row atoms and pseudopotentials, additional functions optimized by Stuttgart group for atoms beyond the second row. Experimental C–H bond strengths were used for all substrates except the alkynes. Alkyne C–H bond strengths were calculated (B3LYP) since experimental values are unavailable [13]. The vertical separation of the lines at $D_{C–H} = 100$ kcal/mol is 9.6 kcal/mol. Reproduced with permission of the RSC from Jiao et al. [20]

alkyls [24]. The calculated Fe–C bond strength for $–CH(CH_3)Ph$, however, was found to lie significantly above the line. Landis also calculated relative metal–carbon bond strengths for a series of $H_nM–R$ complexes where R = Me, Et, ^{i}Pr, ^{t}Bu, CH_2F, vinyl, and C≡CH. For 27 different metals (Sc–Au), he observed slopes for M–C vs. C–H plots in the range 1.2–1.9 [25].

Eisenstein and Perutz calculated slopes for fluoroarene activation in [CpRe(CO)L], [CpRhL], and [CpIrL] (L = CO, PH_3) that were 10–20% larger for L = PH_3 than for L = CO [26]. These calculations are in good agreement with the experimental effects seen here for exchange of CNR by PMe_3.

Two other studies worth mentioning here involve the activation of polyfluorinated benzenes $C_6H_nF_{6-n}$ with [Tp′RhL] precursors where L = CNneopentyl or PMe_3. In these reports, a linear correlation is seen between $D_{rel}(M–Ar^F)$ and $D_{ArF–H}$ [15, 27]. However, the slopes observed are 2.14 and 2.15, respectively. Here, replacement of CNneopentyl by PMe_3 appears to have no effect on the range of Rh–C bond strengths. The range of C–H bond strengths spans only 1.5 kcal mol^{-1}, so perhaps the range is too small to see a meaningful trend.

8 Conclusions

This chapter presented studies of C–H activation of sp, sp^2, and sp^3 hybridized carbon containing substrates by reactive [Tp′RhL] precursors (L = CNneopentyl, PMe_3, $P(OMe)_3$). By using the relationship between the kinetics of hydrocarbon reductive elimination and the competition for C–H activation, the thermodynamics for the various activations could be determined. Knowledge of the driving force for a reaction (ΔG^0) allows the determination of the relative rhodium–carbon bond energy. Examination of the trends in M–C bond strength showed four important features.

First, for the parent hydrocarbons (alkanes, alkenes, alkynes), there is a linear relationship between the rhodium–carbon bond strength and the strength of the carbon–hydrogen bond being broken. Second, the range of rhodium–carbon bond strengths exceeds the range of carbon–hydrogen bond strengths by 38–55% depending on the spectator L ligand, resulting in a slope for this linear correlation that is greater than one. This is consistent with a product-driven equilibrium. Third, for substituted methyl derivatives (i.e., Rh–CH_2X, X = F, Cl, CN, OR, Ph, vinyl, keto), the Rh–C bond is about 7 kcal/mol stronger than what would be expected based upon the C–H bond being broken. This "extra" bond strength was attributed to an increase in the ionic character of the metal–carbon bond. Fourth, it was found that a σ-donating L ligand increases the slope of the M–C/C–H correlation, whereas π-acceptors decrease this slope.

Finally, DFT calculations of these same systems with the same substrates show good agreement with the experimentally observed trends. For these systems, however, the DFT calculations overestimate the slopes of the correlations by about 10–12%.

Acknowledgment We thank the U.S. Department of Energy, grant FG02-86ER13569, for their support of this work.

References

1. Hessell ET, Jones WD (1992) Organometallics 11:1496
2. Blaha JP, Dewan JC, Wrighton MS (1986) Organometallics 5:899
3. Bradley MG, Roberta DA, Geoffroy GL (1981) J Am Chem Soc 103:379
4. Geoffroy GL, Bradley MG (1978) Inorg Chem 17:2410
5. Klahn-Oliva AH, Sineer RD, Sutton D (1986) J Am Chem Soc 108:3107
6. Ghosh CK, Graham WAG (1987) J Am Chem Soc 109:4126
7. Jones WD, Hessell ET (1992) J Am Chem Soc 114:6087
8. Jones WD, Hessell ET (1993) J Am Chem Soc 115:554
9. Jones WD, Wick DD (1999) Organometallics 18:495
10. Wick DD, Northcutt TO, Lachicotte RJ, Jones WD (1998) Organometallics 17:4484
11. Northcutt TO, Wick DD, Vetter AJ, Jones WD (2001) J Am Chem Soc 123:7257
12. Wick DD, Reynolds KA, Jones WD (1999) J Am Chem Soc 121:3974

13. Choi G, Morris J, Brennessel WW, Jones WD (2012) J Am Chem Soc 134:9276
14. Jiao Y, Evans ME, Morris J, Brennessel WW, Jones WD (2013) J Am Chem Soc 135:6994
15. Evans ME, Burke CL, Yaibuathes S, Clot E, Eisenstein O, Jones WD (2009) J Am Chem Soc 131:13464
16. Wick DD, Jones WD (2009) Inorg Chim Acta 362:4416
17. Paneque M, Perez PJ, Pizzano A, Poveda ML, Taboada S, Trujillo M, Carmona E (1999) Organometallics 18:4304
18. Jiao Y, Morris J, Brennessel WW, Jones WD (2013) J Am Chem Soc 135:16198
19. Tolman CA (1977) Chem Rev 77:313
20. Jiao Y, Brennessel WW, Jones WD (2014) Chem Sci 5:804
21. Clot E, Mégret C, Eisenstein O, Perutz RN (2006) J Am Chem Soc 128:8350
22. Bennett JL, Wolczanski PT (1997) J Am Chem Soc 119:10696
23. Schock LE, Marks TJ (1988) J Am Chem Soc 110:7701
24. Vela J, Vaddadi S, Cundari TR, Smith JM, Gregory EA, Lachicotte RJ, Flaschenriem CJ, Holland PL (2004) Organometallics 23:5226
25. Uddin J, Morales CM, Maynard JH, Landis CR (2006) Organometallics 25:5566
26. Clot E, Mégret C, Eisenstein O, Perutz RN (2009) J Am Chem Soc 131:7817
27. Tanabe T, Brennessel WW, Clot E, Eisenstein O, Jones WD (2010) Dalton Trans 10495

Top Organomet Chem (2016) 56: 91–114
DOI: 10.1007/3418_2015_118

Published online: 16 June 2015

Catalytic C–H Bond Functionalization of Cyclopropane Derivatives

Daniela Sustac Roman and André B. Charette

Abstract The present work describes a comprehensive review of the functionalization of cyclopropyl C–H bonds via transition-metal catalysis. Compared to the enormous number of publications related to direct sp^2 and sp^3 bond transformations in the last two decades, the first full account of direct cyclopropyl C(sp^3)–H bond functionalization was only disclosed in 2011. Both intra- and intermolecular transformations are detailed in the review, including asymmetric reactions. In addition, mechanistic aspects of various Pd-catalyzed cyclopropane functionalizations are discussed.

Keywords C–H functionalization · Catalysis · Cyclopropane · Palladium

Contents

1 Introduction 92
2 Early Contributions from the Yu and Sanford Groups 92
3 Intramolecular Direct Functionalization of Cyclopropanes 95
4 Intermolecular Direct Functionalization of Cyclopropanes 102
5 Enantioselective Direct Functionalization of Cyclopropanes 106
6 Conclusion and Outlook 110
References 110

D. Sustac Roman and A.B. Charette (✉)
Centre in Green Chemistry and Catalysis, Department of Chemistry, Université de Montréal, P.O. Box 6128, Montréal, QC, Canada H3C 3J7
e-mail: andre.charette@umontreal.ca

1 Introduction

The cyclopropane ring is a versatile building block in organic synthesis [1]. Cyclopropanes possess unique physical, chemical, and electronic properties as a result of ring strain (27.5 kcal/mol) [2, 3]. Found in numerous natural products, the smallest carbocycle has been both a challenge and an inspiration for synthetic organic chemists [4, 5]. Cyclopropanes are also commonly encountered in current drug targets, where they act as conformational restrictors, thereby orienting a molecule into its bioactive conformation and potentially increasing its potency or providing an improvement in metabolic stability of certain compounds [6]. Recently, the cyclopropane ring was ranked 10th in a top 100 list of the most frequently used rings in the synthesis of small molecule drugs, thus highlighting its continual relevance in medicinally active compounds [7].

Significant efforts have been dedicated to the syntheses of cyclopropanes in both racemic or enantioenriched forms [8–10]. Cyclopropanes may also act as precursors en route toward accessing more chemical complexity, via involvement in various reactions such as cycloadditions, ring openings, or cross-couplings. In particular, there is ample literature precedence for the functionalization of cyclopropanes via cross-coupling reactions [11]. The cyclopropane can act as either the "nucleophile" (organometallic reagent) or "electrophile" (cyclopropyl halide). Both roles can require numerous synthetic steps to achieve the pre-functionalized partners, resulting in unnecessary waste. One solution to the problem of pre-functionalization would be to use only one pre-functionalized coupling partner and employ the cyclopropyl C–H bond as a functional group. The inherent ring strain of the three-membered ring and orbital rehybridization results in enhanced acidity of cyclopropane C–H bonds, thereby facilitating such transformations. A commonly encountered problem in the activation of alkanes with transition metals is their propensity for β-hydride elimination [12]. In cyclopropanes, β-hydride elimination would result in the formation of a cyclopropene species, which is unfavorable thermodynamically [11]. While C–H bond functionalization at sp^2 and sp^3 centers has been vastly explored in the last decades [13–16], full reports concerning cyclopropanes have only lately appeared in the literature. The current chapter presents a comprehensive review of the direct transformations of the cyclopropane C–H bond via transition-metal catalysis.

2 Early Contributions from the Yu and Sanford Groups

The functionalization of cyclopropanes such as **1** via amide-directed metalation followed by quenching with an electrophile (e.g., iodine) is well known in the literature (Scheme 1a) [17, 18]. However, it was not until 2005 that the first example of a transition-metal-catalyzed direct functionalization process of a cyclopropane C–H bond was disclosed [19]. The use of a chelating oxazoline-based auxiliary (derived from (*S*)-*tert*-leucinol) enabled iodination of primary C(sp^3)–H

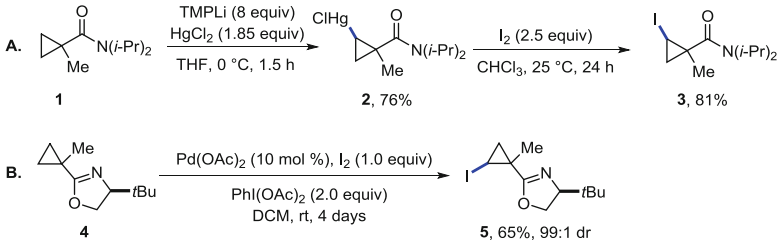

Scheme 1 Cyclopropane functionalization via (**a**) amide-directed metalation and (**b**) Pd-catalyzed diastereoselective iodination

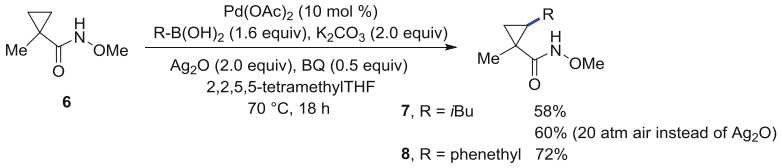

Scheme 2 Yu's Pd-catalyzed alkylation with boronic acids

bonds under Pd catalysis at room temperature. In one example, the secondary C–H group at the β-position of cyclopropyl substrate **4** was exclusively monoiodinated in 65% yield, in preference to the methyl group (Scheme 1b). However, long reaction times (4 days) were required. The oxazoline auxiliary could subsequently be removed under acidic conditions to provide the corresponding cyclopropane carboxylic acid in 99% *ee*.

Later, Yu and coworkers investigated the coupling of C(sp^3)–H bonds with boronic acids, employing $Pd(OAc)_2$ as the catalyst and benzoquinone (BQ)/Ag_2O as oxidants [20] (Scheme 2). The strongly binding, but easily removed, *O*-methyl hydroxamic acid was employed as directing group. The use of 2,2,5,5-tetramethyltetrahydrofuran as solvent was necessary, as it was believed that the bulky solvent not only prevented homocoupling of the boronic acid but also *β*-hydride elimination. Phenethyl and *iso*-butyl boronic acids were employed as coupling partners to provide the corresponding cyclopropyl alkylated products **7** and **8** in 72% and 58% yields, respectively. To improve the practicality of the transformation, the Ag(I) salt could be replaced by air (20 atm) as oxidant.

A unique example of direct olefination of a cyclopropane was also disclosed by the Yu lab [21]. An electron-deficient arylamide was employed as directing group, as the previously employed oxazoline or hydroxamic acid was unreactive in the alkenylation. The proposed mechanism for the reaction involves an amide-directed C–H insertion of the Pd(II) catalyst into the cyclopropane methylene C–H bond of **9**, followed by olefin carbopalladation and β-hydride elimination to provide intermediate **10** (Scheme 3a). Pd(0) is re-oxidized back to Pd(II) by Ag(I)/Cu(II), and a tandem 1,4-addition between the amide moiety of **10** and the acrylate provides the corresponding γ-lactam **11** as the sole isolated product. In the presence of an

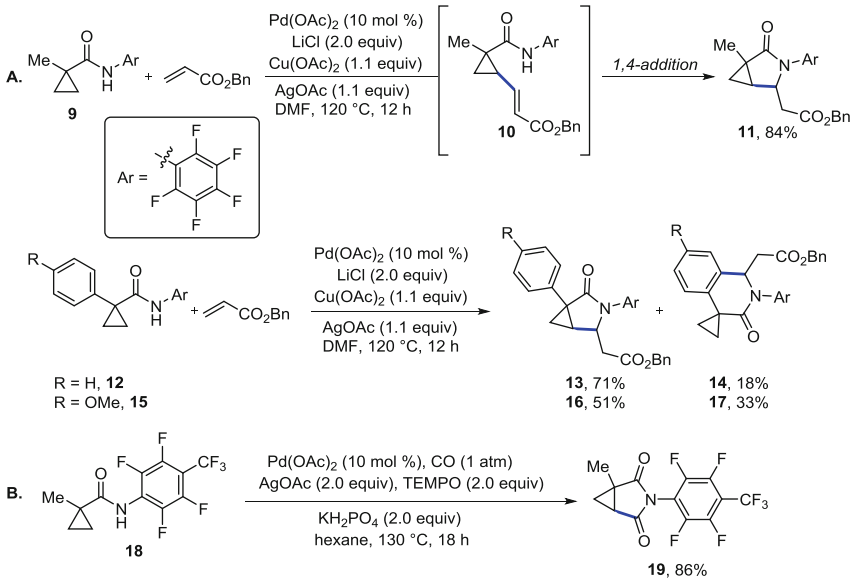

Scheme 3 Yu's (**a**) direct olefination and (**b**) direct carbonylation of cyclopropanes

α-methyl substituent, the cyclopropane C–H bond is olefinated exclusively in 84% yield to deliver a mixture of *cis*-/*trans*-isomers. However, if an α-aryl substituent is present, significant amounts (18% or 33% yield, respectively) of the competitive sp^2 olefination products **14** and **17** are obtained. Direct cyclopropane carbonylation in the presence of an *N*-arylamide auxiliary is also possible under Pd catalysis [22]. After an amide-directed Pd activation of the cyclopropyl C–H bond of **18**, a migratory insertion of CO takes place, and the subsequent Pd intermediate undergoes C–N reductive elimination to provide a succinimide product **19** in 86% yield (Scheme 3b). More recently, Chatani demonstrated cyclopropyl carbonylation in the presence of an *N*,*N*-bidentate group under $Ru_3(CO)_{12}$ catalysis [23].

Sanford and Kubota investigated the functionalization of cyclopropanes under oxidative conditions, employing directing groups such as oximes or pyridines [24]. Iodination of the cyclopropyl C–H bond was found to be dependent on the steric and electronic environment of the auxiliary; for example, in the absence of the methyl group at the α-position of oxazoline **16**, there was no conversion to product (Scheme 4a). Various substituted pyridines (**21**, **23**, and **25**) could direct the iodination, albeit in low yields, even after long reaction times (Scheme 4a). Attempts at cyclopropane acetoxylation with $PhI(OAc)_2$ using various directing groups, as shown for substrates **4** and **27**, resulted in ring opening of the three-membered ring leading to allylic acetates **28** and **29** (Scheme 4b). In a subsequent communication, Sanford and coworkers disclosed one example of alkenylation of a cyclopropyl C–H bond, resulting in the formation of cyclized pyridinium product **30** in a modest 43% yield (Scheme 4c) [25]. The reaction employed a cationic Pd

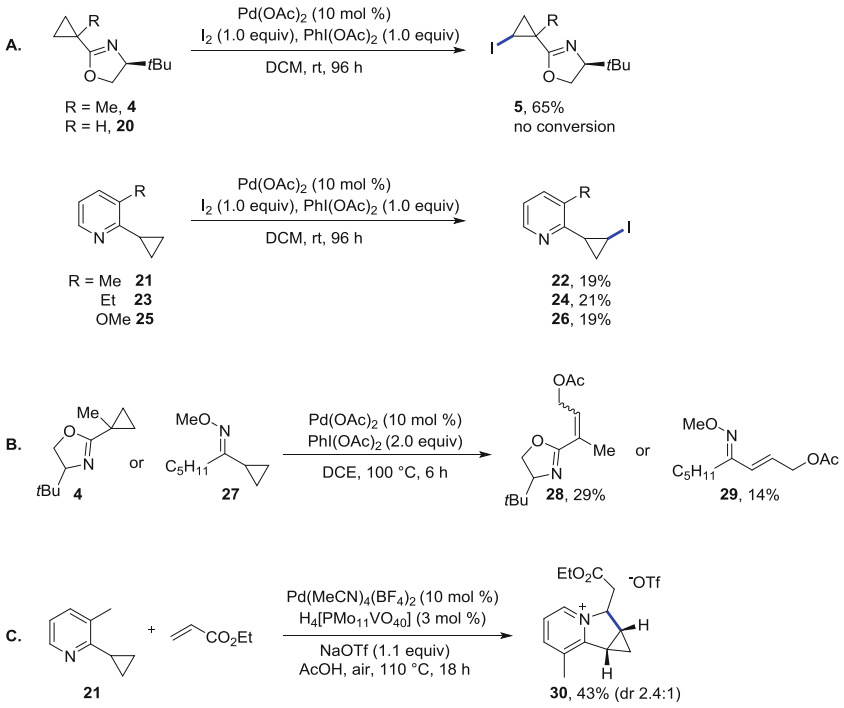

Scheme 4 Cyclopropane functionalization reactions from the Sanford group (**a**) iodination, (**b**) acetoxylation, and (**c**) alkenylation

catalyst, as well as a vanadium-based heteropolyacid ($H_4[PMo_{11}VO_{40}]$) and air as co-oxidants.

3 Intramolecular Direct Functionalization of Cyclopropanes

Similar to the intramolecular functionalization of aryl or alkyl substrates, use of a heteroatom containing-tether not only limits the degree of freedom in the system but also allows for coordination of a transition metal, thus facilitating the reaction.

Rousseaux, Liegault, and Fagnou reported the elegant formation of quinoline and tetrahydroquinoline derivatives via a Pd(0)-catalyzed C–H activation of cyclopropane methylene bond [26]. Both bromophenyl and chlorophenyl cyclopropyl carbamates **31** and **32** were found to be suitable substrates for the transformation into dihydroquinoline **33**, albeit under slightly different conditions (Scheme 5). It was found that the resulting dihydroquinolines **33** were prone to decomposition; thus protocols for either oxidation or reduction of the unstable intermediates were developed. A variety of substituents (nitro, cyano, trifluoromethyl, methoxy, ester)

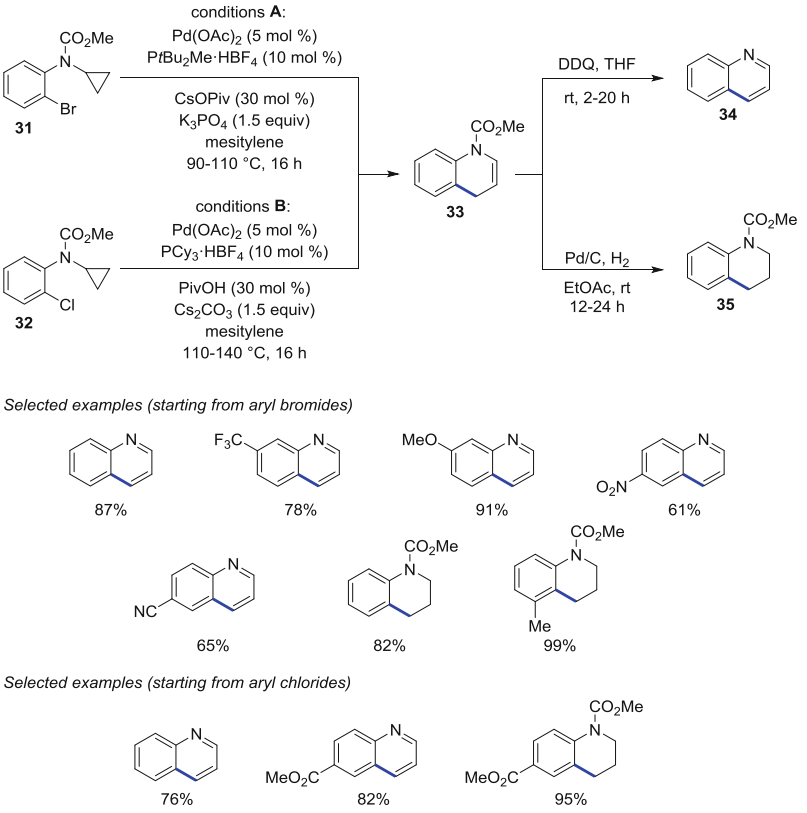

Scheme 5 Synthesis of quinoline and tetraquinoline derivatives via intramolecular cyclopropyl C–H functionalization

were tolerated in the positions *para* and *meta* to the bromide or chloride. A methyl in the *ortho* position provided the corresponding tetrahydroquinoline in 99% yield, demonstrating that the reaction is not sensitive to steric effects.

The authors then investigated the reaction pathway, focusing on whether a concerted metalation–deprotonation (CMD) step occurred prior to the cyclopropane ring opening (recent examples of Pd-catalyzed ring opening of cyclopropanes: [27, 28], [29]). In the absence of a pivalate source, no dihydroquinoline **33** was observed in the cyclization, underlining the involvement of pivalate in the CMD step. Traces of cyclopropyl product **36** were isolated from the reaction of chlorophenyl cyclopropyl carbamate **32**, suggesting the presence of **36** as a possible intermediate in the mechanism (Scheme 6). However, a subsequent control reaction demonstrated that **36** does not undergo ring opening when submitted to the reaction conditions. The result supports the mechanistic proposal that the C–H activation step occurs prior to ring opening and the ring opening of the cyclopropane precedes reductive elimination.

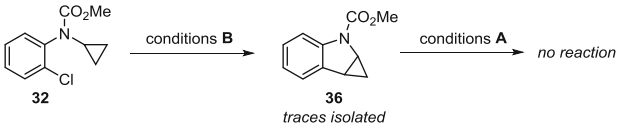

Scheme 6 Control reactions

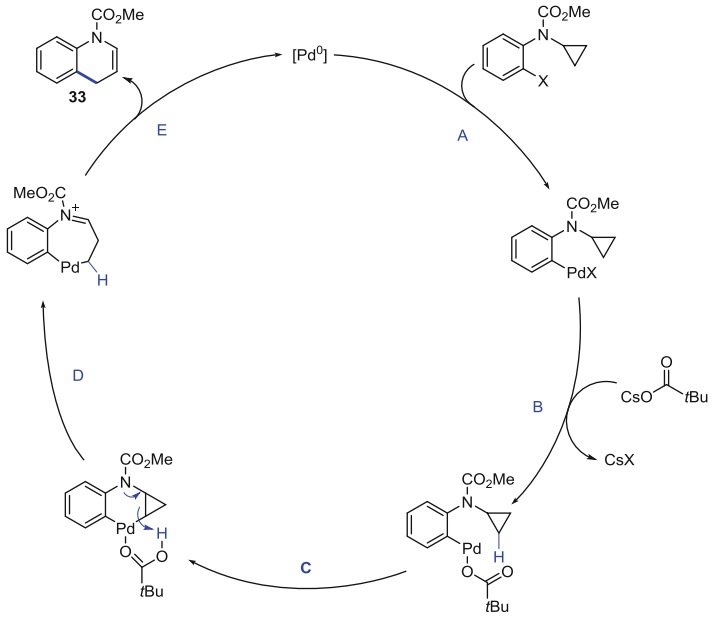

Scheme 7 Proposed reaction mechanism for the formation of dihydroquinoline **33**

Based on the studies, the following mechanism was proposed: oxidative addition of Pd(0) into the aryl halide bond (step A, Scheme 7) is followed by ligand exchange to provide a Pd(II)-pivalate species (step B). Then, pivalate-assisted CMD of the cyclopropyl C–H bond results in the formation of a six-membered palladacycle (step C), which undergoes a cyclopropane ring opening/proton transfer to release ring strain (step D). Deprotonation and reductive elimination (step E) provides the dihydroquinoline **33**.

A further example of cyclopropyl C–H activation followed by ring opening and cyclization was reported by the Charette group in the synthesis of novel seven-membered benzo[*c*]azepine-1-one products [30]. Both bromo- and iodo-cyclopropyl benzamides **37** and **38** were effective substrates for the transformation, providing two isomeric benzazepine-type products **39** and **40** in excellent overall yield (Scheme 8a). When each isomer was separately resubmitted to the reaction conditions, no change was observed for **39**, while **40** slightly isomerized to **39**, suggesting that **40** is the kinetic product and **39** the thermodynamic one. When cyclopropyl benzamide **37** is submitted to Fagnou's reaction conditions with

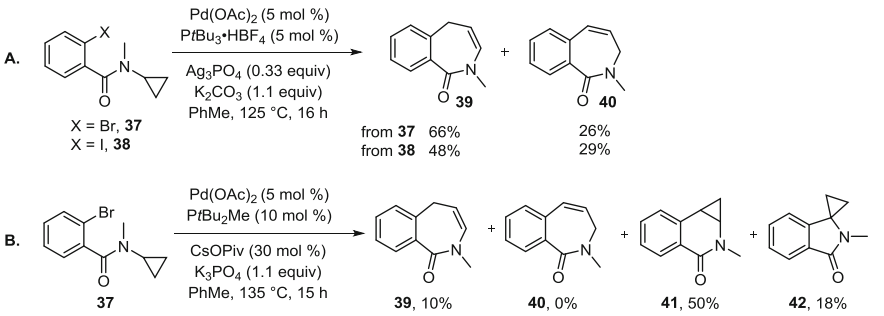

Scheme 8 Synthesis of benzo[*c*]azepine-1-ones, (**a**) optimized reaction conditions, (**b**) pivalate-promoted reaction

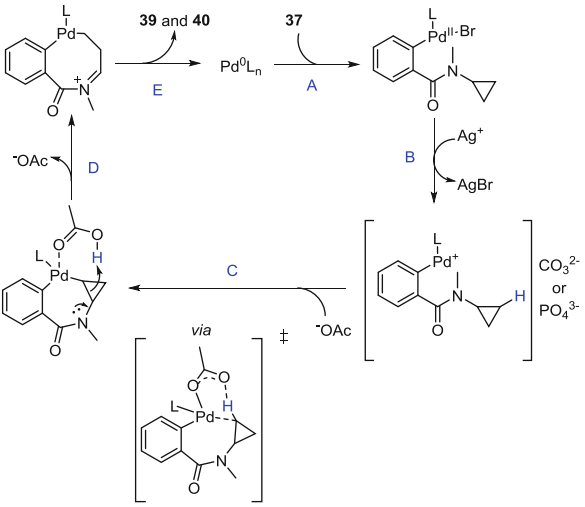

Scheme 9 Plausible mechanism for the formation of benzo[*c*] azepine-1-ones

cesium pivalate, a mixture of spirooxindoles **41** and **42**, as well as benzazepine **39,** is produced, suggesting the intermediacy of **41** in the reaction pathway. However, similar to the control reaction performed in the former Fagnou's report (Scheme 6), **41** was fully recovered when submitted to the optimized reaction conditions. In contrast to other uses of Ag(I) salts as halide sequesters or oxidants, the authors highlight the employment of exactly 1 equiv. Ag^+ as a halide abstractor to provide a reactive cationic Pd species.

The proposed mechanism involves an initial oxidative addition (step A, Scheme 9), followed by halide abstraction by the silver ion to provide a highly reactive cationic Pd species (step B). Acetate-mediated CMD (step C) provides a rare seven-membered ring palladacycle which undergoes ring opening (step D), followed by deprotonation/reductive elimination (step E) to provide the desired products.

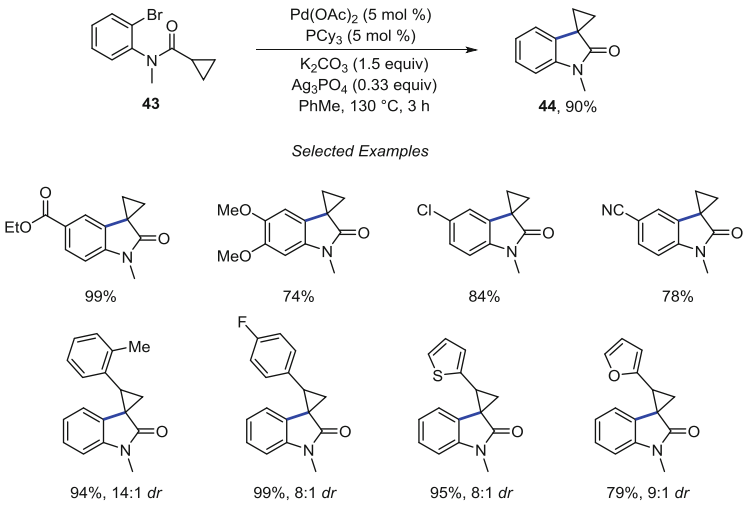

Scheme 10 Pd-catalyzed, Ag-mediated synthesis of 3,3′-cyclopropyl spirooxindoles

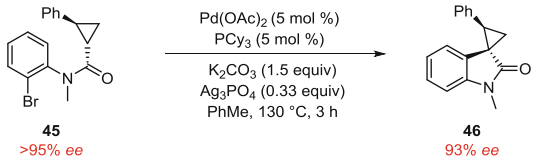

Scheme 11 Epimerization studies of enantioenriched **45**

Additionally, Charette and coworkers disclosed the synthesis of biologically active 3,3′-cyclopropyl oxindole **44** via a Pd-catalyzed, Ag-promoted C–H functionalization of cyclopropanecarboxamide **43** derived from 2-bromoaniline (Scheme 10) [31]. Substitution on the aryl ring or on the cyclopropane, including heterocycles such as furan or thiophene, was well tolerated. A mixture of diastereomers was obtained when aryl substitution was present on the cyclopropane. X-ray crystallography confirmed the structure of both diastereomers.

To investigate whether an enolate arylation was occurring, the authors prepared enantioenriched cyclopropane substrate **45** and submitted it to the reaction conditions (Scheme 11). After 3 h, all starting material was consumed, and spirooxindole product **46** showed little erosion of enantioselectivity. Furthermore, the kinetic isotope effect was determined via parallel reactions to be 3.9, identifying C–H cleavage as a rate-determining step. This observation is not consistent with an enolate-like pathway. Furthermore, the use of a weak base (K_2CO_3) makes the enolate pathway quite unlikely.

Based on all the observations, the mechanism shown in Scheme 12 was proposed. An initial oxidative addition step A is followed by bromide abstraction by Ag^+ to give a cationic Pd species (step B), which can undergo a concerted

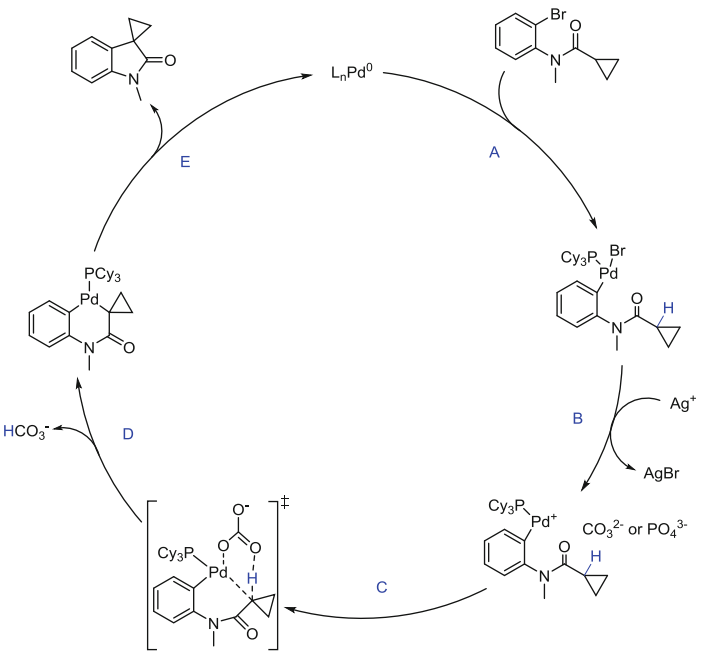

Scheme 12 Proposed reaction mechanism for the synthesis of 3,3′-cyclopropyl spirooxindoles

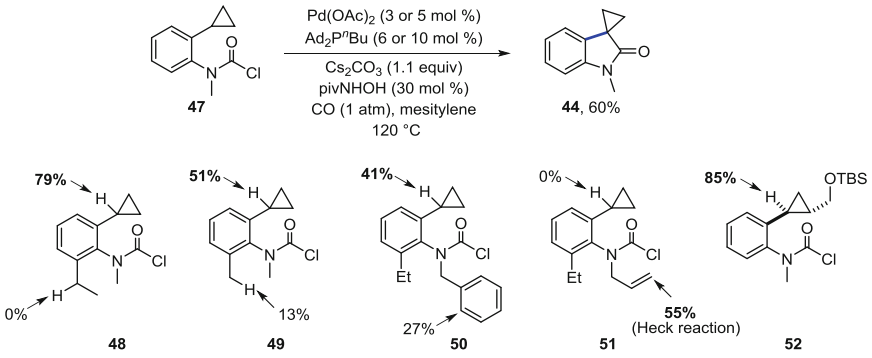

Scheme 13 Takemoto's synthesis of spirooxindoles and order of reactivity experiments

metalation–deprotonation step mediated by carbonate (or phosphate, C and D). The six-membered palladacycle then undergoes reductive elimination (step E) to give the product and regenerate the Pd^0 catalyst.

A related synthesis of 3,3′-cyclopropyl oxindoles was reported by Takemoto et al. [32]. Carbamoyl chloride **47**, containing a cyclopropyl ring at the *ortho* position, undergoes a Pd-catalyzed cyclization onto the benzylic C–H bond of the cyclopropane to provide the corresponding spirooxindole **44** in 60% yield (Scheme 13). Intramolecular competition reactions investigated the chemoselectivity of the

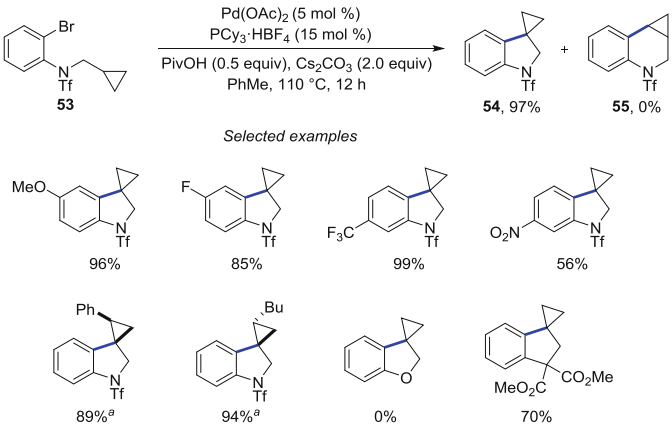

Scheme 14 Pd-catalyzed, pivalate-promoted synthesis of cyclopropyl spiroindolines. [a]With PPh_3 (15 mol%)

cyclization on the cyclopropane C–H bond versus ethyl (**48**), methyl (**49**), phenyl (**50**), and alkene (**51**). The order of reactivity under the optimized conditions was determined to be the Heck reaction > cyclopropyl C(sp^3)–H activation > C(sp^2)–H activation > methyl C(sp^3)–H activation. In addition, the stereochemistry of the starting material is transmitted to the substrate, as *trans*-substituted **52** provided the corresponding *trans*-spirooxindole in 85% yield.

The Cramer group further reported a synthesis of cyclopropyl spiroindolines [33]. Cyclopropyl substrate **53**, containing a triflyl-protected aniline, undergoes a Pd(0)-catalyzed, pivalic acid-mediated methine C–H activation via a CMD process (Scheme 14). Remarkably, only the five-membered spiroindoline **54** is isolated which can be explained through the easier formation of a six- versus seven-membered palladacycle intermediate. Various functional groups are tolerated in the transformation, including substitution on the cyclopropane with an aryl or alkyl group. In the latter cases, the stereochemistry of the starting material (either *cis* or *trans*) is transferred to the products. A malonate-containing substrate can successfully replace the *N*-triflyl group, but the oxygen analog failed to cyclize to the desired product. In case of 2,6-dibromoaniline **56**, the intramolecular cyclopropane arylation could be followed by a Suzuki coupling to provide **57** in 77% yield or intermolecular C–H arylation to provide **58** in 78% yield in a domino-type reaction (Scheme 15). The triflyl protecting group can be removed by reaction with Red-Al.

Baudoin et al. showed that both methine and methylene cyclopropane C–H bonds can be activated under Pd catalysis to provide the corresponding indanes **60** and **62** (Scheme 16) [34]. The methine functionalization is more efficient (68% vs. 39% yield), due to the formation of a less strained five-membered ring.

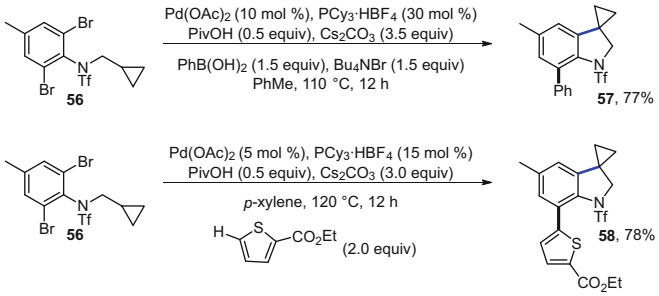

Scheme 15 Domino cyclopropane arylation followed by Suzuki coupling or heterocycle arylation

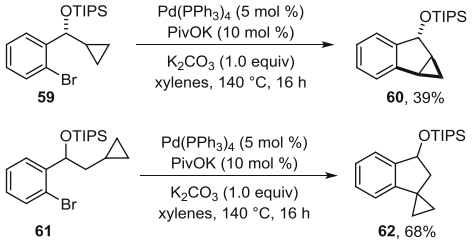

Scheme 16 Intramolecular cyclization onto methylene and methine cyclopropane C–H bonds

4 Intermolecular Direct Functionalization of Cyclopropanes

The concept of bidentate coordination being able to promote sp^2 or sp^3 C–H activation has been well known in the literature [35]. In comparison to monodentate coordination, bidentate groups maintain a higher degree of stereochemical control around the metal center, which enables the formation of more rigid cyclometalated species. Daugulis et al. introduced the picolinamide and aminoquinolinamide auxiliaries for Pd-catalyzed direct arylation of C(sp^2)–H and C(sp^3)–H centers with aryl iodides [36, 37]. The initial report by Daugulis inspired many other groups to utilize the abovementioned auxiliaries in a wide range of transformations, including C(sp^3)–H arylation or C–heteroatom bond formation [38].

In 2013, Babu et al. [39] and Charette et al. [40] disclosed the direct arylation of cyclopropanes employing the aminoquinolamide and picolinamide auxiliaries, respectively. Thus, the Babu group showed that the methylene C–H bond of cyclopropyl substrate **63** can be functionalized with excess aryl iodide in the presence of catalytic $Pd(OAc)_2$ and stoichiometric AgOAc (Scheme 17) [39]. 2-Methylthioanilide **67** could also be employed as auxiliary; however the arylated cyclopropanes **68** and **69** were obtained in lower yields. Monoarylated cyclopropanes **64–66** and **68–69** were obtained as the *cis*-diastereomer; moreover, *cis*-diarylated cyclopropanes can be obtained when excess (8 equiv.) aryl iodide is employed. It is also possible to access mixed triarylated cyclopropylcarboxamides

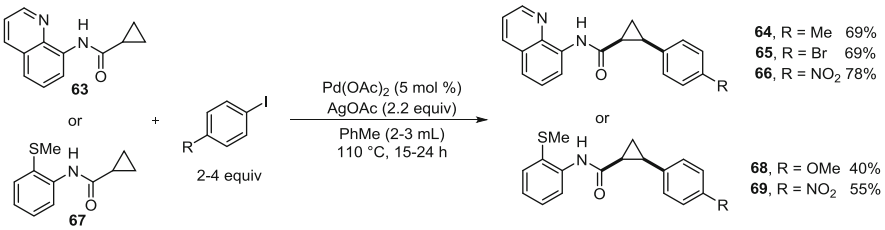

Scheme 17 Aminoquinolamide and 2-methylthioanilide-enabled arylation of cyclopropanes

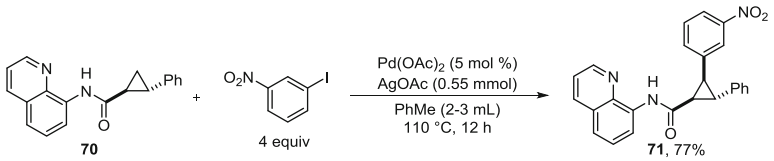

Scheme 18 Synthesis of trisubstituted cyclopropanes

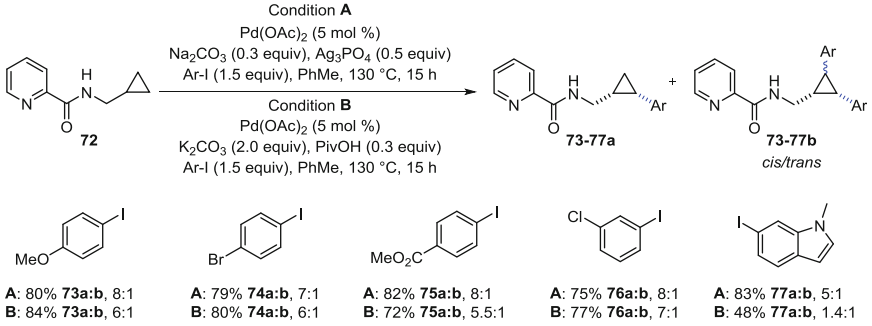

Scheme 19 Picolinamide-directed arylation of cyclopropanes with (hetero)aryl iodides

such as **71** starting from *trans*-disubstituted cyclopropane **70** (Scheme 18). Later, Zeng et al. disclosed one example of the arylation of aminoquinolamide cyclopropane **63** with 4-bromoanisole; however, the yield was only 18% even after 36 h at 140°C [41].

The latter report from the Charette lab disclosed two distinct reaction conditions for the arylation of cyclopropylmethyl picolinamide **72**, employing either excess Ag^+ in the form of Ag_3PO_4 (condition A) or catalytic PivOH (condition B), along with catalytic $Pd(OAc)_2$ (Scheme 19) [40]. The *cis*-diastereomer **73–77a** is obtained exclusively, but in many cases traces of diarylated cyclopropanes **73–77b** (*cis* and *trans*) were observed. The picolinamide group could be transformed into the corresponding *tert*-butylcarbamate by reaction with Boc_2O, followed by oxidative cleavage in the presence of LiOH and H_2O_2. Only aryl iodides were tolerated as coupling partners in the reports from Babu and Charette.

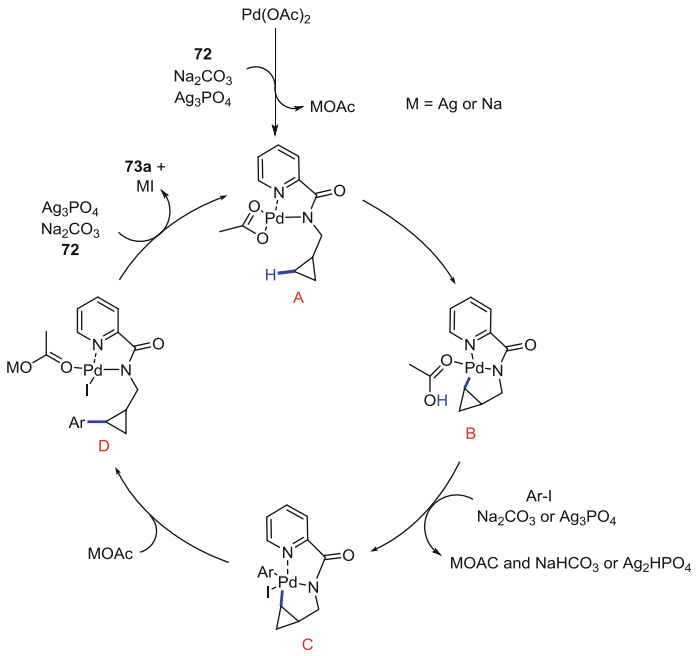

Scheme 20 Proposed mechanism for picolinamide-enabled cyclopropane arylation

Mechanistic evidence from the Daugulis lab [36, 37] and others [42] supports a Pd(II)/(IV) pathway for bidentate-directed C–H functionalization. Sustac and Charette also investigated the mechanism of their cyclopropane arylation [40]. It was determined that an acetate source was necessary for the reaction to proceed, because it is presumably involved in the CMD step. Both Pd(0) and Pd(II) sources could be employed in the Ag-mediated reaction. The silver source is proposed to aid with catalyst regeneration by removing iodide or, in the case of Pd(0) sources, to oxidize them to Pd(II). The proposed mechanism is shown in Scheme 20. Coordination of $Pd(OAc)_2$ to the picolinamide **72** to give complex **A** occurs with loss of one acetate molecule. Then, acetate-mediated concerted metalation–deprotonation provides complex **B**. Oxidative addition of the aryl iodide gives rise to a highly unstable Pd^{IV} complex **C**, which undergoes reductive elimination to provide complex **D**. Loss of iodide mediated by Ag_3PO_4 or Na_2CO_3 and product dissociation and coordination of Pd^{II} to another picolinamide molecule **72** close the catalytic cycle.

The aminoquinolinamide auxiliary was also shown to mediate the construction of 1,1,2-trisubstituted arylcyclopropanes [43]. Substrate **78**, bearing a *cis*-substituted cyclopropyl moiety, reacted smoothly with a variety of (hetero)aryl iodides in a Pd-catalyzed, Ag-mediated transformation (Scheme 21). Notably, substituents such as an aldehyde, a hydroxyl, or an unprotected indole were tolerated under the reaction conditions. Additionally, the reactivity of *trans*-cyclopropyl substrate **79** was investigated (Scheme 21). The challenge here was

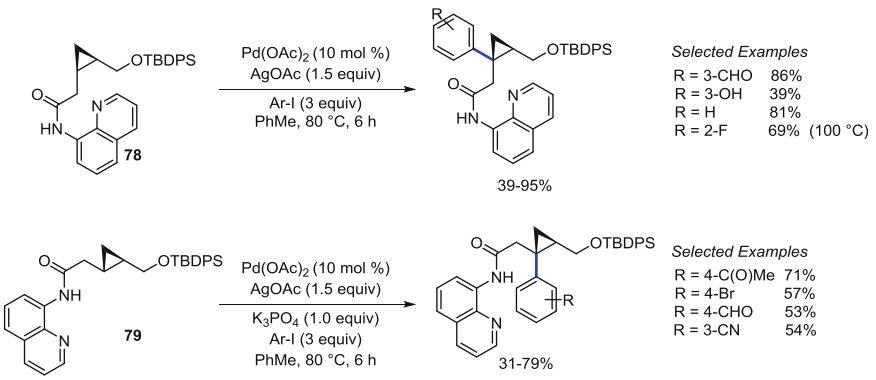

Scheme 21 Synthesis of quaternary centers starting from *cis*- or *trans*-substituted cyclopropanes

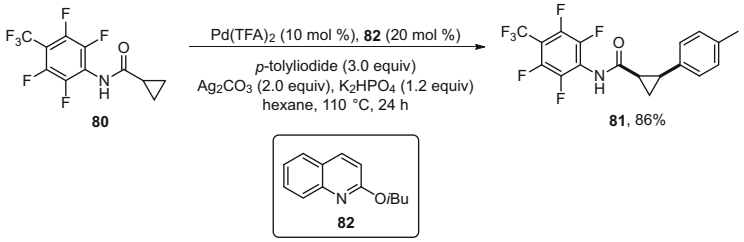

Scheme 22 Pd-catalyzed arylation of cyclopropane **80** enabled by ligand **81**

overcoming the steric effect of the bulky TBDPS group. It was discovered that adding the base K_3PO_4 improved the yield of the reaction (41% without vs. 75% with 1 equiv. K_3PO_4). Various aryl iodides acted as coupling partners in modest to good yields; in general, the yields were lower than in the case of the *cis*-substrate, presumably due to steric effects. Nonetheless, the reaction represents one of the few examples of intermolecular formation of quaternary centers via tertiary C(sp^3)–H functionalization of cyclopropanes.

The Yu group employed a weakly coordinating *N*-arylamide group for the monoarylation of a cyclopropane **80** with *p*-iodotoluene in the presence of 2-isobutoxyquinoline (**82**) as the ligand (Scheme 22) [44]. The ligand had the property of being "mutually repulsive": it allowed for single coordination of Pd to its pyridine portion but also coordination of Pd to the arylamide group of **80**. Such a coordination mode results in an overall lowering the transition state energy of the C(sp^3)–H activation.

Furthermore, selective monoarylation of 1-aminocyclopropane-1-carboxylic acid derivative **83** was achieved in the presence of alkoxy-substituted quinoline **85** in good yield (Scheme 23) [45]. Only one diastereomer of the unnatural amino acid derivative **84** was produced.

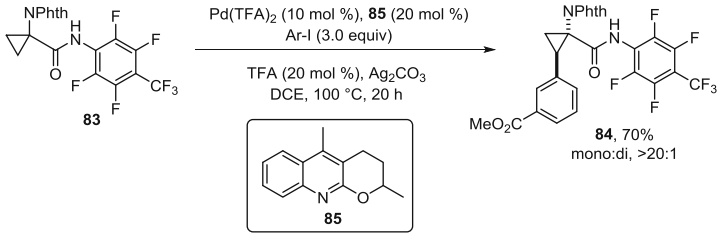

Scheme 23 Selective cyclopropane monoarylation in the presence of alkoxy-quinoline **85**

5 Enantioselective Direct Functionalization of Cyclopropanes

The asymmetric synthesis of cyclopropanes has attracted continual efforts in organic synthesis, due to their relevance in natural products and biologically active compounds. The prevalent methods employed include halomethylmetal mediated processes in the presence of chiral auxiliaries/catalysts (Simmons–Smith-type reactions), transition-metal-catalyzed decomposition of diazoalkanes, Michael-induced ring closures, or asymmetric metalations [8–10, 46]. However, the asymmetric preparation of unfunctionalized cyclopropanes remains relatively undisclosed. The enantioselective activation of unactivated C–H bonds via transition-metal catalysis is an area of active research in organic chemistry [47–49]. Recently, a few groups investigated the enantioselective synthesis of cyclopropanes by direct functionalization reactions.

An intramolecular process for the asymmetric Pd-catalyzed C–H arylation of cyclopropanes was published by the Cramer group [50]. An initial screening of different classes of ligands found TADDOL-type phosphoramidites promising in the synthesis of tetrahydroquinoline **87**. Fine-tuning of the TADDOL structure revealed that ligand **86**, containing 3,5-xylyl substituents, along with the addition of catalytic amounts of pivalic acid to the reaction, provided the best yields and enantiomeric excesses (Scheme 24). The transformation also represented a rare example of the formation of a seven-membered palladacycle as a reaction intermediate. Notably, the cyclization can be performed with catalyst loadings as low as 1 mol%, without affecting the yield or enantioselectivity. Various α-substituted cyclopropanes were tolerated in the reaction to provide the corresponding tetrahydroquinolines **87**–**90**. Of note, the presence of a phenyl or benzyl group in compounds **88** and **89**, respectively, did not result in a competing C(sp^2)–H functionalization. In contrast, the absence of α-substitution led to the synthesis of spiroindolines (Scheme 14, vide supra). The triflyl group of **88** was cleaved by reaction with Red-Al in an excellent 99% yield.

A system consisting of a chiral NHC ligand and a Pd(0) catalyst was shown to activate racemic cyclopropyl substrate **91** in a publication by Kündig et al. [51]. The reaction was not selective as a 1:1 mixture of products arising from the reaction of

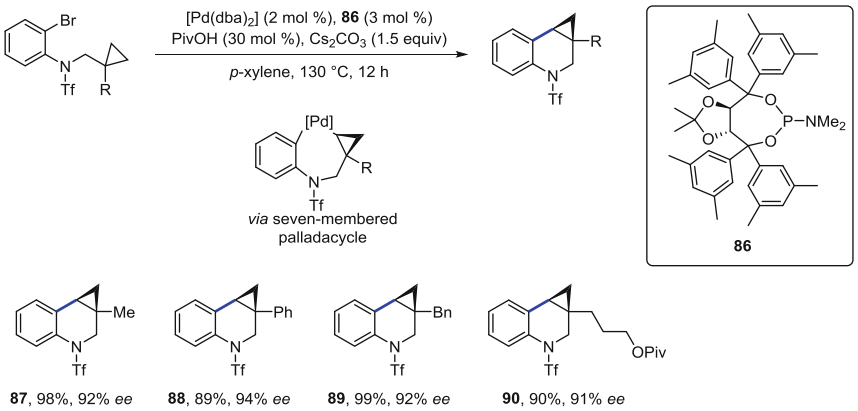

Scheme 24 Pd-catalyzed enantioselective aylation of cyclopropanes in the presence of TADDOL-derived ligand **86**

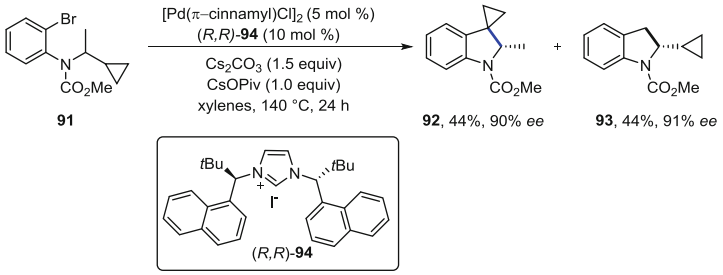

Scheme 25 Enantioselective cyclopropane functionalization promoted by NHC ligand **94**

the cyclopropyl methine C–H bond (compound **92**) and methyl C–H bond (compound **93**) was obtained (Scheme 25).

In 2011, the Yu group disclosed the first example of intermolecular enantioselective C–H functionalization of cyclopropanes [52]. Initially, the cross-coupling of amide cyclopropane **95** with phenylboronic acid pinacol ester (Ph-BPin) was investigated in the absence of a chiral ligand. It was established that the transformation takes place at 100°C, in the presence of $Pd(OAc)_2$ as the catalyst, giving rise to a 2:1 mixture of mono- and diarylated *cis*-cyclopropanes **96** and **97**, respectively. Alkyl potassium trifluoroborates were also compatible coupling partners, when the base was changed to Li_2CO_3 (Scheme 26).

A thorough screen of amino acids and their derivatives led to the application of chiral ligand **98** derived from phenylalanine in the intermolecular arylation of cyclopropane derivatives (Scheme 27) [52]. Albeit not practical, the addition of the catalyst and ligand in two batches at 40°C was optimal for the yield and enantioselectivity. Traces of water were also required in the transformation, and it was speculated that water aided in the transmetalation step. Ph-BPin was the best nucleophile, while the employment of alkyl boronic esters required increased

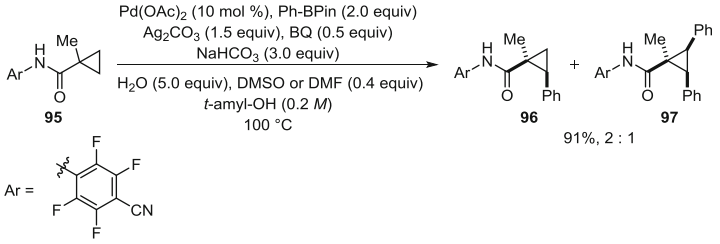

Scheme 26 Optimized conditions for coupling of amide cyclopropane **95** with phenyl boronic ester

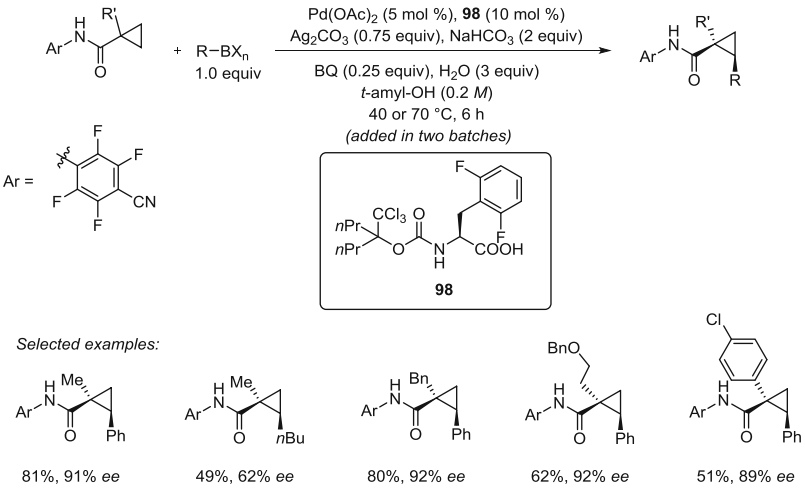

Scheme 27 Enantioselective arylation of cyclopropanes in the presence of mono-protected amino acid ligand **98** and selected examples

temperatures (70°C), leading to slightly lower yields and enantioselectivities. It was also necessary to block the α-position of the cyclopropane in all examples, leading in some cases to lengthy syntheses of the starting materials. Nonetheless, groups such as methyl, isopropyl, cyclopentyl, β-benzyl ethers, γ-protected amines, or even aryls were tolerated in the α-position.

Most recently, the Yu group employed a triflyl-protected amine as a directing group in the asymmetric, intermolecular, and Pd-catalyzed functionalization of cyclopropylmethylamine **99** with aryl iodides (Scheme 28) [53]. Judicious screening of chiral mono-*N*-protected amino acids revealed Boc-L-Val-OH as the ideal ligand. In general, amino acid side chains that were branched (vs. linear) provided better enantioselectivities, while carbamates (e.g., Boc, Fmoc, Cbz) were desirable as *N*-protecting groups. Remarkably, the reaction provided exclusively the monoarylated product **100**, as in all cases the remaining mass balance consisted of unreacted starting material. Furthermore, in contrast to the previous report [52], the presence of a substituent in the α-position of the cyclopropane was not required for reactivity.

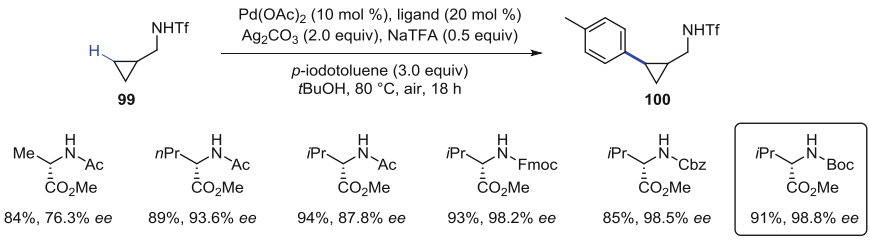

Scheme 28 Screen of ligands for the arylation of cyclopropane **99**

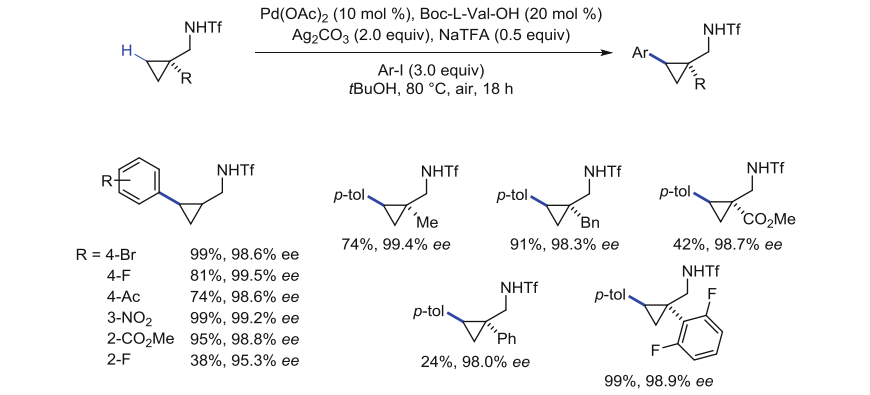

Scheme 29 Enantioselective arylation of cyclopropanes with various aryl iodides

The cyclopropyl methylene C–H bond was exclusively functionalized in the presence of competing aryl, benzyl, or methyl C–H bonds (Scheme 29). Additionally, a wide array of substituted aryl iodides could be employed as coupling partners in excellent yields and enantioselectivities; notably, an ester substituent on the cyclopropane was tolerated, affording the corresponding product in 42% yield. However, heteroaryl iodides were unreactive which represents a limitation to the methodology.

In contrast with the initial report employing boronic esters that follow a Pd(II)/(0) pathway [52], the current methodology is proposed to occur via a Pd(II)/(IV) mechanism. No reaction was observed in the presence of a Pd(0) source or in the absence of the silver salt. A plausible catalytic cycle involves an initial C–H activation step of palladium complex **A** to provide palladacycle **B**, followed by oxidative addition of the aryl iodide to give a highly reactive Pd(IV) complex **C**, which undergoes rapid reductive elimination to provide the desired product and a Pd(II) complex **D** (Scheme 30). The last step is loss of iodide, mediated by the silver salt. The use of the weakly coordinating –NHTf group by the Yu lab has allowed for the development of the first intermolecular and enantioselective C(sp^3)–H activation via a Pd(II)/(IV) catalytic cycle.

Scheme 30 Plausible mechanism for cyclopropane arylation via a Pd(II)/(IV) pathway

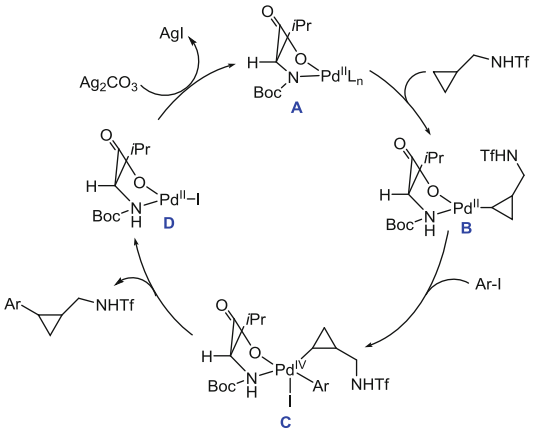

6 Conclusion and Outlook

Over the last decade, continued interest in transition-metal-catalyzed C(sp^3)–H bond functionalization reactions has allowed for the development of several methodologies for direct transformations of cyclopropanes. Intramolecular reactions resulted in the synthesis of biologically relevant cyclopropyloxindoles, as well as access to complex quinoline- or benzazepine-type products. Intermolecular transformations employed strongly binding auxiliaries or weakly coordinating directing groups to achieve arylation of cyclopropanes. A significant breakthrough represented the asymmetric direct arylation of cyclopropanes; in particular, contributions from the Yu group have put forward the use of mono-protected amino acids as chiral ligands in Pd(0)/(II) or Pd(II)/(IV) catalysis. Although at the moment the use of Pd salts as catalysts for the activation of cyclopropanes is predominant, it is desirable that less expensive metals such as Cu, Fe, Ni, or Co are also explored for the transformation.

References

1. Wong HNC, Hon MY, Tse CW, Yip YC, Tanko J, Hudlicky T (1989) Use of cyclopropanes and their derivatives in organic synthesis. Chem Rev 89(1):165–198
2. de Meijere A (1979) Bonding properties of cyclopropane and their chemical consequences. Angew Chem Int Ed 18(11):809–826
3. Exner K, Schleyer PR (2001) Theoretical bond energies: a critical evaluation. J Phys Chem A 105(13):3407–3416
4. Chen DYK, Pouwer RH, Richard J-A (2012) Recent advances in the total synthesis of cyclopropane-containing natural products. Chem Soc Rev 41(13):4631–4642
5. Pietruszka J (2003) Synthesis and properties of oligocyclopropyl-containing natural products and model compounds. Chem Rev 103(4):1051–1070

6. Reichelt A, Martin SF (2006) Synthesis and properties of cyclopropane-derived peptidomimetics. Acc Chem Res 39(7):433–442
7. Taylor RD, MacCoss M, Lawson ADG (2014) Rings in drugs. J Med Chem 57(14):5845–5859
8. Lebel H, Marcoux J-F, Molinaro C, Charette AB (2003) Stereoselective cyclopropanation reactions. Chem Rev 103(4):977–1050
9. Pellissier H (2008) Recent developments in asymmetric cyclopropanation. Tetrahedron 64 (30–31):7041–7095
10. Gagnon A, Duplessis M, Fader L (2010) Arylcyclopropanes: properties, synthesis and use in medicinal chemistry. Org Prep Proc Int 42:1–73
11. Rubin M, Rubina M, Gevorgyan V (2007) Transition metal chemistry of cyclopropenes and cyclopropanes. Chem Rev 107(7):3117–3179
12. Ackermann L (2010) Metal-catalyzed direct alkylations of (hetero)arenes via C-H bond cleavages with unactivated alkyl halides. Chem Commun 46(27):4866–4877
13. Engle KM, Mei T-S, Wasa M, Yu J-Q (2012) Weak coordination as a powerful means for developing broadly useful C–H functionalization reactions. Acc Chem Res 45(6):788–802
14. Neufeldt SR, Sanford MS (2012) Controlling site selectivity in palladium-catalyzed C–H bond functionalization. Acc Chem Res 45(6):936–946
15. Lyons TW, Sanford MS (2010) Palladium-catalyzed ligand-directed C–H functionalization reactions. Chem Rev 110(2):1147–1169
16. Alberico D, Scott ME, Lautens M (2007) Aryl–aryl bond formation by transition-metal-catalyzed direct arylation. Chem Rev 107(1):174–238
17. Eaton PE, Daniels RG, Casucci D, Cunkle GT, Engel P (1987) Amide activation for cyclopropane ortho-lithiation. J Org Chem 52(10):2100–2102
18. Zhang M-X, Eaton PE (2002) BuMgNiPr2: a new base for stoichiometric, position-selective deprotonation of cyclopropane carboxamides and other weak CH acids. Angew Chem Int Ed 41(12):2169–2171
19. Giri R, Chen X, Yu J-Q (2005) Palladium-catalyzed asymmetric iodination of unactivated C–H bonds under mild conditions. Angew Chem Int Ed 44(14):2112–2115
20. Wang D-H, Wasa M, Giri R, Yu J-Q (2008) Pd(II)-catalyzed cross-coupling of sp3 C–H bonds with sp2 and sp3 boronic acids using air as the oxidant. J Am Chem Soc 130(23):7190–7191
21. Wasa M, Engle KM, Yu J-Q (2010) Pd(II)-catalyzed olefination of sp3 C–H bonds. J Am Chem Soc 132(11):3680–3681
22. Yoo EJ, Wasa M, Yu J-Q (2010) Pd(II)-catalyzed carbonylation of C(sp3)–H bonds: a new entry to 1,4-dicarbonyl compounds. J Am Chem Soc 132(49):17378–17380
23. Hasegawa N, Shibata K, Charra V, Inoue S, Fukumoto Y, Chatani N (2013) Ruthenium-catalyzed cyclocarbonylation of aliphatic amides through the regioselective activation of unactivated C(sp3)–H bonds. Tetrahedron 69(22):4466–4472
24. Kubota A, Sanford MS (2011) Palladium-catalyzed ligand-directed oxidative functionalization of cyclopropanes. Synthesis 2011(16):2579–2589
25. Stowers KJ, Fortner KC, Sanford MS (2011) Aerobic Pd-catalyzed sp3 C–H olefination: a route to both N-heterocyclic scaffolds and alkenes. J Am Chem Soc 133(17):6541–6544
26. Rousseaux S, Liegault B, Fagnou K (2012) Palladium(0)-catalyzed cyclopropane C-H bond functionalization: synthesis of quinoline and tetrahydroquinoline derivatives. Chem Sci 3 (1):244–248
27. Dos Santos A, El Kaïm L, Grimaud L, Ramozzi R (2012) Palladium-catalyzed ring opening of aminocyclopropyl Ugi adducts. Synlett 2012(3):438–442
28. Rosa D, Orellana A (2011) Palladium-catalyzed cross-coupling of cyclopropanols with aryl halides under mild conditions. Org Lett 13(1):110–113
29. He Z, Yudin AK (2006) Palladium-catalyzed oxidative activation of arylcyclopropanes. Org Lett 8(25):5829–5832
30. Ladd CL, Roman DS, Charette AB (2013) Palladium-catalyzed ring-opening of cyclopropyl benzamides: synthesis of benzo[c]azepine-1-ones via C(sp3)–H functionalization. Tetrahedron 69(22):4479–4487

31. Ladd CL, Sustac Roman D, Charette AB (2013) Silver-promoted, palladium-catalyzed direct arylation of cyclopropanes: facile access to spiro 3,3′-cyclopropyl oxindoles. Org Lett 15 (6):1350–1353
32. Tsukano C, Okuno M, Takemoto Y (2013) Synthesis of spirooxindoles from carbamoyl chlorides via cyclopropyl methine C(sp^3)–H activation using palladium catalyst. Chem Lett 42(7):753–755
33. Saget T, Perez D, Cramer N (2013) Synthesis of functionalized spiroindolines via palladium-catalyzed methine C–H arylation. Org Lett 15(6):1354–1357
34. Janody S, Jazzar R, Comte A, Holstein PM, Vors J-P, Ford MJ, Baudoin O (2014) Synthesis of 1-indanols and 1-indanamines by intramolecular palladium(0)-catalyzed C(sp3)–H arylation: impact of conformational effects. Chem Eur J 20(35):11084–11090
35. Alsters PL, Engel PF, Hogerheide MP, Copijn M, Spek AL, van Koten G (1993) Rigid five- and six-membered C, N, N′-bound aryl-, benzyl-, and alkylorganopalladium complexes: sp2 vs. sp3 carbon-hydrogen activation during cyclopalladation and palladium(IV) intermediates in oxidative addition reactions with dihalogens and alkyl halides. Organometallics 12 (5):1831–1844
36. Shabashov D, Daugulis O (2010) Auxiliary-assisted palladium-catalyzed arylation and alkylation of sp2 and sp3 carbon – hydrogen bonds. J Am Chem Soc 132(11):3965–3972
37. Zaitsev VG, Shabashov D, Daugulis O (2005) Highly regioselective arylation of sp3 C–H bonds catalyzed by palladium acetate. J Am Chem Soc 127(38):13154–13155
38. Rouquet G, Chatani N (2013) Catalytic functionalization of C(sp2)–H and C(sp3)–H bonds by using bidentate directing groups. Angew Chem Int Ed 52(45):11726–11743
39. Parella R, Gopalakrishnan B, Babu SA (2013) Auxiliary-enabled Pd-catalyzed direct arylation of methylene C(sp3)–H bond of cyclopropanes: highly diastereoselective assembling of di- and trisubstituted cyclopropanecarboxamides. Org Lett 15(13):3238–3241
40. Sustac Roman D, Charette AB (2013) C–H functionalization of cyclopropanes: a practical approach employing a picolinamide auxiliary. Org Lett 15(17):4394–4397
41. Wei Y, Tang H, Cong X, Rao B, Wu C, Zeng X (2014) Pd(II)-catalyzed intermolecular arylation of unactivated C(sp3)–H bonds with aryl bromides enabled by 8-aminoquinoline auxiliary. Org Lett 16(8):2248–2251
42. He G, Chen G (2011) A practical strategy for the structural diversification of aliphatic scaffolds through the palladium-catalyzed picolinamide-directed remote functionalization of unactivated C(sp3)–H bonds. Angew Chem Int Ed 50(22):5192–5196
43. Hoshiya N, Kobayashi T, Arisawa M, Shuto S (2013) Palladium-catalyzed arylation of cyclopropanes via directing group-mediated C(sp3)–H bond activation to construct quaternary carbon centers: synthesis of cis- and trans-1,1,2-trisubstituted chiral cyclopropanes. Org Lett 15(24):6202–6205
44. Wasa M, Chan KSL, Zhang X-G, He J, Miura M, Yu J-Q (2012) Ligand-enabled methylene C (sp3)–H bond activation with a Pd(II) catalyst. J Am Chem Soc 134(45):18570–18572
45. He J, Li S, Deng Y, Fu H, Laforteza BN, Spangler JE, Homs A, Yu J-Q (2014) Ligand-controlled C(sp3)–H arylation and olefination in synthesis of unnatural chiral α–amino acids. Science 343(6176):1216–1220
46. Lauru S, Simpkins NS, Gethin D, Wilson C (2008) Enantioselective synthesis of cyclopropylcarboxamides using s-BuLi-sparteine-mediated metallation. Chem Commun 42:5390–5392
47. Giri R, Shi B-F, Engle KM, Maugel N, Yu J-Q (2009) Transition metal-catalyzed C-H activation reactions: diastereoselectivity and enantioselectivity. Chem Soc Rev 38 (11):3242–3272
48. Nakanishi M, Katayev D, Besnard C, Kündig EP (2011) Fused indolines by palladium-catalyzed asymmetric C–C coupling involving an unactivated methylene group. Angew Chem Int Ed 50(32):7438–7441

49. Martin N, Pierre C, Davi M, Jazzar R, Baudoin O (2012) Diastereo- and enantioselective intramolecular C(sp3)–H arylation for the synthesis of fused cyclopentanes. Chem Eur J 18 (15):4480–4484
50. Saget T, Cramer N (2012) Palladium(0)-catalyzed enantioselective C–H arylation of cyclopropanes: efficient access to functionalized tetrahydroquinolines. Angew Chem Int Ed 51 (51):12842–12845
51. Katayev D, Larionov E, Nakanishi M, Besnard C, Kündig EP (2014) Palladium–N-heterocyclic carbene (NHC)-catalyzed asymmetric synthesis of indolines through regiodivergent C (sp3)–H activation: scope and DFT study. Chem Eur J 20(46):15021–15030
52. Wasa M, Engle KM, Lin DW, Yoo EJ, Yu J-Q (2011) Pd(II)-catalyzed enantioselective C–H activation of cyclopropanes. J Am Chem Soc 133(49):19598–19601
53. Chan KSL, Fu H-Y, Yu J-Q (2015) Palladium(II)-catalyzed highly enantioselective C–H arylation of cyclopropylmethylamines. J Am Chem Soc 137(5):2042–2046

Top Organomet Chem (2016) 56: 115–132
DOI: 10.1007/3418_2015_136

Published online: 23 July 2015

Silver-Mediated Direct sp^3 C–H Bond Functionalization

Taigang Zhou and Zhang-Jie Shi

Abstract Direct sp^3 C–H bond functionalization is an efficient, straightforward, and powerful method to construct new C–X (X=C, N, F, S) bonds from nonfunctionalized aliphatic motif of organic molecules, which has been used in late-stage modification of complex molecules. In this chapter, the recent developments of silver-mediated direct sp^3 C–H functionalizations are reviewed, categorized by C–C bond formation (C–H insertion), C–N bond formation (intramolecular and intermolecular amination/amidation), C–F bond formation, and C–S bond formation.

Keywords C–X (X=C, N, F, S) formation • Silver • sp^3 C–H functionalization

Contents

1 Introduction 116
2 Silver-Mediated Direct sp^3 C–H Transformations 117
2.1 Direct C–C Bond Formation 117
2.2 Direct C–N Bond Formation 121
2.3 Direct C–F Bond Formation 127
2.4 Direct C–SCF_3 Bond Formation 128
3 Conclusions and Perspective 129
References 130

T. Zhou
College of Chemistry, Peking University, Beijing 100871, China

Z.-J. Shi (✉)
College of Chemistry, Peking University, Beijing 100871, China

State Key Laboratory of Organometallic Chemistry, Chinese Academy of Sciences, Shanghai 200032, China
e-mail: zshi@pku.edu.cn

Abbreviations

BHT	2,6-Di-tert-butyl-4-methylphenol
Bo	Benzo
bp	4,7-Diphenyl-1,10-phenanthroline
d.r.	Diastereoselectivity ratio
DCE	Dichloroethane
DCM	Dichloromethane
EDA	Ethyl diazoacetate
h	Hour(s)
L	Ligand
L-Men	L-Menthyl
Me	Methyl
Ns	*p*-Nitrosulfonyl
Ph	Phenyl
Py	Pyridine
Pyr	Pyrrole
rt	Room temperature
$scCO_2$	Supercritical carbon dioxide
^{t}Bubipy	4,4′-Di-*tert*-butyl-2,2′-bipyridine
THF	Tetrahydrofuran
Tp	Tris(pyrazolyl)borate
tpa	Tris(2-pyridylmethyl)amine
Ts	*p*-Toluenesulfonyl

1 Introduction

As a noble metal, silver becomes one of the most important metals in the life of human beings, which has been used as currency and ornaments by humans for thousands of years. Nowadays, silver and its salts have been widely used in photography, electrical equipment, jewelry, as well as transition metal for catalysis in chemistry. In chemical research, silver complexes were usually thought to be low activity and used as either co-catalysts [1, 2] or Lewis acids [3] for decades. In recent years, a wide range of important organic transformation has been catalyzed by silver complexes, including C–H insertion, amination/amidation, fluorination, hydrosilylation, decarboxylation, and so on [4–12].

Direct sp^3 C–H bond functionalization has attracted much attention in the past few decades, which presents high efficient, atom-economical pathways to construct new functional groups from easily available chemicals. Most of present C–H bond transformations need to use expensive metals, such as palladium, rhodium, iridium, etc. [13]. Compared to these metals, silver is relatively economically attractive and has been proved highly efficient for C–H activation in recent years, in particular, silver-mediated sp^3 C–H bond transformation. Diverse Ag complexes exhibited

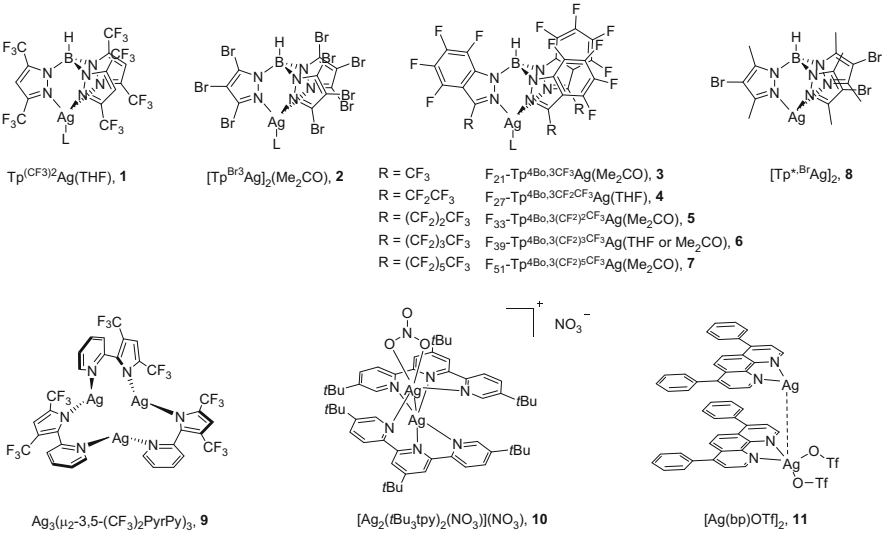

Scheme 1 Silver complexes involved in sp^3 C–H bond transformation

their unprecedented reactivity in this field, which will be discussed in the text (Scheme 1). This chapter will focus on a variety of sp^3 C–H functionalizations catalyzed by different silver complexes.

2 Silver-Mediated Direct sp^3 C–H Transformations

2.1 Direct C–C Bond Formation

C–C bond formation is a major task in synthetic chemistry, and direct C–C bond formation through sp^3 C–H transformation is an ideal method. Up to date, only a few examples were reported via silver catalysts in this field. In 1996, Burgess and coworkers described the earliest work of silver-mediated intramolecular carbene insertion toward C–H bonds (Scheme 2) [14]. They examined 96 potential systems of ligand/metal/solvent combinations to optimize such a C–H insertion reaction. Silver hexafluoroantimonate(V) ($AgSbF_6$) together with bis(oxazolidine) ligand L* in THF showed an unexpected activity and gave desired insertion products in moderate yield (44%) and diastereoselectivity (2.7:1).

A family of tris(pyrazolyl)borate (Tp) silver complexes (Scheme 1, catalysts **1**–**7**) have been independently developed by Dias and Pérez's groups, which proved to be efficient for carbene insertion in sp^3 C–H bonds with diazoacetates [8, 15–24]. For example, in 2004, Dias, Lovely, and coworkers reported early examples of carbene insertion into sp^3 C–H bond of alkanes and ethers by silver with tris(pyrazolyl)borate complex **1** [18, 19]. In this reaction, using neat alkane as substrate

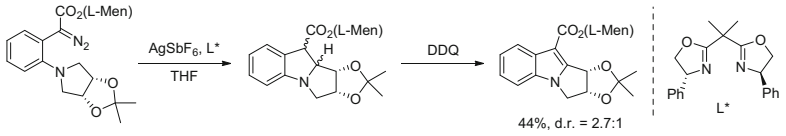

Scheme 2 Intramolecular carbene insertion into C–H bond with silver catalyst

and solvent, 5 mol% [$Tp^{(CF3)2}$]Ag(THF) **1** as catalyst (Scheme 1), and ethyl diazoacetate (EDA) as a carbene source, the desired carbene insertion products were observed with moderate to excellent yield (41–88%, Scheme 3). All primary, secondary, and tertiary sp^3 C–H bonds of alkanes worked well in this transformation. The regioselectivity for the carbene insertion was favored at the primary and secondary sites. However, cyclic ethers were not suitable substrates and showed low activity, presumably due to highly coordinating ability of cyclic ethers.

Pérez's group has focused on modification of tris(pyrazolyl)borate silver complexes for several years. In 2005, Pérez and coworkers developed a highly active silver catalyst [$Tp^{Br3}Ag]_2(Me_2CO)$ **2** for the transformation of sp^3 C–H bond of alkanes with carbene species (Scheme 3) [20]. Compared to silver catalyst **1**, the substitution of ligand in silver catalysts **2** was changed from CF_3 (catalyst **1**) to Br (catalyst **2**) and showed higher efficiency of carbene insertion into sp^3 C–H bonds of various alkanes with EDA. However, the drawback of these silver catalysts is the high catalyst loading (5%) with quite a low turnover numbers. Thus, efficient silver complexes for this transformation were still highly appealing.

After developing the promising catalyst **2**, Pérez and coworkers further reported a new silver complex with perfluorinated tris(pyrazolyl)borate ligand [F_{21}-$Tp^{4Bo,3CF3}$]Ag(Me_2CO) **3**, which can catalyze carbene insertion into sp^3 C–H bond of alkanes with EDA [21]. A variety of alkanes and cycloalkanes were evaluated in the reaction (Scheme 3). Compared to catalyst **1** and **2**, the similar results were achieved with catalyst **3**, while with a low catalyst loading (0.5%) and high turnover numbers.

In 2011, Asensio, Etienne, Pérez, and coworkers reported a first example of carbene insertion into methane sp^3 C–H bond by silver catalysts (Scheme 4) [22]. The reaction was performed using Tp^XAg (silver complexes **2**, **3**, **4**) as the catalysts and ethyl diazoacetate as a carbene source. $ScCO_2$ as the solvent was the key for the success of this transformation. Although silver catalyst was only sparingly soluble in mixture of methane/$scCO_2$, silver complexes **3** or **4** gave approximately 7% desired insertion product, respectively, whereas complex **2** led to a trace amount of product. Nineteen percent yield of ethyl propionate was obtained after the optimization of conditions. Ethane and *n*-pentane also underwent this transformation in $scCO_2$. Additionally, in 2014, Pérez and coworkers also developed a catalytic method for functionalization of methane and light alkanes with EDA in $scCO_2$ based with these fluorinated silver complexes (catalysts **3**–**7**) [23].

Later on, more fluorinated silver complexes (catalysts **5**–**7**) were developed by Pérez and coworkers [24]. Most of those complexes efficiently catalyzed carbene

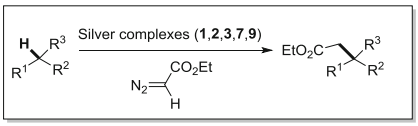

Catalysts	Substrate	yield(%)	Primary site(%)	Secondary site(%)	Tertiary site(%)
				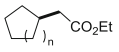	
1		88		100	
3	n=1	70		100	
9		94		100	
1		88		100	
3	n=2	97		100	
9		68		100	
				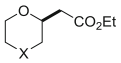	
1	$X=CH_2$	41		100	
1	X=O	0		---	
	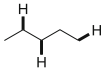			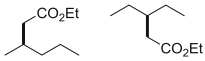	
1		81	41	47	12
2		93	29	57	14
3		86	41	53	6
9		47	12	63	25
			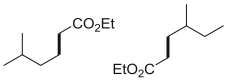	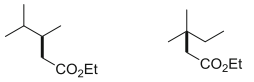	
1		87	59(both)	27	14
2		98	42(both)	37	21
3		93	56(both)	26	18
9		42	20	40	40
			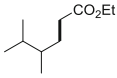		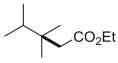
1		85	80		20
2		98	60		40
3		96	75		25
9		44	13		87
		cycles	times(h)		
7		>99	1 1	80	20
		>99	2 2	81	19
		>99	3 2	81	19
		>99	4 5	83	17

Scheme 3 Silver complex-catalyzed carbene insertion into sp^3 C–H bonds

insertion into alkane sp^3 C–H bond with EDA in quantitative yield. More importantly, those silver complexes could be separated and reused several times without loss of efficacy and chemo- and regioselectivities under a fluorous phase (Fomblin or perfluorophenanthrene). For example, by using 2,3-dimethylbutane (1 mL, 7.6 mmol) as the substrate, silver complex **7** (0.005 mmol) F_{51}-Tp$^{4Bo,3(CF2)5CF3}$Ag(acetone) as the catalyst, ethyl diazoacetate (10.5 μL, 0.1 mmol) as a carbene

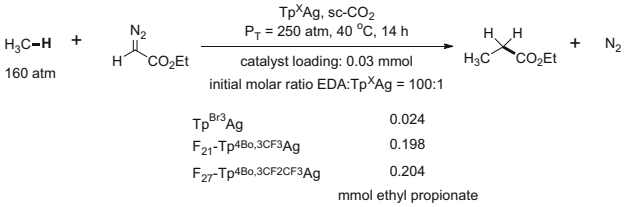

Scheme 4 Silver-mediated methane sp^3 C–H transformation by Pérez et al.

source, and Fomblin HVAC 140/13 (4.0 mL, 1.2 mmol) as the fluorous medium, the desired product and starting material were collected by trap-to-trap vacuum distillation at room temperature after the first catalytic cycle run in good efficiency. Then the fresh starting material (1 mL) and EDA (10.5 μL) were added to the distillation which contained soluble catalyst and the fluorous phase for the second run. This procedure could be repeated several times. The results were shown in Scheme 3. The catalyst **7** was used 4 times and observed identical chemo- and regioselectivity with a slight increase of the reaction time.

Besides a series of tris(pyrazolyl)borate silver complexes, another type of silver complex **9**, discovered by Caulton, Mindiola, and coworkers, could also catalyze carbene insertion into alkane sp^3 C–H bonds [25]. This silver complex was easily prepared from Ag_2O with a bidentated ligand (H(3,5-$(CF_3)_2$PyrPy). This complex was an air- and water-stable complex, existing as a trinuclear form. A series of alkanes, including cyclic, linear, and branched alkanes, were functionalized with complex **9** at 25°C in moderate to excellent yield (Scheme 3). Interestingly, compared with the results from Dias and Pérez's groups by using Tp^XAg complexes, the opposite regioselectivity was observed from Mindiola's group by using complex **9**. For example, the regioselectivity for the carbene insertion into 2,3-dimethylbutane C–H bond with complex **9** favored at the tertiary site over the primary site (ratio 6.7:1, Scheme 3), whereas complex **3** favored at the primary site over tertiary site (ratio 3:1). The yields of functionalization of linear and branched alkanes with complex **9** were moderate due to the formation of fumarate, maleate from EDA, and some unreacted EDA.

In 2013, Lee and coworkers reported silver-mediated intramolecular carbene insertion to sp^3 C–H from alkyne building blocks, mediated by aryne intermediates [26]. In this reaction, using silver trifluoromethanesulfonate (AgOTf, 10 mol%) or $AgSbF_6$ (10 mol%) as the catalyst and toluene as the solvent at 90°C for 5 h, good to excellent yields were obtained for various unsymmetrical and symmetrical bis-1,3-diyne substrates. All primary, secondary, and tertiary C–H bonds could be activated to generate the desired five-membered ring product, and secondary C–H bond was more reactive than primary C–H bond when substrates had two different kinds of available sp^3 C–H bonds (Scheme 5). For example, sp^3 C–H insertion in substrate with two different C–H bonds (entry 4) afforded a mixture of secondary and primary insertion products in high yield (80%) and ratio (13:1).

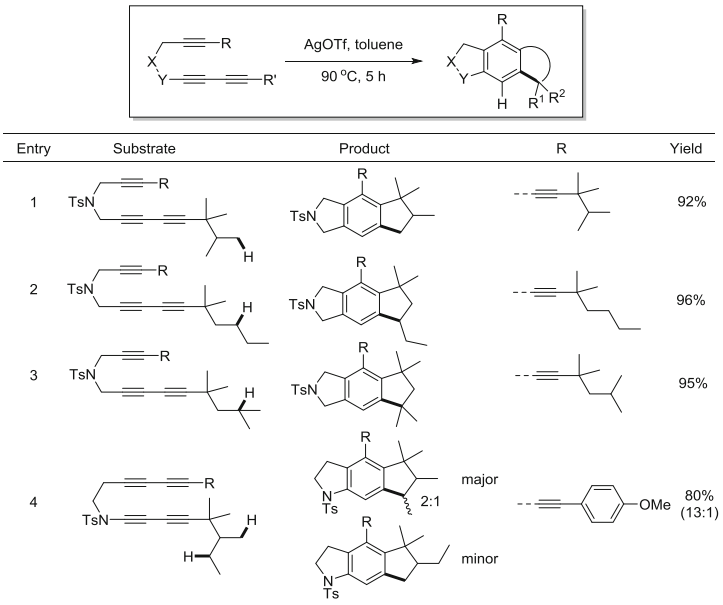

Scheme 5 Silver-mediated sp^3 C–H insertion through aryne intermediates by Lee et al.

2.2 Direct C–N Bond Formation

Nitrogen-containing functional groups are basic and important structural motifs, exiting in biologically active compounds and natural products [27]. The development of new and efficient methods to construct C–N bonds through C–H activation attracted much attention in medicinal chemistry and organic chemistry. Usually, there are two ways to introduce C–N bonds via C–H activation, intramolecular and intermolecular amination/amidation.

2.2.1 Intramolecular Amination/Amidation

In 2004, He and coworkers reported that a disilver (I) complex **10** (Scheme 1) catalyzed intramolecular amidation of sp^3 C–H bonds in both carbamates and sulfamates [28]. Using $AgNO_3$ (4 mol%) with tBu$_3$tpy (4-6 mol%) as the catalyst and $PhI(OAc)_2$ (2.0 equiv.) as the oxidant in MeCN, the intramolecular amidation products were obtained in good to excellent yields (53–90%, Scheme 6). The reaction worked for a range of carbamates and sulfamates, generated five-membered ring and six-membered ring products. In addition, the optical rotation of product will remain as an enantiomerically pure sample during the reaction. This result indicated that the reaction is stereospecific and also provided the evidence to show that the amination involved a silver-mediated nitrene-transfer mechanism.

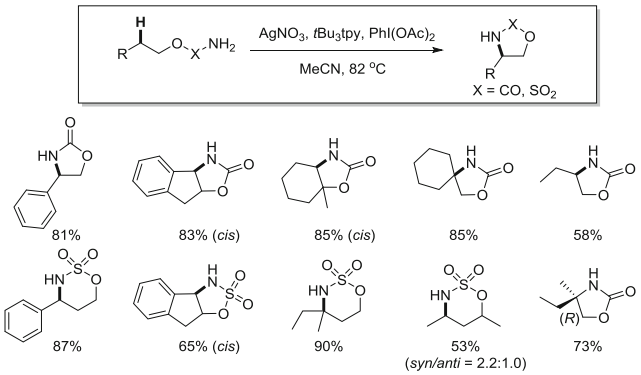

Scheme 6 Silver-mediated intramolecular amination of sp^3 C–H bonds

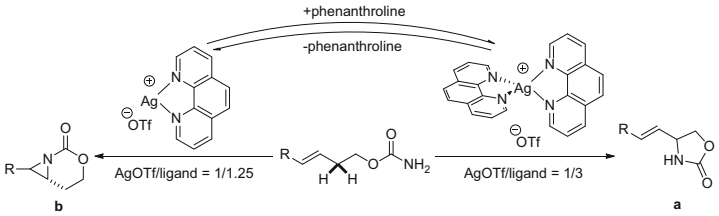

Substrate (AgOTf/ligand = 1/3)	Product a	Product b	Substrate (AgOTf/ligand = 1/3)	Product a	Product dr(*cis*:*trans*)	Product b
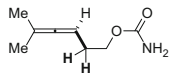	81%	0	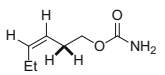	93%	---	0
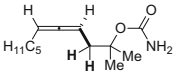	76%	1%	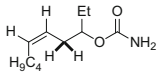	87%	3:1	4%
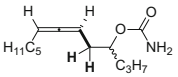	76%	0	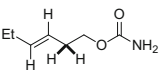	73%	---	11%
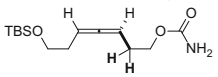	36%	0	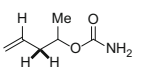	68%	2.4:1	0

Scheme 7 Silver-catalyzed tunable, chemoselective sp^3 C–H amination

However, the substrate scope could not be expanded to amides. Several amides were tried under various reaction conditions; no desired product was obtained.

In 2013, Schomaker and coworkers reported highly chemoselective amidation of C=C and sp^3 C–H bonds by silver catalyst (Scheme 7) [29]. AgOTf was used as the catalyst with phenanthroline as ligand set in the presence of PhIO as the oxidant and 4 Å molecular sieves as additive in DCM. The reaction ran at room temperature. The ratio of AgOTf/ligand is critical since it controlled the reaction pathways to form either aziridination or C–H insertion product. The substrate scopes were

explored to homoallenic and homoallylic carbamates with various substituents. Excellent chemoselectivity and high yields were obtained for this amidation of sp^3 C–H bonds when a 1:3 ratio of AgOTf/ligand was used, while for aziridination when a 1:1.25 ratio of AgOTf/ligand was used.

Later in 2014, ligand-controlled tunable, site-selective silver-catalyzed intramolecular amination/amidation between two different types of C–H bonds has been described by Schomaker and coworkers (Scheme 8) [30]. In the reaction, AgOTf with 4,4′-di-*tert*-butyl-2,2′-bipyridine (^{t}Bubipy) or tris(2-pyridylmethyl)amine (tpa) as the catalyst, PhIO as the oxidant, and 4 Å molecular sieves as additive were used. The sulfamate substrates contained two different types of C–H bonds, including a benzylic C–H bond and an electron-rich tertiary C–H bond. The reactions ran in DCM at room temperature. When AgOTf with ^{t}Bubipy (AgOTf/ligand=1:3) was used as a catalyst, the reaction preferred at an electron-rich tertiary C–H bond. Interestingly, when tpa was used as ligand (AgOTf/ligand=1:1.25), the amidation was favored at a benzylic C–H bond. However, there also were some exceptions. For example, substrate only gave benzylic C–H bond activation with both catalysts, while a higher yield was obtained with (tpa)AgOTf, presumably due to the low bond dissociation energy of benzylic C–H bond (~89 kcal/mol)

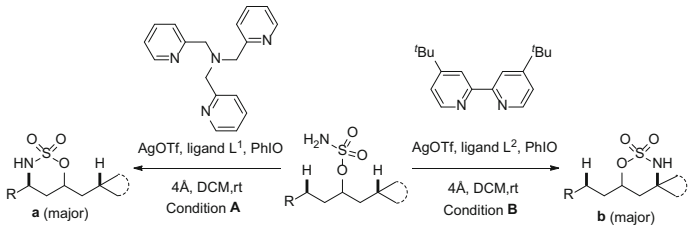

Entry	Substrate		Conditlon A (yield) a	Conditlon A (yield) b	Condition B (yield) a	Condition B (yield) b
1	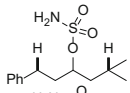		60%	24%	19%	56%
2	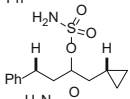		63%	0	28%	0
3	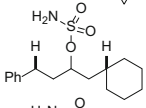		73%	20%	9%	72%
4	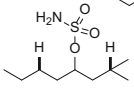		0	94%	0	64%
5	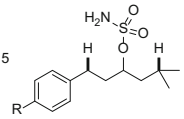	R=OMe	70%	15%	31%	38%
		$R=CF_3$	42%	54%	11%	69%

Scheme 8 Silver-catalyzed, ligand-controlled sp^3 C–H amination by Schomaker et al.

compared to the cyclopropyl C–H bond (~106 kal/mol) (entry 2). The amidation with both catalysts again was obtained at tertiary C–H bond, and similarly (tpa) AgOTf was superior to (^{t}Bubipy)$_2$AgOTf (entry 4).

Very recently, Shi and coworkers reported another beautiful example of silver-catalyzed direct intramolecular amination (Scheme 9) [31]. Primary sp^3 C–H bonds are much less reactive than secondary and tertiary C–H bonds, and activation of primary sp^3 C–H bonds is high challenge and needs to develop a new silver-based catalytic system. In their report, primary sp^3 C–H bond was found preferred to secondary and tertiary C–H bonds. Notably, secondary benzylic C–H and aryl C–H bonds were suitable in the reaction; by using AgOAc (20 mol%) with ^{t}Bubipy (20 mol%) as the catalyst, PhI(OTFA)$_2$ (2.0–4.0 equiv.) as the oxidant, K_2CO_3 (2.0 equiv.) as the base, and PhCl/DCE (1/1) as the solvent at 120°C for 12 h, this amination worked for various triflic amide derivatives and generated only five-membered ring products, while six-membered products were generated through sp^2 C–H amidation. Moderate to good yields are obtained (20–73%). Secondary and tertiary C–H bonds have shown quite a low reactivity in the reaction. The substrates with β-substitution were favorable for amination and usually good yields were

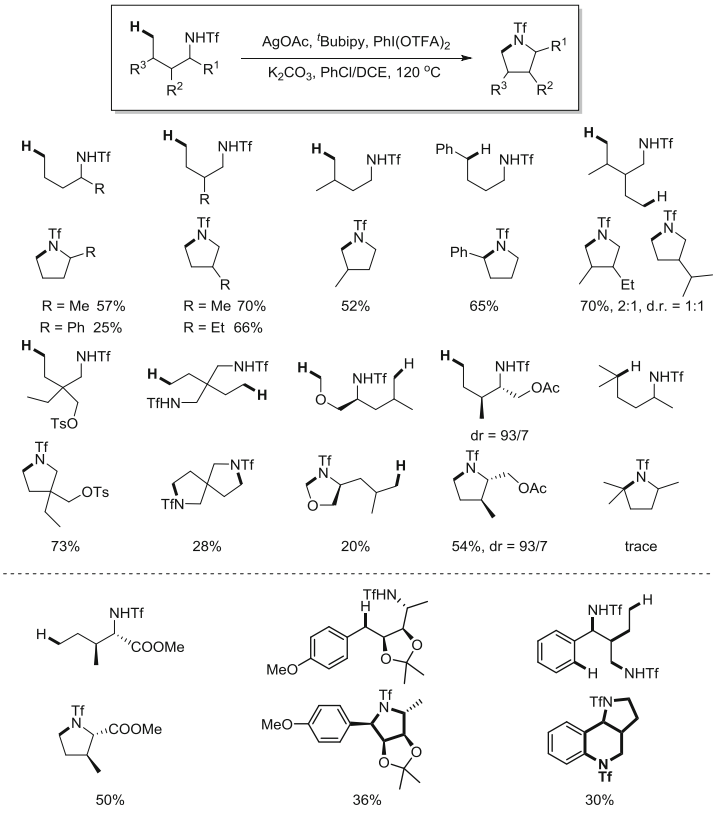

Scheme 9 Silver-mediated directed amination of primary and benzylic C–H bonds by Shi et al.

obtained. However, α-substitution decreased the yields, possibly due to the steric effect. Furthermore, protected linear amino acid ester underwent this transformation and formed 3-methylproline with 50% yield. More complicated core structure of (−)-codonophsinine and (−)-martinellic acid was easily constructed using this powerful method with moderate yields.

2.2.2 Intermolecular Amination

In comparison, intermolecular reaction met high challenges due to both enthalpy and entropy reasons. In 2007, He and coworkers developed a disilver-based new catalyst **11** which showed high efficiency for intramolecular C–H amination reaction (Scheme 10) [32]. Such an intermolecular C–H amination/amidation ran at mild condition. The new catalyst set has successfully been applied to intermolecular amination reaction for the first time (Scheme 11). In the reaction, the catalyst was added in two portions in order to increase the yield. Under typical reaction condition, AgOTf (2 mol%) and ligand (2.4 mol%) were mixed in DCM in a tube for 20 min. Then the substrate (5.0 or 10.0 equiv.), PhI=NNs (1.0 equiv.) and 4 Å molecular sieves (2 g/mmol) were added under N_2 atmosphere. The tube was sealed and heated to 50°C for 2 h before another AgOTf (2 mol%) and ligand (2.4 mol%) mixed in DCM were added. The reaction was carried out at 50°C

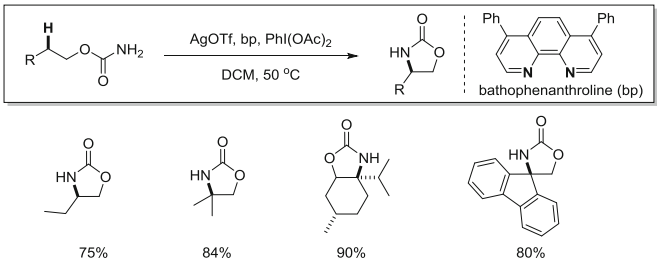

Scheme 10 Silver-mediated intramolecular amination of sp^3 C–H bonds by He et al.

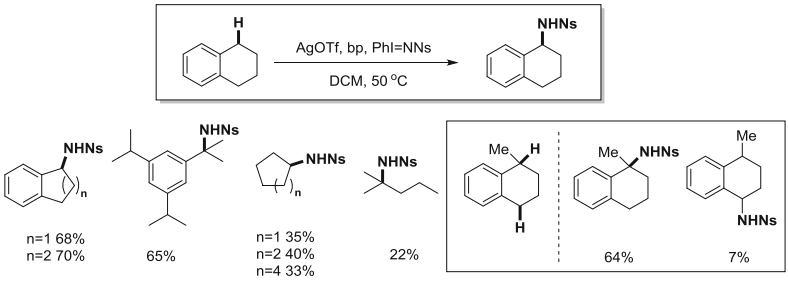

Scheme 11 Silver-mediated intermolecular amination of sp^3 C–H bonds by He et al.

overnight. Good yields were obtained for activating the benzylic C–H bond, while only moderate yields were obtained for inert C–H bond of cyclic alkanes.

In 2008, Díaz-Requejo, Pérez, and coworkers developed a new silver-based catalytic system which proceeded the direct intermolecular amination of alkanes [33]. This new catalyzed system employed complexes $[Tp^{*,Br}Ag]_2$ **8** as catalyst and PhI=NTs ([Ag]/[PhI=NTs]=1/20) as the nitrene source. The reaction was carried out in neat alkane at 80°C for 4 h. Linear and branched alkanes were converted to corresponding isomeric mixtures of amides in moderate to excellent yields (Scheme 12). The amination/amidation was favored at tertiary sites over secondary and primary sp^3 C–H bonds of alkanes, and only a few examples were observed at primary sp^3 C–H bonds. The reaction was inhibited when 2,6-di-*tert*-butyl-4-methylphenol (BHT) was present . Chloroalkanes were observed when CCl_4 was used as solvent. These evidences indicated that the mechanism involved radical species.

Although good results were observed for amination/amidation of alkanes, the reaction needed to carry out in neat substrates. In 2013, Dauban, Díaz-Requejo, Pérez, and coworkers have developed a highly efficient nitrene source sulfonimidamide. Based on their previous studies, complexes $[Tp^{*,Br}Ag]_2$ **8** could catalyze amination/amidation of alkanes (Scheme 12) [34]. In this report, a chiral sulfonimidamide was used as the nitrene source instead of PhI=NTs. High

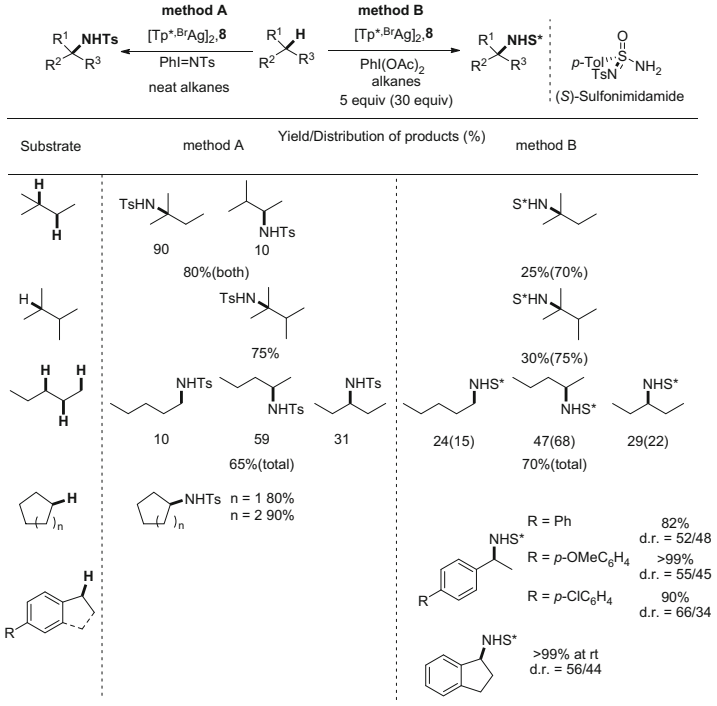

Scheme 12 Sp^3 C–H bond amination using silver complex **8** as catalyst

conversion was obtained for benzylic sp^3 C–H transformation. Important to note, for sp^3 C–H bond of alkane, the silver catalyst **8** showed high activity and gave better yields by using much lower amounts of alkanes.

2.3 *Direct C–F Bond Formation*

Fluorine-containing compounds have unique physical and chemical properties, and they are widely used in material chemistry and medicinal chemistry [35–37]. For example, ^{18}F-labeled organic compounds are used as biological imaging agents for positron emission tomography (PET) [38, 39]. In 2014, Tang and coworkers reported a silver-mediated difluorination of benzylic C–H bonds [40]. In this reaction, they used $AgNO_3$ as catalyst, $Na_2S_2O_8$ as oxidant, and 1-(chloromethyl)-4-fluoro-1,4-diazoniabicyclo[2.2.2]octane bis(tetrafluoroborate) as Selectfluor fluorinating reagent, which is commercially available. Under standard condition, substrate (1.0 equiv.), $AgNO_3$ (10 mol%), $Na_2S_2O_8$ (0.5 equiv.), Selectfluor (3.0 equiv.), and MeCN/H_2O under N_2 were heated to 80°C for several hours. Moderate to excellent yields were achieved (42–93%, Scheme 13). The reaction was tolerating various functional groups, including ketone, ester, carboxylic acid, amide, sulfonamide, aromatic derivatives, and heteroaromatic derivatives. However, higher catalyst loading and excess reagents were needed for some cases. For example, substrates without *ortho*-substituents reacted slowly and usually needed high catalyst loading and large amount of Selectfluor. Obviously, this

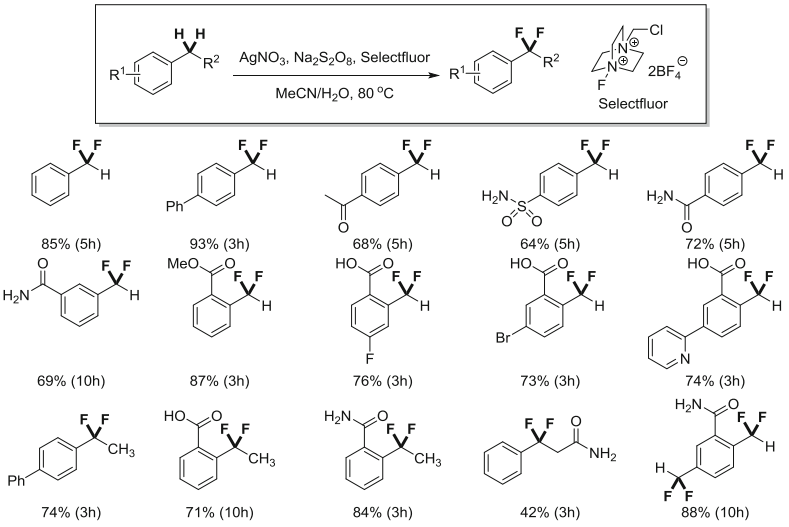

Scheme 13 Silver-mediated difluorination of sp^3 C–H bonds

method provided the most straightforward way to produce 1,1-difluoro substituents at benzylic position.

2.4 Direct C–SCF_3 Bond Formation

Trifluoromethylthio group (SCF_3) is an important structural moiety in new drugs and agrochemicals owing to its strong electronegativity and high lipophilicity [41–44]. Very recently, both Tang and Chen groups have reported direct sp^3 C–H trifluoromethylthiolation using silver (I) trifluoromethanethiolate and persulfate [45, 46]. These developed methods were applied for the late-stage trifluoromethylthiolation of pharmaceutical and agrochemical compounds.

In Tang's work [45], $AgSCF_3$ was used as trifluoromethylthiolation reagent and $Na_2S_2O_8$ as the oxidant. The reaction was carried out under aqueous conditions in air. As standard condition, the substrates (1.0 equiv.), $AgSCF_3$ (2.5 equiv.), $Na_2S_2O_8$ (4.0 equiv.), and MeCN/H_2O/DCE (6:2:1, v/v/v) in 2.00 mL sealed in a vial were warmed to 35°C for 12 h. Moderate to excellent yields (32–94%) of desired products are obtained. The reaction can be carried out at gram scale (Scheme 14). The reaction tolerated various functional groups, including ethers, esters, amino acid derivatives, bromides, and aromatic derivatives. This reaction was favored occurring selectively at tertiary and secondary C–H bonds. Otherwise,

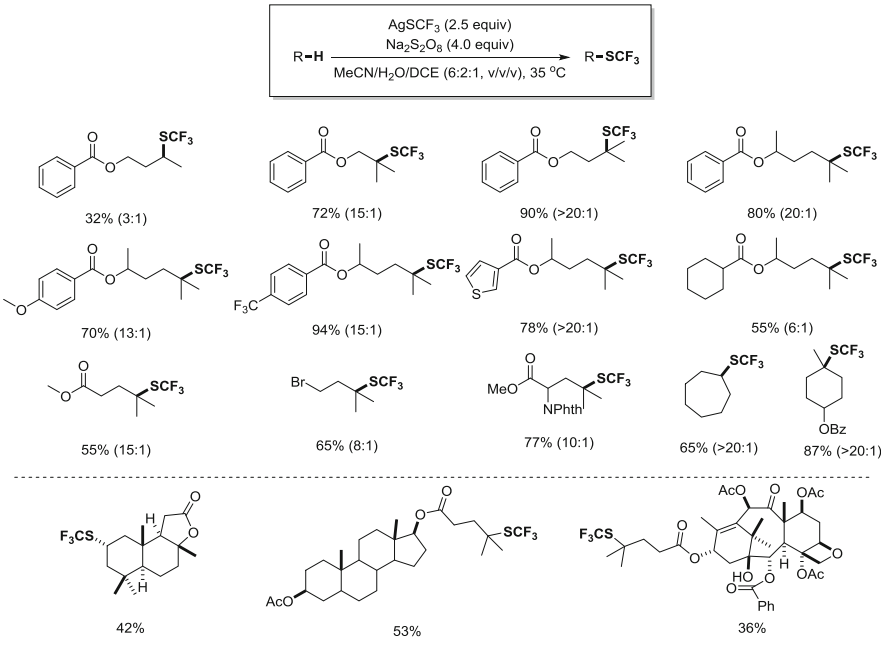

Scheme 14 Silver-mediated trifluoromethylthiolation of sp^3 C–H bonds and applications

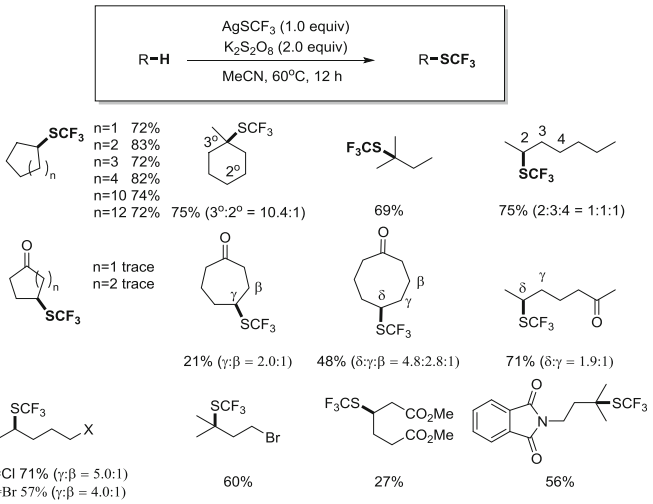

Scheme 15 Silver-mediated trifluoromethylthiolation of sp^3 C–H bonds

this transformation gave a much lower selectivity of trifluoromethylthiolation products. It is important to note that more complex natural products were successfully applied in this trifluoromethylthiolation, exhibiting the potential of this method in medicinal chemistry.

Almost at the same time, Chen and coworkers also reported the similar direct trifluoromethylthiolation of sp^3 C–H bonds by $AgSCF_3/K_2S_2O_8$ [46]. They also used $AgSCF_3$ as trifluoromethylthiolation reagent, but $K_2S_2O_8$ as the oxidant. The reaction was carried out under argon atmosphere. Moderate to excellent yields (18–83%) were obtained under mild conditions (Scheme 15). Similarly, the trifluoromethylthiolation were showed with a better selectivity at tertiary C–H than secondary C–H bonds. Many functional groups were also well tolerated, including ketones, esters, bromides, tertiary alcohols, and phthalimides. However, the presence of the primary and secondary aliphatic alcohols terminated the reaction. The substrates with alkene and alkyne groups were also not workable and resulted in a complicated reaction mixture.

3 Conclusions and Perspective

Although much attention has been paid to silver catalysis in the past several years and significant progress has been achieved in this field of silver-mediated sp^3 C–H bond transformations, compared to the catalysis with other transition metals, the reports in this field are still very limited. In this chapter, we have reviewed a variety of important silver-catalyzed sp^3 C–H transformations, including C–C bond formation, C–N bond formation, C–F bond formation, and C–S bond formation. A

family of tris(pyrazolyl)borate silver complexes and other unique silver complexes were designed, synthesized, and characterized and further proved to be efficient catalysts in this field. Fascinating methodologies were developed for functionalization of different aliphatic C–H bonds, particularly, methane and short alkanes with EDA by perfluorinated tris(pyrazolyl)borate silver complexes in $scCO_2$. Silver-catalyzed/silver-mediated sp^3 C–H amination/amidation, difluorination, and trifluoromethylthiolation provided a great potential for future late-stage functionalization of pharmaceutical and agrochemical compounds. All these developments will blossom a new field to approach the direct aliphatic C–H functionalization. As a cheap noble metal, silver exhibited an exciting feature in catalysis, tunable by the different ligands. We believe that silver will play more and more important roles in direct C–H functionalization with the development of new processes.

Acknowledgment Financial support by MOST (2015CB856600 and 2013CB228102) and NSFC (Nos. 21332001 and 21431008) is gratefully acknowledged. T.Z. was supported in part by the Postdoctoral Fellowship of Peking-Tsinghua Center for Life Sciences and China Postdoctoral Science Foundation Grant (2014 M550546).

References

1. Ladd CL, Sustac Roman D, Charette AB (2013) Org Lett 15:1350
2. Maestre L, Sameera WMC, Díaz-Requejo MM, Maseras F, Pérez PJ (2013) J Am Chem Soc 135:1338
3. Naodovic M, Yamamoto H (2008) Chem Rev 108:3132
4. Yanagisawa A, Takeshita S, Izumi Y, Yoshida K (2010) J Am Chem Soc 132:5328
5. Li Z, He C (2006) Eur J Org Chem 2006:4313
6. Álvarez-Corral M, Muñoz-Dorado M, Rodríguez-García I (2008) Chem Rev 108:3174
7. Yamamoto Y (2008) Chem Rev 108:3199
8. Dias HVR, Lovely CJ (2008) Chem Rev 108:3223
9. Díez-González S, Nolan SP (2008) Acc Chem Res 41:349
10. Munoz MP (2014) Chem Soc Rev 43:3164
11. Weibel J-M, Blanc A, Pale P (2008) Chem Rev 108:3149
12. Harmata M (ed) (2010) Silver in organic chemistry. Wiley, Hoboken
13. Cheng C, Hartwig JF (2015) Chem Rev. doi:10.1021/cr5006414
14. Burgess K, Lim H-J, Porte AM, Sulikowski GA (1996) Angew Chem Int Ed 35:220
15. Doyle MP (2011) ChemCatChem 3:1681
16. Pérez PJ (ed) (2012) Alkane C–H activation by single-site metal catalysis. Springer, Netherlands
17. Rangan K, Fianchini M, Singh S, Dias HVR (2009) Inorg Chim Acta 362:4347
18. Dias HVR, Browning RG, Richey SA, Lovely CJ (2004) Organometallics 23:1200
19. Dias HVR, Browning RG, Richey SA, Lovely CJ (2005) Organometallics 24:5784
20. Urbano J, Belderraín TR, Nicasio MC, Trofimenko S, Díaz-Requejo MM, Pérez PJ (2005) Organometallics 24:1528
21. Despagnet-Ayoub E, Jacob K, Vendier L, Etienne M, Álvarez E, Caballero A, Díaz-Requejo MM, Pérez PJ (2008) Organometallics 27:4779
22. Caballero A, Despagnet-Ayoub E, Mar Díaz-Requejo M, Díaz-Rodríguez A, González-Núñez ME, Mello R, Muñoz BK, Ojo W-S, Asensio G, Etienne M, Pérez PJ (2011) Science 332:835

23. Fuentes MÁ, Olmos A, Muñoz BK, Jacob K, González-Núñez ME, Mello R, Asensio G, Caballero A, Etienne M, Pérez PJ (2014) Chem Eur J 20:11013
24. Fuentes MÁ, Muñoz BK, Jacob K, Vendier L, Caballero A, Etienne M, Pérez PJ (2013) Chem Eur J 19:1327
25. Flores JA, Komine N, Pal K, Pinter B, Pink M, Chen C-H, Caulton KG, Mindiola DJ (2012) ACS Catal 2:2066
26. Yun SY, Wang K-P, Lee N-K, Mamidipalli P, Lee D (2013) J Am Chem Soc 135:4668
27. Lawrence SA (2004) Amines: synthesis, properties and applications. Cambridge University, New York
28. Cui Y, He C (2004) Angew Chem Int Ed 43:4210
29. Rigoli JW, Weatherly CD, Alderson JM, Vo BT, Schomaker JM (2013) J Am Chem Soc 135:17238
30. Alderson JM, Phelps AM, Scamp RJ, Dolan NS, Schomaker JM (2014) J Am Chem Soc 136:16720
31. Yang M, Su B, Wang Y, Chen K, Jiang X, Zhang Y-F, Zhang X-S, Chen G, Cheng Y, Cao Z, Guo Q-Y, Wang L, Shi Z-J (2014) Nat Commun 5
32. Li Z, Capretto DA, Rahaman R, He C (2007) Angew Chem Int Ed 46:5184
33. Gómez-Emeterio BP, Urbano J, Díaz-Requejo MM, Pérez PJ (2008) Organometallics 27:4126
34. Beltran A, Lescot C, Mar Diaz-Requejo M, Perez PJ, Dauban P (2013) Tetrahedron 69:4488
35. O'Hagan D (2008) Chem Soc Rev 37:308
36. Purser S, Moore PR, Swallow S, Gouverneur V (2008) Chem Soc Rev 37:320
37. Wang J, Sánchez-Roselló M, Aceña JL, del Pozo C, Sorochinsky AE, Fustero S, Soloshonok VA, Liu H (2014) Chem Rev 114:2432
38. Ametamey SM, Honer M, Schubiger PA (2008) Chem Rev 108:1501
39. Miller PW, Long NJ, Vilar R, Gee AD (2008) Angew Chem Int Ed 47:8998
40. Xu P, Guo S, Wang L, Tang P (2014) Angew Chem Int Ed 53:5955
41. Leo A, Hansch C, Elkins D (1971) Chem Rev 71:525
42. Leroux F, Jeschke P, Schlosser M (2005) Chem Rev 105:827
43. Manteau B, Pazenok S, Vors J-P, Leroux FR (2010) J Fluor Chem 131:140
44. Xu X-H, Matsuzaki K, Shibata N (2015) Chem Rev 115:731
45. Guo S, Zhang X, Tang P (2015) Angew Chem Int Ed 54:4065
46. Wu H, Xiao Z, Wu J, Guo Y, Xiao J-C, Liu C, Chen Q-Y (2015) Angew Chem Int Ed 54:4070

Top Organomet Chem (2016) 56: 133–154
DOI: 10.1007/3418_2015_122

Published online: 10 June 2015

Applications of Catalytic Organometallic C(sp^3)–H Bond Functionalization

David Dailler, Grégory Danoun, and Olivier Baudoin

Abstract The transition-metal-catalyzed activation of C(sp^3)–H bonds has emerged as powerful strategy to create bonds and introduce functional groups in a direct fashion. This review focuses on recent applications of C(sp^3)–H bond functionalization strategies to the synthesis of biologically active and natural compounds.

Keywords Bioactive molecules · C–H activation · Natural products · Total synthesis · Transition metals

Contents

1 Introduction 134
2 Heteroatom-Directed C–H Activation 134
2.1 Pioneering Stoichiometric Studies 134
2.2 β-Arylation of Carbonyl Compounds 136
2.3 γ-Arylation of Amine Derivatives 140
2.4 Other Directed C–H Functionalizations 144
3 Oxidative-Addition-Initiated C–H Activation 146
4 Conclusion 150
References 151

D. Dailler, G. Danoun, and O. Baudoin (✉)
Université Claude Bernard Lyon 1, CNRS UMR 5246, Institut de Chimie et Biochimie Moléculaires et Supramoléculaires, CPE Lyon, 43 Boulevard du 11 Novembre 1918, 69622 Villeurbanne, France
e-mail: olivier.baudoin@univ-lyon1.fr

1 Introduction

Compared to the wealth of catalytic methods which have been developed for the functionalization of C(sp^2)–H bonds of arenes and heteroarenes, relatively little work has focused on the functionalization of unactivated, nonacidic C(sp^3)–H bonds of alkyl fragments. Most transition-metal-catalyzed C(sp^2)–H functionalization methods involve a C–H activation step in which a C–H bond is cleaved and a carbon–metal bond is formed, a process which has been termed "organometallic" or "inner-sphere" C–H activation [1]. But the organometallic activation of C (sp^3)–H bonds is generally more difficult to achieve, because these bonds are less acidic and lack proximal empty low-energy or filled high-energy orbitals that interact with filled or empty orbitals of the metal, respectively. Despite this intrinsic difficulty, considerable progress has been made in the past decade, and catalytic organometallic C(sp^3)–H bond activation has now become a straightforward and practical tool to build C=C and C(sp^3)–X bonds (X=C or heteroatom) in a complex molecule setting [2–5].

This chapter highlights recent remarkable examples of the fast-growing literature on the application of catalytic organometallic C(sp^3)–H bond functionalization to the synthesis of natural products and active ingredients, of interest for medicine and agrochemistry [6–8]. Reactions involving the cleavage of activated C–H bonds, in α position to heteroatoms or electron-withdrawing groups, or which do not involve organometallic intermediates are not covered herein.

2 Heteroatom-Directed C–H Activation

2.1 Pioneering Stoichiometric Studies

Pioneering applications of heteroatom-directed C(sp^3)–H activation using stoichiometric amounts of metal salts were described by Sames and co-workers in the early 2000s. These studies paved the way for the development of subsequent catalytic methods. In 2000, the total synthesis of the antimitotic natural product (±)-rhazinilam was achieved using a platinum-mediated dehydrogenative C–H bond activation as key step [9]. Several seminal reports had shown that platinum complexes containing nitrogenous bidentate ancillary ligands were prone to undergo C–H activation [10–13]. Exploiting this property, Johnson and Sames employed optimized Schiff base **1** as a bidentate ligand to form the pivotal platinum complex **2** by reaction with a dimethylplatinum reagent $[Me_2Pt(\mu\text{-}SMe_2)]_2$ (Scheme 1). Treatment of **2** with triflic acid afforded a cationic platinum complex **3**, which upon heating in CF_3CH_2OH provided the hydridoplatinum (II) complex **4**, resulting from the selective dehydrogenation of one ethyl group, with excellent yield (90%, NMR yield). Subsequent platinum decomplexation with aqueous KCN followed by cleavage of the imine afforded racemic alkene **5** in 60% overall yield from **1**.

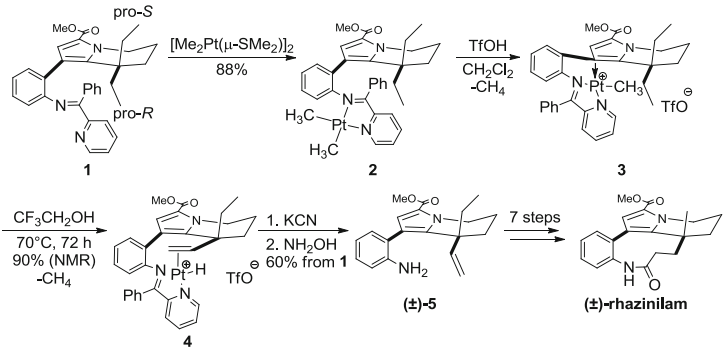

Scheme 1 Synthesis of (±)-rhazinilam involving Pt-mediated alkane dehydrogenation

Alkene **5** was employed to synthesize (±)-rhazinilam in seven additional steps. Sames and co-workers later described an asymmetric version of this approach by differentiating the two enantiotopic ethyl groups using a chiral oxazoline-containing Schiff base [14].

After this first application of a stoichiometric alkane dehydrogenation reaction, Sames and co-workers turned to C(sp^3)–C(sp^2) bond formation via heteroatom-directed C(sp^3)–H bond activation. In 2002, they described the synthesis of the core of teleocidin B4, a complex natural product fragment including two quaternary stereocenters (Scheme 2) [15]. They envisioned that a *tert*-butyl group could act as the cornerstone for the construction of this tetracyclic compound via two directed C–H bond activations. Starting from a tuned Schiff base **6** containing two methoxy substituents to avoid the metalation of arene C–H bonds, a stable six-membered palladacycle **7** was generated by treatment with a stoichiometric amount of $PdCl_2$. The isolation of this intermediate showed the bidentate coordination of the Schiff base and one *ortho*-methoxy group. Palladacycles such as **7** have been known to undergo direct functionalization reactions [16–19]. However, transmetalation with boronic acids had not been reported. Palladacycle **7** reacted with a boronic acid in the presence of Ag_2O to provide the alkenylated product **8** with 65% yield from **6**. Then, treatment of **8** with methanesulfonic acid generated the cyclized product **9**, the precursor of the second C–H activation process, via a Friedel–Crafts alkylation in good yield. Stoichiometric $PdCl_2$ and NaOAc were reacted with **9** to afford a mixture of diastereoisomeric palladacycle **10**, which was directly treated with carbon monoxide and methanol to furnish methyl ester intermediates. Under acidic conditions (silica), the Schiff base was hydrolyzed, followed by spontaneous cyclization, thus providing diastereoisomeric lactams **11** and **12** (65% yield over three steps, d.r. = 1:6). The final stage of the synthesis of the teleocidin core involved indole formation, which was performed in three steps from major diastereoisomer **12**.

Through the preceding syntheses, Sames and co-workers demonstrated the potential of the heteroatom-directed C(sp^3)–H bond activation strategy in total synthesis, which allows to draw nontraditional disconnections in retrosynthetic

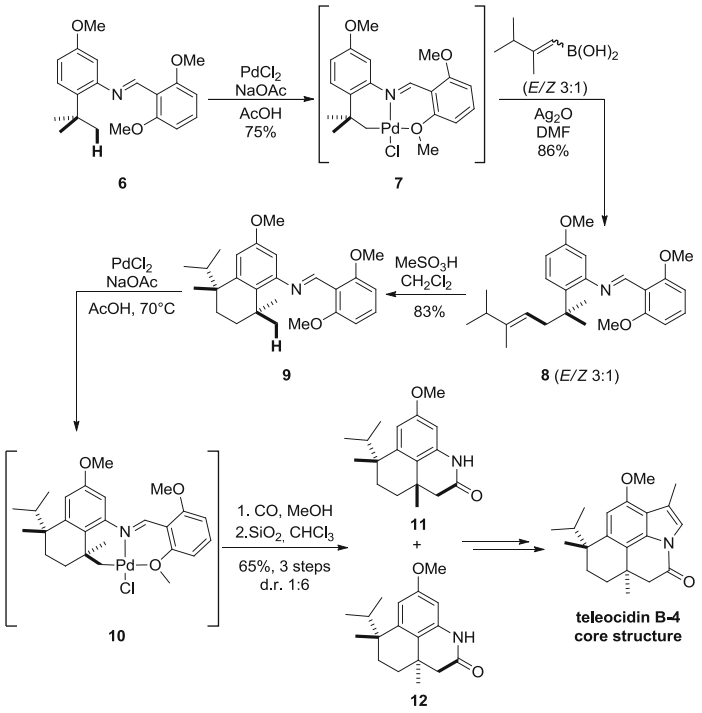

Scheme 2 Synthesis of the core of teleocidin B-4 via multiple Pd-mediated C–H activation

analysis and to construct new bonds in a straightforward manner. However, in these pioneering studies, stoichiometric amounts of metal were necessary to perform the key transformations. Subsequent efforts were devoted to the development of catalytic methods that retain synthetic applicability.

2.2 *β-Arylation of Carbonyl Compounds*

In 2005, taking advantage of bidentate coordinating groups to efficiently bind to a transition metal and to position the latter in proximity to a targeted C–H bond, Daugulis and co-workers described the Pd^{II}-catalyzed regioselective β- and γ-arylation of unactivated $C(sp^3)$–H bonds, by introducing respectively 8-aminoquinoline and picolinamide directing groups [20, 21]. Inspired by this seminal report, numerous developments of new bidentate directing groups and methods have been subsequently reported [22].

In 2006, the group of Corey described a first extension of this concept [23]. Using the 8-aminoquinoline directing group, they could achieve the palladium-catalyzed diastereoselective β- and γ-$C(sp^3)$–H arylation of protected α-amino acid derivatives with aryl iodides and catalytic amounts of $Pd(OAc)_2$.

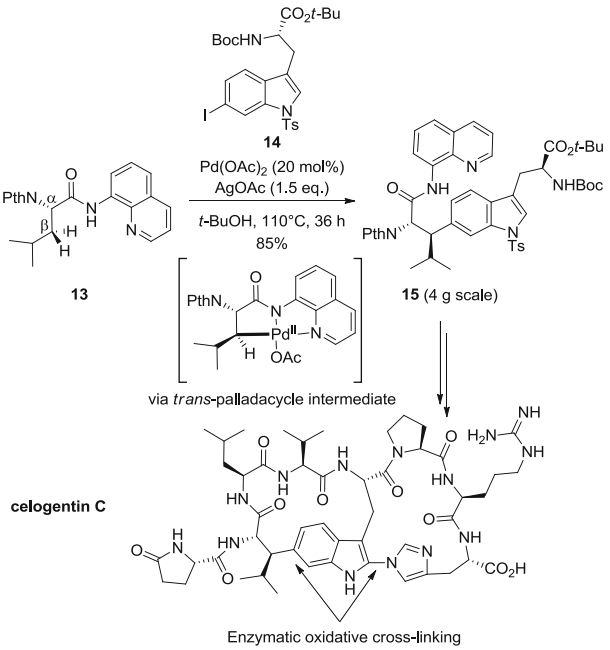

Scheme 3 Total synthesis of celogentin C featuring Pd-catalyzed directed C–H arylation

Following up on this study, Feng and Chen achieved the total synthesis of (–)-celogentin C (Scheme 3) [24]. Inspired by the proposed biosynthesis involving enzymatic oxidative cross-links [25, 26], they envisioned to construct the Leu-Trp C(sp^3)–C(sp^2) bond by regio- and diastereoselective C–H arylation of the Leu motif **13**. After optimization on a model substrate, they could perform the arylation of **13** with iodide **14** in good yield on a multigram scale, using $Pd(OAc)_2$ as the catalyst and AgOAc as the terminal oxidant. A complete diastereoselectivity was observed, which was ascribed to the preferential formation of a *trans*-palladacycle intermediate avoiding the steric clash between the isopropyl and *N*-phthaloyl groups. This Pd^{II} intermediate afforded, after oxidative addition of aryl iodide **14** and C–C reductive elimination, compound **15** with the *erythro* stereochemistry. Interestingly, only the *N*-phthaloyl protecting group could be successfully employed for the arylation process. However, its bulkiness and lability proved to be troublesome during the cleavage of the aminoquinoline auxiliary, for which no mild conditions had been reported. To solve this issue, Chen and co-workers carried out a three-step sequence starting with the transformation of the *N*-phthaloyl group into a smaller azide, followed by Boc-activation of the amide [27] and hydrolysis under Evan's conditions [28]. Overall, the total synthesis of celogentin C was achieved in 23 steps, featuring the first application of catalytic C(sp^3)–H bond functionalization using a bidentate directing group in natural product synthesis.

In 2011, Gutekunst and Baran described both the first example of sequential catalytic C(sp^3)–H arylations in total synthesis and of transition-metal-catalyzed activation of C–H bonds of a cyclobutane ring [29]. This iterative C–H functionalization strategy provided an efficient access to unsymmetrical cyclobutanes of biological interest while avoiding pitfalls of classical cyclobutane synthesis via photoinduced [2+2] cross-dimerization: head-to-head and head-to-tail additions, homodimerization, and *E*/*Z* isomerization of olefin precursors, generally leading to the uncontrolled production of a complex mixture of regio- and stereoisomers [30, 31]. To achieve the synthesis of piperarborenines (Scheme 4), Baran and co-worker selected the [2-(methylthio)phenyl]carbamoyl derivative **16** instead of the 8-aminoquinoline directing group, because the hydrolysis of the former was reported to occur under milder conditions [32]. After optimization, they found that the addition of HFIP and pivalic acid [33] is critical to perform the first C(sp^3)–H arylation with complete regio- and diastereoselectivity, to give *cis*-configured product **17** on gram scale. Taking advantage of divergent epimerization to obtain diastereoisomers **18** and **19** in good yield and stereoselectivity, they successfully performed the second diastereoselective C(sp^3)–H arylation under similar conditions, thus affording tetrasubstituted cyclobutanes **20** and **21**. Piperarborenines B and D were then synthesized from these intermediates in 2–3 steps via transformation of the amide and ester groups into carboxylic acids, followed by condensation with dihydropyridone. Overall, this iterative C–H functionalization strategy allowed to access both natural products in 6–7 steps, 7–12% overall yield. Later on, Baran and co-workers reported an extension of this strategy to the sequential C–H arylation/alkenylation of cyclobutanes, which allowed to synthesize pipercyclobutanamide A, another congener of the same family of natural products [34, 35].

During their studies on the total synthesis of podophyllotoxin based on a Pd-catalyzed C(sp^3)–H arylation strategy (Scheme 5) [36], Ting and Maimone reported subtle conformational effects on reductive elimination pathways. Indeed, when precursor **22** was engaged in directed C(sp^3)–H arylation under usual conditions, β-lactam **23** was unexpectedly isolated as the major product. In the past few years, the direct C–N bond reductive elimination of the nitrogen atom of the amide directing group has been well documented [37–42]. To understand and suppress this undesired pathway, the authors carried out X-ray diffraction analyses of the acetonitrile-bound Pd^{II} complex arising from the C–H activation step. They identified that the environment of this palladacycle is highly congested and affected by the conformation of the cyclohexene ring. As a consequence, they prepared the conformationally distinct substrate **24** as new a precursor of the C–H activation process. After significant optimization including the use of dibenzylphosphate as an additive [43–45], the desired C–C bond formation was performed in 58% yield. To finish, a simple treatment of the arylated product with a TFA/THF/H_2O mixture afforded podophyllotoxin and C-4 *epi*-podophyllotoxin, due to the epimerizable character of the C4 stereogenic center. This strategy provided a five-step synthesis of podophyllotoxin from commercially available bromopiperonal and a straightforward entry into novel arene-modified analogues.

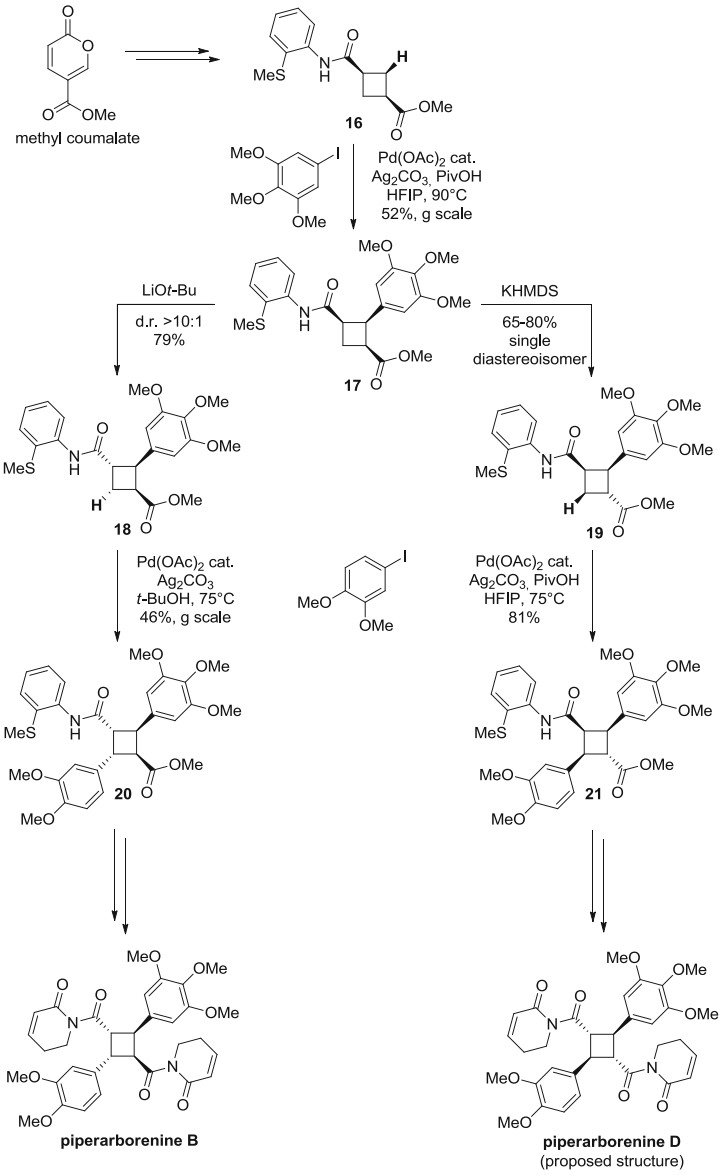

Scheme 4 Total synthesis of piperarborenines via sequential Pd-catalyzed C–H arylations of a cyclobutane core

Recently, further work has been described employing the 8-aminoquinoline directing group for the efficient synthesis of *cis*-3-substituted proline derivatives [46, 47], which are compounds of interests in organocatalysis [48] and drug discovery [49–51].

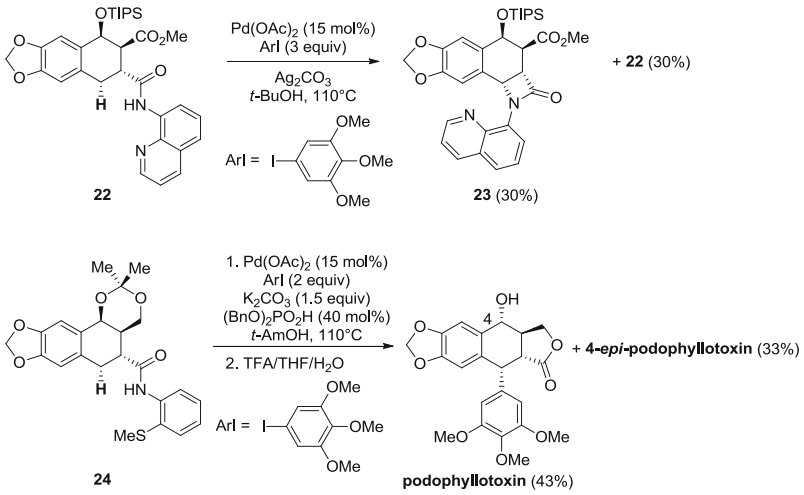

Scheme 5 Total synthesis of podophyllotoxin via Pd-catalyzed directed C–H arylation

2.3 γ-Arylation of Amine Derivatives

Based on the original study of Daugulis and co-workers, who introduced the picolinamide bidentate directing group for the palladium-catalyzed γ-C(sp^3)–H arylation of amine derivatives [20], He and Chen reported major improvements which facilitate synthetic applications [50]. Indeed, they developed milder conditions (80°C, with *t*-BuOH or trifluoroethanol as the solvent), which are compatible with sensitive functional groups and stereogenic centers found in complex molecule settings. Furthermore, based on precedents in peptide chemistry [52], they developed a modified picolinamide directing group which can be removed through intramolecular acyl transfer under mildly acidic conditions. The importance of these modifications was demonstrated through to the formal synthesis of (+)-obafluorin (Scheme 6). The synthetic sequence started from the readily available threonine derivative **25**, which was engaged in the optimized γ-C–H arylation conditions to afford the desired arylated product **26** in 60% yield. The directing group was then smoothly removed under acidic treatment to provide aminoester **27**, which served as an intermediate in the formal synthesis of (+)-obafluorin.

In 2013, Chen and co-workers reported a streamlined approach for the synthesis of tetrahydroquinolines (THQs) via the sequential functionalization of remote C–H bonds [53]. Starting from readily available aryl iodide and aliphatic amine precursors, this strategy involved a three-step sequence including palladium-catalyzed γ-C(sp^3)–H arylation, followed by a previously optimized metal-free ε-C(sp^2)–H iodination reaction [54] and a more classical Cu-catalyzed intramolecular C–N coupling. To test the efficacy of this novel procedure, the authors applied it to the total synthesis of the antimalarial alkaloid (+)-angustureine (Scheme 7) [55]. *N*-Alkylpicolinamide **28** was easily accessible from commercially available (*S*)-(+)-3-

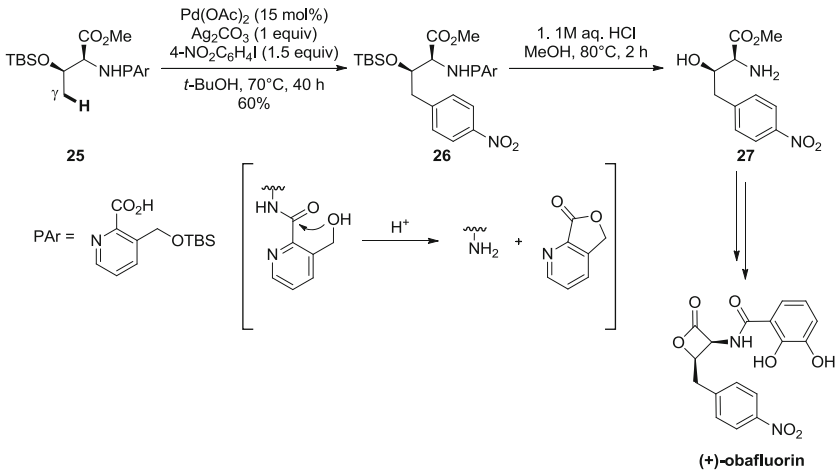

Scheme 6 Formal synthesis of (+)-obafluorin via Pd-catalyzed directed γ-C–H arylation of a threonine derivative

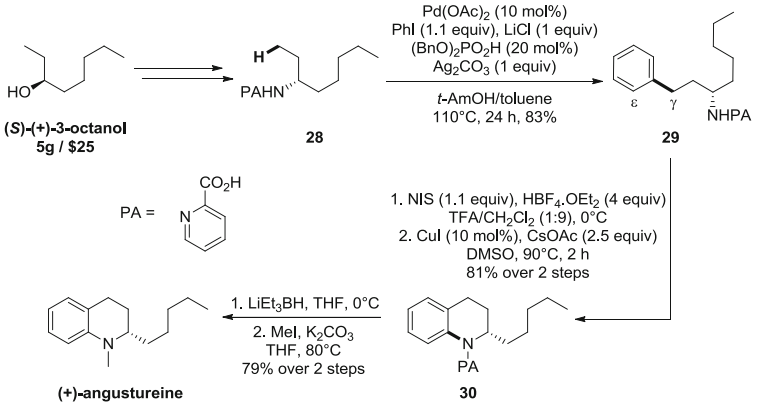

Scheme 7 Synthesis of (+)-angustureine involving Pd-catalyzed directed γ-C–H arylation

octanol. It was engaged in the directed γ-C(sp^3)–H arylation with iodobenzene to afford the desired arylated product **29** in excellent yield. Compound **29** was then treated with NIS and HBF_4 to provide the corresponding *ortho*-iodinated product in mono-selective fashion, which was subsequently engaged in the Cu-catalyzed cyclization to give THQ **30** in 81% yield over two steps. Finally, removal of the PA group from the cyclized compound **30** under reductive conditions followed by *N*-methylation furnished (+)-angustureine in good overall yield.

Despite significant improvements of palladium-catalyzed directed C(sp^3)–H arylation, including the use of less reactive but more cost-attractive aryl bromides [56] or open-air, room-temperature conditions [57], only sporadic examples of

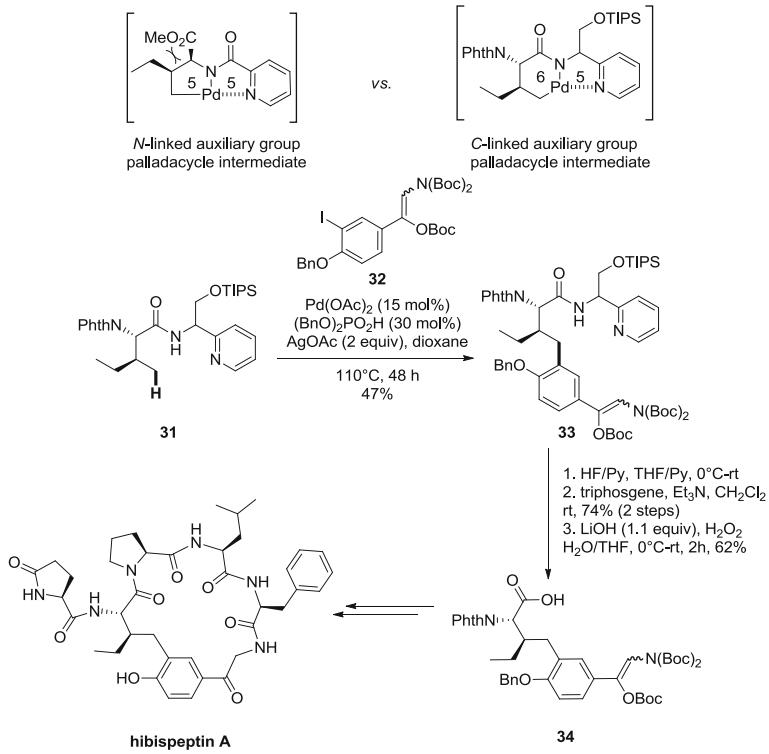

Scheme 8 Synthesis of hibispeptin A featuring a Pd-catalyzed directed γ-C–H arylation with a hindered aryl iodide and a removable directing group

coupling with sterically hindered aryl donors have been reported [58–61]. To address this challenge, Chen and co-workers introduced a new pyridylmethylamine-based directing group, which enabled C–H arylation with sterically hindered *ortho*-substituted aryl iodides [62]. As an illustration, to access the key Ile-Hpa pseudodipeptide moiety in hibispeptin A (Scheme 8), the authors first considered the original *N*-linked picolinamide directing group, which proved efficient in previous γ-C(sp^3)–H arylations of amino acid substrates [20, 58]. Unfortunately, the corresponding γ-Me arylation occurred in low yield (<20%) due to a sterically disfavored *cis*-configuration of the α-CO_2Me and β-Et groups in the five-membered palladacycle intermediate. To solve this low reactivity issue and based on previous studies on the $\gamma-$ arylation of amino acids [23], they explored a series of *C*-linked directing groups that would induce the formation of a less hindered but also less kinetically favored six-membered palladacycle intermediate. They initially found that 2-pyridylethylamine, introduced by Chatani and co-workers [63], provided good arylation yields, but low conversions and loss of chiral integrity during the cleavage of the directing group. Based on their previous studies [58], they designed a new pyridylmethylamine-based directing group which could be

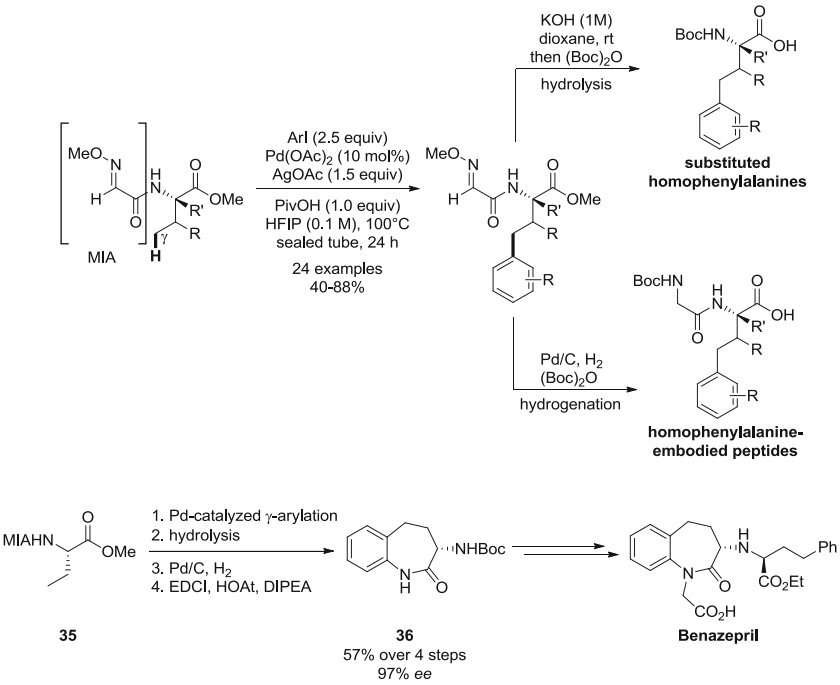

Scheme 9 Formal synthesis of benazepril via Pd-catalyzed γ-C–H arylation using the 2-methoxyiminoacetyl (MIA) directing group

easily removed. The latter was employed to perform the γ-Me arylation of Ile derivative **31** with *ortho*-substituted aryl iodide **32**, which provided the key Ile-Hpa residue **33** in moderate yield. A three-step cleavage sequence then furnished carboxylic acid **34**, a key intermediate of the synthesis of hibispeptin A.

Only a few amine-derived directing groups have been reported, and all of them display drawbacks such as high reaction temperatures (typically 150°C) [59], difficult cleavage [20], or low accessibility [58]. On this basis, Fan and Ma reported a new 2-methoxyiminoacetyl (MIA) directing group for the γ-C(sp^3)-H arylation of amines, which is readily available, operates under moderate reaction temperatures, and can be removed under mild conditions to allow for further functionalization (Scheme 9) [61]. Using this directing group, they could perform the γ-C(sp^3)–H arylation of various 2-aminobutanoic acid derivatives with a broad range of aryl iodides. Furthermore, mild post-functionalizations such as room-temperature hydrolysis or hydrogenation provided homophenylalanine derivatives, which are important motifs in drug discovery, e.g., as peptidomimetics [64]. The synthetic utility of this protocol was demonstrated through the formal synthesis of the antihypertensive agent benazepril. Starting from the simple 2-aminobutanoic acid derivative **35**, lactam **36**, which directly intercepts the synthesis of Ciba-Geigy Corporation, was synthesized in only four steps and good overall yield.

2.4 Other Directed C–H Functionalizations

2.4.1 C–C Bond Formation

Fagnou and co-workers described a completely site-selective C(sp^3)–H or C(sp^2)–H arylation of a broad range of azine and diazine *N*-oxides with aryl halides, involving a Pd^0/Pd^{II} catalytic manifold (Scheme 10) [65, 66]. This switch of regioselectivity is controlled by an intimidate involvement of the base and catalyst. Using a strong base like NaO*t*-Bu, the arylation, which is presumably directed by the *N*-oxide function, selectively occurred at the sp^3 site. This novel C(sp^3)–H arylation methodology was applied to the total synthesis of the alkaloids crykonisine and papaverine, in only three steps after reduction of the *N*-oxide group, and starting from easily available materials.

In 2012, Maes and co-workers reported a new transition-metal-catalyzed methodology for the direct C2–H functionalization of piperidines [67], via pyridine-directed Ru-catalyzed C(sp^3)–H alkylation with alkenes [68]. Based on previous work [69–73], they discovered that a combination of a bulky alcohol (2,4-dimethyl-3-pentanol) and a catalytic amount of a carboxylic acid [74] is necessary to avoid side reactions such as isomerization and/or reduction of the alkene reactant (Scheme 11). They successfully applied this method to the total synthesis of (±)-

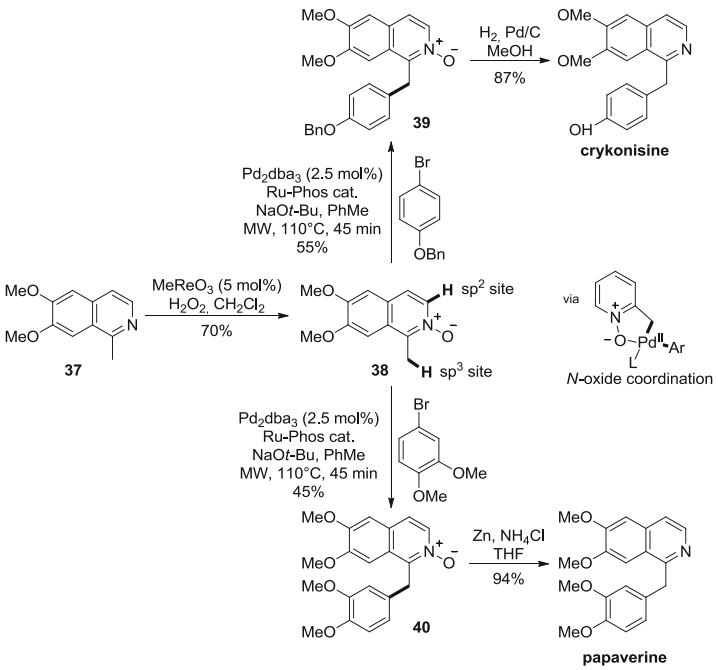

Scheme 10 Synthesis of crykonisine and papaverine via Pd^0-catalyzed site-selective C–H arylation of *N*-oxides

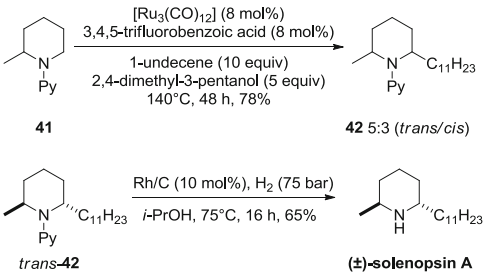

Scheme 11 Synthesis of (±)-solenopsin A via Ru-catalyzed directed C–H alkylation

solenopsin A through a three-step sequence starting from racemic 2-methylpiperidine.

2.4.2 C–N Bond Formation

The formation of four- and five-membered *N*-heterocycles such as azetidines [38–40, 75] and β-lactams [36, 41] through direct C–N bond reductive elimination involving the nitrogen atom of amide directing groups is well documented. Building on these data, Wu and co-workers developed modified conditions to access β-lactams via Pd-catalyzed, C_6F_5I-assisted intramolecular amidation of β-C(sp^3)–H bonds (Scheme 12) [42]. They found that a highly electron-deficient aryl iodide such as C_6F_5I can promote the β-lactam formation pathway (C–N reductive elimination) over the arylation pathway (C–C reductive elimination). Using the 8-aminoquinoline directing group, they synthesized a broad range of β-lactams, including *cis*-fused systems which are difficult to access by other methods, with excellent yield and selectivity. To highlight the synthetic utility of this process, they reported the formal synthesis of β-lactamase inhibitor MK-8712. Starting from readily available L-proline, compound **43** containing the modified 5-OMe-quinoline, easily removable directing group introduced by Chen and co-workers [75] was obtained. The optimized intramolecular C–H amidation afforded *cis*-fused β-lactam **44** in 86% yield. Directing group cleavage with CAN and hydrogenolysis afforded the *cis*-fused product **46**, a key intermediate in the synthesis of the target β-lactamase inhibitor.

2.4.3 C–O Bond Formation

Sharpe and Johnson recently reported a stereocontrolled total synthesis of the indole diterpenoid paspaline (Scheme 13) [76]. In a key step, they envisaged to perform the C–H oxidation of diastereotopic *gem*-dimethyl groups, which would allow to install a pivotal quaternary stereocenter. Inspired by an initial report of Sanford and co-workers [77] and a seminal application in total synthesis by the group of Sorensen [78], they decided to carry out the key selective C–H oxidation of intermediate **47** containing an oxime directing group. Applying Sanford's original condition furnished the desired acetoxylated product **48** in high yield and as a

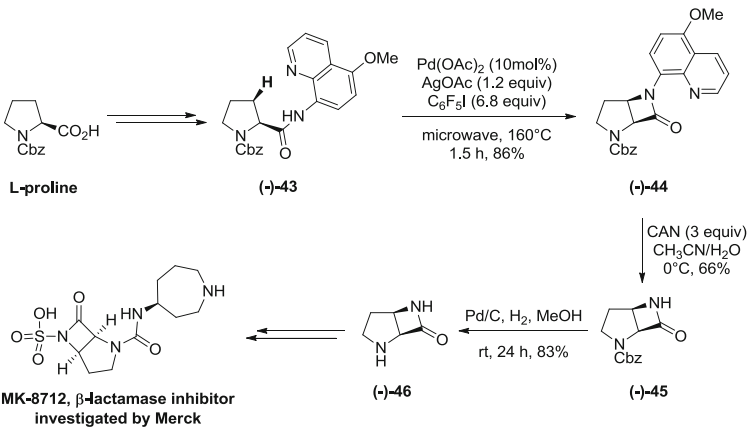

Scheme 12 Synthesis of MK-8712 via Pd-catalyzed intramolecular C–H amidation

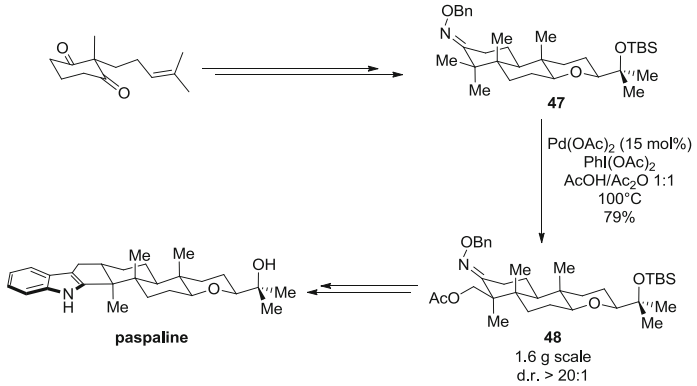

Scheme 13 Synthesis of paspaline via diastereoselective oxime-directed C–H oxidation

single diastereoisomer. This complete diastereoselectivity is thought to originate from the favored conformation of **47**, which places the oxime C–N π-bond and the activated equatorial methyl group in the same plane. A 12-step sequence completed the stereocontrolled synthesis of paspaline.

3 Oxidative-Addition-Initiated C–H Activation

The oxidative addition of a carbon-leaving group bond to a low-valent transition-metal complex may play the same role as the binding to a Lewis basic directing group in order to trigger intramolecular C–H activation [2, 3]. Inspired by Dyker's C–H self-condensation of *ortho*-substituted aryl iodides under ligand-free conditions [79, 80], Baudoin and co-workers reported in 2003 the palladium(0)-catalyzed

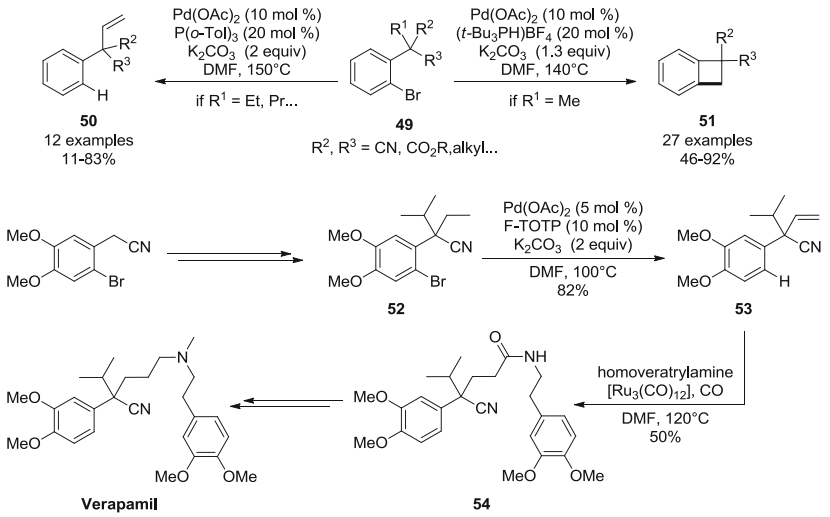

Scheme 14 Synthesis of verapamil involving a selective Pd^0-catalyzed formal dehydrogenation

C(sp^3)–H functionalization of benzylic alkyl groups, giving rise to olefin **50** (formal alkane dehydrogenation) or benzocyclobutene **51** from aryl halide **49** (Scheme 14) [81]. In both cases, they found optimal conditions with DMF as the solvent and K_2CO_3 as the active base. Furthermore, in contrast to Dyker's initial work, no self-condensation was observed thanks to the use of suitable phosphine ligands. Indeed, the formation of olefins **50** was best performed using P(*o*-Tol)$_3$, whereas P(*t*-Bu)$_3$ was found to be optimal to construct benzocyclobutene **51** via a challenging C–C reductive elimination [82]. Further ligand design subsequently allowed to access a greater variety of linear and cyclic olefins under milder conditions [83]. To demonstrate the utility of the dehydrogenation method, the authors applied it to the synthesis of the calcium channel antagonist verapamil [83]. Thus, bromoarene **52**, easily obtained from a commercially available substituted phenylacetonitrile, was engaged into the optimized C–H activation procedure to afford the dehydrogenated product **53** in high yield and with high selectivity in favor of the ethyl *vs*. the isopropyl group. Verapamil was then obtained in good yield (six steps, 17% overall) through a three-step sequence involving ruthenium-catalyzed hydroamidation, *N*-methylation, and chemoselective reduction of the amide function.

In 2009, Baudoin and co-workers reported a new strategy for the synthesis of dihydroisoquinolines, involving sequential C(sp^3)–H arylation and 6-π-electrocyclization, which was applied to the total synthesis of the tetrahydroprotoberberine alkaloid (±)-coralydine (Scheme 15) [84]. First, aryl bromide **55** underwent C–H activation/intramolecular C–C coupling to give benzocyclobutene methyl ester **56** in good yield. Hydrolysis of **56** followed by Curtius rearrangement yielded aminobenzocyclobutene **57**. Condensation of **57** with an appropriate substituted benzaldehyde afforded an imine intermediate, which was directly

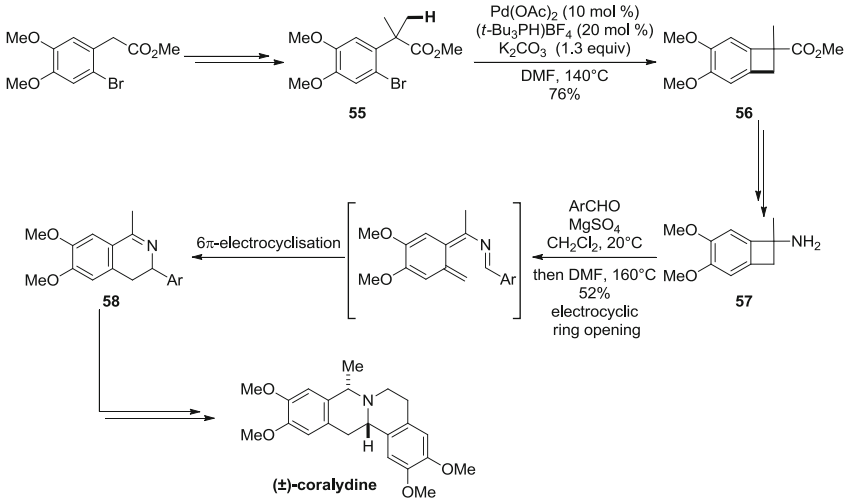

Scheme 15 Synthesis of (±)-coralydine featuring Pd^0-catalyzed intramolecular C–H arylation

engaged in the key thermal tandem electrocyclic ring-opening/6-π-electrocyclization reaction [85], thereby providing dihydroisoquinoline **58** in 52% yield. An additional three-step sequence furnished (±)-coralydine, which was obtained with an overall yield of 6.2% in nine steps.

In 2014, the same research group described the synthesis of valuable 1-indanols and 1-indanamines through a similar intramolecular C–H arylation process (Scheme 16) [86]. In previous reports, (fused) indanes [83, 87, 88] and indanones [88] had been obtained, but only with a quaternary center at the C1 or C2 position, respectively. In the more recent study [86], Baudoin and co-workers proposed suitable conditions to synthesize more interesting, albeit more challenging indanes bearing a tertiary benzylic C1 carbon atom. 1-Indanols and 1-indanamines were obtained under operationally simple conditions and with moderate-to-high yield, depending on the degree of substitution at the C2 position, as a result of Thorpe–Ingold effects. Interestingly, the diastereoselectivity at C1 and C2 was affected by the nature of the heteroatomic substituent at C1. Indeed, a subtle conformational effect allowed to selectively obtain the *trans*-diastereoisomer in the 1-indanamine case, which is a valuable building block for the synthesis of APIs. In contrast, 1-indanols were obtained as the major *cis*-diastereoisomers. Within the framework of a collaboration with Bayer CropScience, this method was applied to the synthesis of racemic *trans*-aminoindane **60**, a known intermediate in the industrial synthesis of the herbicide indaziflam.

As an extension to C–H arylations, Baudoin and co-workers reported the intramolecular alkenylation of unactivated $C(sp^3)$–H bonds. Inspired both by Knochel's intramolecular $C(sp^3)$–H alkenylation of activated benzylic positions [89, 90] and by Ohno's indoline synthesis [91], they developed a unique route toward hexahydroindoles (Scheme 17) [92]. This method afforded sp^3-rich products in

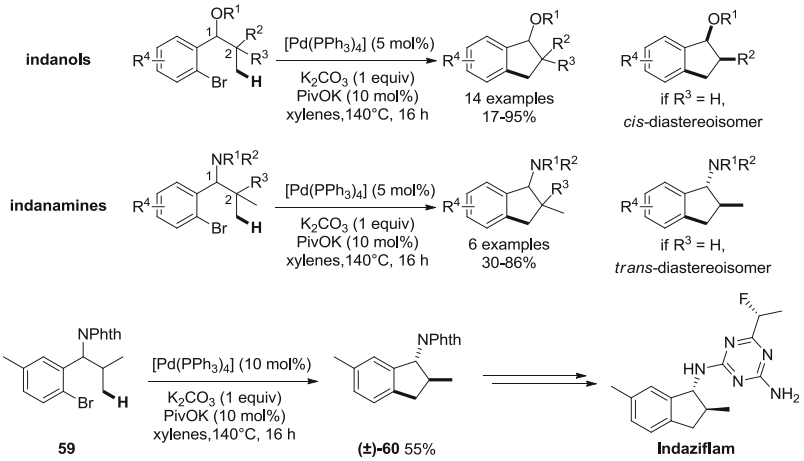

Scheme 16 Formal synthesis of indaziflam involving a conformationally challenging Pd^0-catalyzed intramolecular C–H arylation

good yield with a high degree of regioselectivity. More recently, the same authors reported its application to the synthesis of the bicyclic (Choi) core of aeruginosin marine natural products [93–95]. Cyclohexenyl bromide **61** which was obtained through a six-step synthesis from readily available precursors underwent C(sp^3)–H alkenylation on multigram scale under re-optimized conditions, to provide hexahydroindole **62** in good yield. In parallel, a rapid and divergent access to the hydroxyphenyllactic (Hpla) subunits of the natural products, including those containing chlorine or bromine atoms on the benzene ring, was developed, by using a palladium-catalyzed directed β-C–H arylation of a D-lactic acid derivative (**63**). After screening various directing groups and reaction conditions, the 2-pyridinylisopropyl (PIP) group introduced by Shi and co-workers [41] was found to be the best option to furnish the various required Hpla subunits **64a–c** in good yield and without erosion of optical purity. A multistep sequence involving peptide coupling and deprotections allowed to complete the total synthesis of aeruginosins 98B and 298A, with an unprecedented overall yield and scale for the latter (0.7 g, 8.2% overall yield), and started from simple chiral pool precursors [93]. This strategy also allows to synthesize aeruginosin congeners bearing halogen atoms on the Hpla subunit [94]. This final application highlights the synthetic power of C(sp^3)–H activation, when employed in a strategic manner to streamline complex molecule synthesis.

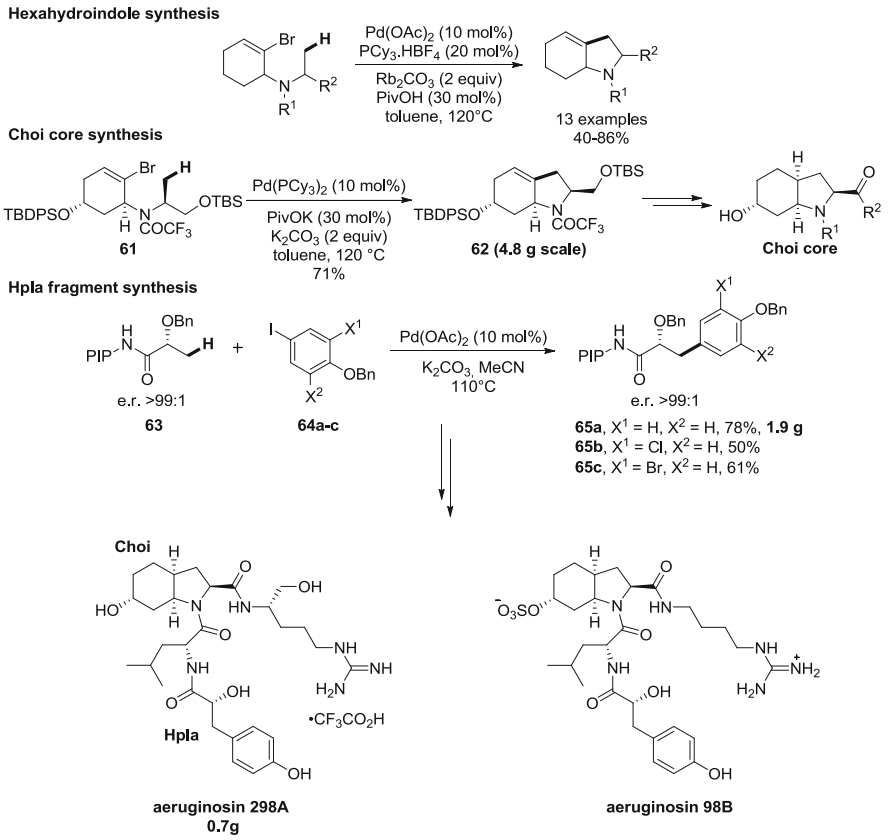

Scheme 17 Total synthesis of aeruginosins featuring two strategic Pd-catalyzed C–H activation reactions

4 Conclusion

In the past decade, catalytic organometallic C(sp^3)–H activation has undergone major progress and has become a powerful tool to create C(sp^3)–X bonds in a very direct manner. An increasing number of applications of the newly developed methods have been reported, both in natural product and API synthesis. The use of C–H bond functionalization in a strategic manner in retrosynthetic analysis is an emerging concept that will deeply impact organic synthesis on the long term, by improving atom and step economy and thus overall efficiency. However, the field is still in its infancy, as one is far from being able to selectively functionalize a given C–H bond in a given organic molecule, and many exciting developments and applications lie ahead.

Acknowledgments The authors thank Région Rhône-Alpes (ARC Santé) and Fondation Pierre Potier pour le Développement de la Chimie des Substances Naturelles et ses Applications for financial support.

References

1. Dick AR, Sanford MS (2006) Tetrahedron 62:2439
2. Jazzar R, Hitce J, Renaudat A, Sofack-Kreutzer J, Baudoin O (2010) Chem Eur J 16:2654
3. Baudoin O (2011) Chem Soc Rev 40:4902
4. Li H, Li BJ, Shi ZJ (2011) Catal Sci Technol 1:191
5. Dastbaravardeh N, Christakakou M, Haider M, Schnürch M (2014) Synthesis 46:1421
6. McMurray L, O'Hara F, Gaunt MJ (2011) Chem Soc Rev 40:1885
7. Gutekunst WR, Baran PS (2011) Chem Soc Rev 40:1976
8. Yamaguchi J, Yamaguchi AD, Itami K (2012) Angew Chem Int Ed 51:8960
9. Johnson JA, Sames D (2000) J Am Chem Soc 122:6321
10. Holtcamp MW, Henling LM, Day MW, Labinger JA, Bercaw JE (1998) Inorg Chim Acta 270:467
11. Johansson L, Ryan OB, Tilset M (1999) J Am Chem Soc 121:1974
12. Wick DD, Goldberg KI (1997) J Am Chem Soc 119:10235
13. Periana RA, Taube DJ, Gamble S, Taube H, Satoh T, Fujii H (1998) Science 280:560
14. Johnson JA, Li N, Sames D (2002) J Am Chem Soc 124:6900
15. Dangel BD, Godula K, Youn SW, Sezen B, Sames D (2002) J Am Chem Soc 124:11856
16. Ryabov AD (1985) Synthesis 233
17. Baldwin JE, Jones RH, Najera C, Yus M (1985) Tetrahedron 41:699
18. Balavoine G, Clinet JC (1990) J Organomet Chem 390:C84
19. Dyker G (1997) Chem Ber/Recl 130:1567
20. Zaitsev VG, Shabashov D, Daugulis O (2005) J Am Chem Soc 127:13154
21. Daugulis O, Roane J, Tran LD (2015) Acc Chem Res 48(4):1053–1064
22. Rouquet G, Chatani N (2013) Angew Chem Int Ed Engl 52:11726
23. Reddy BVS, Reddy LR, Corey EJ (2006) Org Lett 8:3391
24. Feng Y, Chen G (2010) Angew Chem Int Ed 49:958
25. Walsh CT (2004) Science 303:1805
26. Sieber SA, Marahiel MA (2003) J Bacteriol 185:7036
27. Flynn DL, Zelle RE, Grieco PA (1983) J Org Chem 48:2424
28. Evans DA, Britton TC, Ellman JA (1987) Tetrahedron Lett 28:6141
29. Gutekunst WR, Baran PS (2011) J Am Chem Soc 133:19076
30. Filho RB, De Souza MP, Mattos MEO (1981) Phytochemistry 20:345
31. Lewis FD, Quillen SL, Hale PD, Oxman JD (1988) J Am Chem Soc 110:1261
32. Shabashov D, Daugulis O (2010) J Am Chem Soc 132:3965
33. Lafrance M, Gorelsky SI, Fagnou K (2007) J Am Chem Soc 129:14570
34. Gutekunst WR, Gianatassio R, Baran PS (2012) Angew Chem Int Ed 51:7507
35. Gutekunst WR, Baran PS (2014) J Org Chem 79:2430
36. Ting CP, Maimone TJ (2014) Angew Chem Int Ed 53:3115
37. Wasa M, Yu J-Q (2008) J Am Chem Soc 130:14058
38. He G, Zhao Y, Zhang S, Lu C, Chen G (2012) J Am Chem Soc 134:3
39. Nadres ET, Daugulis O (2012) J Am Chem Soc 134:7
40. Ye X, He Z, Ahmed T, Weise K, Akhmedov NG, Petersen JL, Shi X (2013) Chem Sci 4:3712
41. Zhang Q, Chen K, Rao W, Zhang Y, Chen F-J, Shi B-F (2013) Angew Chem Int Ed 52:13588
42. Sun W-W, Cao P, Mei R-Q, Li Y, Ma Y-L, Wu B (2014) Org Lett 16:480
43. Zhang S-Y, He G, Nack WA, Zhao Y, Li Q, Chen G (2013) J Am Chem Soc 135:2124

44. Zhang S-Y, Li Q, He G, Nack WA, Chen G (2013) J Am Chem Soc 135:12135
45. Chen K, Hu F, Zhang S-Q, Shi B-F (2013) Chem Sci 4:3906
46. Affron DP, Davis OA, Bull JA (2014) Org Lett 16:4956
47. Feng R, Wang B, Liu Y, Liu Z, Zhang Y (2015) Eur J Org Chem 2015:142
48. Panday SK (2011) Tetrahedron Asymmetry 22:1817
49. Fatas P, Jimenez AI, Calaza MI, Cativiela C (2012) Org Biomol Chem 10:640
50. Mothes C, Caumes C, Guez A, Boullet H, Gendrineau T, Darses S, Delsuc N, Moumné R, Oswald B, Lequin O, Karoyan P (2013) Molecules 18:2307
51. Taylor RD, MacCoss M, Lawson ADG (2014) J Med Chem 57:5845
52. Linderman RJ, Binet S, Petrich SR (1999) J Org Chem 64:336
53. Nack WA, He G, Zhang S-Y, Lu C, Chen G (2013) Org Lett 15:3440
54. Barluenga J, Álvarez-Gutiérrez JM, Ballesteros A, González JM (2007) Angew Chem Int Ed 46:1281
55. Lin X-F, Li Y, Ma D-W (2004) Chin J Chem 22:932
56. Wei Y, Tang H, Cong X, Rao B, Wu C, Zeng X (2014) Org Lett 16:2248
57. Wang B, Nack WA, He G, Zhang S-Y, Chen G (2014) Chem Sci 5:3952
58. He G, Chen G (2011) Angew Chem Int Ed 50:5192
59. Rodriguez N, Romero-Revilla JA, Fernandez-Ibanez MA, Carretero JC (2013) Chem Sci 4:175
60. He J, Li S, Deng Y, Fu H, Laforteza BN, Spangler JE, Homs A, Yu J-Q (2014) Science 343:1216
61. Fan M, Ma D (2013) Angew Chem Int Ed 52:12152
62. He G, Zhang S-Y, Nack WA, Pearson R, Rabb-Lynch J, Chen G (2014) Org Lett 16:6488
63. Hasegawa N, Charra V, Inoue S, Fukumoto Y, Chatani N (2011) J Am Chem Soc 133:8070
64. Sahoo SP, Caldwell CG, Chapman KT, Durette PL, Esser CK, Kopka IE, Polo SA, Sperow KM, Niedzwiecki LM, Izquierdo-Martin M, Chang BC, Harrison RK, Stein RL, MacCoss M, Hagmann WK (1995) Bioorg Med Chem Lett 5:2441
65. Campeau L-C, Schipper DJ, Fagnou K (2008) J Am Chem Soc 130:3266
66. Schipper DJ, Campeau L-C, Fagnou K (2009) Tetrahedron 65:3155
67. Mitchell EA, Peschiulli A, Lefevre N, Meerpoel L, Maes BUW (2012) Chem Eur J 18:10092
68. Bergman SD, Storr TE, Prokopcová H, Aelvoet K, Diels G, Meerpoel L, Maes BUW (2012) Chem Eur J 18:10393
69. Chatani N, Asaumi T, Ikeda T, Yorimitsu S, Ishii Y, Kakiuchi F, Murai S (2000) J Am Chem Soc 122:12882
70. Chatani N, Asaumi T, Yorimitsu S, Ikeda T, Kakiuchi F, Murai S (2001) J Am Chem Soc 123:10935
71. Pastine SJ, Gribkov DV, Sames D (2006) J Am Chem Soc 128:14220
72. Davies HML, Venkataramani C, Hansen T, Hopper DW (2003) J Am Chem Soc 125:6462
73. Prokopcová H, Bergman SD, Aelvoet K, Smout V, Herrebout W, Van der Veken B, Meerpoel L, Maes BUW (2010) Chem Eur J 16:13063
74. Ackermann L (2011) Chem Rev 111:1315
75. He G, Zhang S-Y, Nack WA, Li Q, Chen G (2013) Angew Chem Int Ed 52:11124
76. Sharpe RJ, Johnson JS (2015) J Am Chem Soc 137(15):4968–4971
77. Desai LV, Hull KL, Sanford MS (2004) J Am Chem Soc 126:9542
78. Siler DA, Mighion JD, Sorensen EJ (2014) Angew Chem Int Ed 53:5332
79. Dyker G (1992) Angew Chem Int Ed 31:1023
80. Dyker G (1994) Angew Chem Int Ed 33:103
81. Baudoin O, Herrbach A, Guéritte F (2003) Angew Chem Int Ed 42:5736
82. Chaumontet M, Piccardi R, Audic N, Hitce J, Peglion J-L, Clot E, Baudoin O (2008) J Am Chem Soc 130:15157
83. Hitce J, Retailleau P, Baudoin O (2007) Chem Eur J 13:792
84. Chaumontet M, Piccardi R, Baudoin O (2009) Angew Chem 121:185
85. Kametani T, Ogasawara K, Takahashi T (1972) J Chem Soc Chem Commun 675

86. Janody S, Jazzar R, Comte A, Holstein PM, Vors J-P, Ford MJ, Baudoin O (2014) Chem Eur J 20:11084
87. Rousseaux S, Davi M, Sofack-Kreutzer J, Pierre C, Kefalidis CE, Clot E, Fagnou K, Baudoin O (2010) J Am Chem Soc 132:10706
88. Pierre C, Baudoin O (2011) Org Lett 13:1816
89. Ren H, Knochel P (2006) Angew Chem Int Ed 45:3462
90. Ren H, Li Z, Knochel P (2007) Chem Asian J 2:416
91. Watanabe T, Oishi S, Fujii N, Ohno H (2008) Org Lett 10:1759
92. Sofack-Kreutzer J, Martin N, Renaudat A, Jazzar R, Baudoin O (2012) Angew Chem Int Ed 51:10399
93. Dailler D, Danoun G, Baudoin O (2015) Angew Chem Int Ed 54:4919
94. Dailler D, Danoun G, Ourri B, Baudoin O (2015) Chem Eur J. doi:10.1002/chem201501370
95. Ersmark K, Del Valle JR, Hanessian S (2008) Angew Chem Int Ed 47:1202

Top Organomet Chem (2016) 56: 155–188
DOI: 10.1007/3418_2015_139

Published online: 19 August 2015

New Concept of C–H and C–C Bond Activation via Surface Organometallic Chemistry

Manoja K. Samantaray, Raju Dey, Santosh Kavitake, and Jean-Marie Basset

Abstract In this chapter we describe the recent applications of well-defined oxide-supported metal alkyls/alkylidenes/alkylidynes and hydrides of group IV, V, and VI transition metals in the field of C–H and C–C bond activation. The activation of ubiquitous C–H and C–C bonds of paraffin is a long-standing challenge because of intrinsic low reactivity. There are many concepts derived from surface organometallic chemistry (SOMC): surface organometallic fragments are always intermediates in heterogeneous catalysis. The study of their synthesis and reactivity is a way to rationalize mechanism of heterogeneous catalysis and to achieve structure activity relationship. By surface organometallic chemistry one can enter any catalytic center by a reaction intermediate leading in fine to single site catalysts. With surface organometallic chemistry one can coordinate to the metal which can play a role in different elementary steps leading for example to C–H activation and Olefin metathesis. Because of the development of SOMC there is a lot of space for the improvement of homogeneous catalysis. After the 1997 discovery of alkane metathesis using silica-supported tantalum hydride by Basset et al. at low temperature (150°C) the focus in this area was shifted to the discovery of more and more challenging surface complexes active in the application of C–H and C–C bond activation. Here we describe the evolution of well-defined metathesis catalyst with time as well as the effect of support on catalysis. We also describe here which metal–ligand combinations are responsible for a variety of C–H and C–C bond activation.

Keywords Alkane metathesis · Metal-Alkylidene · Metal-Alkylidyne · Metal-Hydride · Olefin metathesis · Transition metals

M.K. Samantaray, R. Dey, S. Kavitake, and J.-M. Basset (✉)
KAUST Catalysis Center (KCC), King Abdullah University of Science and Technology, 23955-6900 Thuwal, Saudi Arabia
e-mail: jeanmarie.basset@kaust.edu.sa

Contents

1 Introduction 156
2 Surface Organometallic Chemistry (SOMC) 157
2.1 Various Oxide Supports and Their Functionalities Used in SOMC 158
3 Surface Organometallic Chemistry of Metal Alkyls/Alkylidene and Alkylidyne 160
3.1 Reactivity of Group IV (Zr, Hf, and Ti) Metal Alkyls on Oxide Surfaces 160
4 Metathesis of Alkane 170
4.1 Mechanism for Alkane Metathesis Reaction 170
4.2 Metathesis of Linear Alkanes 172
4.3 Metathesis of Cycloalkanes 176
4.4 Branched Alkanes Metathesis: Metathesis of 2-Methylpropane 179
4.5 Cross Metathesis Between Two Different Alkanes 180
4.6 Hydro-metathesis Reactions 182
5 Conclusions 183
References 184

1 Introduction

The activation of ubiquitous C–H and C–C bonds of paraffins is a long-standing challenge for chemists because of their presence in petroleum and natural gas and their intrinsic low reactivity. In 1997, our group reported the catalytic transformation of acyclic alkanes into their lower and higher homologues using silica-supported tantalum hydride(s) [1] in the absence of hydrogen at low temperature (150°C). This has resulted in the faster development of surface organometallic chemistry (SOMC), a discipline which has progressively emerged as a new area of heterogeneous and homogeneous catalysis where one can prepare relatively well-defined "single-site catalysts" [2]. The first results in the area of C–H and C–C bond activation came from the discovery of single-site catalysts, e.g., $[(\equiv Si–O–)_3Zr–H]$, which were able to catalyze the low-temperature hydrogenolysis of alkanes [3] and later of polyethylene [4].

What was interesting and new in the SOMC approach is the fact that it was bridging the two areas of homogeneous and heterogeneous catalysis which did not overlap enough in the past. During the last 60 years, homogeneous catalysis played an important role in the selective organic transformations of lower to higher value products [5, 6]. Clear understanding of the reaction mechanism at the molecular level and selective formation of the product by tuning the metal center and its ligands are the main reasons for the increasing use of homogeneous catalysts. This resulted from the parallel development of molecular organometallic chemistry [7–11]. In contrast, the heterogeneous catalysts, which are more commonly used in industry than homogeneous catalysis, did not lead to a clear understanding of reaction mechanisms (at least at the atomic and molecular level), although the parallel development of surface science could allow successful story in the identification of elementary steps (e.g., in ammonia synthesis) [12]. The main reason was the small amount of active sites and consequently the difficulty to fully characterize

these active sites and to draw a reliable and predictive structure–activity relationship.

In this chapter, we try to describe SOMC strategy in the recent years to achieve alkane and cycloalkane metathesis with increasing TONs and selectivities. We will explore the surface organometallic chemistry of Group IV, V and VI metals on various supports and the properties of these single-site systems in the area of alkane and cycloalkane metathesis.

2 Surface Organometallic Chemistry (SOMC)

A heterogeneous catalyst is an ideal choice for the great variety of chemical transformations carried out in industry. Homogeneous catalysts, mostly because of their fragility, instability at higher temperature, and difficulty to separate them from the product(s) after reaction, are comparatively less used in industry (although the number of homogeneous processes is steadily increasing with time). However, selective utilization of the small number of active sites in heterogeneous catalyst makes their characterization quasi-impossible, and, as a result, structure–activity relationship is rarely reached which prevents further improvement of these catalysts.

In order to bring the concepts of homogeneous catalysis into heterogeneous catalysis, a new field of catalysis was developed called surface organometallic chemistry (SOMC) (Scheme 1). SOMC led progressively to the discovery of a new area of chemistry [13, 14]. It has been found that organometallic complexes react with surfaces of oxides in a very specific way leading to new materials having an extremely high electron deficiency. As a consequence a very strong reactivity to activate the C–H and C–C bonds of paraffin's was observed. It was discovered when group IV metal alkyls were reacted with silica surfaces. The first discovery of the hydrides of group IV was made in the field of olefin polymerization [15]. These group IV metal alkyls (or hydrides) are tremendously effective for low-temperature hydrogenolysis of most alkanes and polyolefins (similar to Ziegler–Natta depolymerization), activation of methane, and coupling of methane into ethane and hydrogen. A series of new reactions were developed by using this approach [16].

After its origin, SOMC has been extended to the full ensemble of metallic elements of the periodical table, to a huge variety of ligands, and to a huge variety of supports. In addition, SOMC approach is applied in the area of nanoparticles. In almost all cases, we could progressively understand reaction mechanisms and make a clear structure–activity relationship.

SOMC is purely a surface phenomenon where an organometallic complex binds selectively with the surface by covalent (or sometimes ionic or both) bonds. One can then access to its electronic configuration and oxidation state, and this leads to a better understanding of the reaction mechanism. In SOMC, the surface acts as a ligand, which means one can tune the catalytic activity of the organometallic with the surface

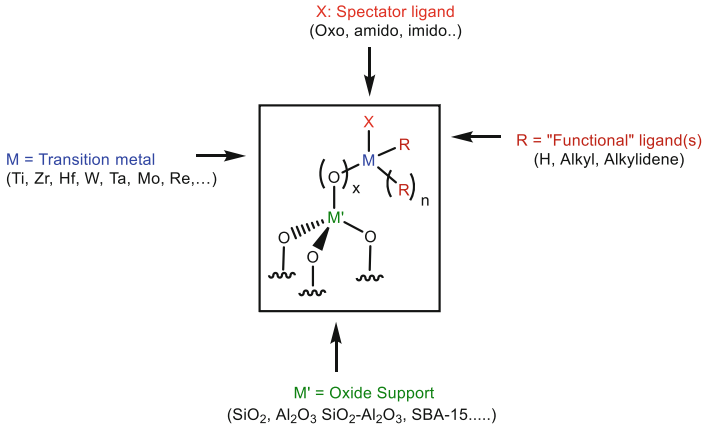

Scheme 1 Schematic presentation of surface organometallic compound

ligand. Surface can play the role of acid–base ligand as well as redox site. Besides this, steric constraints in a porous surface also play an important role in catalysis.

Surface organometallic fragments can also be considered as reaction intermediates in heterogeneous catalysis. Thus, the study of their stoichiometric reactivity allows identification of the elementary steps in a precise way. Thus, as short statement, SOMC is making a strong creative bridge between homogeneous and classical heterogeneous catalysis.

2.1 Various Oxide Supports and Their Functionalities Used in SOMC

To graft organometallic complexes in SOMC, various inorganic materials have been used as a support such as silica, silica–alumina, alumina, magnesia, MCM 41, SBA-15, amino-modified SBA-15, etc. Depending on the nature of the reactive sites on the surface of these materials, different behaviors were observed, leading to sometimes completely different catalytic activity. Before considering the reactivity of metal alkyls with, for example, silica surface, we have to understand the functional groups present on such surface. First, we will consider flame silica Aerosil® from Degussa partially dehydroxylated at various temperatures. This solid has a surface area of ca. $\approx$200 m^2g^{-1} which contains isolated, vicinal, and geminal hydroxyl groups (Scheme 2).

It was generally believed that reactivity of metal alkyls with the partially dehydroxylated silica surface occurs by protonolysis of the *metal*–alkyl bond by the remaining surface silanols. However, progressively it appeared that this is a very narrow description of a complex phenomenon. In a partially dehydroxylated surface, the dehydroxylation produces ≡Si–O–Si≡ groups for which the strain is

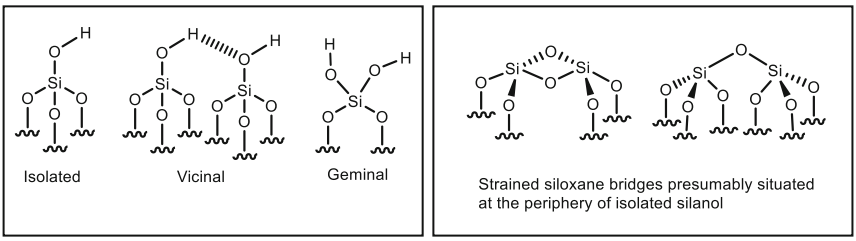

Scheme 2 Various surface silanols and siloxane bridges present on partially dehydroxylated silica

Table 1 Example of various organometallic complexes on oxide surface prepared by SOMC approach

Metal	SOMC species	References
Vanadium	$(\equiv SiO-)V(=NBu^t)(CH_2Bu^t)_2$	[18]
Chromium	$(\equiv SiO-)Cr(CH_2Bu^t)_3$	[19]
Zirconium	$(\equiv SiO-)Zr(CH_2Bu^t)_3$	[4, 20]
Molybdenum	$(\equiv SiO-)Mo(\equiv CMe_3)(CH_2Bu^t)_2$	[21]
Tantalum	$(\equiv SiO-)Ta(=CHBu^t)(CH_2Bu^t)_2$	[22]
Tungsten	$(\equiv SiO-)WMe_5$	[23]
Rhenium	$(\equiv SiO-)Re(\equiv CMe_3)(CH_2Bu^t)_2$	[24]
Osmium	$(\equiv SiO-)Os(\equiv CMe_3)(CH_2Bu^t)_2$	[25]

the result of the pretreatment temperature. Thus, at very high temperature, more strained ≡Si–O–Si≡ groups were produced on silica surface and vice versa.

These strained groups exhibit also a typical reactivity with metal alkyls or metal hydrides

To understand the reaction mechanism for a given reaction on surface and correlate structure–activity relationship, first of all a well-defined "single-site" system is needed. To have a well-defined "single-site" system the silanols must be sufficiently isolated from each other to behave independently. This is the necessary condition to reach the ultimate goal of making "single-site" catalysts. Based on the above concepts, flame silica which has a surface area of ≈200 m^2g^{-1} is usually pretreated at 700, 500, and 200°C under high vacuum (10^{-5} mbar) for 16 h. The corresponding number of silanols is equal to 0.26, 0.42, and 0.86 $mmolg^{-1}$, respectively (measured either by ^1H NMR of simple titration method via MeLi) [17]. For such low values for surface silanol especially in the case of $SiO_{2\text{-}700}$, one can presume that the hydroxyl groups are far away from each other and so well-defined grafted organometallic isolated species will be expected upon reaction with these hydroxyl groups. This is the key point of surface organometallic chemistry.

In Table 1, we have mentioned some examples of grafting of organometallic complexes on various supports by the use of surface organometallic chemistry.

3 Surface Organometallic Chemistry of Metal Alkyls/ Alkylidene and Alkylidyne

3.1 Reactivity of Group IV (Zr, Hf, and Ti) Metal Alkyls on Oxide Surfaces

This area was really at the origin of alkane activation with surface metal hydrides. Those surface metal hydrides were obtained by treatment under hydrogen of silica-supported metal alkyls. The first one in this series was tris-neopentylzirconium surface complex [≡SiO–Zr(Np)$_3$] **1**.

Zirconium tris-neopentyl surface complex **1** was synthesized by the sublimation of tetra-neopentylzirconium complex onto the surface of partially dehydroxylated silica at 500°C [26, 27] and fully characterized by IR, NMR, EXAFS, elemental analysis, and gas quantification methods as well as chemical methods [3, 28, 29]. Furthermore, in order to confirm its surface structure, the grafting experiment was carried out with deuterated silica and tetra-neopentylzirconium. Evolution of 1 mol of deuterated neopentane per mole of grafted zirconium proved that there is a single bond between zirconium and oxygen. This monopodal surface structure was further confirmed by EXAFS experiment with **1**.

While zirconium and titanium lead to a monopodal species on $SiO_{2\text{-}500}$ [30], in the case of [Hf(Np)$_4$] the surface reaction produces a mixture of mono- and bipodal species (Scheme 3) [31]. The mono- and bipodal (70:30) mixture was confirmed by the evolution of gas during the reaction associated with the surface microanalysis: the lower the C/Hf ratio in elemental analysis, the higher the percentage of bipodal species. Further, it was confirmed by solid-state NMR: in ^{13}C NMR, two peaks were found at 106 and 95 ppm corresponding to **C**H$_2$ of neopentyl for monopodal surface complex (**3**) and bipodal surface complex (**4**). However, with $SiO_{2\text{-}800}$, Hf

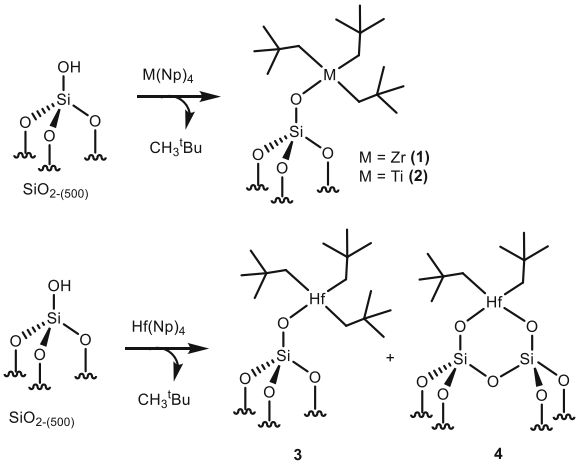

Scheme 3 Synthesis of mono- and bis-grafted group (IV) metal alkyls on $SiO_{2\text{-}500}$

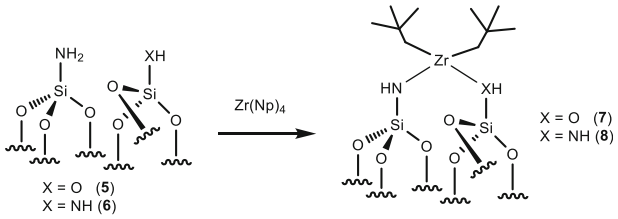

Scheme 4 Grafting of $Zr(Np)_4$ on modified SBA-15

$(NP)_4$ gives only monopodal species which was proved by elemental analysis, gas quantification, and NMR.

The grafting of $Zr(Np)_4$ was not only restricted to silica surface but also to other well-defined oxide surfaces. Recently, amino-modified SBA-15 surfaces were prepared by the reaction of partially dehydroxylated SBA-15 at 1100°C with ammonia at 200 and 500°C to generate [(≡Si–NH_2)(≡Si–OH)] (**5**) and [(≡Si–$NH_2)_2$] (**6**). The advantage of this method is the preparation of adjacent groups in close vicinity. The surface organometallic complexes were prepared by the reaction of [$Zr(Np)_4$] with [(≡Si–NH_2)(≡SiOH)] and [(≡Si–$NH_2)_2$] in pentane for 8 h at room temperature (Scheme 4) [20].

The surface complexes [(≡SiNH–)(≡SiO–)$Zr(Np)_2$] (**7**) and [(≡SiNH–$)_2$Zr $(Np)_2$] (**8**) were fully characterized by solid-state NMR, IR, and TEM. It was also observed in BET experiment that although the surface area decreases slightly due to the grafting of the bulky [$Zr(Np)_3$] fragment, this fragment did not block the opening and the pores of the material. Additionally, bright-field transmission electron microscopy (BF-TEM) obtained with high-resolution TEM (HRTEM) confirms the preservation of the hexagonally ordered mesophase structure [20].

Similarly, $Zr(Np)_4$ and $Ti(Np)_4$ react with silica–alumina partially dehydroxylated at 500°C (SiO_2–$Al_2O_{3\text{-}500}$) to form a 100% monopodal species in case of zirconium [4] and a mixture of 40% mono- and 60% bipodal species in case of titanium [32]. Similarly, when $Ti(CH_2–Ph)_4$ and $Zr(CH_2–Ph)_4$ were grafted onto $SiO_{2\text{-}200}$ and $SiO_{2\text{-}700}$, one could generate, respectively, bipodal and monopodal surface complex [33].

3.1.1 Hydrides of Group IV Metal Alkyls

After synthesis of [(≡SiO–$Zr(Np)_3$] (**1**) and species [(≡SiO–$Ti(Np)_3$] (**2**) [30], the efforts were made to synthesize and identify the corresponding surface organometallic hydride which we believed to be the active catalyst for various types of C–H bond activation reaction. **1** and **2** generate tri-podal monohydride (**9**, **10**) as major component when reacted with H_2 at 150°C [30, 34]. However, **3** generates bipodal bis-hydride (**11**) as major component under H_2 atmosphere at temperature lower than 100°C (Scheme 5) [35]. Similar hydrides were observed when silica–alumina and alumina-supported $Ti(Np)_4$ and $Zr(Np)_4$ were heated at 150°C in the

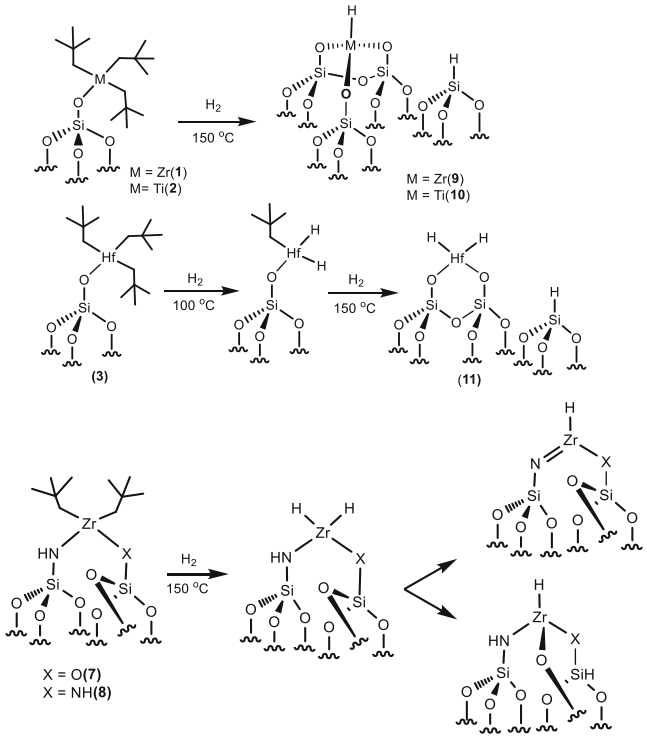

Scheme 5 Metal hydrides of group IV obtained when group IV metal alkyls react with hydrogen

presence of hydrogen [32]. On the other hand under similar conditions, **7** and **8** generated various other hydrides (Scheme 5) [20].

3.1.2 Reactivity of Group V (Ta) Alkyls and Alkylidene on Oxide Surfaces

One of the important aspects of surface organometallic chemistry was achieved when $[Ta(CH_3)_5]$ **12**, which is known to be very unstable at room temperature in solution, was stabilized upon grafting on $SiO_{2\text{-}700}$ surface (a similar observation was observed with $[W(Me)_6]/SiO_{2\text{-}700}$ and will be discussed separately in next section) [36]. $[Ta(CH_3)_5]$ reacts with $SiO_{2\text{-}700}$ at −20°C and generates [≡SiO–Ta $(CH_3)_4$] (**13**) monopodal species. The formation of **13** was confirmed by solid-state NMR, gas quantification methods, as well as elemental analysis (Scheme 6). **13** can easily be transformed into a mixture of mono- and bipodal tantalum–carbene surface complex (**14**) upon heating at 150°C for 4 h. The structure of **14** was precisely confirmed by advanced solid-state NMR, elemental analysis, and gas quantification methods.

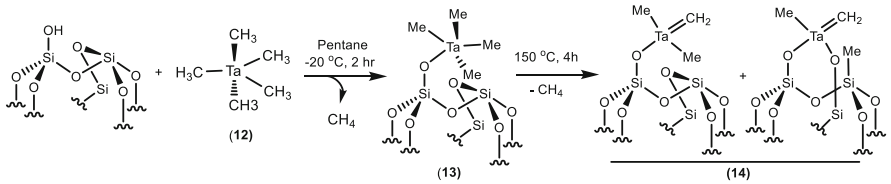

Scheme 6 Grafting of $Ta(CH_3)_5$ on $SiO_{2\text{-}700}$ and formation of mono- and bipodal tantalum-methyl-methylidene surface complex

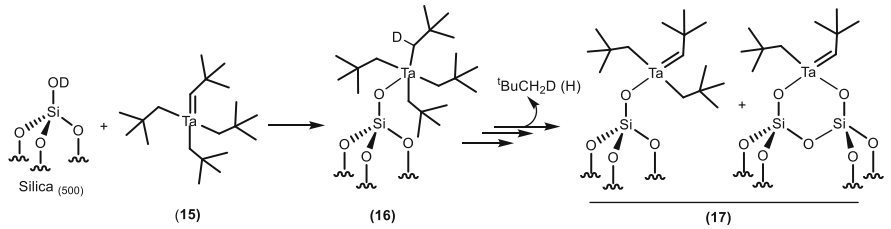

Scheme 7 Formation of mono- and bipodal tantalum-neopentyl-neopentylidene on the surface of $SiO_{2\text{-}500}$

Similarly in previous literature reports, [Ta(=C^{t}Bu)(CH$_2$^{t}Bu)$_3$] (**15**) was grafted on $SiO_{2\text{-}500}$ [37] and $SiO_{2\text{-}700}$ [22], respectively. While in $SiO_{2\text{-}700}$, it gives exclusively monopodal surface organometallic, but in the case of $SiO_{2\text{-}500}$ it gives a mixture of mono- and bipodal surface complex (**17**) via an intermediate **16** (Scheme 7) [37, 38]. The mechanism for the reaction between **15** and $SiO_{2\text{-}500}$ was understood when deuterium labeled $SiO_{2\text{-}500}$ was used. Evolution of more than one mole of neopentane per grafted tantalum (neopentane/Ta = 1.35) [37] indicated the formation of a mixture of mono- and bipodal species on the silica surface (Scheme 7).

The reaction of **15** with deuterated (>90%) silica followed by hydrolysis with D_2O produced 2.6 equiv. of neopentane with the major species as mono-deuterated neopentane (54.4%), followed by 36.7% as bis-deuterated and 5.5% tris-deuterated neopentane along with 3.3% neopentane. The evolution of tris-deuterated neopentane confirmed that the incorporation of deuterium to tantalum carbene occurs during the grafting of ≡SiOD with **15**. Additionally, to confirm the presence of tantalum–carbene species on the surface, **17** was treated with excess of acetone (Scheme 8). Formation of 1 equiv. of **18** per grafted Ta complex confirms the presence of one carbene center per grafted tantalum complex.

Again to confirm the presence of tantalum carbene on silica surface ^{13}C-enriched tantalum–carbene complex, [Ta(=C*H^{t}Bu)(CH$_2$^{t}Bu)$_3$] was grafted on silica$_{-(500)}$. The ^{13}C CP NMR showed a peak at 246 ppm which corresponds to (=**C***H^{t}Bu) along with other peaks confirming the presence of tantalum carbene on the supported complex [39].

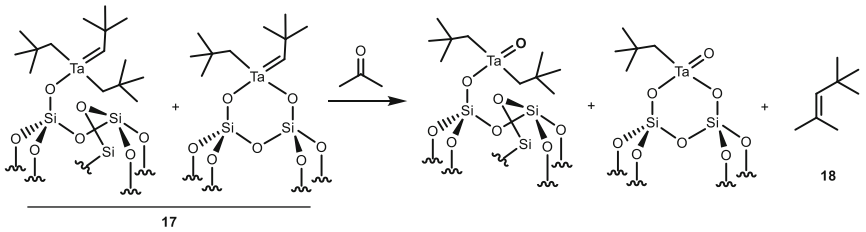

Scheme 8 Pseudo-Wittig reaction between **17** and acetone

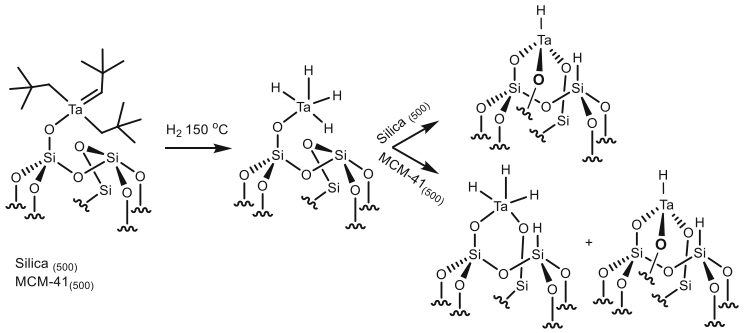

Scheme 9 Evolution of surface tantalum hydride upon heating under hydrogen atmosphere (*bipodal structure in the case of* $SiO_{2\text{-}500}$ *was omitted for clarity*)

MCM-41 partially dehydroxylated at 500°C was also used to understand the behavior of the [Ta(=C^{t}Bu)(CH$_2$^{t}Bu)$_3$] complex on oxide support. Interestingly, NMR, EXAFS, elemental analysis, and gas quantification results support the formation of monopodal species, whereas in the case of $SiO_{2\text{-}500}$, it produces a mixture of mono and bipodal species [40, 41].

3.1.3 Reactivity of Group V (Ta) Hydride on Oxide Surfaces

Interestingly, clearly distinct results were observed when the MCM-41-supported [≡SiOTa(=C^{t}Bu)(CH$_2$^{t}Bu)$_2$] and silica-supported **17** were treated with hydrogen at 150°C (Scheme 8). In the case of silica-supported tantalum monohydride is formed via the intermediacy of tantalum polyhydride which was proved by EXAFS [42], whereas in the case of MCM-41-supported tantalum complex, a mixture of tantalum monohydride (major) and tris-hydride (minor) was formed via tantalum polyhydride [40] (Scheme 9). Upon further heating from 150 to 500°C under hydrogen atmosphere, progressive decrease of the Ta–H peak was observed in IR spectra, and a new surface complex corresponding to [(≡SiO)$_3$Ta] was formed. This can be explained by the fact that at higher temperature, a hydride transfer from

tantalum to silicon and a siloxy transfer from silicon to tantalum were observed [40].

3.1.4 Reactivity of Group VI (W) Alkyls and Alkylidene on Oxide Surfaces

For the exploration of better catalyst for C–H bond activation especially, in the case of alkane metathesis, the focus was shifted from group V to group VI metal catalysts as these metals are well known for olefin metathesis as well as for C–H bond activation. They also were found to make low-temperature hydrogenolysis of alkanes and polymerization of olefin [19, 43]. Similar to group V metal alkyls, group VI metal alkyls can undergo reaction with dehydroxylated silica. Similar to Scheme 7, [W(≡C^{t}Bu)(CH$_2$^{t}Bu)$_3$] (**19**) [Mo(≡C^{t}Bu)(CH$_2$^{t}Bu)$_3$] (**20**) was employed for grafting of group VI metal alkyl on $SiO_{2\text{-}700}$. In general, a pentane solution of an excess of **19** or **20** was added to $SiO_{2\text{-}700}$ at room temperature to obtain [(≡SiO–)W(≡C^{t}Bu)(CH$_2$^{t}Bu)$_2$] [44] (**21**) or [(≡SiO–)Mo(≡C^{t}Bu)(CH$_2$^{t}Bu)$_2$] (**22**) (Scheme 10). The IR spectrum shows a decrease of the ν(≡Si–O–H) band at 3,747 cm^{-1} with the formation of two new series of bands at 3,000–2,700 and 1,500–1,300 cm^{-1} assigned to $\nu_{(CH)}$ and $\delta_{(CH)}$ vibrations.

However, in the case of [Ta(=C^{t}Bu)(CH$_2$^{t}Bu)$_2$], the reaction proceeds with the addition of Si–OH bond onto the Ta=C bond followed by α-H abstraction (Scheme 7), but in the case of [W(≡C^{t}Bu)(CH$_2$^{t}Bu)$_3$] or [Mo(≡C^{t}Bu)(CH$_2$^{t}Bu)$_3$], the addition of Si–OH on W≡C or Mo≡C was not observed when grafted on $SiO_{2\text{-}700}$ (Scheme 10). It forms a monopodal carbyne species on $SiO_{2\text{-}700}$. Gas quantification and elemental analysis confirmed that there are nearly three neopentyl groups per tungsten atom which again corroborates the monopodal structure of the above grafted complex. Furthermore, formation of a carbyne ligand on silica surface was confirmed by ^{1}H, ^{13}C, and HETCOR solid-state NMR with the observation of characteristic peak at 318 ppm for the $\mathbf{C}_{(carbyne)}$. The supported complex **21** was found to be very active in olefin metathesis but exhibited no activity in alkane metathesis. The corresponding hydride [(≡SiO–)W(≡C^{t}Bu)(CH$_2$^{t}Bu)$_2$] was prepared by treating **21** with the excess of hydrogen at 150°C and found to be much less active in alkane metathesis. To generate more electrophilic metal center for better catalytic activity, alumina partially dehydroxylated at 500°C (PDA) was chosen as solid support. Under similar condition, **19** was grafted on $Al_2O_{3\text{-}500}$ at room temperature (Scheme 11).

The supported organometallic complexes were characterized by IR, solid-state NMR, EXAFS, and elemental analysis. All these data taken together confirm that it is a mixture of monopodal carbyne (major) (Scheme 10) along with a minor amount of cationic tungsten with the migration of neopentyl group from tungsten to nearby electrophilic aluminum center. The corresponding polyhydride was prepared from **23** by the treatment of excess of hydrogen at 150°C (Scheme 12). IR spectra showed partial consumption of the Al–OH with simultaneously formation of Al–H bond,

Scheme 10 Grafting of group VI metal alkylidyne on the surface of $SiO_{2\text{-}700}$

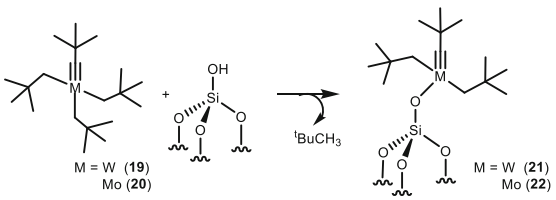

Scheme 11 Grafting of [W(≡C^{t}Bu)(CH$_2$^{t}Bu)$_3$] on the surface of $Al_2O_{3\text{-}500}$ (*for simplicity only Td Al is shown*)

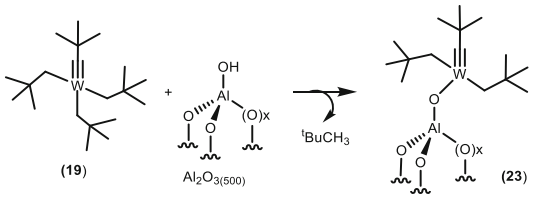

Scheme 12 Formation of tungsten polyhydride on $Al_2O_{3\text{-}500}$

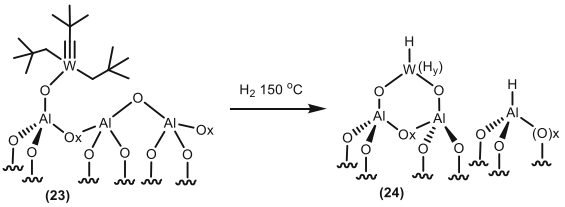

Scheme 13 Proposed mechanism for the non-oxidative coupling of methane catalyzed by the W–H supported onto SiO_2–Al_2O_3 and Al_2O_3

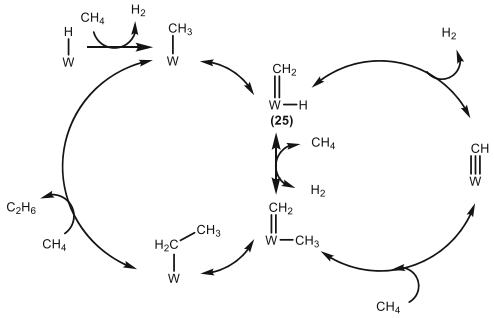

and it indicates the formation of bis-aluminoxy hydride species on the surface of alumina (Scheme 12) [45].

Initial attempts to generate W(carbene)(hydride) from a partial hydrogenation of **21** and **23** failed. W(carbene)(hydride) was believed to be an active catalytic species for alkane metathesis reaction. In 2010, Basset et al. reported direct methylation of tungsten polyhydride with methane at higher temperature followed by α-H abstraction generated tungsten carbene species along with tungsten carbyne species (Scheme 13) [46]. However, **25** was found to be very less active in alkane metathesis reaction.

On the other hand, in an important observation, it was found that highly unstable [W(CH$_3$)$_6$] (**26**) [47] can easily be grafted on the oxide support to generate the

Scheme 14 Grafting of $[W(CH_3)_6]$ on $SiO_{2\text{-}700}$

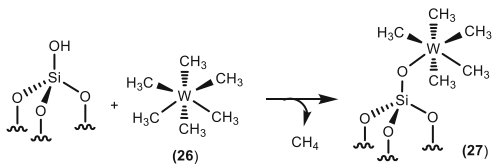

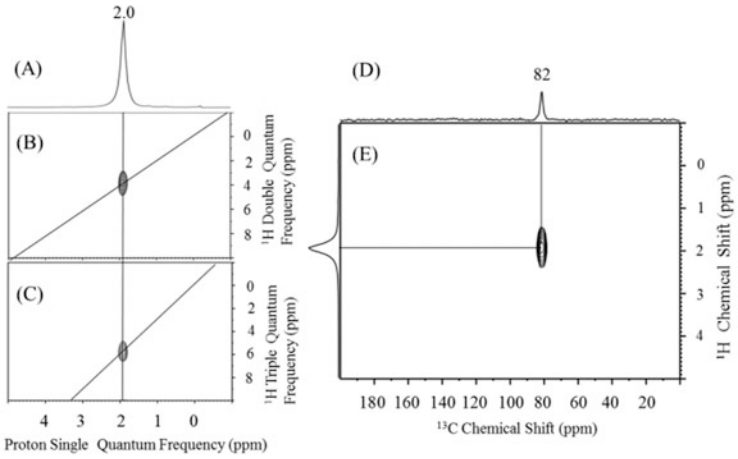

Fig. 1 (*A*) One-dimensional (1D) ^{1}H MAS solid-state NMR spectrum of **27.** (*B*) Two-dimensional (2D) ^{1}H–^{1}H double-quantum (DQ)/single-quantum (SQ) and (*C*) ^{1}H–^{1}H triple-quantum (TQ)/SQ NMR spectra of **27**, (*D*) ^{13}CCP/MAS NMR spectrum of **27**, and (*E*) 2D ^{1}H–^{13}C CP/MAS dipolar HETCOR spectrum of **27**

corresponding stable grafted surface organometallic complex (Scheme 14). When a pentane solution of **26** was allowed to react with $SiO_{2\text{-}700}$ at −50 to −30°C for a required time period, golden yellow solid power was formed [23].

The supported complex $[(\equiv SiO–)W(CH_3)_5]$ (**27**) was fully characterized by advanced solid-state NMR, IR, elemental analysis, and gas quantification method (Fig. 1). ^{13}C solid-state NMR shows a peak at 82 ppm which auto correlates with peak at 2.0 ppm obtained from ^{1}H NMR confirming the formation of **27**. Furthermore, double-quantum (DQ) and triple-quantum (TQ) experiments confirmed the formation of **27** [23]. All combined experimental data along with NMR are in favor of formation of a monopodal complex on silica surface (Fig. 1).

A ^{13}C-enriched sample of **27** was heated in the NMR probe from 25 to 72°C. Maintaining temperature at 72°C for 12 h revealed several NMR signals in the region of 298 and 40–48 ppm. HETCOR spectra showed several correlation cross peaks. Specifically, the ^{13}C peak at 298 ppm correlates with the ^{1}H peak at 7.6 ppm in ^{1}H NMR which confirms the formation of the tungsten carbyne (W≡**CH**) (Scheme 15).

NMR results also confirm that along with all the peaks corresponding to tungsten-methyl-methylidyne, a peak at −0.5 ppm is also observed which auto correlates in double quantum (DQ) and triple quantum (TQ), confirming either the

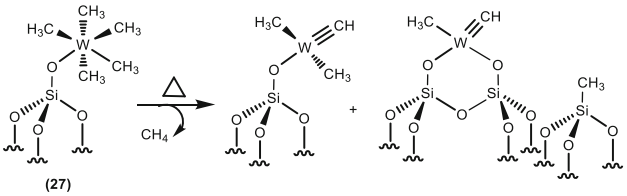

Scheme 15 Formation of tungsten methylidyne (W≡C) species

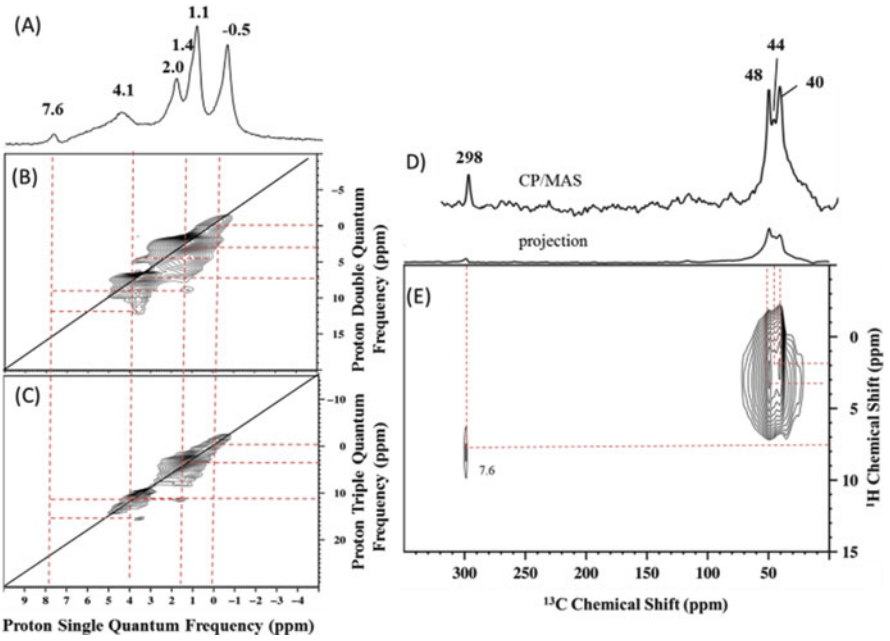

Fig. 2 (*A*) 1D ^{1}H spin-echo MAS solid-state NMR spectrum of $[(\equiv SiO)_xW(\equiv CH)Me_y]$, (*B*) 2D ^{1}H–^{1}H DQ and (*C*) ^{1}H–^{1}H TQ, (*D*) ^{13}CCP/MAS NMR spectrum, and (*E*) 2D CP/MAS HETCOR NMR spectrum

formation of CH_4 while heating the species **27** or methyl migration from W to Si (Fig. 2). Finally, ^{29}Si NMR proves that a peak at −12 ppm is due to methyl migration from W to Si which again confirms that the structure of the decomposed species is a mixture of mono- and bipodal (Scheme 15) [23].

To understand the activity of the $[W(CH_3)_6]$ (**26**) with other oxide supports, the synthesis was extended from silica to silica–alumina. In a similar way, like in silica, $[W(CH_3)_6]$ was grafted on silica–alumina partially dehydroxylated at 500°C. Grafting experiments of $[W(CH_3)_6]$ carried out in pentane at −50 to −30°C resulted in a brown solid **28** (Scheme 16).

The resulting solid **28** was fully characterized using advance solid-state NMR techniques (Fig. 3) along with elemental analysis and gas quantification methods. Solid-state NMR shows two peaks in the ^{13}C NMR: one at −17 ppm belongs to

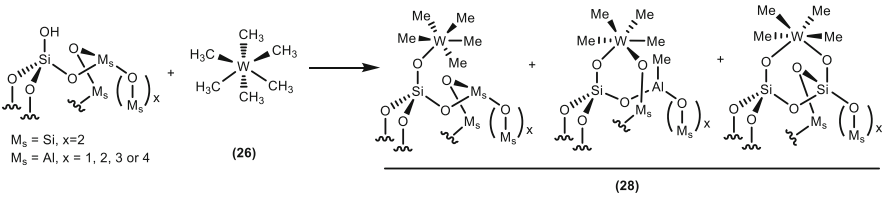

Scheme 16 Grafting of $W(CH_3)_6$ on silica–alumina partially dehydroxylated at 500°C

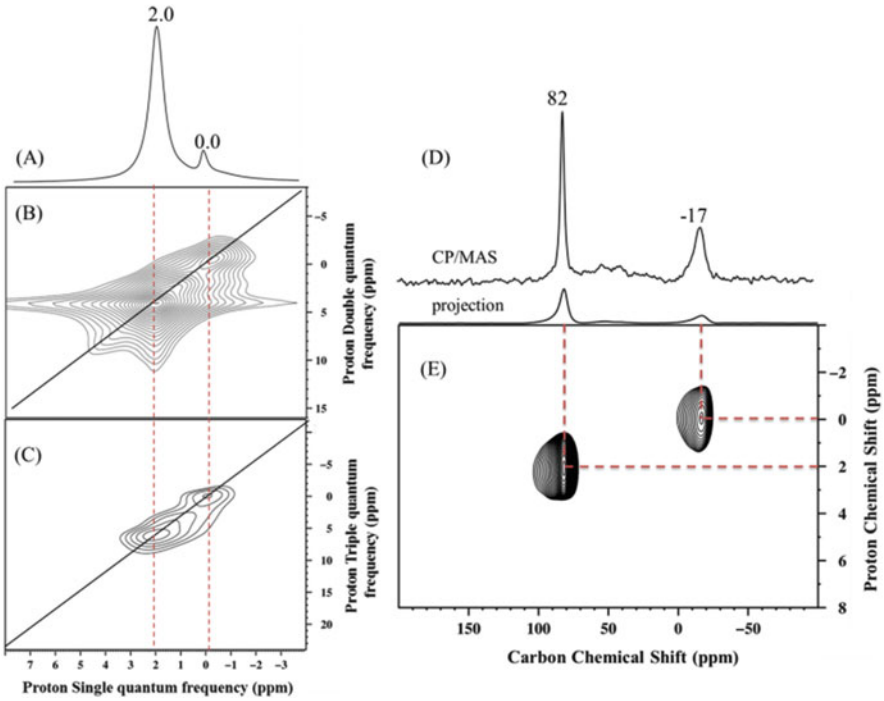

Fig. 3 HETCORE, DQ, and TQ spectra of surface complex **28**

[Al–CH_3] peak which is likely resulting from methyl migration from W to Al [48], and the other at 82 ppm is ascribed to a[W–CH_3] which correlates with the ^{1}H NMR in HETCOR: therefore, all peaks belong to same complex (Fig. 3) [49]. Based on the experimental evidence and characterization data, it was believed that the grafting of **26** on SiO_2–$Al_2O_{3\text{-}500}$ leads to the formation of a mixture of mono- and bipodal surface complex.

In conclusion, all the surface organometallic complexes synthesized and characterized so far are extremely electron deficient and between eight electrons to 12 electrons in the Green formalism [50]. The resulting complexes either alkyls

or hydrides have exhibited very specific properties in catalysis related to alkanes but also olefins.

4 Metathesis of Alkane

Alkane metathesis is a catalytic reaction involving successive breaking and formation of C–H and C–C bonds of alkanes to give lower and higher alkanes homologues [51]. Alkane metathesis reaction can be described by the following general equation:

$$2C_nH_{2n+2} \rightleftharpoons C_{(n-i)}H_{2(n-i)+2} + C_{(n+i)}H_{2(n+i)+2},$$

where $n = 2...n-1$ and $i = 1, 2, 3...n-1$.

In 1997, Basset et al. introduced catalytic transformation of acyclic alkanes into their lower and higher homologues using silica-supported tantalum hydrides [1] in the absence of hydrogen at low temperature (150°C).

Since in the alkane metathesis, one or more C–C bonds can be broken and reformed, it lacks the selectivity in the formation of products, in contrast to the olefin metathesis where only one type of C=C is cleaved and recombined. With certain exceptions, the observed product selectivity in alkane metathesis has been $C_{n+1} > C_{n+2} \gg C_{n+3}...; C_{n-1} > C_{n-2} \gg C_{n-3}...$.

Later it was found that to get a successful activity in alkane metathesis, catalysts need to have a multifunctionality, i.e., (i) activation of the C–H bond resulting in a metal alkyl, (ii) α-H elimination leading to a metallocarbene, (iii) β-H elimination leading to an olefin, (iv) olefin metathesis, and (v) finally successive hydrogenations of the olefins or the carbenes leading to alkanes. The selectivity of products is a consequence of the relative stabilities of metallacyclobutanes intermediates formed during the olefin metathesis [52].

4.1 Mechanism for Alkane Metathesis Reaction

It took a long time to establish the mechanism of this fascinating reaction after its discovery: it was known that silica-supported tantalum hydride reacted with methane at very reasonable temperature (ca. 50°C) to give a tantalum methyl and hydrogen by sigma bond metathesis [51]. A first hypothesis was advanced in which the Ta-alkyl would react directly with the C–C bond of the alkane to give a redistribution of alkyl group by analogy with the redistribution of alkylidene in olefin metathesis and the redistribution of alkylidyne in alkyne metathesis [53]. However, there was no evidence (experimental or theoretical) of such redistribution. Progressively, the surface organometallic chemistry of tantalum and tungsten allowed the observation of primary products in alkane metathesis. It is only recently that all the elementary steps have been isolated with a tantalum tetramethyl linked to silica [36].

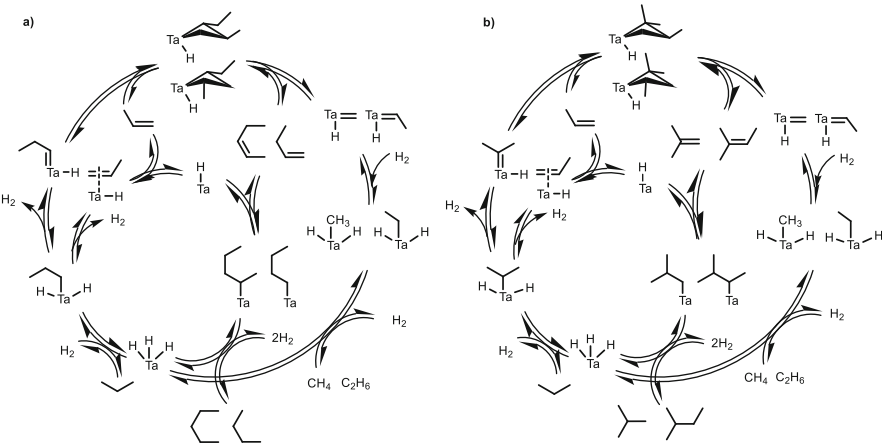

Scheme 17 Proposed mechanism for the propane metathesis (**a**) formation of linear alkanes and (**b**) formation of branched alkanes

Presently, one can summarize as follows the various observations that we made on the mechanism of alkane metathesis:

As already mentioned, it was observed that one mole of hydrogen is liberated when methane is reacted with the tantalum hydride with the formation of tantalum methyl. The reaction with methane above 150°C leads to the formation of the Ta-methyl, Ta-methylene, and Ta-methylidyne species plus H_2 (M = Ta) [40–42, 54]. These observations are a proof that the first step of alkane metathesis is the formation of metal alkyl intermediate via cleavage of the C–H bond of the alkane likely by sigma bond metathesis. Further, detailed mechanistic [22, 55] and experimental kinetic studies revealed that the alkenes and hydrogen are the primary products [56]. Initially, it was believed that the active site was a bis-siloxy tantalum-monohydride, but progressively, evidence came in favor of an equilibrium between bis-siloxy tantalum-monohydride d^2 and bis-siloxy-tantalum-tris-hydride d^0 [57], and the mechanism would fit much better with a bis-siloxy-tantalum-tris-hydride [58].

With this knowledge, a possible mechanism was proposed where the metal hydride activates the C–H bond of alkane to form H_2 and alkyl-M surface species, e.g., in the case of propane using Ta-hydride, it forms *n*- and iso-propyl-Ta. The respective alkyl-Ta species either undergo α-H transfer [59, 60] leading to the two carbene–hydride complexes Ta(H)(=C(CH_3)$_2$) and Ta(H)(=CH–CH_2–CH_3) or β-H transfer [60, 61] forming an olefin–hydride complex Ta(H)(η^2-CH_2=CH–CH_3) (Scheme 17). The resulting propene then leaves the coordination sphere of the Ta (H)(η^2-CH_2=CH–CH_3) and undergoes a homologation process via cycloaddition with the carbenic species to form four differently substituted metallacyclobutanes with methyl or ethyl groups in [1,2] or [1,3] positions (Scheme 17a) [62–65]. These metallacyclobutanes undergo cycloreversion to give new olefins and new carbene–hydride species (Scheme 17b) [66]. This catalytic cycle further continues via hydride addition into the carbene as well as olefin insertion into the hydrides.

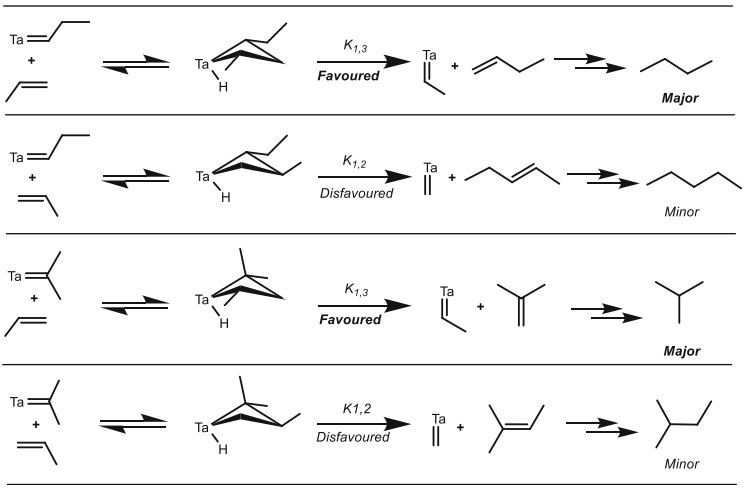

Scheme 18 Stability of metallacyclobutane intermediates in propane metathesis reaction

Subsequently, the alkanes are liberated via a known process of hydrogenation and hydrogenolysis [67] or possibly via σ-bond metathesis [68].

The product selectivity in the case of propane for the formation of linear alkanes was found to be butane (C_{n+1}) in higher amount than pentane (C_{n+2}). This can be clearly explained based on the steric interactions between substituents in [1,2] or [1,3] positions in metallacyclobutane intermediates (Scheme 18) [22, 52].

Very recently it was found that with ^{13}C-labeled C_2H_6, it is possible to isolate the initiation products in metathesis of ethane into propane with [(≡SiO–)TaMe$_4$] (**13**). This can be considered as a breakthrough because for the first time it was found that the reaction mechanism may proceed with a Ta-alkyl; previously, it is believed to proceed by a Ta–H (Scheme 19) ([36, 69]).

4.2 Metathesis of Linear Alkanes

4.2.1 Metathesis of Propane

Synthesis and characterization of several catalyst precursors of [Ta] and [W] on different supports like silica [44], alumina [45], or silica–alumina [70] have been discussed in the previous section. These catalyst precursors were tested mainly in propane metathesis under similar condition in batch reactor at 150°C for 120 h. Catalytic performances revealed that the [SiO_2–$Al_2O_{3\text{-}500}$–W–H] and [$Al_2O_{3\text{-}500}$–W–H] have similar and better activity (TON) than the corresponding silica-supported tantalum-based catalyst precursors (Table 2). It was also observed that the product selectivity for tungsten hydrides is narrower than for tantalum hydrides [71].

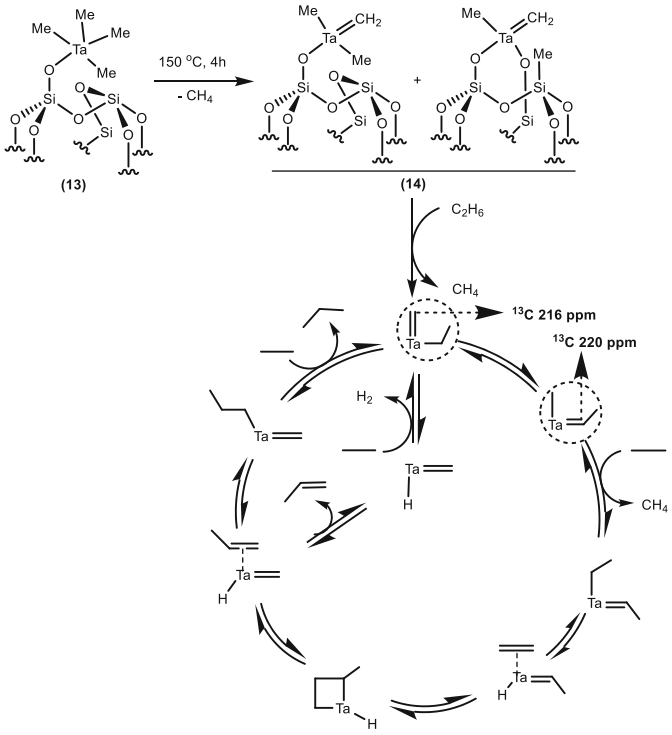

Scheme 19 Proposed mechanism for metathesis of ethane by $Ta(Me)_4$ – precatalyst

Recently, in order to further improve catalytic activity, two new catalyst precursors were developed [(≡SiO–)WMe_5] (**27**) [23] and [(≡SiO–)$TaMe_4$] (**13**) [36]. Such polymethyl complexes possess no β-H and can easily generate in situ the corresponding surface M-methylidene species (M = W [23, 72], Ta [36]) which has been done with little success in the past [44, 73]. The improvement in activity is marginal in the case of **13** compared to that of earlier reported tantalum catalyst precursors. However, the catalyst precursor **27** showed notable improvement than previously reported catalyst precursors with TON of 127 (Table 2, Entry 14).

Further investigation by preparing tungsten complexes on different supports and their corresponding hydride complexes to test their catalytic performances is under progress.

4.2.2 Metathesis of Decane

After tremendous success in propane metathesis (lower alkane) reaction, catalyst precursor **27** was employed for metathesis of *n*-decane (higher alkane). The *n*-decane metathesis reaction carried out at 150°C produced a broad distribution of linear alkanes from methane to C_{30} (triacontane) with trace amount of branched alkanes without any olefinic or cyclic products [74]. Interestingly, the formation of lower

Table 2 Comparison of catalyst precursor activity in metathesis of propane at 150°C for 120 h

No.	Catalyst precursors	TON[a]	Product selectivity (%)[b]						
			CH_4	C_2H_6	C_4H_{10}	i-C_4H_{10}	C_5H_{12}	i-C_5H_{12}	C_6H_{14}
1	$[(\equiv SiO)Ta(=CH^tBu)(CH_2{}^tBu)_2]_{(Si\text{-}700)}$ (**29**)	35	12.8	47.5	22.8	10.4	3.5	2.5	Traces
2	$[(\equiv Al_sO)Ta(=CH^tBu)(CH_2{}^tBu)_2]_{(Al2O3\text{-}500)}$ (**30**)	34	5.0	52.0	32.0	7.0	3.5	1.5	Traces
3	$[(\equiv SiO)Ta(=CH^tBu)(CH_2{}^tBu)_2]_{(SA\text{-}500)}$ (**31**)	33	10.5	47.0	31.2	3.8	4.2	2.3	Traces
4	$[(\equiv SiO)W(\equiv C^tBu)(CH_2{}^tBu)_2]_{(Si\text{-}700)}$ (**21**)	<1	–	–	–	–	–	–	–
5	$[(Al_sO)W(\equiv C^tBu)(CH_2{}^tBu)_2]_{(Al2O3\text{-}500)}$ (**23**)	28	2.7	65.4	20.7	2.9	5.3	1.5	1.0
6	$[(\equiv SiO)W(\equiv C^tBu)(CH_2{}^tBu)_2]_{(SA\text{-}500)}$ (**32**)	29	1.6	61.7	25.7	3.4	5.5	1.3	1.0
7	$[(\equiv SiO)Ta\text{–}H]_{(Si\text{-}700)}$ (**33**)	60	10.0	46.0	30.6	5.1	4.8	2.2	Traces
8	$[(\equiv Al_sO)Ta\text{–}H]_{(Al2O3\text{-}500)}$ (**34**)	60	9.5	47.5	27.9	8.6	4.5	1.5	–
9	$[(\equiv SiO)Ta\text{–}H]_{(SA\text{-}500)}$ (**35**)	59	11.5	46.5	31.4	4.1	4.8	2.2	–
10	$[(\equiv SiO)W\text{–}H]_{(Si\text{-}700)}$ (**36**)	8	5.7	56.0	29.0	2.8	5.1	1.4	–
11	$[(\equiv Al_sO)W\text{–}H]_{(Al2O3\text{-}500)}$ (**24**)	121	2.4	57.3	28.9	3.7	5.0	1.3	1.4
12	$\mathbf{[(\equiv SiO)W\text{–}H]_{(SA\text{-}500)}}$ (**37**)	**123**	1.9	58.0	28.9	3.2	5.2	1.4	1.4
13	$\mathbf{[(\equiv SiO)TaMe_4]_{(Si\text{-}700)}}$ (**13**)	**49**	11.6	45.4	32.8	6.5	5.5	1.7	1.0
14	$\mathbf{[(\equiv SiO)WMe_5]_{(Si\text{-}700)}}$ (**27**)	**127**	2.0	54.0	33.0	4.0	6.0	1.0	Traces

[a]TON is expressed in (mol of propane transformed)/(mol. of W)

[b]The selectivities are defined as the amount of product over the total amount of products

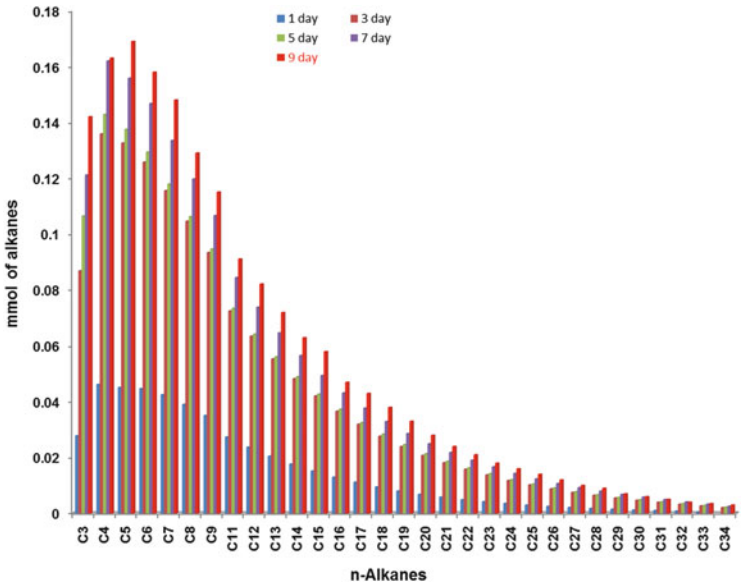

Fig. 4 Product distribution of *n*-decane metathesis for the catalysts $[(\equiv SiO)WMe_5]_{Si\text{-}Al\text{-}500}$

alkane was found to be predominant compared to higher alkanes. This was in sharp contrast to the narrow distribution observed in the case of propane metathesis ($C_{n+1} > C_{n-1}$). Further experiments for metathesis of *n*-hexane to *n*-nonane also showed similar product distribution. The distribution of product was found to be independent of the alkane carbon number. However, such a product distribution was closer to that reported with fully heterogeneous tandem system (Fig. 4). We assume that we have an ISOMET-PARAFFIN process by opposition to ISOMET-OLEFIN [6, 75].

The drastic improvement in the catalytic activity was observed when **27** is replaced by $[SiO_2–Al_2O_{3\text{-}500}–WMe_5]$ (**28**) catalyst precursor [49]. It gave 350 TON as compared to 153 TON using **27** as a catalyst precursor. This clearly shows the effect of the support as a ligand on the activity of catalyst. It should be noted that the product distribution was similar for the catalyst precursors **27** and **28**.

Further investigation on the metathesis of 1-decene (an expected olefin during the alkane metathesis of *n*-decane) and the hydrogenation of the products formed clearly demonstrated that the distribution resulting from alkane and olefin metathesis completely differs with the same catalyst. If there is no double-bond migration, 9-octadecene and ethylene are expected to be the major primary products. Indeed, these primary products are observed, as the temperature reaches 150°C. However, after just 15 min, C_7 to C_{12} and C_{13} to C_{20} olefins are also observed, clearly indicating that some isomerization of double bond occurs leading to several competitive metatheses (Fig. 5).

In the proposed mechanism, for the olefin metathesis, the W-bis-carbene is generated via hydrogen transfer from the methyl to the W-methylidyne in the presence of an olefin. This further undergoes [2+2] cycloaddition with external olefin followed by cycloreversion to give ethylene and W-alkylidene, which reacts

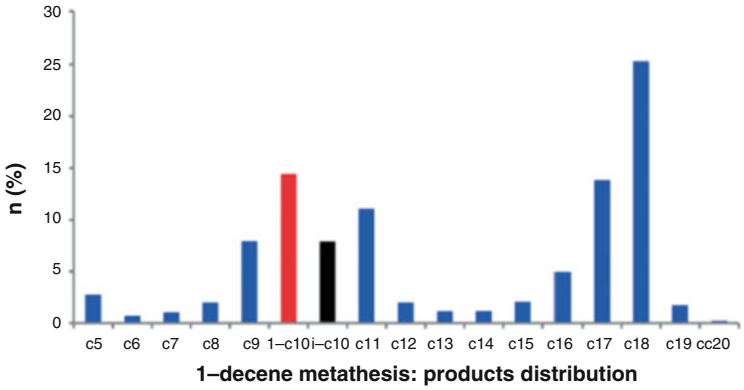

Fig. 5 Product distribution of 1-decene metathesis with [(≡SiO–)WMe_5] catalyst

with an additional olefin to release the final metathesis product (Scheme 20, a). Other olefin formations can be explained through the ethylene insertion and isomerization (Scheme 20, c).

While in alkane metathesis mechanism (Scheme 20, b), the *n*-decane undergoes σ-bond metathesis to generate methane and the W-bis-decyl species which, upon β-H elimination, produces the W–H with a coordinated olefin. Further, the α-hydrogen transfer from the alkyl to alkylidyne forms the hydrido W-bis-carbene [55, 76]. This upon [2+2] cycloaddition and cycloreversion gives an internal olefin and hydrido W-bis-carbene. Successive insertion/elimination steps (by chain walking) [77] give the terminal alkene, which reacts to a new W-alkylidene. The CH activation of the pendant W-hydride with *n*-decane followed by β-H elimination provides 1-decene. A second metathesis between 1-decene and newly formed W-alkylidene followed by hydrogenolysis produces the alkane.

It is noteworthy that the double-bond isomerization step is faster than the overall elementary steps of alkane metathesis. Formation of lower alkanes is due to the tungsten hydride intermediate, favoring chain walking with double-bond migration followed by fast cross metathesis with coordinated ethylene leading to lower alkenes in turn giving lower alkanes on hydrogenation. This intramolecular reaction pathway, without formation of the free olefin, probably is the difference between alkane and olefin metathesis.

4.3 Metathesis of Cycloalkanes

Metathesis of acyclic alkane produces lower and higher homologues of the corresponding alkanes. With the recent improvements in the catalysis using the precatalyst [(≡SiO)WMe_5] (**27**), it was interesting for us to apply similar strategy for acyclic alkanes, e.g., cyclooctane expecting to have easy access to lower and higher homologues of cyclic alkanes.

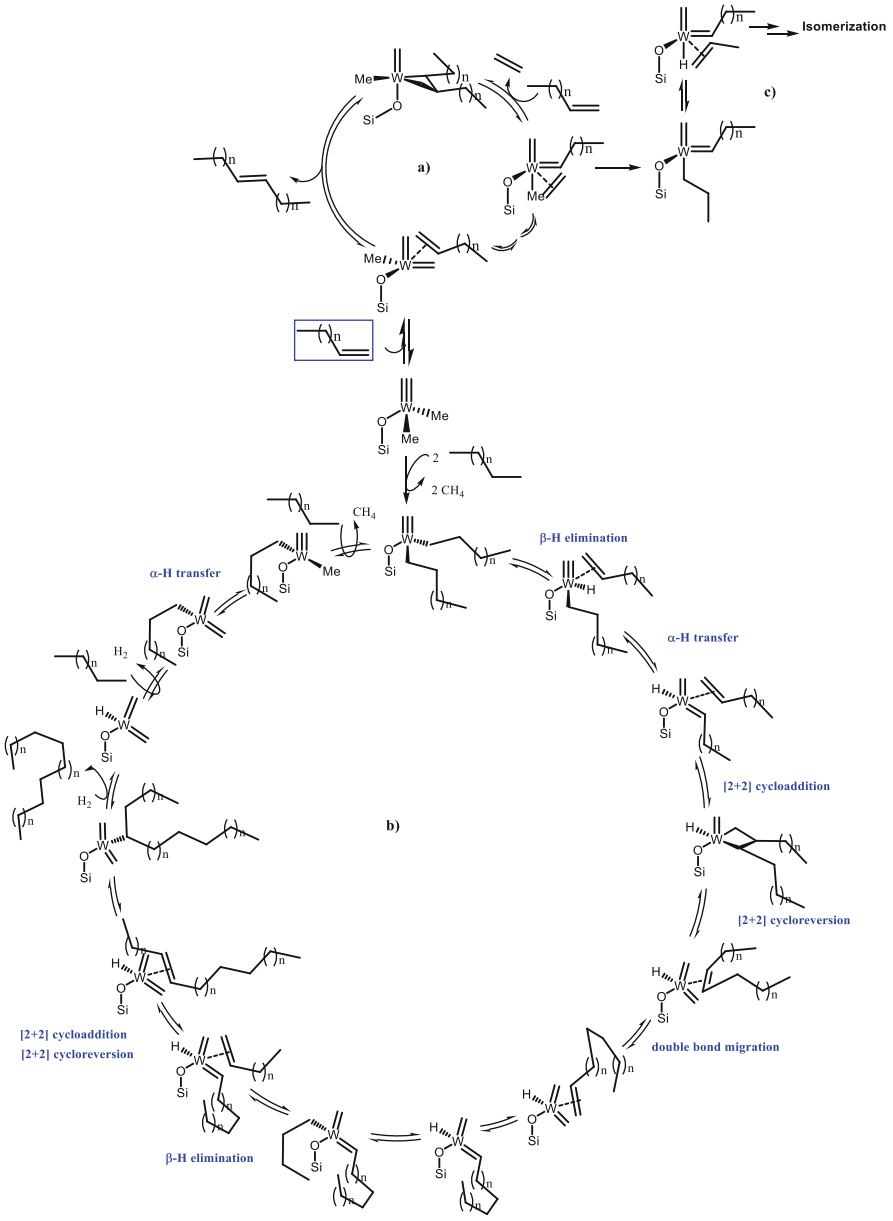

Scheme 20 Proposed mechanism for (*a*) olefin metathesis, (*b*) alkane metathesis, and (*c*) olefin isomerization via ethylene insertion

Recently, metathesis of cyclooctane was reported using the tandem system having the pincer-ligated iridium complexes for hydrogenation/dehydrogenation and Schrock-type Mo-alkylidene complexes for olefin metathesis [78]. However,

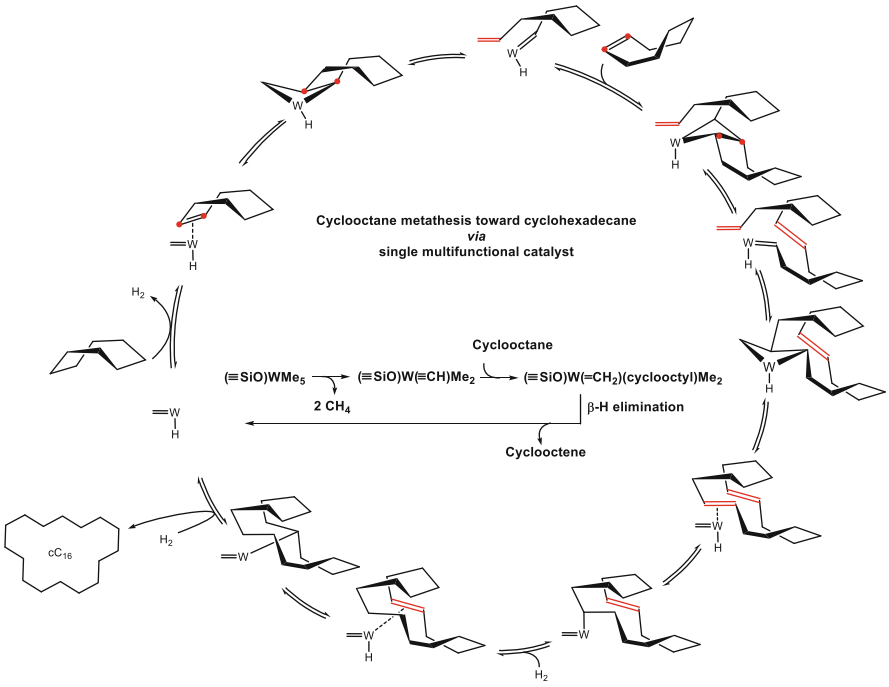

Scheme 21 Proposed mechanism for metathesis of cyclooctane into cyclohexadecane

this system showed >80% formation of polymeric products with cyclic oligomers (C_{16}, C_{24}, C_3, and C_{40}) of cyclooctane.

4.3.1 Metathesis of Cyclooctane

Precatalyst **27** has shown surprising results in the metathesis of cyclooctane and cyclodecane with broad distribution of lower and higher macrocyclic alkanes. Cyclopentane, cyclohexane, and cycloheptane were found to be inactive under similar condition [79].

For example, the cyclooctane metathesis using **27** has shown exceptional distribution of macrocyclic alkanes in the range of C_{12} to C_{40} without any polymeric products [79], wherein the cyclooctane undergoes similar mechanism with C–H bond activation followed by β-H elimination to give W-methylidene hydride and cyclooctene. The cyclooctene undergoes ring-opening–ring-closing metathesis reactions (RO-RCM) via the backbiting of terminal double bond to give 1,9-cyclohexadecadiene. This on hydrogenation gives the cyclohexadecane (Scheme 21). In a similar manner, macrocyclic alkanes (C_{24}, C_{32}, C_{40}) are generated via RO-RCM of cyclooctene.

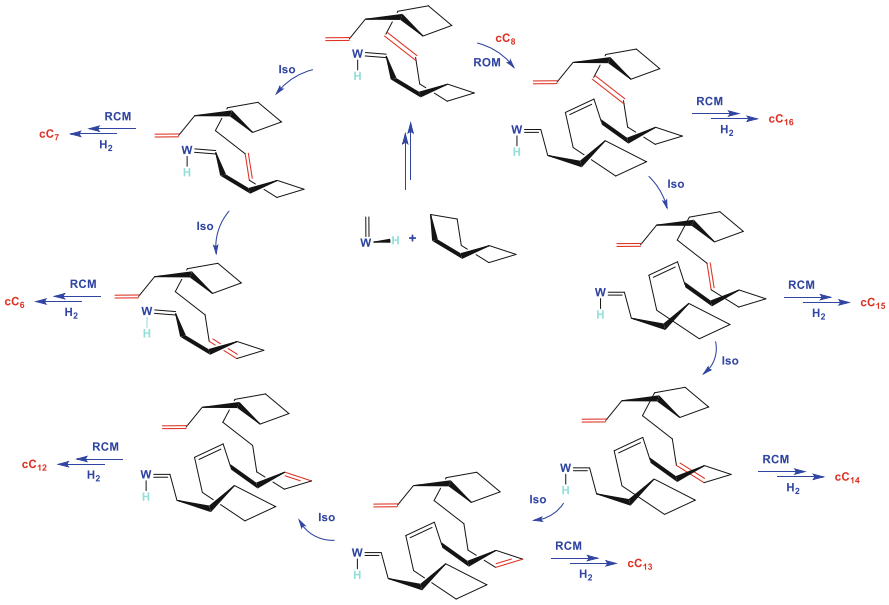

Scheme 22 Proposed mechanism for ring expansion and ring contraction with some selected cyclic and macrocyclic alkanes formation from cyclooctane metathesis. *ROM* ring-opening metathesis, *RCM* ring-closing metathesis, *Iso* double-bond isomerization

The formation of other macrocyclic alkanes and lower cyclic alkanes (C_5, C_6, and C_7) is clearly due to the double-bond isomerization before RCM. This was further proved by the reaction of macrocyclic alkane (C_{12} to C_{40}) at 150°C for 48 h, which did not produce any ring contraction cyclic products (C_5, C_6, and C_7) clearly, indicating that the lower cyclic alkanes are not formed by the secondary metathesis of macrocyclic alkanes (Scheme 22).

The absence of polymeric products is definitely due the low steady-state concentration of cyclooctene formed during the reaction.

4.4 Branched Alkanes Metathesis: Metathesis of 2-Methylpropane

The alkane metathesis of highly branched alkanes and product selectivity also follows the same mechanism with catalyst **24**. A selective and catalytic conversion of 2-methylpropane into 2,3-dimethylbutane (42%), and ethane (41%) (Scheme 23) [80] was observed when 2-methylpropane was passed over the catalyst **24** at 150°C. Conversion was reached up to 8% and 37 TON was achieved over 43 h (Scheme 23).

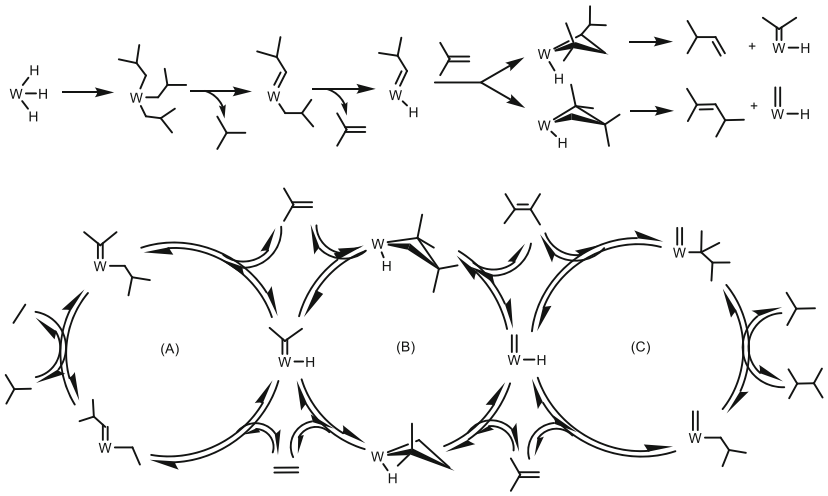

Scheme 23 Proposed mechanism for metathesis of 2-methylpropane

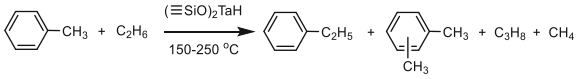

Scheme 24 Cross metathesis of toluene and ethane with silica-supported tantalum hydride

4.5 Cross Metathesis Between Two Different Alkanes

Cross metathesis between two different alkanes represent one of the most difficult challenges in organic chemistry [53]. In 2001, Basset et al. first demonstrated the possibilities of sigma bond metathesis between two different alkanes [55]. In 2004, this same group has reported the cross metathesis between ethane and toluene [81] and methane and propane [82]. Silica-supported tantalum hydride catalyst $\left[(\equiv SiO)_2TaH\right] \rightleftharpoons \left[(\equiv SiO)_2TaH_3\right]$ was employed for cross-metathesis reaction between toluene and ethane at 250°C. Under static condition, it produced mainly ethyl benzene and xylenes as major product along with propane and methane (Scheme 24).

In order to have better understanding, the same reaction was performed with 100% ^{13}C-enriched methyl in toluene and found mainly ^{13}C-mono-labeled ethylbenzene at the α-position (92%), while xylenes were 98% ^{13}C-mono-labeled. Besides this isolation of stable intermediates, such as $[(\equiv SiO)_2Ta–C_2H_5]$, $[(\equiv SiO)_2Ta–CH_2C_6H_5]$, or $[(\equiv SiO)_2Ta–C_6H_4CH_3]$ by ^{13}C CP MAS NMR spectroscopy, the mechanism of the reaction leading to various xylenes is given in Scheme 25.

In this scheme, we assume that in the equilibrium $\left[(\equiv SiO)_2Ta^{(III)}H\right] \rightleftharpoons \left[(\equiv SiO)_2Ta^{(V)}H_3\right]$, it is $[(\equiv SiO)_2TaH_3]$, d^0, which is

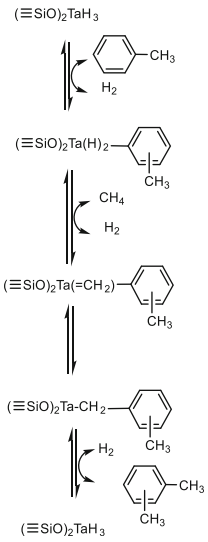

Scheme 25 Possible mechanism of cross metathesis of toluene and methane with silica-supported tantalum tris-hydride

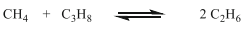

Scheme 26 Cross metathesis of methane and propane in the presence of silica-supported tantalum catalyst

involved in the succession of sigma bond metathesis. The reaction of methane with the $Ta(H)_2$(aryl) is a multistep which is omitted for clarity.

4.5.1 Cross Metathesis Using Methane as Reactant

Although methane is the most abundant hydrocarbon found on earth, until now there is not enough applications found for this important chemical (except the partial oxidation to syngas). Thus, cross metathesis of higher alkane with methane is interesting. This question was raised since the discovery of alkane metathesis reaction in 1997 where it was found that the two molecules of ethane can participate in self-metathesis and give one molecule of methane and one molecule of propane [1]. Thus, it is interesting to see whether it is possible to drive this reaction in the reverse direction, i.e., reacting methane with another alkane to give a mixture of alkanes with incorporation of methane (Scheme 26).

The reaction with propane and methane was investigated under dynamic conditions with very high methane/propane ratio to overcome thermodynamic barrier and favor kinetics. It was found that ethane was selectively produced. This result

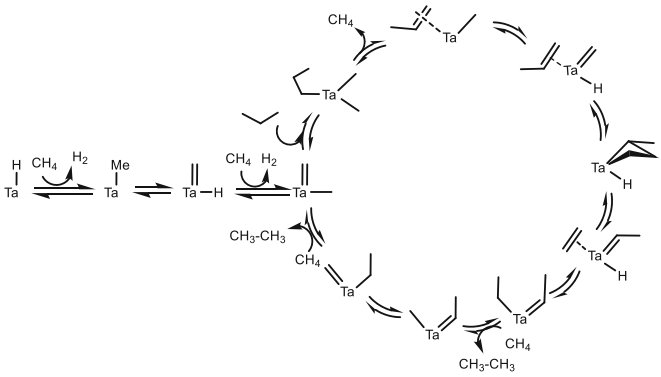

Scheme 27 Possible mechanism for cross metathesis of methane and propane with silica-supported tantalum hydride

was further supported by isotope labeling with ^{13}C-enriched methane. A possible mechanism is given for the better understanding of this reaction (Scheme 27).

4.6 Hydro-metathesis Reactions

Hydro-metathesis of propene under hydrogen atmosphere, in the presence of TaH/KCC-1 catalyst, proceeds smoothly under dynamic reaction condition at 150°C for 65 h with 750 TON [83]. In addition to the expected hydrogenation product, propane, ethane, and butane were formed as major products, and methane, isobutane, and isopentanes formed as minor products in case of propene. Similarly in the case of 1-butene, propane and hexanes were formed as major products, and ethane, propene, pentanes, and heptanes were formed as minor products. In case the of butene, the catalyst was found to be stable even after 75 h and cumulative TON up to 1,150 achieved after 75 h of the reaction [83]. The most important issue with this catalyst is the stability and reusability of this Ta–H/KCC-1 catalyst and the high turnover numbers reached compared with the turnover numbers reported for the Ta–H/SiO_2 catalyst in alkane metathesis reaction.

As expected, this reaction was found to be faster in comparison to alkane metathesis because of the absence of C–H bond activation steps which are assumed to be the difficult step of alkane metathesis reaction. Besides thermodynamic factors, this could also explain the comparative ease for the hydro-metathesis because olefin hydrogenation is thermodynamically favored even at low temperatures.

Based on the experimental fact and following the Chauvin mechanism for alkane metathesis, a probable mechanism was proposed for hydro-metathesis of propene (Scheme 28).

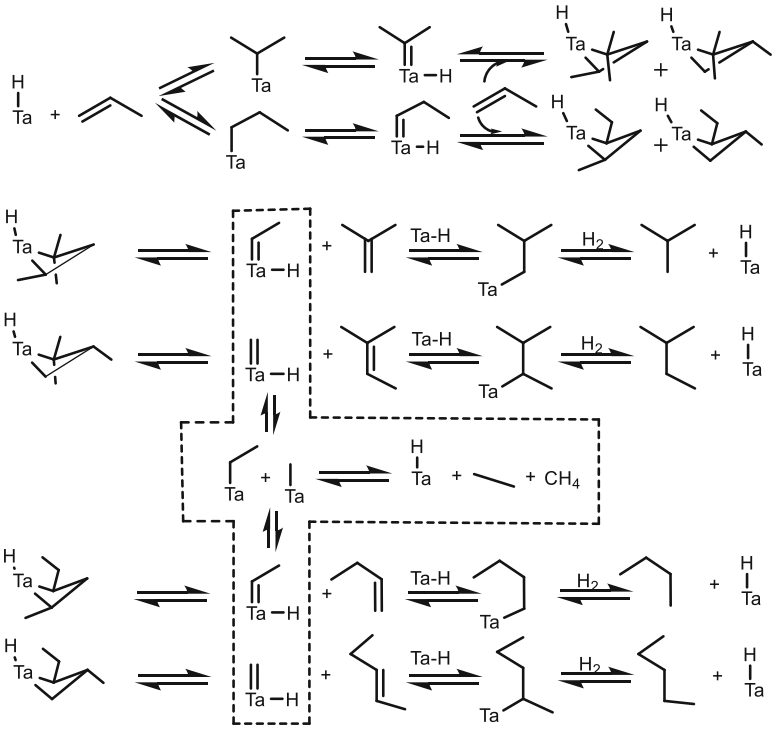

Scheme 28 Possible mechanism of hydro-metathesis of propene with silica-supported tantalum hydride

5 Conclusions

The rules of molecular organometallic chemistry apply when reacting organometallics with surfaces of oxides. A new field has emerged in catalysis called SOMC.

The reasons why the surface organometallic compounds of group IV and V exhibit a high reactivity toward C–H and C–C bonds of alkane are likely multiple:

1. They are highly electron deficient (between eight and 12 electrons in the Green formalism).
2. It was already known in organometallic chemistry that the transition metals of group IV and V can activate C–H bonds of alkanes by sigma bond metathesis, but the number of catalytic examples (see, e.g., the early works of P. Watson H/D exchange and CH_4/CD_4 exchange) [84] was not so high because in solution, the complexes may lose activity by dimerization or any other type of bimolecular interactions. In contrast, isolation on a support of a highly electron-deficient complex prevents any sort of bimolecular deactivation. This is a well-known concept, but it deserves to be repeated.

3. The use of a support as a ligand brings a supplementary electronic and steric parameter.
4. The surface organometallic complexes are thermally much more stable than their molecular counterpart. The example of [(≡Si–O) WMe_5] on silica which is stable up to 100°C is a good example of the ability of a surface to stabilize a molecular compound which is explosive at room temperature! So reactions can be performed on organometallic compounds at very high temperature which is not possible in classical homogeneous catalysis. Such stability allows the observation of carbynes, carbenes, alkyls, amido, imido, and hydrides even at elevated temperatures.

The absence of bimolecular reactions avoids many deactivation processes and allows better lifetime of the catalysts. This is a well-known concept but repetition is a source of pedagogy.

Using a variety of single-site surface complexes bearing simultaneously several types of highly reactive ligands has been at the origin of the various concepts of single-site multifunctional catalysts:

- Monofunctional with metal hydride(s): (Ziegler–Natta depolymerization, hydrogenolysis of waxes, olefin polymerization), metal carbenes (olefin metathesis, ROMP ADMET, etc.)
- Bifunctional with metal hydrides (or alkyls) (conversion of butenes to propylene)
- Trifunctional (conversion of ethylene to propylene, metathesis of alkanes, cycloalkanes, etc.)

References

1. Vidal V, Theolier A, Thivolle-Cazat J, Basset JM (1997) Science 276:99–102
2. Basset JM, Ugo R (2009) Modern surface organometallic chemistry. Wiley-VCH, Weinheim, pp 1–21
3. Corker J, Lefebvre F, Lecuyer C, Dufaud V, Quignard F, Choplin A, Evans J, Basset JM (1996) Science 271:966–969
4. Dufaud VR, Basset JM (1998) Angew Chem Int Ed 37:806–810
5. Goldman AS, Roy AH, Huang Z, Ahuja R, Schinski W, Brookhart M (2006) Science 312: 257–261
6. Huang Z, Rolfe E, Carson EC, Brookhart M, Goldman AS, El-Khalafy SH, MacArthur AHR (2010) Adv Synth Catal 352:125–135
7. Herisson JL, Chauvin Y (1971) Makromol Chem 141:161–176
8. Schrock RR, Murdzek JS, Bazan GC, Robbins J, Dimare M, Oregan M (1990) J Am Chem Soc 112:3875–3886
9. Bazan GC, Oskam JH, Cho HN, Park LY, Schrock RR (1991) J Am Chem Soc 113:6899–6907
10. Schwab P, Grubbs RH, Ziller JW (1996) J Am Chem Soc 118:100–110
11. Nguyen ST, Grubbs RH, Ziller JW (1993) J Am Chem Soc 115:9858–9859
12. Ertl G (1983) J Vac Sci Technol A 1:1247–1253
13. Cariati E, Dragonetti C, Lucenti E, Roberto D, Ugo R (2009) Modern surface organometallic chemistry. Wiley-VCH, Weinheim, pp 639–683

14. Dragonetti C, Ceriotti A, Roberto D, Ugo R (2007) Organometallics 26:310–315
15. Ballard DGH, Courtis A, Holton J, Mcmeeking J, Pearce R (1978) J Chem Soc Chem Commun 994–995
16. Popoff N, Mazoyer E, Pelletier J, Gauvin RM, Taoufik M (2013) Chem Soc Rev 42:9035–9054
17. Nedez C, Theolier A, Lefebvre F, Choplin A, Basset JM, Joly JF (1993) J Am Chem Soc 115: 722–729
18. Wolke SI, Buffon R, Rodrigues UP (2001) J Organomet Chem 625:101–107
19. Ajjou JAN, Scott SL, Paquet V (1998) J Am Chem Soc 120:415–416
20. Bendjeriou-Sedjerari A, Azzi JM, Abou-Hamad E, Anjum DH, Pasha FA, Huang KW, Emsley L, Basset JM (2013) J Am Chem Soc 135:17943–17951
21. Saint-Arroman RP, Chabanas M, Baudouin A, Copéret C, Basset JH, Lesage A, Emsley L (2001) J Am Chem Soc 123:3820–3821
22. Le Roux E, Chabanas M, Baudouin A, de Mallmann A, Copéret C, Quadrelli EA, Thivolle-Cazat J, Basset JM, Lukens W, Lesage A, Emsley L, Sunley GJ (2004) J Am Chem Soc 126: 13391–13399
23. Samantaray MK, Callens E, Abou-Hamad E, Rossini AJ, Widdifield CM, Dey R, Emsley L, Basset JM (2014) J Am Chem Soc 136:1054–1061
24. Chabanas M, Baudouin A, Copéret C, Basset JM (2001) J Am Chem Soc 123:2062–2063
25. Berthoud R, Rendon N, Blanc F, Solans-Monfort X, Coperet C, Eisenstein O (2009) Dalton Trans 5879–5886
26. Quignard F, Lecuyer C, Choplin A, Olivier D, Basset JM (1992) J Mol Catal 74:353–363
27. Niccolai GP, Basset JM (1998) Nato ASI 3 High Technol 44:111–124
28. Quignard F, Lecuyer C, Bougault C, Lefebvre F, Choplin A, Olivier D, Basset JM (1992) Inorg Chem 31:928–930
29. Saint-Arroman RP, Basset JM, Lefebvre F, Didillon B (2005) Appl Catal A Gen 290:181–190
30. Rosier C, Niccolai GP, Basset JM (1997) J Am Chem Soc 119:12408–12409
31. Tosin G, Santini CC, Taoufik M, De Mallmann A, Basset JM (2006) Organometallics 25: 3324–3335
32. Larabi C, Merle N, Norsic S, Taoufik M, Baudouin A, Lucas C, Thivolle-Cazat J, de Mallmann A, Basset JM (2009) Organometallics 28:5647–5655
33. Popoff N, Espinas J, Pelletier J, Macqueron B, Szeto KC, Boyron O, Boisson C, Del Rosal I, Maron L, De Mallmann A, Gauvin RM, Taoufik M (2013) Chem Eur J 19:964–973
34. Rataboul F, Baudouin A, Thieuleux C, Veyre L, Copéret C, Thivolle-Cazat J, Basset JM, Lesage A, Emsley L (2004) J Am Chem Soc 126:12541–12550
35. Tosin G, Santini CC, Baudouin A, De Mallman A, Fiddy S, Dablemont C, Basset JM (2007) Organometallics 26:4118–4127
36. Chen Y, Abou-hamad E, Hamieh A, Hamzaoui B, Emsley L, Basset JM (2015) J Am Chem Soc 137:588–591
37. Dufaud V, Niccolai GP, Thivolle-Cazat J, Basset JM (1995) J Am Chem Soc 117:4288–4294
38. Lefort L, Chabanas M, Maury O, Meunier D, Copéret C, Thivolle-Cazat J, Basset JM (2000) J Organomet Chem 593:96–100
39. Chabanas M, Quadrelli EA, Fenet B, Copéret C, Thivolle-Cazat J, Basset JM, Lesage A, Emsley L (2001) Angew Chem Int Ed 40:4493–4496
40. Soignier S, Taoufik M, Le Roux E, Saggio G, Dablemont C, Baudouin A, Lefebvre F, de Mallmann A, Thivolle-Cazat J, Basset JM, Sunley G, Maunders BM (2006) Organometallics 25:1569–1577
41. Saggio G, Mallmann A, Maunders B, Taoufik M, Thivolle-Cazat J, Basset J-M (2002) Organometallics 21:5167–5171
42. Vidal V, Theolier A, Thivolle-Cazat J, Basset JM, Corker J (1996) J Am Chem Soc 118: 4595–4602
43. Delley MF, Nunez-Zarur F, Conley MP, Comas-Vives A, Siddiqi G, Norsic S, Monteil V, Safonova OV, Copéret C (2014) Proc Natl Acad Sci U S A 111:11624–11629

44. Le Roux E, Taoufik M, Chabanas M, Alcor D, Baudouin A, Copéret C, Thivolle-Cazat J, Basset JM, Lesage A, Hediger S, Emsley L (2005) Organometallics 24:4274–4279
45. Le Roux E, Taoufik M, Copéret C, de Mallmann A, Thivolle-Cazat J, Basset JM, Maunders BM, Sunley GJ (2005) Angew Chem Int Ed 44:6755–6758
46. Szeto KC, Norsic S, Hardou L, Le Roux E, Chakka S, Thivolle-Cazat J, Baudouin A, Papaioannou C, Basset JM, Taoufik M (2010) Chem Commun 46:3985–3987
47. Galyer L, Mertis K, Wilkinson G (1975) J Organomet Chem 85:C37–C38
48. Marks TJ (1992) Acc Chem Res 25:57–65
49. Samantaray MK, Dey R, Abou-Hamad E, Hamieh A, Basset JM (2015) Chem Eur J 21: 6100–6106
50. Green MLH (1995) J Organomet Chem 500:127–148
51. Basset JM, Copéret C, Soulivong D, Taoufik M, Thivolle-Cazat J (2006) Angew Chem Int Ed 45:6082–6085
52. Leconte M, Basset JM (1979) J Am Chem Soc 101:7296–7302
53. Basset JM, Copéret C, Soulivong D, Taoufik M, Cazat JT (2010) Acc Chem Res 43:323–334
54. Vidal V, Theolier A, Thivolle-Cazat J, Basset JM (1995) J Chem Soc Chem Commun 991–992
55. Copéret C, Maury O, Thivolle-Cazat J, Basset JM (2001) Angew Chem Int Ed 40:2331–2334
56. Basset JM, Copéret C, Lefort L, Maunders BM, Maury O, Le Roux E, Saggio G, Soignier S, Soulivong D, Sunley GJ, Taoufik M, Thivolle-Cazat J (2005) J Am Chem Soc 127:8604–8605
57. Avenier P, Taoufik M, Lesage A, Solans-Monfort X, Baudouin A, de Mallmann A, Veyre L, Basset JM, Eisenstein O, Emsley L, Quadrelli EA (2007) Science 317:1056–1060
58. Pasha FA, Cavallo L, Basset JM (2014) ACS Catal 4:1868–1874
59. Vanasselt A, Santarsiero BD, Bercaw JE (1986) J Am Chem Soc 108:8291–8293
60. Parkin G, Bunel E, Burger BJ, Trimmer MS, Vanasselt A, Bercaw JE (1987) J Mol Catal 41: 21–39
61. Sharp PR, Astruc D, Schrock RR (1979) J Organomet Chem 182:477–488
62. Wallace KC, Dewan JC, Schrock RR (1986) Organometallics 5:2162–2164
63. Wallace KC, Liu AH, Dewan JC, Schrock RR (1988) J Am Chem Soc 110:4964–4977
64. Turner HW, Schrock RR (1982) J Am Chem Soc 104:2331–2333
65. Mclain SJ, Sancho J, Schrock RR (1979) J Am Chem Soc 101:5451–5453
66. Schinzel S, Chermette H, Copéret C, Basset JM (2008) J Am Chem Soc 130:7984–7987
67. Chabanas M, Vidal V, Copéret C, Thivolle-Cazat J, Basset JM (2000) Angew Chem Int Ed 39: 1962–1965
68. Watson PL (1983) J Am Chem Soc 105:6491–6493
69. Chen Y, Ould-Chikh S, Abou-Hamad E, Callens E, Mohandas JC, Khalid S, Basset JM (2014) Organometallics 33:1205–1211
70. Le Roux E, Taoufik M, Baudouin A, Copéret C, Thivolle-Cazat J, Basset JM, Maunders BM, Sunley GJ (2007) Adv Synth Catal 349:231–237
71. Taoufik M, Le Roux E, Thivolle-Cazat J, Copéret C, Basset JM, Maunders B, Sunley GJ (2006) Top Catal 40:65–70
72. Callens E, Abou-Hamad E, Riache N, Basset JM (2014) Chem Commun 50:3982–3985
73. Buffon R, Leconte M, Choplin A, Basset JM (1994) J Chem Soc Dalton 1723–1729
74. Riache N, Callens E, Espinas J, Dery A, Samantaray MK, Dey R, Basset JM (2015) Catal Sci Technol 5:280–285
75. Kundu S, Choliy Y, Zhuo G, Ahuja R, Emge TJ, Warmuth R, Brookhart M, Krogh-Jespersen K, Goldman AS (2009) Organometallics 28:5432–5444
76. Rascon F, Coperet C (2011) J Organomet Chem 696:4121–4131
77. Domski GJ, Rose JM, Coates GW, Bolig AD, Brookhart M (2007) Prog Polym Sci 32:30–92
78. Ahuja R, Kundu S, Goldman AS, Brookhart M, Vicente BC, Scott SL (2008) Chem Commun 253–255
79. Riache N, Callens E, Samantaray MK, Kharbatia NM, Atiqullah M, Basset JM (2014) Chem Eur J 20:15089–15094

80. Merle N, Stoffelbach F, Taoufik M, Le Roux E, Thivolle-Cazat J, Basset JM (2009) Chem Commun 2523–2525
81. Taoufik M, Schwab E, Schultz M, Vanoppen D, Walter M, Thivolle-Cazat J, Basset JM (2004) Chem Commun 1434–1435
82. Soulivong D, Copéret C, Thivolle-Cazat J, Basset JM, Maunders BM, Pardy RBA, Sunley GJ (2004) Angew Chem Int Ed 43:5366–5369
83. Polshettiwar V, Thivolle-Cazat J, Taoufik M, Stoffelbach F, Norsic S, Basset JM (2011) Angew Chem Int Ed 50:2747–2751
84. Watson PL, Parshall GW (1985) Acc Chem Res 18:51–56

Top Organomet Chem (2016) 56: 189–208
DOI: 10.1007/3418_2015_132

Published online: 29 July 2015

Transfer Dehydrogenations of Alkanes and Related Reactions Using Iridium Pincer Complexes

David Bézier and Maurice Brookhart

Abstract This chapter covers advances during the past 5 years in using iridium pincer complexes for transfer dehydrogenations of alkanes as well as related reactions which couple dehydrogenation with other transformations. Several new pincer complexes are described which have emerged during this period and which have added not only to the scope of available catalysts but also to the range of substrates and products generated. Transfer dehydrogenation has been linked with other reactions to produce catalytic systems that carry out alkane metatheses, generate benzene bearing a long-chain linear alkyl group from ethyl benzene and linear alkanes, couple alkanes with alkenes, and use transfer dehydrogenation in combination with Diels–Alder chemistry to produce *para*-xylene from ethylene as the sole feedstock.

Keywords Alkane functionalization · C–H activation · Dehydrogenation · Iridium pincer catalysts

Contents

1 Introduction 190
2 Alkane Dehydrogenation 192
3 Applications to the Synthesis of Aromatics 195
4 Applications to the Synthesis of Long-Chain Alkanes 199
5 Dehydrogenation of Functionalized Organic Molecules 201
6 Moving Forward by Using O_2 as Hydrogen Acceptor 203
7 Summary and Future Challenges 204
References 205

D. Bézier and M. Brookhart (✉)
Department of Chemistry, University of North Carolina at Chapel Hill, Chapel Hill, NC 27599-3290, USA
e-mail: mbrookhart@unc.edu

1 Introduction

Alkanes are the primary feedstock from which the majority of the world's chemicals are derived. They are the primary constituents of petroleum and natural gas and the associated low boiling components of natural gas. Coal, natural gas, and biomass are also sources of alkanes produced via gasification of these materials to syngas (CO/H_2) followed by Fischer–Tropsch catalysis resulting in a stochastic distribution of linear hydrocarbons.

Alkenes as well as aromatics are derived from alkanes through dehydrogenation. Alkenes and aromatics are highly versatile intermediates which can be converted to a wide array of value-added chemicals and materials including detergents, pharmaceutical intermediates, and polymers. Alkenes are primarily produced via "cracking" alkanes over heterogeneous dehydrogenation catalysts at very high temperatures (500–900°C) [1]. Such "acceptorless" dehydrogenations are endothermic (ca. 28–30 kcal/mol), but the large positive entropy gained from loss of H_2 renders these processes exergonic at such high temperatures. Additionally, aromatics are also made by heterogeneous dehydrogenations of various hydrocarbon feedstocks. Such high-temperature processes often result in low selectivities and generation of by-products.

There has been growing interest in homogeneous alkane dehydrogenations due to the possibility of obtaining higher selectivities and the prospects for production of functionalized alkenes via dehydrogenation of functionalized alkanes. Homogeneous dehydrogenations are normally carried out at much lower temperatures which require the use of a hydrogen acceptor to render the reactions thermodynamically feasible [Eq. (1)]. In the majority of the cases examined to date, the acceptor molecule has been an alkene, rendering the overall reaction close to thermoneutral.

$$\mathrm{R\text{-}CH_2\text{-}CH_2\text{-}R' + A \longrightarrow R\text{-}CH{=}CH\text{-}R' + AH_2} \quad (1)$$

A = alkene

Early studies of catalytic intermolecular dehydrogenations were reported independently by Felkin and Crabtree. In a series of papers [2–4], Felkin employed phosphine-stabilized polyhydrides of rhenium, ruthenium, and iridium as catalysts. Conditions were generally mild (25–150°C), but turnover numbers were low (2–70). The primary screening reaction employed both by Felkin and Crabtree, which has become standard today for screening transfer dehydrogenations, used *t*-butylethylene (TBE) as acceptor to dehydrogenate cyclooctane (COA) [Eq. (2)]. The favorable ΔG° of −6 kcal/mol avoids reversibility issues, and the bulky *t*-butylethylene acceptor binds weakly to metal centers and possesses no allylic hydrogens, thus avoiding potential catalyst deactivation through strong binding or formation of a π-allyl species.

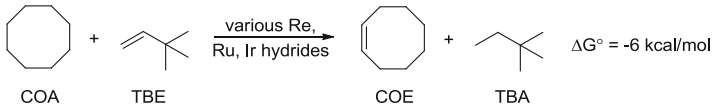

(2)

Crabtree started his investigations by using the cationic Ir(III) complex $IrH_2(acetone)_2(PPh_3)_2^+$ followed by neutral Ir(III) carboxylates $(PR_3)_2IrH_2(\eta^2\text{-}O_2CCF_3)$ (R = cyclohexyl, p-C_6H_5) as catalysts for thermal and photochemical dehydrogenations [5–7]. As with the case for Felkin's polyhydride studies, turnover numbers were generally low, but driving the reaction with light allowed acceptorless dehydrogenation of cyclooctane to be achieved [8]. In related studies, the groups of Saito [9], Tanaka [10], and Goldman [11] independently showed that photolysis of $Rh(Cl)(CO)(PMe_3)_2$ in linear and cyclic alkanes resulted in conversion to alkenes with high turnover numbers. Goldman showed a related system, $Rh(Cl)(L)(PMe_3)_2$ (L = PCy_3 or $P(^iPr)_3$), as well as the dimer, $[ClRh(PMe_3)_2]_2$, could be activated with H_2 in the presence of an acceptor to generate the active species $Rh(Cl)(PMe_3)_2$ which could achieve rapid transfer dehydrogenation [12–15]. A drawback of the system is that under H_2, alkene hydrogenation competes with alkane dehydrogenation. A thorough mechanistic study was reported.

A major breakthrough in transfer dehydrogenation of alkanes was achieved in 1996 by Jensen, Kaska, and coworkers [16, 17]. They reported that the iridium pincer complex (^{tBu4}PCP)IrH_2, **1a**, was highly reactive and exceptionally thermally stable for transfer dehydrogenation of COA employing TBE as the acceptor [Eq. (3)]. For example, at 200°C the turnover frequency was reported to be 12/min with no noticeable catalyst decomposition over 7 days.

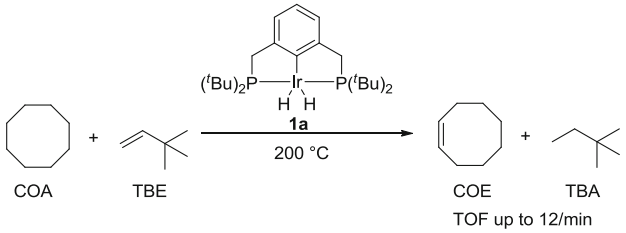

(3)

The report by Jensen and Kaska stimulated extensive work using various iridium pincer complexes for alkane transfer dehydrogenations and related chemistry. Indeed, iridium pincer complexes have dominated this area of research. Some of the highlights during the period 1996–2010 include the modification of the complex (^{tBu4}PCP)IrH_2, **1a**, by changing substituents on the phosphine (**1b**–**1c**) [18–20], adding functional groups to the aromatic backbone (**1d**–**1f**) [21–24], replacing the phosphines by phosphinite groups (**2a**–**2d**) [25–28], and incorporating an anthracenyl group in the backbone (**3a**) (Fig. 1) [29]. The mechanism of the alkane dehydrogenation reaction using **1a** [22, 30–33] and **2a** [22, 25, 26] was thoroughly investigated.

The above work has been extensively reviewed [34–37]; the reader is directed to these publications for an in-depth coverage. This chapter will be devoted to more

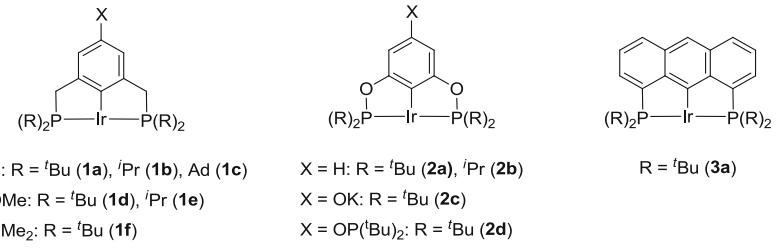

Fig. 1 Examples of active PCP iridium pincer complexes for alkane dehydrogenation

recent advances employing iridium pincer complexes in transfer dehydrogenation reactions and closely related chemistry.

2 Alkane Dehydrogenation

It has been shown that iridium pincer complexes containing electron-rich alkylphosphines are highly efficient catalysts for alkane dehydrogenation reactions. However, the Roddick group demonstrated that iridium complexes bearing electron poor phosphines can also efficiently catalyze the dehydrogenation of alkanes [38]. The iridium complex containing bis(trifluoromethyl)phosphine groups (^{CF3}PCP)Ir(η^4-COD), **4** (Fig. 2), was shown to catalyze the transfer dehydrogenation of COA with TBE (1:1) giving TONs up to 660 after 58 h (initial TOF = 40 h^{-1}) at 200°C. Due to inhibition by TBE, by using a 5:1 COA/TBE ratio, higher initial activities (TOF = 155 h^{-1}) and TONs (2,580 after 24 h) were obtained. This catalyst showed relatively minor inhibition by cyclooctene (COE), and no inhibition was detected with N_2 or H_2O. Using the same catalyst, very low activity was observed for the dehydrogenation of linear alkanes with TBE at 150°C (TONs = 81 after 48 h), and moderate TONs were obtained for the acceptorless dehydrogenation of cyclodecane (TONs = 92 after 24 h).

The Yamamoto group reported the use of 7-6-7 fused-ring PCP iridium catalysts (7–6–7-^{R}PCP)Ir(H)(Cl), **5a**, (R = *i*Pr) and **5b** (R = Ph) for alkane transfer dehydrogenation (Fig. 3) [39]. After activation with NaO^{t}Bu, TONs up to 3,510 and 4,140 were obtained with catalysts **5a** and **5b**, respectively, after 36 h at 200°C when using a COA/TBE ratio of 1.5:1. While both catalysts **5a** and **5b** showed no inhibition by product formation, the latter allowed highest TONs (4,821 at 230°C after 24 h) due to its higher stability. The catalyst **5a** is also an active catalyst for the transfer dehydrogenation of linear alkanes. By using a ratio *n*-octane/norbornene of 1.5:1, TONs up to 1,100 were obtained at 200°C after 12 h. However, due to its low solubility in *n*-octane, the catalyst **5b** showed no activity under similar conditions.

Huang and coworkers synthesized a new phosphinothious/phosphinite (^{iPr4}PSCOP)Ir pincer complex, **6** (Fig. 4) [40]. Upon activation with NaO^{t}Bu, this complex exhibits exceptionally high activity for transfer dehydrogenation of COA

Fig. 2 (^{CF3}PCP)Ir(η^4-COD) complex reported by Roddick [38]

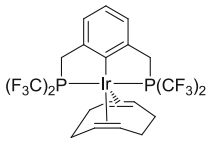

4

Fig. 3 (7–6–7-^{R}PCP)Ir complexes reported by Yamamoto [39]

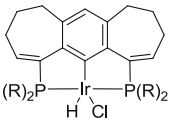

R = ^{i}Pr (**5a**), R = Ph (**5b**)

Fig. 4 Iridium complexes reported by Huang [40, 41]

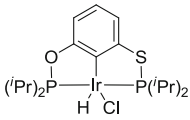

6

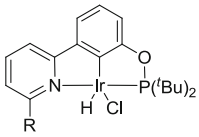

R = H (**7a**), R = Me (**7b**), R = ^{t}Bu (**7c**)

with TBE as the hydrogen acceptor. By using a COA/TBE ratio of 1:1, TONs up to 5,900 were achieved after 15 h at 200°C with an initial rate of 2,910 TO h^{-1}. Due to slight inhibition with TBE, this rate was increased to 5,600 TO h^{-1} by using a COA/TBE ratio of 4.8:1. This catalytic system also demonstrated high efficiency for the transfer dehydrogenation of *n*-octane with TOF up to 1,400 h^{-1} when the reaction was carried out at 200°C with TBE (0.5 M). Under these conditions, a selectivity of 33% for the formation of 1-octene was observed after 5 min due to fast isomerization of the terminal olefin. The olefin isomerization mechanism by iridium pincer catalysts was shown by Goldman and Brookhart to proceed via a π-allyl mechanism involving a η^3-allyl iridium hydride intermediate [42]. At the same temperature, by increasing the TBE concentration to 3 M, TONs up to 1,200 were obtained.

The Huang group also reported iridium complexes of novel NCP pincer ligands containing pyridine and phosphinite arms (^{R}NCOP^{tBu})Ir(H)(Cl), **7a–7c** (Fig. 4) [41]. While complexes **7b** (R = Me) and **7c** (R = ^{t}Bu) after activation with NaO^{t}Bu showed quite low catalytic activity for the cyclooctane transfer dehydrogenation (TONs up to 6), the less sterically hindered complex **7a** (R = H) activated with NaO^{t}Bu exhibited TONs up to 466 with initial rates of 1,010 TO h^{-1} when using a COA/TBE ratio of 14:1 at 150°C. TONs of 78, 28, and 19 were obtained for the dehydrogenation of *n*-octane with TBE (0.5 M) at 150°C when using the catalytic systems NaO^{t}Bu plus **7a**, **7b**, and **7c**, respectively. Due to a fast isomerization process, the selectivity for the formation of 1-octene was low (7% after 5 min with **7a**).

The Brookhart group reported the use of PC(sp^3)P–Ir(ethylene) pincer complexes, **8a–8d**, based on the triptycene ligand (Fig. 5) [43] (for earlier reports of similar iridium triptycene complexes, see [44–47]). The complex **8a** (R = *i*Pr)

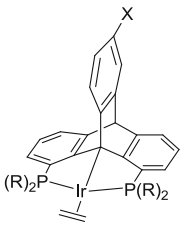

R = ^{i}Pr, X = H (**8a**); R = ^{i}Pr, X = NMe_2 (**8b**)
R = Cy, X = H (**8c**), R = Cp, X = H (**8d**)

Fig. 5 PC(sp^3)P−Ir (ethylene) complexes reported by Brookhart [43]

showed high activity for the dehydrogenation of COA with TBE (1:1) giving TONs of 910, 2,590, and 2,820 after 0.5, 4, and 24 h, respectively. The higher TONs obtained with **8a** compared to (^{t}Bu4POCOP)IrH_2, **2a**, were explained by the difference of binding affinities of these two complexes for TBE and COE. The complex **8a** has a similar affinity for these two alkenes, in contrast to **2a** which favors COE over TBE, thus inhibiting the catalytic activity by the product formation (COE) as the reaction proceeds. Surprisingly, very low activities (TONs ≈40) were observed when using catalysts **8c** (R = Cy) and **8d** (R = Cp). The complex **8a** also exhibited high catalytic activity (TOF up to 2,400 h^{-1}) and stability (TON = 6,000 after 10 h) for the dehydrogenation of *n*-octane with TBE (6M) at 200°C. By decreasing the reaction temperature to 100°C with 0.5 M of TBE, 1-octene represented up to 27% of all the octenes after 1 h of reaction (TON = 34). Under these conditions, full conversion of TBE to TBA (TON = 500) was obtained after 29 h. The complex **8b** bearing a NMe_2CH_2 substituent on the triptycene backbone was synthesized and successfully supported on alumina by following a previously reported strategy [24]. Modest catalytic activity was observed for the transfer dehydrogenation of COA with TBE when using this supported catalyst due to a fast decomposition of the catalytic system, most likely due to the reaction between the alumina support and the iridium center.

By replacing the phenyl backbone of the PCP ligand by a cyclohexyl backbone, the Wendt group succeeded in the synthesis of the aliphatic iridium complex (PCyP)Ir(H)(Cl), **9** (Fig. 6) [48]. The catalytic activity of this complex activated with NaO^{t}Bu was found to be very low (TONs up to 50) for the transfer dehydrogenation of COA by TBE (1:1) at 200°C due to fast decomposition of the active species. By decreasing the temperature to 120°C with the use of a ratio COA/TBE of 24:1 at 120°C, TONs up to 200 have been achieved. The acceptorless dehydrogenation of COA was also carried out at 150°C giving low TONs (≈5).

The most active iridium dehydrogenation catalysts are based on pincer ligands bearing phoshine or phosphinite groups. However, non-phosphine-based iridium pincer catalysts were also recently developed. The Braunstein group synthesized iridium complexes based on pincer ligands bearing *N*-heterocylic carbenes (NHCs) (Fig. 7). After activation with NaO^{t}Bu, the species generated from the bis(NHC) complex **10** was inactive for alkane transfer dehydrogenation [49]. Similarly, the active catalyst generated from the complex **11** bearing one normal and one

Fig. 6 (PCyP)Ir(H)(Cl) complex reported by Wendt [48]

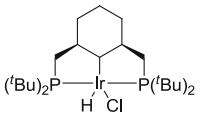

9

Fig. 7 CCC iridium complexes reported by Braunstein [49, 50]

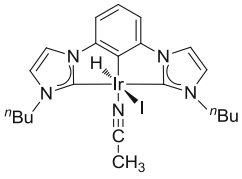

10

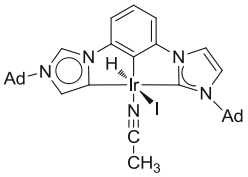

11

abnormal NHC ligand showed very low activity for the dehydrogenation of COA with TBE (8:1) at 200°C (TONs = 4 after 10 h) due to its low stability and low solubility in the reaction media [50].

The Chianese group synthesized more rigid bis(NHC) iridium complexes, **12a**–**12f**, which were shown to be active pre-catalysts for the acceptorless dehydrogenation of alkanes (Fig. 8) [51, 52]. For the acceptorless dehydrogenation of COA, the catalytic systems generated in situ from **12c**, **12d**, and **12e** with NaO^{t}Bu gave TONs of 103, 84, and 35, respectively, after 12 h at reflux of COA (bp = 150°C). The catalytic activity of **12c** appears to exhibit no inhibition in the presence of COE or N_2. By using the higher-boiling cyclodecane, TONs up to 102 were achieved with the pre-catalyst **12c** after 22 h. Acceptorless dehydrogenation of linear alkanes was also carried out. TONs up to 97 were obtained when using the pre-catalyst with *n*-undecane, which is comparable to the results obtained from the most active iridium PCP catalysts. Under similar conditions, pre-catalysts **12c** and **12d** showed lower reactivity (TON = 50).

Other non-phosphine-based catalysts active for alkane dehydrogenation were developed by the Jensen group [53]. The complex ($^{t\text{Bu4}}$AsOCOAs)IrHCl, **13** (Fig. 9), combined with NaO^{t}Bu catalyzed the transfer dehydrogenation of COA with TBE (1:1) giving TONs of up to 930 after 24 h with initial rates of 600 TO h^{-1} at 200°C. The leveling off in catalytic activity was explained by inhibition by the COE product, as well as thermal decomposition of the catalyst over time.

3 Applications to the Synthesis of Aromatics

As the global demand for chemicals grows, so does that for aromatics, which constitute a significant fraction of the major building blocks of the chemical industry. As petroleum is displaced by natural gas, and as decreased gasoline refining (in favor of diesel [54]) limits production of aromatic by-products, the

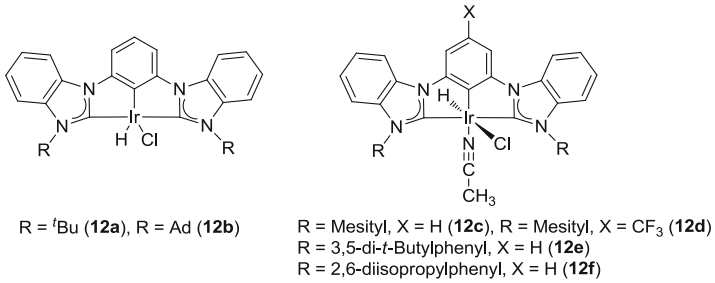

Fig. 8 CCC iridium complexes reported by Chianese [51, 52]

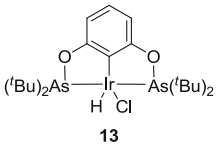

Fig. 9 (^{tBu4}AsOCOAs)IrHCl complex reported by Jensen [53]

synthesis of aromatics from alkanes becomes increasingly attractive. Heterogeneously catalyzed dehydroaromatization of *n*-alkanes is known to occur at very high temperatures (>500°C) but with low yields and low selectivity [55–60].

By using iridium pincer catalysts, Goldman and Brookhart developed the dehydroaromatization of *n*-alkanes which allows the formation of alkylaromatics in the presence of an excess of hydrogen acceptors [61]. This reaction occurs via sequential dehydrogenation of alkanes generating conjugated trienes which undergo electrocyclization to give cyclohexadienes which are then further dehydrogenated to yield the aromatic products [Eq. (4)].

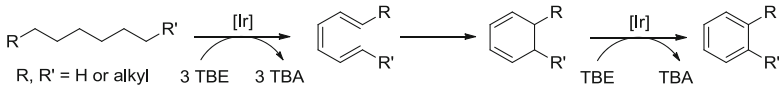

(4)

Through the screening of numerous iridium pincer catalysts, high activities were obtained when using the complexes **1b**, **14a**, and **3b** with 4 equiv. of TBE (relative to the *n*-alkane) (Fig. 10). The newly reported hybrid phosphine/phosphinite (^{iPr4}PCOP)Ir, **14a**, emerged as the most effective catalyst allowing the conversion of *n*-hexane to benzene with a yield of 44% (670 mM) after heating a solution of 6.13 M TBE with 1.53 M *n*-hexane for 120 h at 165°C. The dehydroaromatization of *n*-octane was achieved even more efficiently generating aromatics with a yield of 86% including *o*-xylene and ethylbenzene with a 7:1 ratio. Propene was able to replace the expensive TBE as hydrogen acceptor albeit with lower yields (38%).

Moreover, starting from *n*-decane or *n*-dodecane, this protocol resulted in the formation of non-branched *n*-alkylarenes which are not accessible via the classical industrial route involving Friedel–Crafts alkylation of arenes with linear olefins. For example, when the dehydroaromatization of *n*-decane was catalyzed by **14a**,

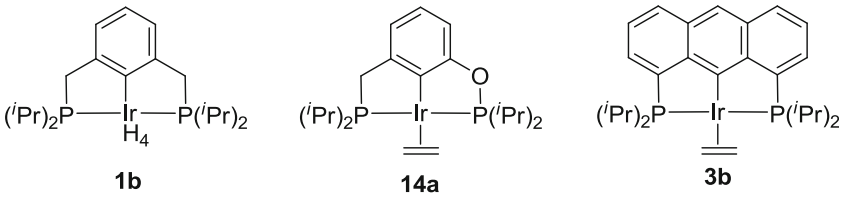

Fig. 10 Active catalysts for *n*-alkane dehydroaromatization [61]

o-propyltoluene was the major product along with *n*-butylbenzene, 1,2-diethylbenzene, and benzene [Eq. (5)].

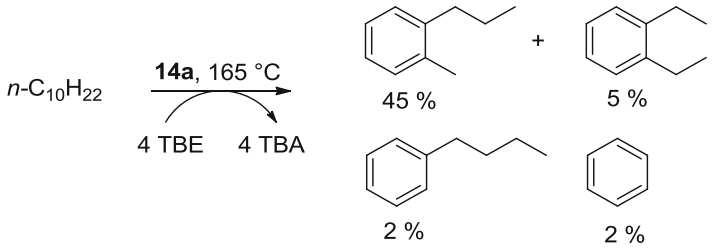

(5)

Another protocol for the synthesis of *n*-alkylarenes was recently developed by Schrock, Goldman, and coworkers [Eq. (6)] [62]. This process combines a Schrock-type olefin metathesis catalyst (Mo or W) with an iridium pincer dehydrogenation catalyst and results in the conversion of ethylbenzene and *n*-alkanes to long-chain *n*-alkyl arenes via the reaction sequence shown in Eq. (6). This reaction termed "Alkyl Group Cross-Metathesis" (AGCM) was carried out at 180°C, and best results were obtained with the use of W(NAr′)(C_3H_6)(pyr)(OHIPT) (Ar′ = 2,6-$Me_2C_6H_3$, OHIPT = 2,6-(2,4,6-$^iPr_3C_6H_2$)$_2C_6H_3O$) as the olefin metathesis catalyst and (^{tBu4}PCP)IrH_2, **1a**, as the dehydrogenation/hydrogenation catalyst. For example, the reaction between *n*-octane and ethylbenzene after 24 h yielded a mixture of 1-phenyloctane (240 mM), 1-phenylheptane (60 mM), and tetradecane (20 mM).

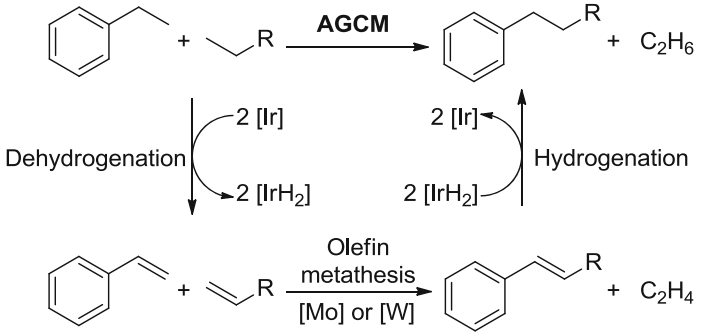

(6)

An alternative route to the most valuable constituent of the BTX (benzene, toluene, xylene) mixture, *p*-xylene, has been reported by Brookhart and coworkers

[63]. *p*-Xylene is one of the highest volume chemical intermediates derived from petroleum. Its primary use is for the production of the dimethyl ester of terephthalic acid, which is copolymerized with ethylene glycol to produce polyethylene terephthalate (PET). Traditionally, *p*-xylene is produced by catalytic reforming of various crude oil streams, followed by a difficult separation of the mixture containing benzene, toluene, *o*-xylene, *m*-xylene, and *p*-xylene. Taking advantage of the abundance of ethane in the USA via the recent shale gas boom, the use of ethylene (obtained from cracking of ethane) [64] has drawn growing interest as a feedstock. By using ethylene as the sole feedstock, the Brookhart group developed the synthesis of *p*-xylene, uncontaminated by the *ortho* and *meta* isomers [Eq. (7)]. The stepwise synthesis relies on the disproportionation of 1-hexene (which can be obtained from the trimerization of ethylene) to 2,4-hexadiene catalyzed by an iridium pincer complex (0.04 mol%) at 180°C. Through a catalyst screening, best results were obtained when using the catalyst ($^{i\text{Pr4}}$Anthraphos)Ir(C_2H_4), **3b** (TON = 777 after 3.5 h), with moderate activities observed with $^{i\text{Pr4}}$PC(sp^3)P−Ir (ethylene), **8a** (TON = 506 after 3.5 h) [43], and ($^{i\text{Pr4}}$PCOP)Ir(ethylene), **14** (TON = 214 after 3.5 h). The mixture was subjected to a Diels–Alder cyclization at 250°C with ethylene (600 psi) resulting in the complete formation of 3,6-dimethylcyclohexene and 3-ethylcyclohexene (ratio 8:1). The dehydrogenation of these two compounds was carried out at 400°C over Pt/Al_2O_3 giving a mixture of *p*-xylene and ethylbenzene (ratio 8.5:1) in 93% and 88% yields, respectively.

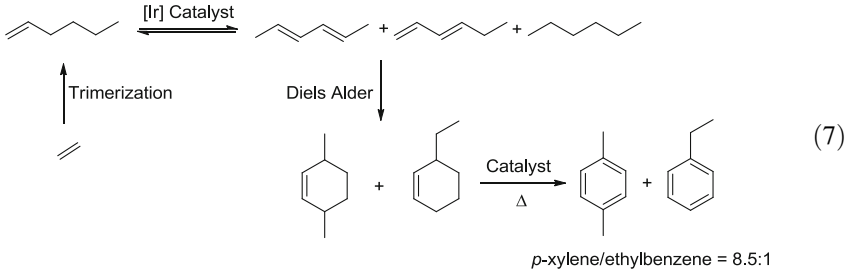

(7)

A one-pot procedure was also developed [Eq. (8)]. Heating 1-hexene at 250°C with 600 psi of ethylene for 24 h in the presence of 0.32 mol% of **3b** after 192 h resulted in nearly complete conversion with respect to hexenes (93%) yielding 3,6-dimethylcyclohexene (66%), ethylcyclohexene (12%), and aromatics (10%). This mixture is readily converted to *p*-xylene and ethyl benzene using classical heterogeneous catalysts such as Pt on alumina. This was the first example of ethylene serving as a hydrogen acceptor in alkane dehydrogenation. The yield of hexadienes (and ultimately *p*-xylene) is no longer limited by the equilibrium disproportionation of 1-hexene to hexadienes and *n*-hexane, making this one-pot approach to 3,6-dimethylcyclohexene a more attractive route for *p*-xylene synthesis from ethylene. A similar strategy was used for the synthesis of piperylene and toluene via the tandem transfer dehydrogenation of pentane or pentene followed by a Diels–Alder reaction with ethylene [65].

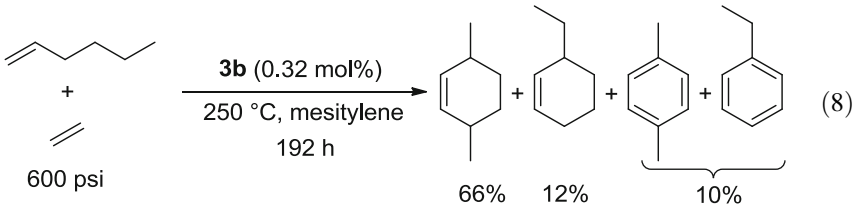

(8)

4 Applications to the Synthesis of Long-Chain Alkanes

Alkane metathesis has potential applications on an enormous scale. Most notably, it would allow the "upgrading" of low carbon number *n*-alkanes (C_3–C_8) to chains with higher carbon number which are ideal for diesel and jet fuel. Lighter *n*-alkanes can be obtained via Fischer–Tropsch chemistry from syngas [66–69], from direct biomass reduction, or even from CO_2 reduction with the use of sustainable energy sources. Moreover, light alkanes are found in vast amounts in natural gas and petroleum reserves, equivalent to >10% of current world oil reserves. While heterogeneous alkane metathesis catalysts have been reported [70–73], the first homogeneous alkane metathesis catalytic system was developed by Goldman, Brookhart, and coworkers in 2006 based on tandem transfer dehydrogenation and olefin metathesis [Eq. (9)] [74, 75]. The system exhibits high efficiency with overall product concentrations of 1.25 and 2.05 M obtained from 7.6 M *n*-hexane using 10 mM (^{tBu4}PCP)IrH_2, **1a**, and (^{tBu4}POCOP)IrH_2, **2a**, respectively, in combination with the Mo catalyst, **15** (16 mM), after 1 day at 125°C. In addition to decane and ethane, *n*-alkanes of intermediate chain lengths are formed and represent a large fraction of the total alkene product. Due to the low stability of the Mo catalyst, **15**, the overall yield was limited.

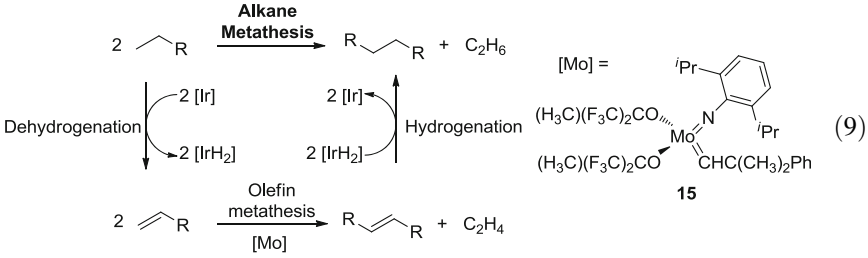

(9)

Other catalysts have been used to increase the substrate scope, yield, and selectivity of this reaction [19, 76–78]. Particularly, the Goldman group investigated the use of the mixed phosphine/phosphinite catalyst (^{tBu4}PCOP)Ir(H_2), **14b**, which was found to be four times faster than (^{tBu4}PCP)IrH_2, **1a**, and eight times faster than (^{tBu4}POCOP)IrH_2, **2a** [79] (Fig. 11). More interestingly, the less sterically hindered (^{tBu2}PCOP^{iPr2})Ir(ethylene), **14c**, was found to be even more active

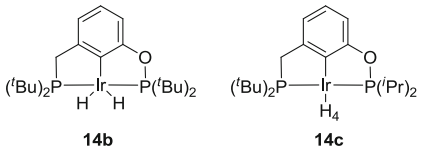

Fig. 11 Active co-catalysts in tandem alkane metathesis [79]

with rates four times greater than ($^{t\text{Bu4}}$PCOP)Ir(ethylene), **14b**. However, ($^{i\text{Pr4}}$PCOP)Ir(H_2), **14a**, was not as productive as the two other catalysts presumably due to lower stability.

Alkane–alkene coupling, another strategy to upgrade light hydrocarbons, was recently reported by Bercaw and Labinger [80–82]. This process takes advantage of the mixed nature of many light by-product streams which contain both alkanes and alkenes as substrates. The ideal reaction [Eq. (10)] involves a tantalum-based catalyst to dimerize the alkene component of the mixed feedstock to afford the C_{2n} alkene. Subsequent transfer hydrogenation by an iridium pincer catalyst allows the conversion of the alkane component to the 1-alkene while hydrogenating the C_{2n} product to an alkane. The 1-alkene is next catalytically dimerized with a second equivalent of 1-alkene, and the cycle can continue. The net reaction corresponds to the coupling of the alkane and alkene to give the higher alkane without the formation of any lighter by-products. This process involves alkane dehydrogenation by a pincer-ligated iridium complex (**1a**, **1b**, or **2a**) and alkene dimerization by Cp*$TaCl_2$(ethylene), **16**, which is inert to internal olefins. Best results were obtained by slowly adding 1-hexene (1,200 mM) to a mixture containing ($^{t\text{Bu4}}$PCP)Ir(H_2), **1a** (5 mM), and Cp*$TaCl_2$(ethylene), **16** (8 mM), in *n*-heptane (solvent) which resulted in the generation of C_{13} alkenes (obtained from hexane/heptene coupling) and C_{14} alkenes with a yield of 40% (C_{13}+C_{14}) and a cooperativity of 91% [Eq. (11)]. The "cooperativity" was defined by Bercaw and Labinger as the amount of 1-heptene generated by dehydrogenation that is incorporated into C_{13} and C_{14} alkenes. The absence of C_{13}/C_{14} alkanes indicates that the last step of the catalytic cycle (hydrogenation of the long-chain alkene) cannot be completed. When using ($^{t\text{Bu4}}$POCOP)Ir(H_2) **2a** as the co-catalyst, no desired products (C_{13}/C_{14}) were detected due to the fast isomerization of 1-heptene to internal heptenes which are inert to coupling by **16**. Moreover, this tandem catalytic system can be applied to the dimerization of *n*-heptane with TBE (which is inert to dimerization). The use of ($^{i\text{Pr4}}$PCP)Ir(H_2) **1b** (2 mM) with **16** (8 mM) and 250 mM of TBE in *n*-heptane at 100°C for 18 h resulted in ~50% conversion and the generation of C_{14} alkenes in 18% yield. Styrene was also investigated as an alternate hydrogen acceptor. The conversion of styrene/heptane mixtures by the Ta/Ir tandem system led to the formation of heptene dimers, with up to 58% overall yield of heptane-derived products.

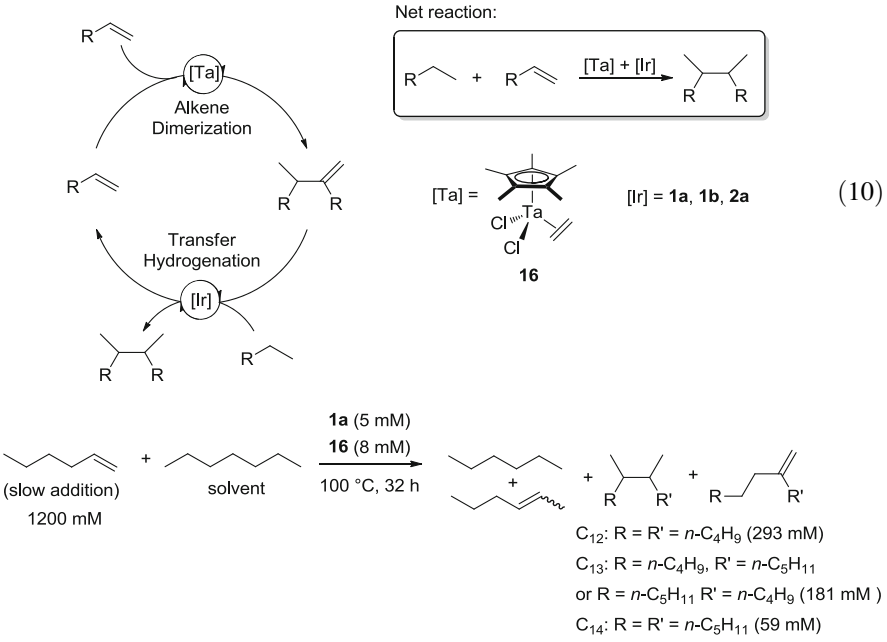

(10)

(11)

5 Dehydrogenation of Functionalized Organic Molecules

Despite the large number of highly active catalysts for alkane dehydrogenation, surprisingly little work has been extended to functionalized substrates. An early report by Jensen and Kaska showed modest reactivity (~57 TONs) for the dehydrogenation of tetrahydrofuran with TBE by using ($^{t\text{Bu4}}$PCP)Ir(H_2), **1a**, as the catalyst at 150°C [83]. Using the same catalyst, the dehydrogenation of tertiary amines to form enamines in the presence of TBE at 90°C was reported by Goldman, again with modest TONs (≈10) [84]. A similar reaction developed by the Wendt group with (PCyP)Ir(H)(Cl), **9**, as catalyst required higher temperatures (120°C) to obtain comparable activity [48]. In the context of hydrogen storage, acceptorless dehydrogenation of *N*-ethylperhydrocarbazole by ($^{t\text{Bu4}}$PCP)Ir(H_2), **1a**, ($^{i\text{Pr4}}$PCP)Ir(H_2), **1b**, and ($^{t\text{Bu4}}$POCOP)Ir(H_2), **2a**, was developed by Jensen [85]. They later found that ($^{t\text{Bu4}}$POCOP)Ir(H_2), **2a**, was able to selectively dehydrogenate the heterocycle ring of various indolic and carbazolic molecules [Eq. (12)] [86].

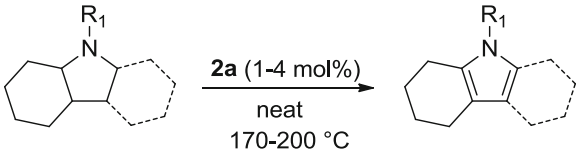

(12)

Recently, Huang demonstrated a much broader scope of heterocycle dehydrogenations using the hybrid phosphinothious/phosphinite (^{iPr4}PSCOP)Ir(H)(Cl) pincer complex **6** activated with NaO^{t}Bu [40]. A large variety of O- and N-containing heterocycles were successfully dehydrogenated at 120°C in the presence of TBE [Eq. (13)]. For example, 2,3-dihydrobenzofuran gives benzofuran in high yield with low catalyst loading (0.1 mol%). Higher catalyst loading (5 mol%) was required to dehydrogenate tetrahydrofuran to furan and piperidine to pyridine.

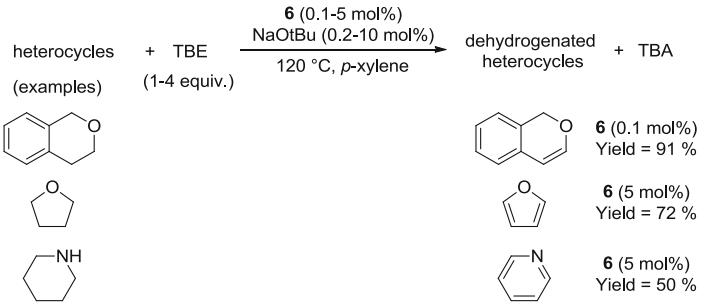

(13)

Brookhart and coworkers recently showed that catalysts (^{iPr4}Anthraphos)Ir(H)(Cl), **3b**, ^{iPr4}PC(sp^3)P−Ir(H)(Cl), **8a**, and (^{iPr4}POCOP)Ir(H)(Cl), **2b**, were effective for the dehydrogenation of cyclic and acyclic ethers using TBE as a hydrogen acceptor at 120°C after activation with NaO^{t}Bu [Eq. (14)] [87]. For example, THF and *N*-methylmorpholine were converted to furan and 2,3-dehydro-*N*-methylmorpholine with TONs of 660 and 325, respectively, using the pre-catalyst **3b**. Acyclic ethers represent a more challenging class of substrates. The small, electron-rich alkene products are strong ligands for Ir(I) complexes and thus readily inhibit catalysis. However, it was observed that diethyl ether was dehydrogenated with all three catalysts, though pre-catalyst **8a** gave the best result providing 90 TONs with 0.2 mol% loading. The dehydrogenation of cyclic and acyclic ether substrates using ethylene as the hydrogen acceptor was demonstrated for the first time. Under mild conditions at 120°C, a series of ether heterocycles can be dehydrogenated with up to 375 TONs producing ethane as the hydrogenated product. The pre-catalyst **8a** was particularly active in this protocol, producing good yields for all the substrates surveyed. For example, the reaction of *N*-methylmorpholine with ethylene catalyzed by **8a** (0.5 mol%)/NaO^{t}Bu (1 mol%) selectively formed 2,3-dehydro-*N*-methylmorpholine in 57 % yield, lower than the 78% yield obtained with TBE [Eq. (15)].

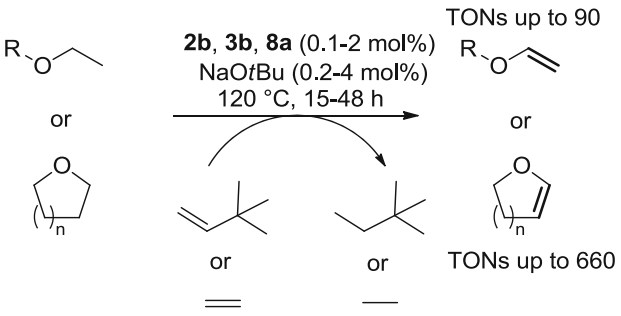

(14)

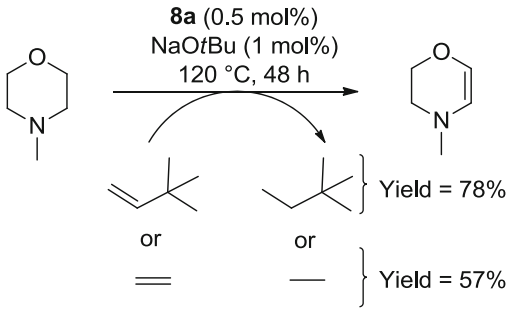

(15)

6 Moving Forward by Using O_2 as Hydrogen Acceptor

Oxidative dehydrogenation of light alkanes offers a potentially attractive route to alkenes, since the reaction is exothermic and avoids the thermodynamic constraints of non-oxidative routes by forming water as a by-product [Eq. (16)]. This methodology has been intensively studied for the conversion of ethane to ethylene and propane to propene via the use of heterogeneous catalysts [88, 89]. Homogeneous systems for such reactions have not yet been reported, but they could complement heterogeneous catalysts via the use of milder conditions and application to a larger substrate scope including longer-chain alkanes.

$$C_nH_{2n+2} + 0.5\,O_2 \longrightarrow C_nH_{2n} + H_2O \quad (\Delta H^\circ \approx -28\ \text{kcal.mol}^{-1}) \tag{16}$$

Goldberg, Heinekey, Goldman, and coworkers have recently made progress towards achieving this goal. They found that the Ir(III) bis-acetate complex (^{dm}phebox)Ir(OAc)$_2$(OH$_2$) (^{dm}phebox = 2,6-bis(4,4-dimethyloxazolinyl)-3,5-dimethylphenyl), **17**, can achieve stoichiometric C–H activation of arenes and alkanes [Eq. (17)] [90]. With benzene, C–H activation takes place to form (^{dm}phebox)Ir(OAc)(Ph), **18**, at 100°C, and with *n*-octane, an aliphatic C–H bond is activated followed by a β-hydride elimination to give (^{dm}phebox)Ir(OAc)(H), **19**, and octene after 72 h at 200°C. The dehydrogenation mediated by **17** results from C–H activation at an Ir(III) center via a concerted metalation–deprotonation pathway [91], in contrast with the reactions of phosphine-based pincer iridium systems.

A fast isomerization of the kinetic product 1-octene to internal octenes has been observed. The stoichiometric alkane dehydrogenation mediated by **17** is not inhibited by the presence of N_2 and α-olefins, and the rate of the reaction seems to be accelerated by the presence of water. Complex **17** can be regenerated from **19** by reacting with O_2 and HOAc [92]. This suggests that a catalytic cycle involving O_2 as hydrogen acceptor is plausible. However, preliminary attempts to make this reaction catalytic have been thwarted by catalytic instability towards O_2 at the temperature required for alkane dehydrogenation.

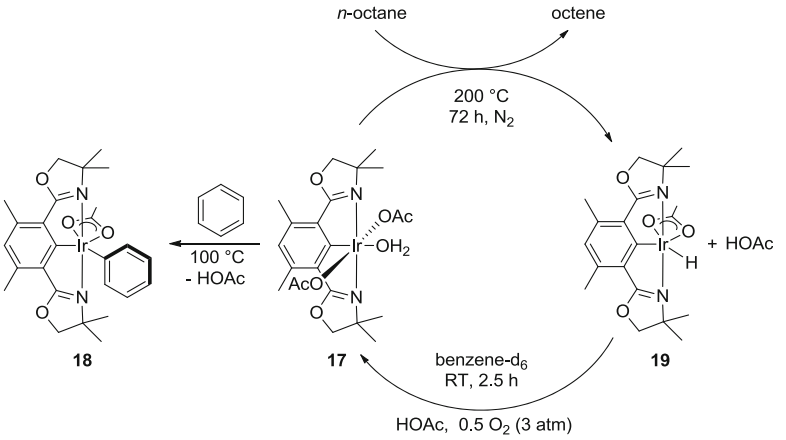

(17)

7 Summary and Future Challenges

The period 2011–2015 has seen continued development of a wide variety of new iridium pincer complexes active for transfer dehydrogenations of alkanes. These include iridium complexes which have incorporated, for example, electron-deficient PCP ligands, CCC pincer ligands bearing NHC carbene arms, $PC_{sp3}P$ ligands exhibiting a cyclohexyl or triptycene unit in the backbone, $PC_{sp2}P$ ligands based on an anthracene and a rigid fused 7-6-7 ring structure, hybrid PCP systems bearing mixed phosphine/phosphinite (PCOP) and phosphinothious/phosphinite (PSCOP) arms, and a pincer ligand, AsOCOAs, in which phosphorus atoms have been replaced by arsenic. Several of these systems have shown improved thermal stabilities and/or turnover numbers with respect to alkane transfer dehydrogenations. A major unsolved problem in simple transfer dehydrogenations is the selective generation of valuable α-olefins from linear alkanes. While several iridium pincer systems show kinetic selectivity for formation of α-olefins, subsequent olefin isomerization results in loss of selectivity at high conversion. While *t*-butyl ethylene and to a lesser extent norbornene have been used as efficient acceptors, for practical applications less expensive, more readily available acceptors need to be developed. Use of ethylene and propylene as acceptors has recently seen success and will likely be a focus of future studies. The ideal acceptor would of course be dioxygen, and recent results from Goldberg, Goldman, and Heinekey suggest this is

plausible. There has been increasing interest and advances in catalyst development for dehydrogenations of functionalized systems, in particular dehydrogenations of heterocyclic amines and ethers. Applications to more complex molecules and late stage functionalizations of pharmaceuticals represent attractive future endeavors in this area.

This period has also seen numerous advances in coupling transfer dehydrogenation with a second transformation. Increased efficiency in homogeneous alkane metathesis has been reported, but achieving high selectivity for converting the C_n alkane to ethane and the C_{2n-2} alkane has proved elusive. The high temperatures required for pincer iridium-catalyzed dehydrogenation result in short lifetimes of the olefin metathesis catalysts, so a challenge to be addressed is to develop a highly thermally stable olefin metathesis catalyst or a homogeneous dehydrogenation catalyst that functions efficiently at much lower temperatures. Other attractive processes which likely will see more development include alkyl group cross-metathesis whereby ethyl benzene plus a linear alkane can be converted to benzene bearing a linear long-chain alkyl group, alkane–alkene coupling employing tandem iridium and tantalum catalysts, and combining Diels–Alder reactions of dienes produced through hydrogen transfer reactions to ultimately lead to valuable aromatics such as *p*-xylene and toluene. Coupling other catalytic reactions involving olefins to their generation via dehydrogenation is also an area ripe for further exploitation.

Acknowledgments We gratefully acknowledge the financial support of the National Science Foundation as part of the Center for Enabling New Technologies through Catalysis (CENTC), Phase II Renewal, CHE-1205189.

References

1. Weissermel K, Arpe H-J (2008) Olefins. In: Industrial organic chemistry. Wiley, Weinheim, pp 59–89
2. Baudry D, Ephritikhine M, Felkin H, Holmes-Smith R (1983) J Chem Soc Chem Commun 788–789
3. Felkin H, Fillebeen-Khan T, Gault Y, Holmes-Smith R, Zakrzewski J (1984) Tetrahedron Lett 25:1279–1282
4. Felkin H, Fillebeen-khan T, Holmes-Smith R, Yingrui L (1985) Tetrahedron Lett 26:1999–2000
5. Burk MJ, Crabtree RH, Parnell CP, Uriarte RJ (1984) Organometallics 3:816–817
6. Burk MJ, Crabtree RH, McGrath DV (1985) J Chem Soc Chem Commun 1829–1830
7. Burk MJ, Crabtree RH (1987) J Am Chem Soc 109:8025–8032
8. Aoki T, Crabtree RH (1993) Organometallics 12:294–298
9. Nomura K, Saito Y (1988) J Chem Soc Chem Commun 161–162
10. Sakakura T, Sodeyama T, Tokunaga Y, Tanaka M (1988) Chem Lett 263–264
11. Maguire JA, Boese WT, Goldman AS (1989) J Am Chem Soc 111:7088–7093
12. Maguire JA, Boese WT, Goldman ME, Goldman AS (1990) Coord Chem Rev 97:179–192
13. Maguire JA, Goldman AS (1991) J Am Chem Soc 113:6706–6708
14. Maguire JA, Petrillo A, Goldman AS (1992) J Am Chem Soc 114:9492–9498
15. Wang K, Goldman ME, Emge TJ, Goldman AS (1996) J Organomet Chem 518:55–68

16. Gupta M, Hagen C, Flesher RJ, Kaska WC, Jensen CM (1996) Chem Commun 2083–2084
17. Gupta M, Hagen C, Kaska WC, Cramer RE, Jensen CM (1997) J Am Chem Soc 119:840–841
18. Liu F, Pak EB, Singh B, Jensen CM, Goldman AS (1999) J Am Chem Soc 121:4086–4087
19. Kundu S, Choliy Y, Zhuo G, Ahuja R, Emge TJ, Warmuth R, Brookhart M, Krogh-Jespersen-K, Goldman AS (2009) Organometallics 28:5432–5444
20. Punji B, Emge TJ, Goldman AS (2010) Organometallics 29:2702–2709
21. Krogh-Jespersen K, Czerw M, Zhu K, Singh B, Kanzelberger M, Darji N, Achord PD, Renkema KB, Goldman AS (2002) J Am Chem Soc 124:10797–10809
22. Zhu K, Achord PD, Zhang X, Krogh-Jespersen K, Goldman AS (2004) J Am Chem Soc 126:13044–13053
23. Ray A, Zhu K, Kissin YV, Cherian AE, Coates GW, Goldman AS (2005) Chem Commun 3388–3390
24. Huang Z, Brookhart M, Goldman AS, Kundu S, Ray A, Scott SL, Vicente BC (2009) Adv Synth Catal 351:188–206
25. Goettker-Schnetmann I, White P, Brookhart M (2004) J Am Chem Soc 126:1804–1811
26. Goettker-Schnetmann I, Brookhart M (2004) J Am Chem Soc 126:9330–9338
27. Goettker-Schnetmann I, White PS, Brookhart M (2004) Organometallics 23:1766–1776
28. Morales-Morales D, Redón R o, Yung C, Jensen CM (2004) Inorg Chim Acta 357:2953–2956
29. Haenel MW, Oevers S, Angermund K, Kaska WC, Fan H-J, Hall MB (2001) Angew Chem Int Ed 40:3596–3600
30. Renkema KB, Kissin YV, Goldman AS (2003) J Am Chem Soc 125:7770–7771
31. Kanzelberger M, Singh B, Czerw M, Krogh-Jespersen K, Goldman AS (2000) J Am Chem Soc 122:11017–11018
32. Krogh-Jespersen K, Czerw M, Summa N, Renkema KB, Achord PD, Goldman AS (2002) J Am Chem Soc 124:11404–11416
33. Krogh-Jespersen K, Czerw M, Goldman AS (2002) J Mol Catal A Chem 189:95–110
34. Choi J, MacArthur AHR, Brookhart M, Goldman AS (2011) Chem Rev 111:1761–1779
35. Morales-Morales D (2009) Iridium-mediated alkane dehydrogenation. In: Oro LA, Claver C (eds) Iridium complexes in organic synthesis. Wiley-VCH, Weinheim, pp 325–344
36. Choi J, Goldman A (2011) Ir-catalyzed functionalization of C–H bonds. In: Andersson PG (ed) Iridium catalysis, vol 34. Springer, Berlin/Heidelberg, pp 139–167
37. Findlater M, Choi J, Goldman A, Brookhart M (2012) Alkane dehydrogenation. In: Pérez PJ (ed) Alkane C–H activation by single-site metal catalysis, vol 38. Springer, Netherlands, pp 113–141
38. Adams JJ, Arulsamy N, Roddick DM (2012) Organometallics 31:1439–1447
39. Shi Y, Suguri T, Dohi C, Yamada H, Kojima S, Yamamoto Y (2013) Chem Eur J 19:10672–10689
40. Yao W, Zhang Y, Jia X, Huang Z (2014) Angew Chem Int Ed 53:1390–1394
41. Jia X, Zhang L, Qin C, Leng X, Huang Z (2014) Chem Commun 50:11056–11059
42. Biswas S, Huang Z, Choliy Y, Wang DY, Brookhart M, Krogh-Jespersen K, Goldman AS (2012) J Am Chem Soc 134:13276–13295
43. Bézier D, Brookhart M (2014) ACS Catal 4:3411–3420
44. Azerraf C, Gelman D (2008) Chem Eur J 14:10364–10368
45. Azerraf C, Gelman D (2009) Organometallics 28:6578–6584
46. Levy R, Azerraf C, Gelman D, Rueck-Braun K, Kapoor PN (2009) Catal Commun 11:298–301
47. Musa S, Romm R, Azerraf C, Kozuch S, Gelman D (2011) Dalton Trans 40:8760–8763
48. Polukeev AV, Gritcenko R, Jonasson KJ, Wendt OF (2014) Polyhedron 84:63–66
49. Raynal M, Pattacini R, Cazin CSJ, Vallée C, Olivier-Bourbigou H, Braunstein P (2009) Organometallics 28:4028–4047
50. Zuo W, Braunstein P (2012) Organometallics 31:2606–2615
51. Chianese AR, Mo A, Lampland NL, Swartz RL, Bremer PT (2010) Organometallics 29:3019–3026
52. Chianese AR, Drance MJ, Jensen KH, McCollom SP, Yusufova N, Shaner SE, Shopov DY, Tendler JA (2014) Organometallics 33:457–464

53. Brayton DF, Beaumont PR, Fukushima EY, Sartain HT, Morales-Morales D, Jensen CM (2014) Organometallics 33:5198–5202
54. Colton W (2012) The outlook for energy: a view to 2040. ExxonMobil report, p 19. http://www.exxonmobil.com/Corporate/files/news_pub_eo.pdf
55. Spitsyn VI, Pirogova GN, Korosteleva RI, Kalinina GE (1988) Dokl Akad Nauk SSSR 298:149–151 [Phys Chem]
56. Arata K, Hino M, Matsuhashi H (1993) Appl Catal A 100:19–26
57. Davis RJ (1994) Heterog Chem Rev 1:41–53
58. Meriaudeau P, Naccache C (1997) Catal Rev Sci Eng 39:5–48
59. Davis BH (1999) Catal Today 53:443–516
60. Smieskova A, Rojasova E, Hudec P, Sabo L (2004) Appl Catal A 268:235–240
61. Ahuja R, Punji B, Findlater M, Supplee C, Schinski W, Brookhart M, Goldman AS (2011) Nat Chem 3:167–171
62. Dobereiner GE, Yuan J, Schrock RR, Goldman AS, Hackenberg JD (2013) J Am Chem Soc 135:12572–12575
63. Lyons TW, Guironnet D, Findlater M, Brookhart M (2012) J Am Chem Soc 134:15708–15711
64. He C, You F (2014) Ind Eng Chem Res 53:11442–11459
65. Kundu S, Lyons TW, Brookhart M (2013) ACS Catal 3:1768–1773
66. Leckel D (2009) Energy Fuels 23:2342–2358
67. Dry ME (2002) Catal Today 71:227–241
68. Dry ME (2002) J Chem Technol Biotechnol 77:43–50
69. Hildebrandt D, Glasser D, Hausberger B, Patel B, Glasser BJ (2009) Science 323:1680–1681
70. Burnett RL, Hughes TR (1973) J Catal 31:55–64
71. Vidal V, Theolier A, Thivolle-Cazat J, Basset J-M (1997) Science (Washington, DC) 276:99–102
72. Basset JM, Coperet C, Lefort L, Maunders BM, Maury O, Le Roux E, Saggio G, Soignier S, Soulivong D, Sunley GJ, Taoufik M, Thivolle-Cazat J (2005) J Am Chem Soc 127:8604–8605
73. Le Roux E, Taoufik M, Copéret C, de Mallmann A, Thivolle-Cazat J, Basset J-M, Maunders BM, Sunley GJ (2005) Angew Chem Int Ed 44:6755–6758
74. Goldman AS, Roy AH, Huang Z, Ahuja R, Schinski W, Brookhart M (2006) Science 312:257–261
75. Haibach MC, Kundu S, Brookhart M, Goldman AS (2012) Acc Chem Res 45:947–958
76. Ahuja R, Kundu S, Goldman AS, Brookhart M, Vicente BC, Scott SL (2008) Chem Commun 253–255
77. Bailey BC, Schrock RR, Kundu S, Goldman AS, Huang Z, Brookhart M (2009) Organometallics 28:355–360
78. Huang Z, Rolfe E, Carson EC, Brookhart M, Goldman AS, El-Khalafy SH, MacArthur AHR (2010) Adv Synth Catal 352:125–135
79. Nawara-Hultzsch AJ, Hackenberg JD, Punji B, Supplee C, Emge TJ, Bailey BC, Schrock RR, Brookhart M, Goldman AS (2013) ACS Catal 3:2505–2514
80. Leitch DC, Lam YC, Labinger JA, Bercaw JE (2013) J Am Chem Soc 135:10302–10305
81. Leitch DC, Labinger JA, Bercaw JE (2014) Organometallics 33:3353–3365
82. Labinger J, Leitch D, Bercaw J, Deimund M, Davis M (2015) Top Catal 58:494–501
83. Gupta M, Kaska WC, Jensen, CM (1997) Chem Commun 461–462
84. Zhang X, Fried A, Knapp S, Goldman AS (2003) Chem Commun 2060–2061
85. Wang Z, Tonks I, Belli J, Jensen CM (2009) J Organomet Chem 694:2854–2857
86. Brayton DF, Jensen CM (2014) Chem Commun 50:5987–5989
87. Lyons TW, Bezier D, Brookhart M (Submitted)
88. Cavani F, Ballarini N, Cericola A (2007) Catal Today 127:113–131
89. Gärtner CA, van Veen AC, Lercher JA (2013) ChemCatChem 5:3196–3217
90. Allen KE, Heinekey DM, Goldman AS, Goldberg KI (2013) Organometallics 32:1579–1582
91. Pahls DR, Allen KE, Goldberg KI, Cundari TR (2014) Organometallics 33:6413–6419
92. Allen KE, Heinekey DM, Goldman AS, Goldberg KI (2014) Organometallics 33:1337–1340

Index

A
Acetoxylation, 94
Addition, cyclo-, 21–23, 92, 171, 175, 176
  oxidative, 67, 97, 99, 104, 109, 137, 146
Aeruginosins, 149
Alkane–alkene coupling, 200
Alkanes, dehydroaromatization, 196
  functionalization, 189
  metathesis, 155, 170, 199
    tandem, 200
Alkenes, 20, 23, 38, 88, 171, 176, 190, 203
  acyclic, 8, 15
  alkylation, 144
  dehydrogenation, 190, 192
Alkyl group cross-metathesis (AGCM), 197
Alkylamines, 56
Alkylarenes, 196
Alkylation, 7, 20, 24, 38, 53
Alkylidenes, 155, 160, 170
Alkylidynes, 155, 160, 170, 176
Alkyliron(II) complexes, 2
Alkynes, 10, 12, 21, 70, 75–88, 120
  metathesis, 170
Alkynyl hydrides, 79
Alkynylation, 28, 49, 53
Amination/amidation, 116, 121
Amines, 4, 15, 55, 108, 201
  γ-arylation, 140, 143
Aminobenzocyclobutene, 147
2-Aminobutanoic acid derivatives, 143
1-Aminocyclopropane-1-carboxylic acid, 105
Aminoquinolamide, 102
Aminoquinoline, 19, 22, 27, 31, 35, 44, 136, 145
  based *N*,*N*-bidentate amide, 50
Angustureine, 140
Aromatic compounds, 47
Arylacetylenes, 49
Arylamines, hetero-, 54
Arylation, 14, 20, 27, 34, 51, 136
  arylpyridines, 4, 6
  carbonyl compounds, 136
Arylboronic acids, 12
Arylpyridines, 3
Azoles, 21, 43, 49, 51, 55, 58

B
Benazepril, 143
Benzazepines, 97
Benzo[*c*]azepine-1-one, 97
Bi(heteroaryl)s, annulative metalation, 54
Biaryls, 24, 51
Bioactive molecules, 133
2-Biphenylmagnesium, 12
Bis(diphosphine)iron, 13
Bond strengths, 67
Borylation, 20
  iron-catalyzed, 13
Bromopiperonal, 138
t-Butylethylene (TBE), 72, 190
2-Butynyl hydride, 80

C
C–C bonds, 1, 47, 117, 144, 155
C–F bonds, 115, 127
C–H bonds, activation, 1, 19, 67, 133, 155
  heteroatom-directed, 134
  oxidative addition, 146

C–H bonds (*cont.*)
functionalization, 19, 91, 115
C–H/C–H coupling, 48
C–H/N–H coupling, 54
C–H/X–H coupling, 57
C–N bonds, 41, 47, 115, 121
C–S bonds, 32, 39, 115
Carbonylation, 20, 31, 39, 40, 94
Catalysis, 91
Celogentin C, 137
Chelation assistance, 19
1-(Chloromethyl)-4-fluoro-1,4-diazoniabicyclo[2.2.2]octane bis (tetrafluoroborate), 127
Chlorophenyl cyclopropyl carbamates, 95
Concerted metalation–deprotonation (CMD), 20, 25, 36, 44, 96, 101, 104, 203
Copper, 47, 49
Coralydine, 147
Cross-dehydrogenative couplings, 15, 30
Cross metathesis, 180
Crykonisine, 144
Cycloadditions, 92, 171, 175
oxidative, 21–23
Cycloalkanes, metathesis, 157, 176
Cyclodecane, dehydrogenation, 192
1,9-Cyclohexadecadiene, 178
Cyclohexadecane, 178
Cyclohexadienes, 196
Cyclohexenyl bromide, 149
Cyclometalation, 2, 20, 25, 39
Cyclooctane, 176–179, 190–193
dehydrogenation, 190
metathesis, 176, 178
Cyclopropanes, 69, 74, 91–110
Cyclopropenes, 92
Cyclopropyl benzamide, 97
Cyclopropyl carboxamides, 102
Cyclopropyl halide, 92
Cyclopropyl methyl picolinamide, 103
Cyclopropyl oxindole, 99
Cyclopropyl spirooxindoles, 100

D
Decane, metathesis, 173
Decarboxylation, 116
1-Decene metathesis, 176
Dehydroaromatization, 196
Dehydrogenation, oxidative, 203
transfer, 189
Dehydrogenative coupling, 47
aromatic, 59
DFT, 63 ,67
Di-*tert*-butyl-4-methylphenol (BHT), 26
Dialkylphosphonates, 59
Diaryl sulfides, 40
Diarylmagnesium, 6
Diarylzinc, 3
Difluorination, 127
Dihydroquinolines, 95
2,3-Dimethylbutane, 179
3,6-Dimethylcyclohexene, 198
Directing groups, 2
Disulfides, 34

E
Epimerization, 99
Ethane, metathesis, 173
Ethane/toluene, cross metathesis, 180
Ethylbenzene, 196
Ethylcyclohexene, 198
Ethylene, 203

F
Ferracycles, 5
Fischer–Tropsch catalysis, 190
Fluorination, 116

G
Grignard reagents, 4

H
Hafnium, 160
Halogenation, 48, 49
N-Heterocyclic carbenes (NHCs), 58
Hexadienes, 198
Hexafluoro-2-propanol (HFIP), 58
Hexahydroindoles, 148
Hexenes, 198
Hibispeptin, 142
Homophenylalanine derivatives, 143
Hydro-metathesis, 182
Hydrocarbons, activation by [Tp′Rh(CNR)], 68
[Tp′Rh(PMe_3)], 77
[Tp′Rh($P(OMe)_3$)], 82
Hydrosilylation, 116
Hydroxyphenyllactic (Hpla) subunits, 149

I
1-Indanamines, 148

1-Indanols, 148
Indaziflam, 149
Iridium, 2, 20, 116
  pincer catalysts, 177, 189
Iridium triptycene, 193
Iron, 1
Iron–isocyanide, 11
Iron–xantphos, 15
Isocyanide, 11
Isonitrile, 11

K
Kinetic isotope effect (KIE), 60
Kinetics, 67

L
Lactamase inhibitor, 145
Lactams, 135, 143, 145
  β-, 41, 138
  γ-, 93
Late-transition metals, 2

M
Metal-alkylidynes, 155
Metal-hydrides, 155
Metallacyclobutanes, 171
Metathesis catalysts, 155, 199, 205
Methane/propane, cross metathesis, 182
2-Methoxyiminoacetyl (MIA), 143
N-Methylbenzamides, 3
Methylene isoindolinone, 50
2-Methylpropane, metathesis, 179
Methylthioanilide, 102
MK-8712, 145
Molybdenum, 199

N
Naphthalenes, 13
Natural products, 133
Neopentylisocyanide, 82
Nickel, 19, 20
Nitrosylation, 43
Nucleophiles, 1, 48, 57, 92, 107

O
Obafluorin, 140
Olefins, 68, 170, 175, 196, 200
  cyclic, 147
  isomerization, 177
  metathesis, 155
  poly-, 157
Organomagnesium, 6
Organozinc, 6
Oxazolinylaniline, 50

P
Palladacycles, 97, 100, 106, 109, 135, 138, 142
Palladium, 2, 20, 49, 91
Papaverine, 144
Paspaline, 145
Peptidomimetics, 143
2-Phenylpyridine, 55, 58
Phthalimide, 56
Picolinamide, 102
Piperarborenines, 138
Pipercyclobutanamide, 138
Piperylene, 198
Platinum, 134
Podophyllotoxin, 138
Polyethylene terephthalate (PET), 198
Polyfluoroarenes, 51, 55
Polyhydrides, phosphine-stabilized, 190
Prefunctionalization, 48
Proline, *cis*-3-substituted, 139
Propane, 69, 180, 181
  metathesis, 172, 175, 182
Propene, 171, 182, 196, 203
  hydro-metathesis, 182, 183
o-Propyltoluene, 197
Pseudo-Wittig reaction, 164
2-Pyridinylisopropyl (PIP), 149
Pyridinylpropylamine, 50
N-(2-Pyrimidyl)indoles, 56
Pyrroles, 12

Q
Quinolylamine directing group, 6

R
Reductive elimination, 67
Rh–C bonds, 72, 80, 84
Rhazinilam, 134
Rhodium, 2, 20, 67
Ring-opening–ring-closing metathesis reactions (RO-RCM), 178
Ruthenium, 2, 20

S
Schrock-type metathesis catalysts (Mo/W), 177, 197
Schwartz's reagent, 42

Selectfluor fluorinating reagent, 127
Silver, 56, 98, 104, 109, 115–129
Silver hexafluoroantimonate(V), 117
Silylation, 20
  iron-catalyzed, 13
Solenopsin A, 145
Spirooxindoles, 98
Sulfoximine, 55
Surface organometallic chemistry (SOMC), 155, 157
Syngas, 190

T
Tantalum, 159, 163, 170, 200, 205
Tantalum carbene, 162, 163
Tantalum hydrides, 155, 156, 164, 170–172, 180–183
Teleocidin B4, 135
Terephthalic acid, dimethyl ester, 198
Tetrahydrofuran, dehydrogenation, 201
Tetrahydroprotoberberine, 147
Tetrahydroquinolines (THQs), 95, 106, 140
Tetramethyltetrahydrofuran, 93
Tetraneopentylzirconium, 160
Thermodynamics, 67
Thiolation, 32, 40, 58
Titanium, 86, 160, 161
Toluene, 198
Toluene/methane, cross metathesis, 181
Total synthesis, 133
[Tp′Rh(CNR)], 68
Transfer dehydrogenations, 190
  alkanes, 189
Transition metals, 2, 48, 68, 92, 133, 155
Trifluoromethylthiolation, silver-mediated, 128
Triisopropylsilyl (TIPS), 28
Trimethylphosphite, 82
Tris(pyrazolyl)borate (Tp) silver complexes, 117
Tungsten, 159, 165, 170, 173
Tunsten carbyne, 166, 167
Tungsten hydrides, 172, 176
Tungsten methylidyne, 168
Tungsten polyhydride, 166

V
Vanadium, 95
Verapamil, 147

X
Xylenes, 180, 196–198

Z
Zirconium tris-neopentyl surface complex, 160